TESIS DE LA UNIVERSIDAD DE ZARAGOZA

2025 254

Seyed Hesamoddin Bidooki

Characterization of Molecular Mechanisms of TXNDC5 and Its Role in Squalene Response Using Various Drug Delivery Systems in the AML12 Cell Line

Director/es
de la Osada García, Jesús
de Matos Fernandes, Susana
Navarro Ferrando, María Ángeles

ISSN 2254-7606

Prensas de la Universidad Universidad Zaragoza

Universidad de Zaragoza
Servicio de Publicaciones

ISSN 2254-7606

Universidad Zaragoza
1542

Tesis Doctoral

CHARACTERIZATION OF MOLECULAR MECHANISMS OF TXNDC5 AND ITS ROLE IN SQUALENE RESPONSE USING VARIOUS DRUG DELIVERY SYSTEMS IN THE AML12 CELL LINE

Autor

Seyed Hesamoddin Bidooki

Director/es

de la Osada García, Jesús
de Matos Fernandes, Susana
Navarro Ferrando, María Ángeles

UNIVERSIDAD DE ZARAGOZA
Escuela de Doctorado

Programa de Doctorado en Bioquímica y Biología Molecular

2025

Universidad Zaragoza
1542

Tesis Doctoral

Characterization of Molecular Mechanisms of TXNDC5 and Its Role in Squalene Response Using Various Drug Delivery Systems in the AML12 Cell Line

Autor

Seyed Hesamoddin Bidooki

Director/es

Prof. Dr. Jesús Osada García

Prof. Dr. Susana de Matos Fernandes

Prof. Dr. María Ángeles Navarro Ferrando

UNIVERSIDAD DE ZARAGOZA

UNIVERSIDAD DE PAU Y LA REGION DE ADOUR

Escuela de Doctorado

Programa de Doctorado en Bioquímica y Biología Molecular

2025

Characterization of Molecular Mechanisms of TXNDC5 and Its Role in Squalene Response Using Various Drug Delivery Systems in the AML12 Cell Line

Autor

Seyed Hesamoddin Bidooki

Director/es

Prof. Dr. Jesús Osada García

Prof. Dr. Susana de Matos Fernandes

Prof. Dr. María Ángeles Navarro Ferrando

Departamento de Bioquímica y Biología Molecular y Celular
Instituto de Ciencias Analíticas y Físicoquímica del Medio Ambiente y los Materiales

UNIVERSIDAD DE ZARAGOZA
UNIVERSIDAD DE PAU Y LA REGION DE ADOUR

February 2025

DEDICATION

To my beloved parents, Dr. Seyed Kazem Bidoki and Fatemeh Arefanian

Your unwavering love, endless support, and countless sacrifices have been the cornerstone of my journey. Through every challenge and triumph, your faith in me has been my greatest source of strength. This accomplishment is a reflection of the values, perseverance, and encouragement you've instilled in me. I am forever grateful for everything you have done to help me reach this moment.

And to my dear fiancée, Maedeh Vahdatazad

Thank you for your constant love, patience and understanding. Your support has been my anchor, and your belief in me has kept me going through the most difficult times. This thesis is as much yours as it is mine, for without you this journey would have been incomplete.

With all my love and gratitude, I dedicate this work to all of you.

ACKNOWLEDGEMENTS

I'm so grateful to have had the chance to complete this PhD thesis! It's been one of the most challenging and rewarding experiences of my life, and I couldn't have done it without the support, guidance, and encouragement of so many amazing people. I just want to say a big, heartfelt thank you to everyone who has been on this journey with me.

I'd like to start by thanking my thesis directors, Prof. Dr. Jesús Osada García, Prof. Dr. Susana de Matos Fernandes, and Prof. Dr. Maria Angeles Navarro Ferrando. You've been so supportive and helpful throughout this process, and I'm truly grateful to have had them as guides. I can't thank you enough for all your amazing expertise, thoughtful insights, and unwavering guidance. You've shaped this work in ways I could never have imagined! From the very beginning to the very end, your kind words and helpful feedback encouraged me to think critically and to do my best. I feel so lucky to have had such inspiring mentors. They believed in me and helped me to overcome so many obstacles along the way.

I'd also like to thank my wonderful colleagues and fellow researchers at the Department of Biochemistry and Cellular and Molecular Biology. I'd also like to thank Dr. Roberto Martínez Beamonte, Dr. Javier Sánchez Marco, and Dr. Roubi Hamid Ahmad Abuobeid for all their help and support. You were always there for me with your valuable advice, guidance, and encouragement, and I'm so grateful to have had you on my side. I'm so grateful to Prof. Dr. Mª Jesús Rodriguez-Yoldi and Prof. Dr. Carmen Arnal. You were so helpful, offering lots of great advice and support along the way. Thanks to you, I was able to complete my manuscripts and thesis successfully! I'd like to send a big, warm thank you to Cristina Barranquero, Santiago Morales Andres, Dr. Luis Herrera-Marcos, Tania Herrero-Continente, Raylen Escobar and Isabel Baviano Rayego. Your friendship and collaboration made even the most challenging moments totally manageable. Thank you all so much! The wonderful conversations and collaborations we've had have been such a source of inspiration and growth for us both. I'm so grateful to you all for challenging my ideas, sharing your knowledge, and offering your support during this journey. I've been so lucky to work alongside such a brilliant and dedicated team, who have made my experience so rich and rewarding. I'd also like to thank Prof. Dr. Julio Montoya, Prof. Dr. Eduardo Ruiz Pesini, Ana Vela Sebastián, Sonia Emperador, Irene Jiménez, Ester López, Melissa Carvajal, and Vicky Peña for all your help, support, and encouragement. You were always there for me and made me feel so welcome and comfortable from day one. You were kind enough to let me use your instruments and equipment, and you even gave me all the training I needed!

I want to thank my wonderful parents, Dr. Seyed Kazem Bidoki and Fatemeh Arefanian, from the bottom of my heart. You have always believed in me, made incredible sacrifices, and taught me the values of perseverance and hard work. I am so grateful for everything you have done for me! You've always been my biggest supporters, always reminding me to follow my dreams and never give up, even when the road ahead seemed tough.

To my sweet little brother, Seyed Sobhan Bidoki, you've been a constant source of joy and laughter, always reminding me to keep perspective and stay positive. Your youthful enthusiasm and unconditional support mean the absolute world to me, my dear brother.

To my amazing fiancée, Maedeh Vahdatazad, your support has been absolutely incredible. I can't thank you enough for your patience, understanding, and for being my constant companion throughout this journey. You've been there through the highs and lows,

always ready with a word of encouragement or a shoulder to lean on when things got tough. I don't know what I would have done without you! Your faith in me has never wavered, and I'm so grateful for that. I'm also really thankful to your family, Farshid Vahdatazad and Leila Hatamzad, who have welcomed me with open arms and given me so much love and encouragement along the way. Your support has meant the world to me, and I feel so lucky to be part of your family.

To my dear friends Arash Matinahmadi and Alireza Tavakolpournegari, I want to thank you from the bottom of my heart for being there for me, for your wonderful sense of humor, your understanding, and for providing much-needed moments of distraction and relief from the demands of research. From long chats to shared giggles to just being there when I needed a break, you've made this journey so much less lonely and so much more enjoyable. I'd like to give a big, heartfelt thank you to my Iranian friend in Zaragoza, Mehrzad Javadzadeh. He's been there for me every step of the way with his unwavering friendship and support, and I'm so grateful!

Finally, I would like to express my gratitude to everyone who contributed to this thesis in some way, big or small—whether through academic guidance, emotional support, or personal advice. You have all played a crucial role in helping me reach this point, and I am deeply appreciative of each and every one of you. This thesis is as much a reflection of your love and support as it is of my work, and for that, I will be forever grateful.

ABBREVIATIONS

AML12	Alpha mouse liver cell line
ALD	Alcohol-related liver disease
ALT	Alanine aminotransferase
AST	Aspartate aminotransferase
ATF6	Activating transcription factor 6
ATP	Adenosine triphosphate
AMPK	AMP-activated protein kinase
ATM	Ataxia-telangiectasia mutated
ATF4	Activating transcription factor 4
APMAP	Adipocyte plasma membrane-associated protein
APOA1	Apolipoprotein A1
APOB	Apolipoprotein B
ACC	Acetyl CoA carboxylase
ACOX1	Peroxisomal acyl CoA oxidase
ATGs	Transcriptional activator of autophagy-related genes
ASK1	Apoptotic signal-regulating kinase 1
BA	Bile acids
CT Scan	Computed tomography scan
CK-18	Cytokeratin-18
CF	Cardiac fibrosis
CXCL8	Interleukin 8
CS	Crystalline silica
CRISPR	Clustered regularly interspaced short palindromic repeats
C2C12	Mouse myoblast cell line
CDKs	Cyclin-dependent kinases
COS-7	Monkey African green kidney fibroblasts
CNTs	Carbon nanotubes
CALR	Calreticulin
CRN	Clinical Research Network
ChREBP	Carbohydrate responsive element binding protein
CPT1A	Carnitine palmitoyl transferase 1A
DNA	Deoxyribonucleic acid
DDR	DNA damage response
DM	Diabetes mellitus
DDIT3	DNA damage-inducible transcript 3
DNAJA3	DnaJ heat shock protein family (Hsp40) member A3
DLS	Dynamic light scattering
DR5	Death receptor 5
DNL	*De novo* lipogenesis
DGAT2	Diacylglycerol acyltransferase 2
DGAT	Diacylglycerol transferase
DAGs	Diacylglycerols

ER	Endoplasmic reticulum
ERAD	ER-associated degradation
EIF2AK3	Eukaryotic translation initiation factor 2-alpha kinase 3
ERN1	Serine/threonine-protein kinase/endoribonuclease inositol-requiring enzyme 1
ERp46	Endoplasmic reticulum protein 46
EndoPDI	Endothelial protein disulfide isomerase
ECM	Extracellular matrix
EDEM3	ER degradation enhancing alpha-mannosidase like protein 3
EVOO	Extra virgin olive oil
EMA	European Medicines Agency
FIB-4	Fibrosis-4 index
FPP	Farnesyl pyrophosphate
FAs	Fatty acids
FAS	Fatty acid synthase
FABP	Fatty acid binding protein
FAT	Fatty acid translocase
FLIP	Fatty liver inhibition progression
FDA	United States Food and Drug Administration
GLP-1	Glucagon-like peptide type 1
G6P	Glucose 6-phosphate
GSTM6	Glutathione S-transferase, mu 6
GSTP3	Glutathione S-transferase pi 3
GSTT1	Glutathione S-transferase, theta 1
GPX4	Glutathione peroxidase 4
GSH	Glutathione
HDL	High-density lipoprotein
HSR	Heat shock response
HSPs	Heat shock proteins
HSF1	Heat shock factor 1
HIFs	Hypoxia-inducible factors
HSPA8	Heat shock protein family A (Hsp70) member 8
HSPA5	Heat shock protein family A (Hsp70) member 5
HSPA9	Heat shock protein family A (Hsp70) member 9
HF	Heart failure
HCC	Hepatocellular carcinoma
HEK293T	Human embryonic kidney cells 293T
HeLa	Henrietta lacks cancer cells
Hsp90aa1	Heat shock protein 90, alpha (cytosolic), class A member 1
HSCs	Hepatic stellate cells
HMG-CoA	β-Hydroxy β-methylglutaryl-CoA
HepG2	Human hepatoma cell line
IL-6	Interleukin 6
INSIG	Insulin-induced gene

IGFBP1	Insulin-like growth factor-binding protein-1
iPLA2	Calcium independent phospholipase A2
IPP	Isopentenyl pyrophosphate
Jurkat	Immortalized line of human T lymphocyte cells
JNK	C-Jun N-terminal kinases
KO	Knockout
KGF	Keratinocyte growth factor
LF	Liver fibrosis
LPS	Lipopolysaccharides
LDL	Low-density lipoprotein
MRI	Magnetic resonance imaging
MIQE	Minimum information for publication of quantitative real-time
MBOAT7	Membrane-bound O-acyltransferase domain-containing protein 7
MAPK	Mitogen-activated protein kinase
METTL3	N6-adenosine-methyltransferase
MD	Mediterranean diet
MTT	3-(4 5-dimethylthiazol-2-yl)-2 5-diphenyltetrazolium bromide
MDA-MB-231	M.D. Anderson-metastatic breast 231
MIN6	Mouse insulinoma cell line 6
Mfn2	Mitofusin 2
MCF-7	Michigan cancer foundation-7
m6A	N6-methyladenosine
mTOR	Mechanistic target of rapamycin
mTORC1	Mammalian target of rapamycin complex
MAGs	Monoacylglycerols
MVA	Mevalonate pathway
mtGPAT	Mitochondrial glycerol-3-phosphate acyltransferase
MASLD	Metabolic dysfunction-associated steatotic liver disease
MUFA	Monounsaturated fatty acids
Npm1	Nucleophosmin 1
NAFLD	Non-alcoholic fatty liver disease
NASH	Non-alcoholic steatohepatitis
NFS	NAFLD fibrosis score
NEFA	Non-esterified fatty acids
NR4A1	Nuclear receptor subfamily 4 group A member 1
NMSC	Non-melanoma skin cancer
NF-κB	Nuclear factor kappa B
NIH-3T3	Mouse NIH/Swiss embryo fibroblasts
Oplah	5-oxoprolinase (ATP-hydrolyzing)
OA	Oleanolic acid
PCR	Polymerase chain reaction
PUFA	Polyunsaturated fatty acids
PBC	Primary biliary cholangitis
PSC	Primary sclerosing cholangitis

PNPLA3	Patatin-like phospholipase domain-containing protein 3
PDIA15	Protein disulfide isomerase family A member 15
PDI	Protein disulfide isomerase
PPARα	Peroxisomal proliferator-activated receptor alpha
PRDX4	Peroxiredoxin 4
PRDX5	Peroxiredoxin 5
PRDX6	Peroxiredoxin 6
PRDX6B	Peroxiredoxin 6B
PI3k	Phosphoinositide-3 kinase
PKB	Protein kinase B
PCA	Polyalkyl (cyano) acrylates
PLA	Poly (lactic acid)
PGA	Poly (glycolic acid)
PLGA	Poly (lactic-co-glycolic acid)
PLGA NPs	PLGA nanoparticles
PEG	Polyethylene glycol
PPIB	Peptidylprolyl isomerase B
ROS	Reactive oxygen species
RER	Rough endoplasmic reticulum
RIDD	Regulated IRE1-dependent decay
RAAS	Renin-angiotensin-aldosterone system
RKO	Human colon carcinoma cell line
RPS14	Ribosomal protein S14
RNA	Ribonucleic acid
STAT3	Signal transducer and activator of transcription 3
SREBP1c	Sterol regulatory element binding protein 1 c
SFA	Saturated fatty acids
SSR2	Signal sequence receptor, beta
SEC61A1	Sec61 alpha 1 subunit
Serpina1a	Serine (or cysteine) peptidase inhibitor, clade A, member 1A
Serpina1b	Serine (or cysteine) peptidase inhibitor, clade A, member 1B
Serpina3m	Serine (or cysteine) peptidase inhibitor, clade A, member 3M
SEM	Scanning electron microscope
SCAP	SREBP cleavage-activated protein
SER	Smooth endoplasmic reticulum
SRP	Signal recognition particle
SNPs	Single nucleotide polymorphisms
SPEA	Serum prolidase enzyme activity
sRAGE	Soluble receptor for advanced glycation end product
SAF	Steatosis, activity and fibrosis
SiO_2	Silicon dioxide
TNF-α	Tumor necrosis factor-alpha
TGs	Triglycerides
TRAF2	Receptor-associated tumor necrosis factor 2

TEI	Total energy intake
TAGs	Triacylglycerols
TM6SF2	Transmembrane 6 superfamily member 2
TXNDC5	Thioredoxin domain-containing protein 5
TRX	Thioredoxin
TGFβ	Transforming growth factor beta
TP53	Tumor protein p53
TBP	TATA-box binding protein
TiO_2	Titanium dioxide
TEM	Transmission electron microscopy
UPR	Unfolded protein response
UPRmt	Mitochondrial unfolded protein response
UTR	Untranslated region
UPS	Ubiquitin/proteasome system
VLDL	Very low-density lipoproteins
WT	Wild-type
XBP1	X-box binding protein 1
ZrO_2	Zirconium dioxide

Table of Contents

ABBREVIATIONS..... 1
I. ABSTRACT (ENGLISH)..... 10
I. RESUMEN (ESPAÑOL)..... 11
I. RÉSUME (FRANÇAIS) 12
II. INTRODUCTION.....13
1. Liver Anatomy and Physiology..... 14
1.1. Structure of the Liver..... 14
1.1.1. Lobes and Segments..... 14
1.1.2. Hepatic Lobule……..... 15
1.2. Functions of the Liver..... 16
1.2.1. Metabolism of Lipids, Proteins and Carbohydrates..... 16
1.2.2. Detoxification and Drug Metabolism..... 17
1.2.3. Bile Production and Excretion..... 17
1.2.4. Other Liver Functions..... 18
2. Liver Disease..... 18
2.1. Definition and Classification of Liver Diseases..... 18
2.2. Common Symptoms and Signs of Liver Disease..... 18
2.3. Causes of Liver Disease..... 19
3. MASLD……..……..... 19
3.1. Epidemiology of MASLD..... 20
3.2. Diagnosis and Assessment of MASLD..... 20
3.3. Pathology of MASLD..... 21
3.4. Lipid Metabolism in MASLD..... 22
3.4.1. Absorption of NEFA from Plasma..... 23
3.4.2. Hepatic *De Novo* Lipogenesis (DNL)..... 24
3.4.3. Fatty Acid Oxidation…..... 26
3.4.4. Plasma Secretion of Hepatic Lipids…….... 27
3.4.5. Bile Acids……..... 28
3.4.6. Non-Esterified Cholesterol……..... 28
3.4.7. Macroautophagy..... 28
3.5. Carbohydrates and Insulin Metabolism in MASLD..... 28
3.6. Nuclear Receptors in MASLD……..... 29
3.7. Cell Death in MASLD……..... 29
4. Cellular Stress..... 30
4.1. Overview of Cellular Stress..... 30
4.2. Oxidative Stress in MASLD..... 32
4.3. ER and its Stress in MASLD..... 32
4.3.1. ER……..... 32
4.3.2. Protein synthesis and stress modulation..... 33
4.3.2.1. ERN1 (IRE1) Pathway..... 34
4.3.2.2. EIF2AK3 (PERK) Pathway..... 35
4.3.2.3. ATF6 Pathway……..... 35
4.3.3. ER Stress and lipid homeostasis……..... 35
4.3.4. ER Stress Inducers..... 37
5. TXNDC5..... 37
5.1. Overview of TXNDC5..... 37
5.2. *TXNDC5* Gene and Protein Structure..... 38
5.3. TXNDC5 and Fibrosis-Related Pathologies..... 41
5.4. The Role of TXNDC5 in Chronic Diseases..... 42

5.4.1. TXNDC5 and Diabetes Mellitus..... 42
5.4.2. TXNDC5 and Heart Diseases..... 43
5.4.3. TXNDC5 and Liver Cancer..... 44
5.5. TXNDC5 and Dietary Patterns..... 45
6. Mediterranean Diet..... 46
6.1. Overview and Key Components of the Mediterranean Diet..... 46
6.2. The Role of Healthy Fats in the MD..... 47
6.3. EVOO..... 47
6.4. Bioactive Compounds in EVOO..... 48
6.5. Squalene..... 49
6.5.1. Squalene and Biological Role..... 50
6.5.2. Squalene and Cholesterol Synthesis..... 51
7. Nanoparticles..... 53
7.1. Definition and Characteristics..... 53
7.2. Classification Based on Composition..... 54
7.2.1. Metal Nanoparticles..... 54
7.2.2. Ceramic Nanoparticles..... 55
7.2.3. Carbon-based Nanoparticles..... 55
7.2.4. Polymeric Nanoparticles..... 55
7.2.4.1. PLGA..... 57
7.2.4.2. Chitosan..... 58
8. Role of AML12 Cell Line in Hepatic Research..... 59
III. OBJECTIVES (ENGLISH) 61
III. OBJETIVOS (ESPAÑOL) 61
IV. PUBLICATIONS..... 62
1. Endoplasmic Reticulum Protein TXNDC5 Interacts with PRDX6 and HSPA9 to Regulate Glutathione Metabolism and Lipid Peroxidation in the Hepatic AML12 Cell Line..... 64
2. TXNDC5 Plays a Crucial Role in Regulating Endoplasmic Reticulum Activity through Different ER Stress Signaling Pathways in Hepatic Cells..... 88
3. Squalene Loaded Nanoparticles Effectively Protect Hepatic AML12 Cell Lines against Oxidative and Endoplasmic Reticulum Stress in a TXNDC5-Dependent Way..... 116
4. Chitosan Nanoparticles, a Novel Drug Delivery System to Transfer Squalene for Hepatocyte Stress Protection..... 139
V. DISCUSSION..... 154
1. Endoplasmic Reticulum Protein TXNDC5 Interacts with PRDX6 and HSPA9 to Regulate Glutathione Metabolism and Lipid Peroxidation in the Hepatic AML12 Cell Line..... 155
2. TXNDC5 Plays a Crucial Role in Regulating Endoplasmic Reticulum Activity through Different ER Stress Signaling Pathways in Hepatic Cells..... 160
3. Squalene Loaded Nanoparticles Effectively Protect Hepatic AML12 Cell Lines against Oxidative and Endoplasmic Reticulum Stress in a TXNDC5-Dependent Way..... 167
4. Chitosan Nanoparticles, a Novel Drug Delivery System to Transfer Squalene for Hepatocyte Stress Protection..... 171
VI. CONCLUSIONS (ENGLISH) 179
VI. CONCLUSIONES (ESPAÑOL) 181
VII. REFERENCES..... 183

I. ABSTRACT

ABSTRACT (ENGLISH)

Metabolic dysfunction–associated steatotic liver disease (MASLD), previously known as non-alcoholic fatty liver disease (NAFLD) is induced by fat accumulation within the liver. Endoplasmic reticulum (ER) stress, oxidative stress, and mitochondrial dysfunction are necessary elements in the development of MASLD. Thioredoxin domain-containing 5 (TXNDC5) is a member of the thioredoxin family and plays a pivotal role as an ER chaperone involved in maintaining cellular homeostasis in stress conditions. Nevertheless, the precise molecular mechanisms through which TXNDC5 exerts its effects on hepatocytes under conditions of oxidative and ER stress remain incompletely understood. The objective of this study was to investigate the effects of TXNDC5 on squalene action, a natural antioxidant found in virgin olive oil, delivered through various drug delivery systems to enhance its bioavailability. Squalene was encapsulated in PLGA and chitosan nanoparticles with the aim of enhancing its cellular uptake in AML12 (alpha mouse liver) cells and TXNDC5-deficient AML12 cells (KO) produced by CRISPR/Cas9 technology. Characterization of the nanoparticles by electron microscopy, dynamic light scattering, zeta potential analysis, and high-performance liquid chromatography confirmed efficient encapsulation and inclusion of squalene at different concentrations. The encapsulation of squalene in chitosan nanoparticles demonstrated a significantly enhanced cellular uptake in comparison to the PLGA and ethanol drug carriers. This enables the administration of higher doses, which enhance hepatocyte viability and reduce ROS levels, effectively compensating for the adverse effects of TXNDC5 deficiency in the context of hepatocyte stress protection.

Cell viability assays showed that TXNDC5 has an important role in modulating cell viability under conditions of oxidative and ER stress, as evidenced by the fact that squalene effectively reduced ROS in AML12 cells while increasing ROS in TXNDC5-deficient cells. Squalene was observed to enhance cell viability under conditions of ER stress by decreasing the expression of ER stress markers, including ERN1 and EIF2AK3, and by inducing the expression of protective proteins such as GPx4. To ascertain the function of TXNDC5 in AML12 and KO cell lines, tunicamycin, palmitic acid, and thapsigargin were utilized as stressors. The results from protein expression of the most prominent ER stress markers revealed that among them, the proteins ERN1 and EIF2AK3 were downregulated and HSPA5 was upregulated. Tunicamycin has disrupted the protein levels of HSPA5, ERN1, and EIF2AK3 in KO cells. Palmitic acid modified the protein levels of the ER stress sensors, such as ATF6, HSPA5, and EIF2AK3. TXNDC5 interacted with PRDX6 and HSPA9, proteins involved in the redox regulation of lipid peroxidation and glutathione, and with the loss of TXNDC5, these pathways do have reduced activities, as was recorded by reduced lipid and glutathione peroxidation. Thereby, loss of TXNDC5 impacted mitochondrial functions and specifically disrupted the mRNA levels coding genes that participate in an oxidative stress response and protein folding process.

In conclusion, these findings show that TXNDC5 is a modulator of multiple signaling pathways involved in oxidative and ER-induced stresses in hepatocytes, which squalene, given through PLGA and chitosan nanoparticles, prevents the action of these stresses and supports its protective action by the underlying therapeutic implications for modulation of TXNDC5 with a drug-target delivery system to protect the liver.

RESUMEN (ESPAÑOL)

Enfermedad hepática esteatótica asociada a disfunción metabólica (MASLD), anteriormente conocida como enfermedad del hígado graso no alcohólico (NAFLD) es inducida por la acumulación de grasa en el hígado. El estrés del retículo endoplasmático (RE), el estrés oxidativo y la disfunción mitocondrial son elementos necesarios en el desarrollo de la MASLD. La proteína que contiene dominios tiorredoxina tipo 5 (TXNDC5) es un miembro de la familia de las tiorredoxinas y desempeña un papel fundamental como chaperona del RE involucrada en el mantenimiento de la homeostasis celular en condiciones de estrés. Sin embargo, los mecanismos moleculares precisos a través de los cuales TXNDC5 ejerce sus efectos sobre los hepatocitos en condiciones de estrés oxidativo y del RE siguen siendo incompletos. El objetivo de este estudio fue investigar los efectos de TXNDC5 sobre la acción del escualeno, un antioxidante natural que se encuentra en el aceite de oliva virgen, administrado a través de varios sistemas de administración de fármacos para mejorar su biodisponibilidad. El escualeno se encapsuló en nanopartículas de PLGA y quitosano con el objetivo de mejorar su captación celular en células AML12 (hígado de ratón alfa) y células AML12 deficientes en TXNDC5 (KO) producidas mediante tecnología CRISPR/Cas9. La caracterización de las nanopartículas mediante microscopía electrónica, dispersión dinámica de la luz, análisis del potencial zeta y cromatografía líquida de alta resolución confirmó la encapsulación eficiente y la inclusión de escualeno en diferentes concentraciones. La encapsulación de escualeno en nanopartículas de quitosano demostró una absorción celular significativamente mejorada en comparación con los portadores de fármacos PLGA y etanol. Esto permite la administración de dosis más altas, que mejoran la viabilidad de los hepatocitos y reducen los niveles de ROS, compensando eficazmente los efectos adversos de la deficiencia de TXNDC5 en el contexto de la protección contra el estrés de los hepatocitos.

Los ensayos de viabilidad celular mostraron que TXNDC5 tiene un papel importante en la modulación de la viabilidad celular en condiciones de estrés oxidativo y de ER, como lo demuestra el hecho de que el escualeno redujo eficazmente los ROS en las células AML12 mientras aumentaba los ROS en las células deficientes en TXNDC5. Se observó que el escualeno mejora la viabilidad celular en condiciones de estrés de ER al disminuir la expresión de marcadores de estrés de ER, incluidos ERN1 y EIF2AK3, e induciendo la expresión de proteínas protectoras como GPx4. Para determinar la función de TXNDC5 en las líneas celulares AML12 y KO, se utilizaron tunicamicina, ácido palmítico y tapsigargina como factores de estrés. Los resultados de la expresión de proteínas de los marcadores de estrés del RE más destacados revelaron que, entre ellos, las proteínas ERN1 y EIF2AK3 estaban disminuidas y HSPA5 estaba aumentada. La tunicamicina ha alterado los niveles de proteínas de HSPA5, ERN1 y EIF2AK3 en las células KO. El ácido palmítico modificó los niveles de proteínas de los sensores de estrés del RE, como ATF6, HSPA5 y EIF2AK3. TXNDC5 interaccionaba con PRDX6 y HSPA9, proteínas involucradas en la regulación redox de la peroxidación lipídica y el glutatión, y con la pérdida de TXNDC5, estas vías tienen actividades reducidas, como se registró por la reducción de la peroxidación lipídica y del glutatión. Por lo tanto, la pérdida de TXNDC5 afectó las funciones mitocondriales y alteró específicamente los niveles de ARNm que codifican genes que participan en una respuesta al estrés oxidativo y en el proceso de plegamiento de proteínas.

En conclusión, estos hallazgos muestran que TXNDC5 es un modulador de múltiples vías de señalización involucradas en el estrés oxidativo e inducido por ER en los hepatocitos, y que el escualeno, administrado a través de nanopartículas de PLGA y quitosano, previene la acción de estos estreses y apoya su acción protectora por las implicaciones terapéuticas subyacentes para la modulación de TXNDC5 con un sistema de administración de fármacos a dianas para proteger el hígado.

RÉSUME (FRANÇAIS)

Maladie hépatique stéatosique associée à un dysfonctionnement métabolique (MASLD), anciennement connue sous le nom de stéatose hépatique non alcoolique (NAFLD) est induite par l'accumulation de graisse dans le foie. Le stress du réticulum endoplasmique (RE), le stress oxydatif et le dysfonctionnement mitochondrial sont des éléments nécessaires au développement de la MASLD. La protéine qui contient la thioredoxine de type 5 (TXNDC5) est un membre de la famille des thioredoxines et joue un rôle central en tant que chaperon du RE impliqué dans le maintien de l'homéostasie cellulaire dans des conditions de stress. Néanmoins, les mécanismes moléculaires précis par lesquels le TXNDC5 exerce ses effets sur les hépatocytes dans des conditions de stress oxydatif et du RE restent incomplètement compris. L'objectif de cette étude était d'étudier les effets du TXNDC5 sur l'action du squalène, un antioxydant naturel présent dans l'huile d'olive vierge, délivré par divers systèmes d'administration de médicaments pour améliorer sa biodisponibilité. Le squalène a été encapsulé dans des nanoparticules de PLGA et de chitosane dans le but d'améliorer son absorption cellulaire dans les cellules AML12 (foie de souris alpha) et les cellules AML12 déficientes en TXNDC5 (KO) produites par la technologie CRISPR/Cas9. La caractérisation des nanoparticules par microscopie électronique, diffusion dynamique de la lumière, analyse du potentiel zêta et chromatographie liquide haute performance a confirmé l'encapsulation et l'inclusion efficaces du squalène à différentes concentrations. L'encapsulation du squalène dans des nanoparticules de chitosane a démontré une absorption cellulaire significativement améliorée par rapport aux vecteurs de médicaments PLGA et éthanol. Cela permet l'administration de doses plus élevées, qui améliorent la viabilité des hépatocytes et réduisent les niveaux de ROS, compensant efficacement les effets indésirables du déficit en TXNDC5 dans le contexte de la protection contre le stress des hépatocytes.

Les tests de viabilité cellulaire ont montré que TXNDC5 joue un rôle important dans la modulation de la viabilité cellulaire dans des conditions de stress oxydatif et ER, comme en témoigne le fait que le squalène réduit efficacement les ROS dans les cellules AML12 tout en augmentant les ROS dans les cellules déficientes en TXNDC5. Il a été observé que le squalène améliore la viabilité cellulaire dans des conditions de stress ER en diminuant l'expression des marqueurs de stress ER, notamment ERN1 et EIF2AK3, et en induisant l'expression de protéines protectrices telles que GPx4. Pour déterminer la fonction de TXNDC5 dans les lignées cellulaires AML12 et KO, la tunicamycine, l'acide palmitique et la thapsigargine ont été utilisés comme facteurs de stress. Les résultats de l'expression protéique des marqueurs de stress ER les plus importants ont révélé que parmi eux, les protéines ERN1 et EIF2AK3 étaient régulées à la baisse et HSPA5 était régulée à la hausse. La tunicamycine a perturbé les niveaux de protéines de HSPA5, ERN1 et EIF2AK3 dans les cellules KO. L'acide palmitique a modifié les niveaux de protéines des capteurs de stress du RE, tels que ATF6, HSPA5 et EIF2AK3. TXNDC5 a interagi avec PRDX6 et HSPA9, des protéines impliquées dans la régulation redox de la peroxydation lipidique et du glutathion, et avec la perte de TXNDC5, ces voies ont des activités réduites, comme cela a été enregistré par la réduction de la peroxydation lipidique et du glutathion. Ainsi, la perte de TXNDC5 a eu un impact sur les fonctions mitochondriales et a spécifiquement perturbé les niveaux d'ARNm codant les gènes qui participent à une réponse au stress oxydatif et au processus de repliement des protéines.

En conclusion, ces résultats montrent que TXNDC5 est un modulateur de multiples voies de signalisation impliquées dans les stress oxydatifs et induits par le RE dans les hépatocytes, que le squalène, administré par l'intermédiaire de nanoparticules de PLGA et de chitosane, empêche l'action de ces stress et soutient son action protectrice par les implications thérapeutiques sous-jacentes de la modulation de TXNDC5 avec un système d'administration de médicaments ciblés pour protéger le foie.

II. INTRODUCTION

1. Liver Anatomy and Physiology

1.1. Structure of the Liver

1.1.1. Lobes and Segments

The liver is the largest organ in the body, representing 2% of the total body weight [1]. It is divided into a number of lobes that vary depending on the species. In the case of humans, there are right and left lobes, the latter having two other lobes (quadrate lobe and caudate lobe). In the case of pigs and mice, there are also 4 lobes. The caudate lobe is situated in close proximity to the inferior vena cava on the posterior aspect of the liver, while the quadrate lobe is located in the vicinity of the gallbladder on the anterior inferior surface of the liver (Figure 1). Notwithstanding their distinct anatomical characteristics, both the caudate and quadrate lobes are functionally considered part of the left lobe [2,3]. From the standpoint of function, the liver is subdivided into eight segments in accordance with the vascular supply and biliary drainage characteristics, as delineated by Couinaud's classification scheme. The previously stated segments are crucial since they each have their own biliary drainage and a separate blood supply from the portal vein and hepatic artery. The left hemiliver is made up of segments I through IV, including segment I, which is the caudate lobe. The right lobe is made up of segments V through VIII, each of which occupies a distinct anatomical and functional area. Because it enables the removal of particular segments to treat liver cancers or perform transplants while maintaining the function of the remaining liver, this segmentation is crucial in surgical resection [2,4].

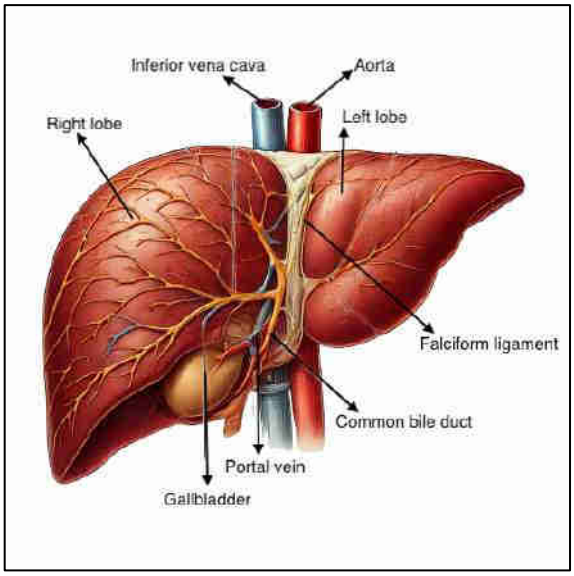

Figure 1. Structure of the liver. Created by BioRender.com, accessed on 20 September 2024. Adapted from ref [2].

1.1.2. Hepatic Lobule

The functional unit of the liver is called the hepatic lobule. This structure is organized around a central vein (or centrilobular) that will carry blood to the hepatic veins and then to the vena cava. In the lumen of the hepatic sinusoids, the blood from the hepatic arterioles and the portal vein is collected, and after being exposed to the exchange of nutrients and metabolites with the hepatocytes, it will be drained by the central vein [3,5]. This constitutes a unique irrigation in the organism, in which two vessels supply blood to an organ (portal vein and hepatic artery, while only one drains it (hepatic vein). As shown in Figure 2, hepatocytes are the main cells of this structure and are arranged, like the spokes of a wheel, in the form of cellular plates with a thickness of 2 cells. Within these plates are the bile canaliculi that collect the bile produced by the hepatocytes and take it to the bile duct, and on the other side of these hepatocytes, around the cellular plates, is the space of Disse, which is a narrow space between the hepatocytes and the endothelial cells in which nutrients, metabolites and even a large percentage of plasma proteins pass through [3,5]. This space is drained by the lymphatic system. In this space appear the Ito cells, also called hepatic stellate cells, whose function is to store vitamin A, and in case of liver injury they transdifferentiate into fibrogenic and proliferative myofibroblasts and produce extracellular matrix [3,5]. Finally, in the hepatic lobules appear the hepatic sinusoids, formed by discontinuous endothelial cells that can be interspersed with Kupffer cells, macrophages responsible for purifying the blood from the colon of the bacilli [2,6]. This complex histological structure enables the efficient processing of blood and the execution of a range of essential functions, including metabolic, detoxification, and synthetic processes (Figure 3) [2,6].

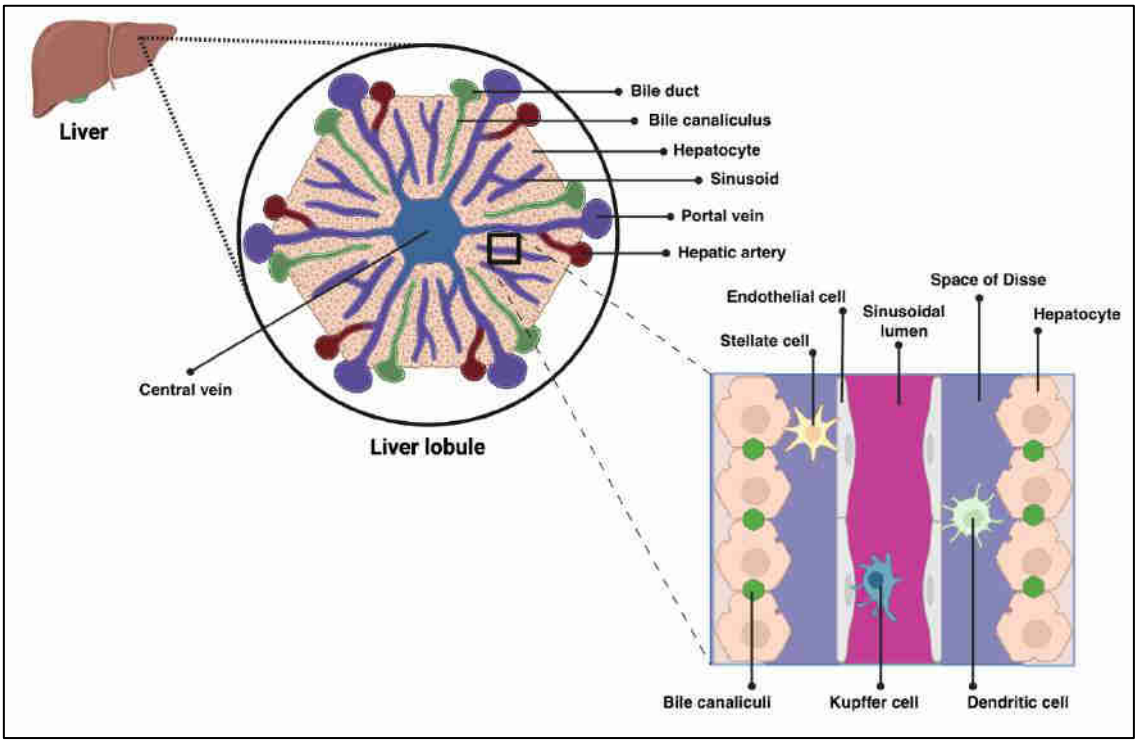

Figure 2. Structure of the liver lobule. Created by BioRender.com, accessed on 23 September 2024. Adapted from ref [7].

1.2. Functions of the Liver

1.2.1. Metabolism of Lipids, Proteins and Carbohydrates

Within lipid metabolism, the liver synthesizes almost all the lipids in the body and normally, it secretes them to the rest of the body for consumption or storage. The cells will use them for the synthesis of membranes, intracellular structures and chemical substances (such as for the synthesis of steroid hormones by the gonads and the adrenal gland) [8,9]. Thus, the liver has some specific functions in lipid metabolism, such as the oxidation and synthesis of fatty acids, the synthesis of phospholipids and of almost all lipoproteins and the synthesis of large quantities of cholesterol, most of which will be excreted with bile, but about 20% will be transported to the rest of the tissues together with the phospholipids in the lipoproteins [8,10].

Regarding protein metabolism, the liver makes a key contribution both in the degradation of proteins through the deamination of amino acids and the formation of urea for the elimination of ammonia from the body and in the formation of plasma proteins (with the exception of gamma globulins) and in the synthesis and interconversion of the different amino acids and synthesis of compounds derived from amino acids [8,10].

Within carbohydrate metabolism, hepatocytes are capable of converting galactose and fructose into glucose, carrying out gluconeogenesis, storing large quantities of glucose in the form of glycogen, and using hydrocarbons to modify proteins or lipids. Due to these functions, the liver is a key organ for maintaining blood glucose, since when there is a postprandial increase in blood glucose, it is capable of storing this excess glucose in the form of glycogen, which can reach between 5-10% of the volume of the liver [11–13]. Thanks to this action, it can later, in a moment of hypoglycemia, release glucose from glycogen and even produce it (if necessary) from triglycerides or proteins and give it to the rest of the body; this phenomenon is known as the glucose buffering function of the liver [11]. This function is regulated by the insulin and glucagon hormones. Insulin stops gluconeogenesis in the liver and inactivates hepatic phosphorylase, preventing glycogen catabolism. On the other hand, it stimulates the activity of glycogen synthase. In addition, it increases the uptake of blood glucose by the hepatocyte, increasing the activity of the glucokinase enzyme that converts glucose to glucose-6-P and prevents it from being able to freely leave the hepatocyte. Insulin not only intervenes in the carbohydrate metabolism of the liver but also in the lipid metabolism, since when this glucose can no longer be stored in the form of glycogen, it stimulates its transformation into fatty acids that will initially be distributed with lipoproteins to the rest of the tissues and that, in case of saturation of the organism, can also be stored in the liver [10,11]. While insulin exerts its effect in a postprandial situation, glucagon acts in the opposite situation, in which blood glucose begins to decrease, as in a prolonged fast, producing an antagonistic effect to that of insulin. Glucagon stimulates glycogenolysis through the elevation of cAMP in the hepatocyte, which leads to an increase in free glucose in the hepatocyte that will be secreted into the bloodstream. Glucagon is also capable of stimulating gluconeogenesis if glycogenolysis has not restored blood glucose [10–13].

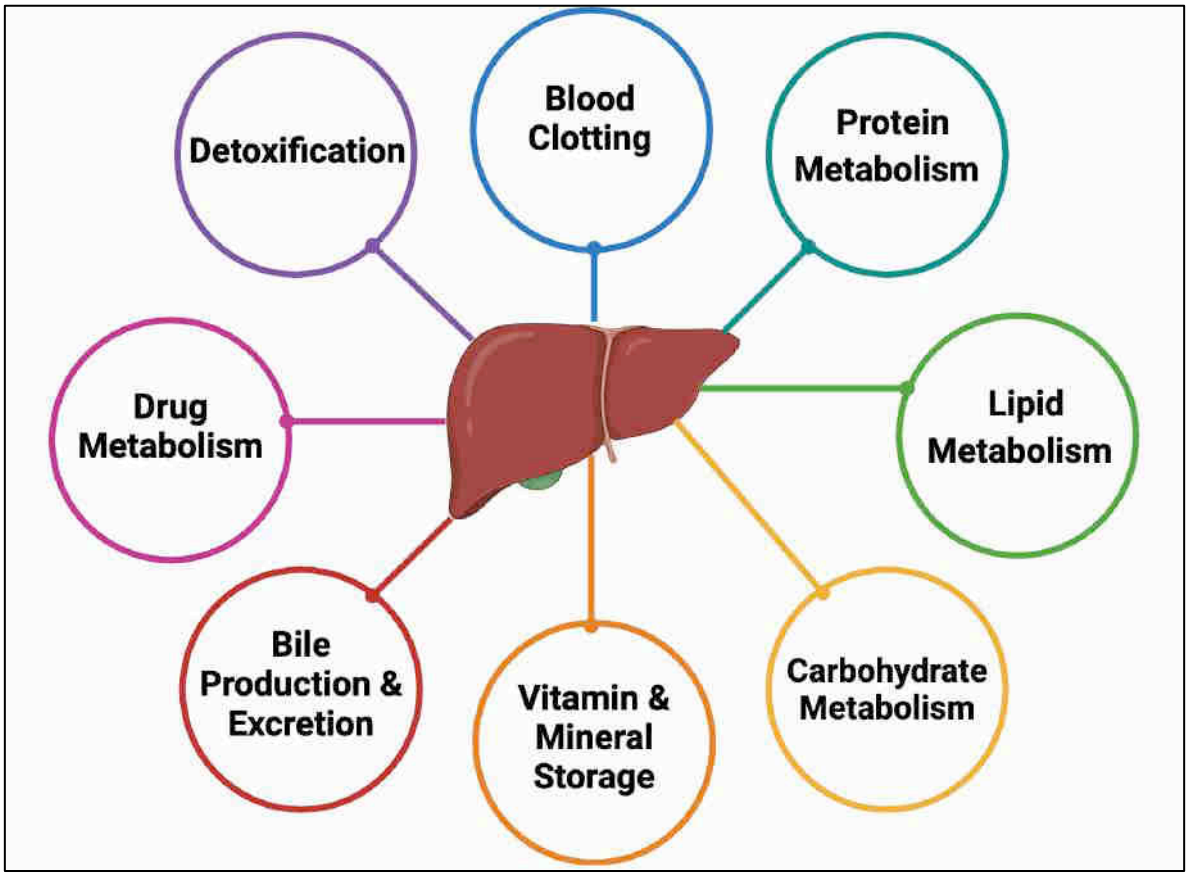

Figure 3. Liver functions. Created by BioRender.com, accessed on 23 September 2024. Adapted from ref [10,11].

1.2.2. Detoxification and Drug Metabolism

Plates of hepatocytes are arranged with sinusoids separating them. This structure is essential for guiding the hepatocytes' excretion of detoxifying products into the bloodstream and bile. In addition, detoxification enzymes are abundant throughout the cytosol and the vast network of the endoplasmic reticulum (ER) [14]. Endotoxins and exotoxins are detoxified by hepatocytes. In phase I, cytochrome P450 enzymes buried in the ER membranes oxidize and reductively break down lipophilic poisons. Phase II enzymes that catalyze conjugation reactions use many of the phase I products as substrates. In general, water-soluble waste products that are eliminated through sweat, urine, or bile are produced using endogenous cofactors [10,14,15].

1.2.3. Bile Production and Excretion

Another major contribution of the liver in the body is the synthesis and excretion of bile, whose function is the digestion and absorption of fats, since on the one hand they act as detergents and emulsify the large fat particles in food into smaller particles that are more easily attacked by lipases, and on the other hand they actively promote the absorption of fats. In addition, bile constitutes a means of excreting waste products from the blood such as bilirubin or excess cholesterol [15,16]. Bile salts are produced from cholesterol, which is first converted

into cholic or chenodeoxycholic acid and then combined with glycine or taurine into glyco- and tauro-conjugated bile acids, these and their sodium salts are excreted through bile. In the absence of bile salts, about 40% of the ingested lipids would be excreted in the feces, with the subsequent energy deficit due to the loss of nutrients [10,15,16].

1.2.4. Other Liver Functions

Finally, other important functions performed by the liver are the synthesis of coagulation molecules (fibrinogen, prothrombin, factor VII, etc.) [17], the storage of vitamins (vitamin A, D and B12) [15,18] and iron (in the form of ferritin) and the elimination and detoxification of toxins, drugs, hormones and other substances [10]. All these implications in the different metabolic pathways give us an idea of the metabolic complexity of the liver, and also allow us to observe that hepatocytes behave as true energy philanthropists, releasing energy to the rest of the body when it needs it and storing it when the rest of the body does not need it [19–21].

2. Liver Disease

2.1. Definition and Classification of Liver Diseases

Based on the underlying cause, the severity, and the time of onset, liver disorders are a broad category of diseases that impact the structure and function of the liver and are categorized as either acute or chronic. Acute liver diseases have a rapid onset and are frequently the result of viral infections, toxins, or drug-induced liver injury [22–24]. In severe cases, they can progress to acute liver failure. Chronic liver diseases develop over an extended period of time, frequently as a consequence of persistent conditions such as viral hepatitis (B and C), alcohol-related liver disease, or non-alcoholic fatty liver disease (NAFLD). Long-term damage from them may include liver cancer or cirrhosis. Furthermore, classification can be based on the underlying cause, which may include environmental toxins (like alcohol and drug-induced liver injury), genetic predispositions (like hemochromatosis), infectious agents (like viruses, including hepatitis viruses A, B, and C, as well as other pathogens), or autoimmune responses (like autoimmune hepatitis). A framework for the diagnosis and management of the different forms of liver disease is provided by this broad classification system [22–24].

2.2. Common Symptoms and Signs of Liver Disease

The signs and symptoms of liver disease often appear gradually and might vary depending on the seriousness of the problem and its underlying cause. Fatigue, appetite loss, nausea, and abdominal pain are some of the first signs of liver illness, especially in the upper right quadrant where the liver is located. More obvious symptoms, such as jaundice (yellowing of the skin and eyes), dark urine, pale feces, and itchy skin, may appear as liver function declines. These signs point to a problem with bile flow or bilirubin processing. In more severe phases, there may be edema or ascites in the legs and abdomen, easy bleeding or bruises, and hepatic encephalopathy, which is characterized by memory or cognition issues. The liver's

decreased capacity to control blood coagulation, fluid balance, and toxin elimination is reflected in these symptoms. Significant liver dysfunction is indicated by these symptoms, which also usually point to the existence of underlying diseases such as cirrhosis, hepatitis, or liver failure [22–25].

2.3. Causes of Liver Disease

Viral hepatitis is a collective term used to describe a group of infectious diseases that cause inflammation of the liver. The five viruses that primarily cause hepatitis are hepatitis A, B, C, D, and E. Of particular concern are chronic hepatitis B and C, as they have the potential to progress to more serious liver conditions, including cirrhosis and liver cancer [26]. Genetic liver diseases are defined as inherited conditions that affect liver function due to mutations in specific genes [27]. The most prevalent genetic liver disorders include hemochromatosis, Wilson's disease, and alpha-1 antitrypsin deficiency [28–30]. A mutation that results in excessive iron absorption and storage in the liver is the underlying cause of hemochromatosis [29]. Autoimmune and cholestatic liver diseases are conditions characterized by disruption of the body's immune system or bile flow, which ultimately results in liver damage [31]. Two illustrative examples are primary biliary cholangitis (PBC) and primary sclerosing cholangitis (PSC). In PBC, the body's immune system targets the small bile ducts within the liver, leading to bile duct proliferation and subsequent liver damage. In PSC, the larger bile ducts within and outside the liver become inflamed and scarred, resulting in obstructed bile flow and an increased risk of cirrhosis and bile duct cancer [32,33]. Alcohol-related liver disease (ALD) is a spectrum of liver conditions caused by excessive alcohol consumption. Prolonged and excessive consumption of alcohol can result in alcoholic hepatitis, a severe inflammatory condition marked by jaundice, pain in the liver area, and elevated levels of liver enzymes in the blood. Over time, prolonged alcohol abuse results in the formation of scar tissue, or fibrosis, which may subsequently progress to cirrhosis [24,25]. NAFLD or as recently named metabolic dysfunction-associated steatotic liver disease (MASLD) [34] is a condition characterized by the accumulation of excess fat in the liver of individuals who consume minimal to no alcohol. It is closely associated with metabolic syndrome, obesity, type 2 diabetes, insulin resistance, and dyslipidemia [35–37].

3. MASLD

This disease is currently the most common liver pathology in Western countries and is expected to be the main cause of liver transplants in the coming years. MASLD covers the first stage, in which there is an accumulation of fat greater than 5% of the liver volume in the absence of inflammation. When the disease evolves in the presence of the inflammatory component, it is called steatohepatitis (NASH or non-alcoholic steatohepatitis) [38]. The third stage of the disease is characterized by the appearance of scar tissue deposits in the liver, known as liver fibrosis [39]. A treatment at this point would not be able to return to the previous stage, since it is irreversible, but it would prevent progress to the next stage or cirrhosis. Liver cirrhosis is characterized by the presence of foci of necrosis and cell proliferation together with the previously observed fibrosis and inflammation. Finally, the pathology could worsen when

these foci of proliferative cells dedifferentiate into cancer cells, known as hepatocellular carcinoma (HCC) [35–37]. The progression of liver damage is shown in Figure 4.

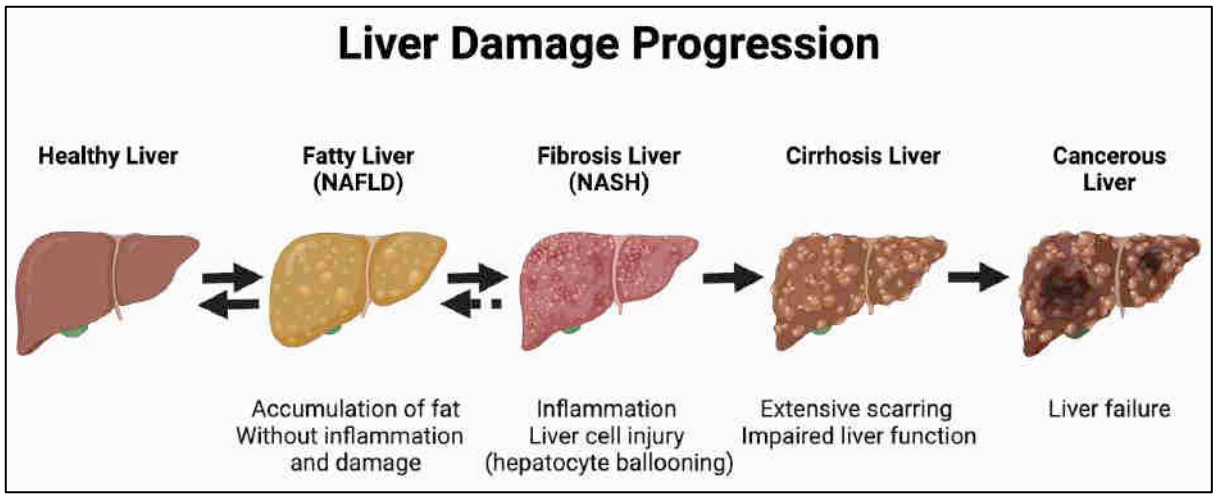

Figure 4. Liver disease stages. Created by BioRender.com, accessed on 24 September 2024. Adapted from ref [35–37].

3.1. Epidemiology of MASLD

MASLD is currently considered to affect 20-34% of the population. However, this percentage varies greatly across the globe [24,25,40]. For example, in a study by Younossi et al., which collected the results obtained from 729 studies from more than 20 countries and included a total of more than 8 million people, they observed that the lowest prevalence was in Africa, where it was 13.5%, while the highest was in South America, 30.5%, and the Middle East, 31.8% [41]. In Europe, the prevalence is 23.7%, with Italy at the top, 49.6% [41]. In Spain, thanks to a study by Caballeria et al., we know that the prevalence is 25.8%. Other factors that greatly influence its prevalence are the existence of other metabolic diseases, such as hyperlipidemia (69.2%), obesity (51.3%), hypertension (39.3%), type two diabetes (22.5%), or metabolic syndrome (42%) [42].

3.2. Diagnosis and Assessment of MASLD

Prevalence rates give a rough idea of the situation across the globe. However, they are often imprecise as the diagnosis of MASLD is complicated and different studies have used different diagnostic methods. These are classified as non-invasive and invasive (liver biopsy) methods [43,44].

Ultrasound is the most widely used method in the clinic with asymptomatic patients, as it is very economical, fast and harmless. However, it shows very low specificity and sensitivity when the percentage of steatosis is below 30% and requires trained personnel to interpret the equipment readings. Computed tomography scans (CT scans) technique is based on exposure to X-rays, and the comparison between the densities of the liver and spleen. In the case of steatosis, the density of the liver is lower than that of the spleen. However, this method involves

exposure to radiation and can be distorted by external factors such as edema or copper accumulation in the liver. CT would not be better than ultrasound in its diagnosis, but it would offer a quantitative method [43,44]. The magnetic resonance imaging (MRI) technique is based on the observation of hydrogens, which show different patterns depending on whether they are part of water or fat. Thanks to this, the fat density of the liver can be measured. This technique can show a very high precision in diagnosis. of steatosis. However, the equipment capable of carrying out this analysis is very expensive and scarce and is unable to differentiate between simple steatosis and steatohepatitis [43,44]. Transient elastography (FibroScan) is a non-invasive method based on ultrasound to measure the degree of fibrosis in the liver. The combination of fibroscan with one of the serum panels may become the best noninvasive method for measuring MASLD [43,44]. So far, non-invasive biomarkers and scoring systems, such as the NAFLD Fibrosis Score (NFS) or the Fibrosis-4 Index (FIB-4) and many proteins have been studied as possible biomarkers of MASLD such as TNFα, IL-6, pentraxin, ferritin, SPEA (Serum Prolidase Enzyme Activity), sRAGE (soluble Receptor for Advanced Glycation End Product) and CK-18 (Cytokeratin-18) [45,46]. Of all of them, the one that has offered the best results is CK- 18 However, it still does not meet the specificity and sensitivity characteristics necessary for clinical use [43,44].

Currently, liver biopsy followed by histopathological examination is the most accurate diagnostic method for MASLD. However, it still has its limitations. In addition to being an invasive method that can cause hepatitis, performing a liver biopsy only detects the presence of hepatitis B. uses a small section of the liver (approximately 1/50,000th of a part), leaving most of it unstudied [43,44]. Three standards are being used for the histological diagnosis of NASH: the Brunt system, the NASH CRN (Clinical Research Network), and the SAF (Steatosis, Activity and Fibrosis) and FLIP (Fatty Liver Inhibition Progression) algorithms, but there is no consensus on which of them would be the most appropriate. Despite this difficulty in its diagnosis, it is undoubtedly highly prevalent in the population today, and this is a problem because until a few decades ago it had not been diagnosed in humans. This justifies the need to learn more about its pathophysiology [43,44].

3.3. Pathology of MASLD

Insulin resistance, which is intimately linked to obesity and metabolic syndrome, is the first step in the pathogenesis of MASLD. Increased lipolysis brought on by insulin resistance causes an overabundance of non-esterified fatty acids (NEFA) to circulate in the circulation. Triglycerides (TGs) are created when the liver absorbs these fatty acids (FAs), which eventually causes hepatic steatosis, or the buildup of fat inside the hepatocytes. Furthermore, the liver's capacity to export these fats as very low-density lipoproteins (VLDL) may be diminished, thereby exacerbating the accumulation of fat [47]. The progressive accumulation of fat in hepatocytes results in heightened oxidative stress, mitochondrial dysfunction, and the generation of reactive oxygen species (ROS). Damage to liver cells and the start of lipid peroxidation are the outcomes of this oxidative stress, which also triggers the liver's inflammatory processes. The liver releases pro-inflammatory cytokines like TNF-α and IL-6 when immune cells like Kupffer cells (liver macrophages) are activated in response to the

injury. These cytokines further promote liver inflammation [47,48]. Overall, the liver plays a fundamental role in the synthesis, storage, degradation, packaging and distribution of carbohydrates, proteins and fatty acids, being orchestrated by a complex network of metabolic signaling pathways, hormones, nuclear receptors and transcription factors. Deregulation in any of these pathways leads to lipid acquisition, incorporation of circulatory fatty acids, or *de novo* lipogenesis (DNL), which exceeds the compensatory capacity of removing them from the liver (oxidation, VLDL secretion and production and excretion of bile acids) will cause hepatic steatosis. This situation can cause oxidative stress, ER stress, compromised mitochondrial function and increased oxidation in peroxisomes and cytochromes leading to cellular damage and disease progression [35–37]. The summary of pathways that regulate the pathology of MASLD is shown in Figure 5.

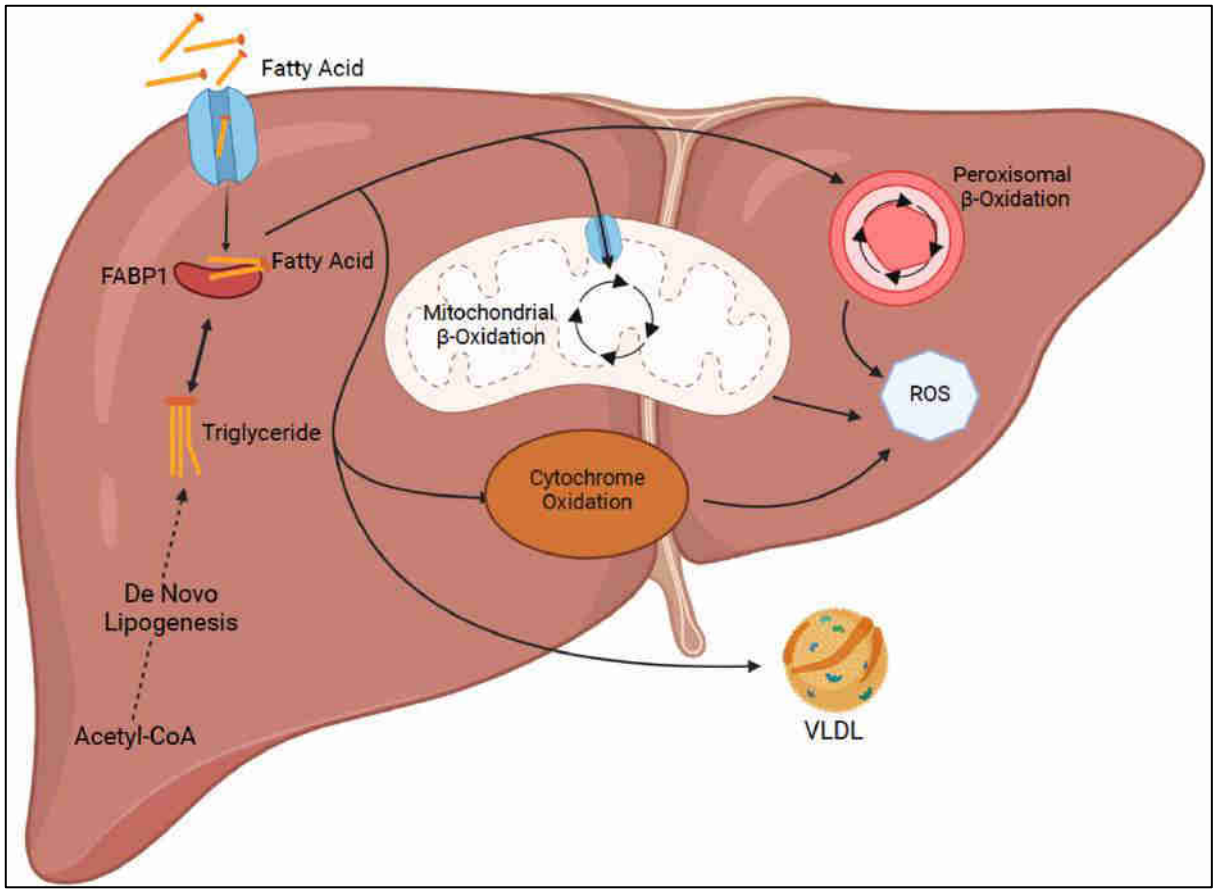

Figure 5. Major pathways regulating lipid acquisition and disposal inside the liver. Adapted from ref [49].

3.4. Lipid Metabolism in MASLD

The liver is the central organ that controls lipid homeostasis through several highly regulated biochemical pathways, which we will discuss in detail below. The liver is responsible for regulating the secretion of triglycerides and cholesterol through lipoprotein metabolism, using both fatty acids from food intake, or in fasting situations, from adipocytes or synthesizing

them. Finally, it also regulates cholesterol metabolism, by controlling both the synthesis and the plasma surplus through the secretion and recycling of lipoproteins [50,51].

3.4.1. Absorption of NEFA from Plasma

Plasma levels of NEFA have been shown to correlate with apoptosis in hepatocytes and may activate it. These FAs come mainly from lipolysis in adipocytes (80%), although they can be derived from triglycerides from food intake (20%). In a fasting state, lipolysis occurs in adipose tissue stimulated by catecholamines, and glucagon. It is blocked by insulin, so lipolysis would be triggered in a state of insulin resistance, increasing FAs in plasma regardless of the nutritional situation [52,53]. Although the mechanisms of NEFA uptake are not completely clear, it seems that the passive diffusion of these towards the liver is residual and their entry depends on fatty acid transporters (FAT or fatty acid transporters). When they reach the membrane, a transmembrane complex is formed consisting of a fatty acid binding protein (FABP), caveolin, a fatty acid translocase (FAT/CD36), and a calcium-independent phospholipase (iPLA2β) that allows the flow of FAs into the hepatocyte by binding through specific membrane receptors. This mechanism can be regulated by peroxisomal proliferator-activated receptor alpha (PPARα) together with leptin and insulin. The proteins that form this complex have been the subject of several studies for their possible role in the development of MASLD, with high concentrations of these fatty acid transporters being found in patients with MASLD [53–55].

Among the FABPs, FABP1 is the main hepatic isoform, responsible for transport for storage in the form of TGs and thus exerting a protective effect against NEFA cytotoxicity. It is also able to mediate the transport of PPAR ligands to the nucleus of hepatocytes (Figure 6). NEFA lipotoxicity to the liver causes the activation of Toll-like receptors and initiates the extrinsic cascade of apoptosis, the predominant form of liver damage in NASH. FAs interfere with nuclear receptor signaling, promoting insulin resistance, and ER stress, as well as stimulating the production of TNFα and its receptor. Activation of the TNFα receptor increases the expression of SREBP1c (sterol regulatory element binding protein 1 c), a transcription factor that induces hepatic lipogenesis and lipid accumulation. TNFα-mediated effects are antagonistic to adiponectin, being decreased in steatohepatitis [56,57]. The conversion of NEFA into TG and its accumulation in lipid droplets appears to be hepatoprotective, although it is typical of hepatic steatosis. This conversion occurs through the action of the mitochondrial glycerol-3-phosphate acyltransferase (mtGPAT) and diacylglycerol acyltransferase 2 (DGAT2) enzymes. These processes are controlled by the transcription factors SREBP-1c, LXR, FXR (Liver/ Farnesoid X receptor) and ChREBP (Carbohydrate responsive element binding protein), which links both lipid and glucose metabolism (Figure 6). In addition to the quantity, the type of NEFA that appears in the steatotic liver is also altered, with a substantial accumulation of saturated fatty acids (SFA), such as palmitic (C16:0) and stearic (C18:0) in relation to monounsaturated and polyunsaturated fatty acids (MUFA and PUFA) [58,59].

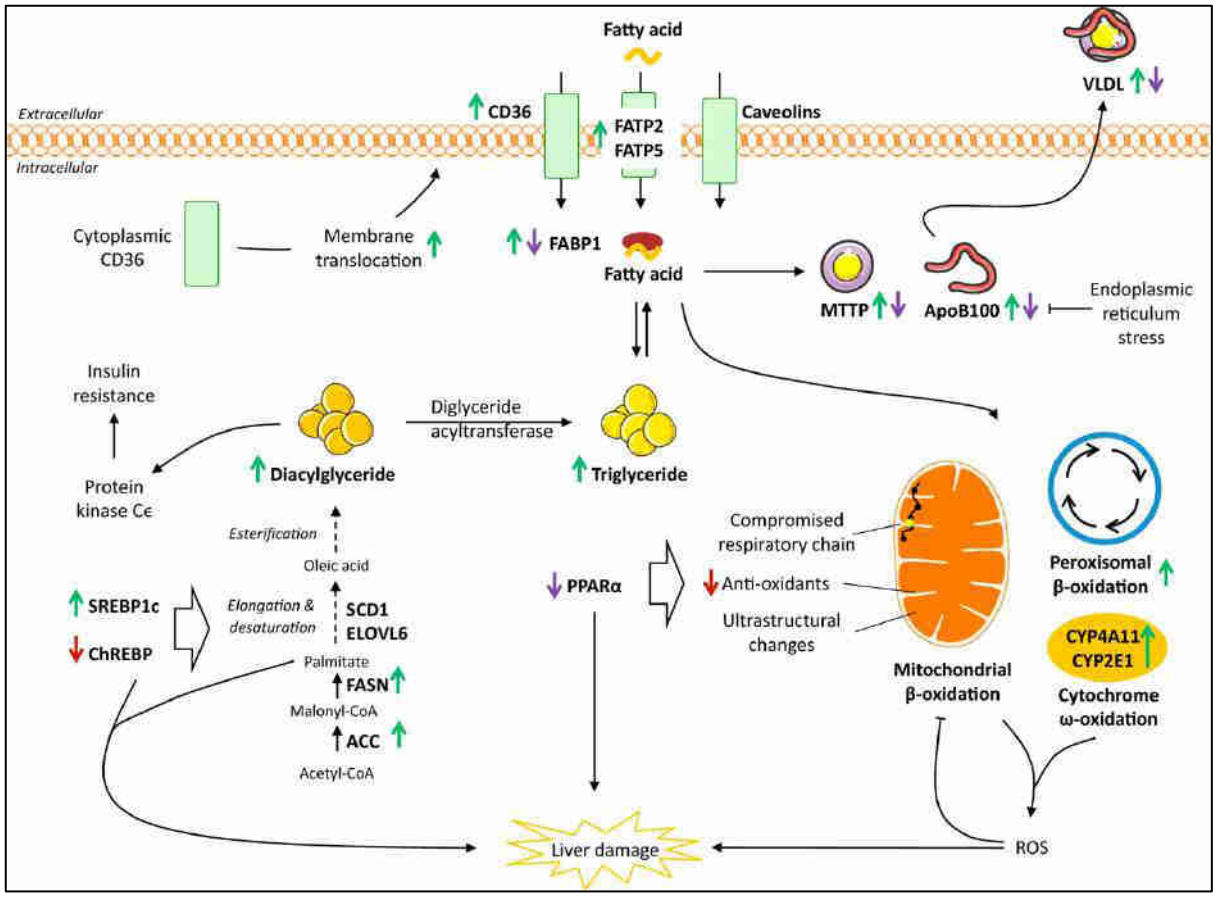

Figure 6. Effects on hepatic lipid metabolism in MASLD. Adapted from ref [51]

3.4.2. Hepatic *De Novo* Lipogenesis (DNL)

DNL consists of the synthesis of FAs from carbohydrates, which occurs in the liver in situations of energy excess. This process is a fundamental and complex pathway that uses products of glycolysis for lipid biosynthesis. Increased DNL has been associated with several metabolic diseases, the most prevalent being MASLD. Although hepatic TG accumulation is the result of uptake of NEFA released by lipolysis in adipocytes (56%), DNL (26%) and diet (15%), in lipogenic pathway, plays an important role. In patients with MASLD, the FA in TG had a higher saturation level, pointing towards the DNL pathway [60]. The two main enzymes are acetyl CoA carboxylase (ACC) and fatty acid synthase (FAS), which together are responsible for converting acetyl CoA and malonyl CoA into FA. The function of ACC is the addition of a carboxyl to acetyl CoA to form malonyl CoA. A hydrocarbon chain is then generated by adding two carbon groups, until reaching 16-18. For the synthesis of TGs, FAs bound to CoA bind to glycerol, generating lysophosphatidic acid, which captures a new fatty acid-producing phosphatidic acid. After dephosphorylation, the resulting diacylglycerol acid is converted into a TG by the enzyme diacylglycerol transferase (DGAT). The transcriptional regulation of DNL has two main pathways: SREBP1c and ChREBP, both induced by the action of insulin and high glucose concentrations (Figure 7) [58–60].

It is in this context that the proteolytic release of SREBP1c from the Golgi membrane, where it is inactive, and its translocation to the nucleus occurs. This release occurs as a result of the interaction with two ER membrane proteins, SCAP (SREBP cleavage-activated protein) and INSIG (insulin-induced gene). When SCAP changes its conformation, due to phosphorylation events or sterol binding, INSIG dissociates from the complex, leaving the MEDADL amino acid sequence of SREBP1c exposed and therefore cleaved by two proteases S1P and S2P. This releases the active form that is translocated to the nucleus [61,62]. This activation can occur through two pathways controlled by the insulin receptor, both starting with the PI3k (phosphoinositide-3 kinase)/PKB (protein kinase B) pathway, one resulting in the phosphorylation of the nascent SREBP1c and the other with the activation of LXRα. On the other hand, there is the mTORC1 (mammalian target of rapamycin complex) pathway, which is activated when PKB is constitutively activated, causing an increase in the mature form of SREBP1c and an increase in DNL (Figure 7). In this way, insulin action via PI3K/PKB promotes SREBP1c processing, activating DNL, with the transcriptional expression of many genes involved in FA synthesis such as FAS, ACC, or DGAT as previously discussed [63]. ChREBP, in contrast to SREBP1c, is activated by the postprandial increase in glucose in hepatocytes. Briefly, the glycolysis rate increases to compensate for cytosolic glucose with the entry of blood glucose through insulin-independent transporters GLUT2. ChREBP activation appears to be modulated by the large number of metabolites generated during glycolysis, although the mechanism is unknown. It is postulated that glucose 6-phosphate (G6P) may have a global role, although in hepatocytes fructose-2,6-bisphosphate is proposed. The outcome is still uncertain, but it promotes the expression of central DNL genes such as FAS, ACC, or pyruvate kinase (PK1) [64,65].

Finally, ACC1, the main hepatic isoform, is regulated at several levels. First, it is found in low-activity dimers that, when polymerized, increase their activity in response to insulin. Second, it has allosteric regulators such as citrate and glutamate, promoting its polymerization and consequent increase in activity, while molecules such as malonyl-CoA act as allosteric repressors inhibiting its activity. Finally, ACC1 is phosphorylated in cells by hormones such as glucagon or adrenaline, inactivating it. This phosphorylation seems to be carried out by the AMP-dependent protein kinase (AMPK) pathway instead of by PKA. In addition, glutamate appears to promote the activity of an ACC phosphatase, thereby regulating the activity of this enzyme in another way [60]. All these mechanisms are summarized in Figure 7.

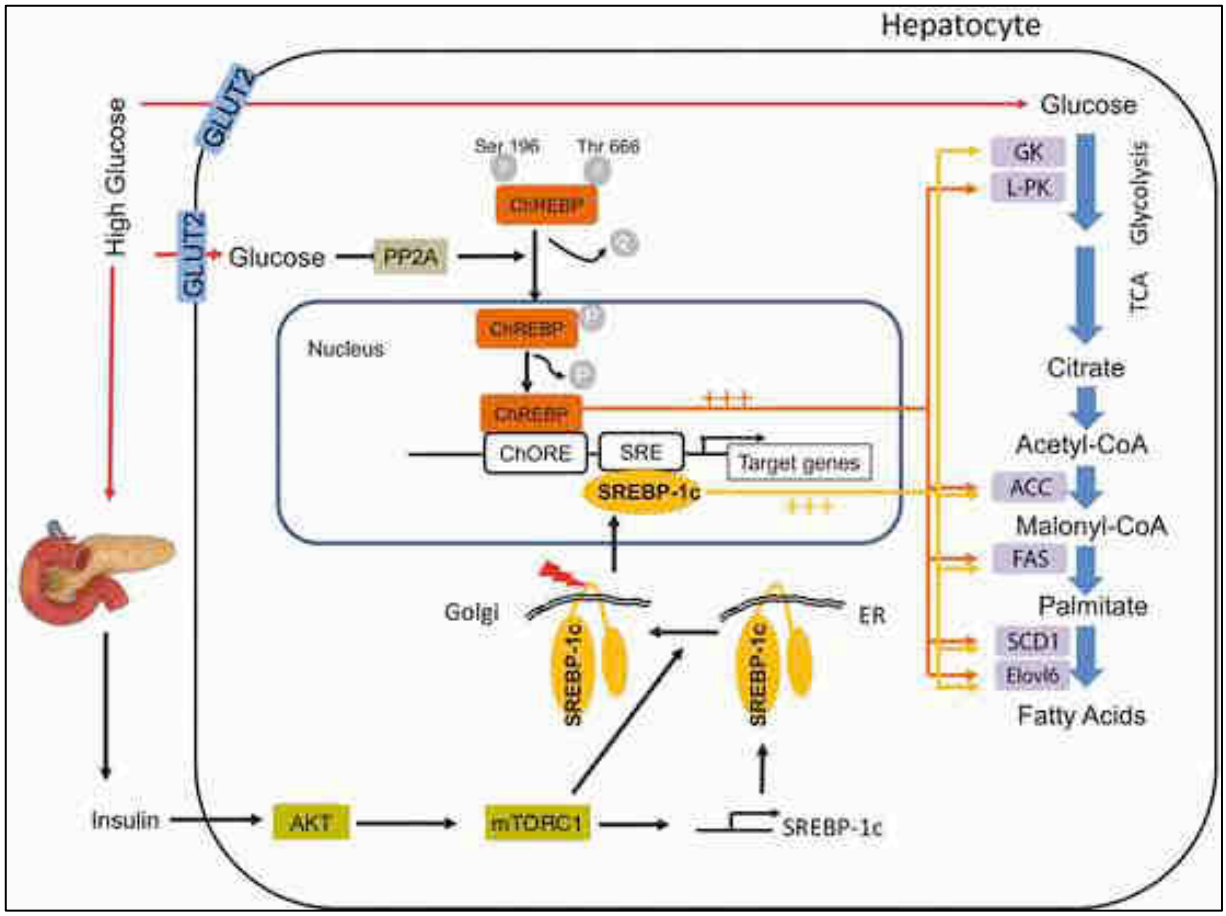

Figure 7. Summary of SREBP1c- and ChREBP-mediated regulation of *de novo* lipogenesis. Adapted from ref [66].

3.4.3. Fatty Acid Oxidation

Fatty acid oxidation (FAO) is the most energy-efficient way for homeostasis compared to other macronutrient subtypes. FAO begins in the cytoplasm, where acyl CoA synthase binds FAs to coenzyme A, forming acyl CoA. From this point, oxidation occurs mainly in the mitochondria, although it can occur in peroxisomes or through the action of cytochromes in the ER [46,50,67,68]. The entry of acyl CoA into the mitochondria usually occurs through the enzyme carnitine palmitoyl transferase 1A (CPT1A) located in the outer mitochondrial membrane, with passive diffusion transport being a minority. CPT1A can only transport acyl CoA of 18 C or less, implying a pass through the peroxisome to reduce its length if the incoming FA is greater than or equal to 18 C. The oxidation of these FAs in the peroxisome occurs from peroxisomal acyl CoA oxidase (ACOX1). Its absence causes accumulation of long-chain acids, fibrosis, oxidative stress and inflammation, emphasizing the role of long-chain FAO in MASLD [50,69].

In the mitochondria, malonyl CoA, a precursor of lipid synthesis, allosterically regulates CPT1A, accumulating after activation of the insulin receptor. In the postprandial state, the oxidation of FAs is reduced, stimulating their synthesis, storage and peripheral distribution. Oxidation in the mitochondria or β-oxidation produces electrons in the form of

NADH and $FADH_2$, which are carried to the electron transport chain to generate ATP and acetyl CoA that will be degraded in the Krebs cycle or in the case of the absence of glucose and a high lipid content, transformed into ketone bodies [50,70]. When there is an excess of lipids, the mitochondrial mechanisms of protection against oxidative damage are overwhelmed, causing damage to mitochondrial DNA and reducing mitochondrial activity. In this way, a vicious circle is established that forces mitochondrial dysfunction and oxidative stress. When mitochondrial function decreases, an alternative FAO route is used, and ω oxidation happens in the ER [69]. Cytochromes CYP4A, CYP4A11, CYP2E1 and CYP2A1 are responsible for microsomal ω-oxidation, which, although it reduces hepatic lipid content, generates lipid peroxidation, significant levels of ROS, oxidative stress and dicarboxylic acids that cause inflammation. On the other hand, the inhibition of CPT1A due to an excess of malonyl CoA can in turn block β-oxidation, activating ω-oxidation without the need for mitochondrial dysfunction [50,71]. FA oxidation is controlled by insulin and PPARα. This factor also stimulates the formation of ketone bodies through the transcriptional regulation of the mitochondrial enzyme HMG-CoA synthase. PPARα expression is related to lipid homeostasis as well as inflammation, stimulating fatty acid transport proteins and apolipoprotein B-related enzymes on the one hand and promoting the ability of JNK1 and NF-KB to bind to DNA, causing hepatic inflammation on the other hand. However, it decreases during steatohepatitis [71,72].

3.4.4. Plasma Secretion of Hepatic Lipids

TG secretion is another option for the liver to reduce lipid content. Due to their hydrophobic nature, FAs can only be secreted after they have been incorporated as TG into water-soluble VLDL particles together with cholesterol, phospholipids and apolipoproteins. VLDL particles are formed in the ER, where APOB100 is loaded with lipids in a process catalyzed by the enzyme MTTP (microsomal triglyceride transfer protein) (Figure 6). Nascent VLDL are subsequently transferred to the Golgi apparatus, and during this process, they will be loaded with more lipids until the mature VLDL particle is formed. Thus, a VLDL contains a single APOB100 molecule and a variable TG content. As implied, APOB100 and MTTP are key components in VLDL secretion and in maintaining hepatic lipid homeostasis. This leads to the conclusion that patients with defects in the MTTP or APOB genes show hepatic steatosis secondary to problems secreting TGs [73]. It has been observed that TG secretion through VLDLs increases with intrahepatic lipid content, however, it reaches a maximum when the fat content of the liver exceeds 10%, compromising the compensatory capacity of this system to prevent increased lipid accumulation in the liver. Despite the greater secretion of VLDL-TG in patients with hepatic steatosis than in healthy individuals, APOB100 secretion remains stable, suggesting that patients with MASLD do not secrete more lipoproteins, but the same ones, but larger and richer in TG [73]. Despite the variation among studies, it is clear that plasma lipid secretion in MASLD can be biphasic, initially increasing until reaching a plateau or even a decrease. This situation contributes to hepatic steatosis, lipotoxicity and liver damage, promoting disease progression and fibrosis [67,73,74].

3.4.5. Bile Acids

Bile acids (BAs), in addition to being a partial lipid excretion route, can act as a ligand for nuclear hormone receptors, with FXR being the main target. In the liver, FXR is a negative regulator of BA synthesis, interfering with the conversion of cholesterol to BAs initiated by CYP7A1 through the stimulation of a protein called SHP (small heterodimer partner), and also facilitating BA absorption in the distal ileum. FXR decreases glycolysis through the inhibition of ChREBP and lipogenesis through the SHP-SREBP-1c axis. Activation of hepatic FXR leads to the reduction of FA and TG, increases β-oxidation through the induction of PPARα, and decreases the expression of apolipoprotein C3, involved in the assembly of VLDL [75–77].

3.4.6. Non-Esterified Cholesterol

In hepatic steatosis, unesterified cholesterol accumulates in hepatocytes and their organelles as a result of increased cholesterol synthesis and cholesterol ester hydrolysis and decreased cholesterol export and BA synthesis. Regarding increased cholesterol synthesis, hydroxy-methyl-glutaryl CoA reductase (HMG-CoA reductase) is the key enzyme for cholesterol synthesis and is regulated by sterol regulatory-element binding protein (SREBP)-2. Furthermore, overfeeding with free cholesterol has been shown to lead to the accumulation of toxic oxysterols that contribute to ROS generation, mitochondrial and ER stress, and liver damage. These deleterious effects are not limited to the hepatocyte since the abundant free cholesterol stimulates Kupffer cells and ITO cells which mediate inflammation and fibrosis [74,78–81].

3.4.7. Macroautophagy

Another process related to lipid homeostasis in the liver is macroautophagy. This lysosomal pathway, during fasting, leads to the fusion of lysosomes and lipid droplets to form autophagosomes, which when degraded release FAs that will be catabolized by β-oxidation. This process is inhibited by the mammalian target of rapamycin (mTOR), which is inactive during fasting. In an insulin-resistant state, mTOR and calpain are overactivated. The latter is a repressor of ATGs (Transcriptional activator of autophagy-related genes). In this regard, it has been observed in mice that defective macroautophagy leads to an increase in lipid droplets in the liver and, on the other hand, other authors found in models for genetic and nutritional obesity, a decrease in the expression of ATGs. Furthermore, it has been seen in patients with obesity that the induction of the mTOR pathway activates SREBP-1c, promotes ER stress and inhibits autophagy [82–84].

3.5. Carbohydrates and Insulin metabolism in MASLD

MASLD and carbohydrate metabolism are closely related. On the one hand, many of the substrates required for DNL come from CHO metabolism (e.g. DNL requires reducing power (NADPH) derived from the pentose phosphate pathway) and on the other hand most of the nuclear factors that regulate lipid metabolism are also important mediators of insulin

signaling, such as the transcription cofactors ChREBP and SREBP1c. It has been known for some time that high-carbohydrate diets induce insulin resistance, oxidative stress, lipogenesis, and MASLD. Excess glucose is normally stored as glycogen under the influence of insulin, but can also provide TG: glycerol via triose phosphate and FAs via acetyl CoA (via the Krebs cycle). It is also known that high glucose concentrations in hepatocyte culture can induce ER stress and apoptosis due to metabolic imbalance, this phenomenon is known as glucotoxicity [85].

3.6. Nuclear Receptors in MASLD

Nuclear receptors are transcription factors capable of sensing changes in the environment or hormonal signals and regulating gene transcription to adapt to these changes, thus orchestrating the vital functions of cells and the organism. In humans, there are 48 nuclear receptors categorized into 7 subfamilies NR0-NR6. In general, nuclear receptors depend on the ligand that regulates the cellular machinery through transcription. Certain specific members of the NR1 subfamily (LXR, PPAR, FXR, CAR and PXR) have been shown to be especially important in the development of MASLD [86–88].

3.7. Cell Death in MASLD

Several mechanisms of cell death in hepatocytes during hepatic steatosis have been observed: apoptosis, ferroptosis, necroptosis and pyroptosis (Figure 8) [81]. The main mechanism described is apoptosis. It can occur via an intrinsic pathway, activated by intracellular stress, such as oxidative stress or organelle dysfunction (ER stress, lysosomal permeabilization and mitochondrial dysfunction) or it can occur via an extrinsic pathway, initiated by the binding of death ligands, such as FAS or TRAIL to their respective receptors [89,90]. Both intrinsic and extrinsic pathways converge on a caspase effector to mediate apoptosis. Ferroptosis is an iron-dependent type of non-apoptotic cell death. It is driven by the accumulation of lipid peroxides, unlike the universal forms of cell death (autophagy, apoptosis, and necrosis). Biochemically, it is usually accompanied by increased lipid peroxidation, elevated ROS levels, and related genetic changes in cytoskeleton and mitochondria in the development and reversal of steatosis in human hepatocytes. The regulation of ferroptosis is closely linked to the metabolism of amino acids, iron, and lipids, and associated pathways. Consequently, mounting evidence emphasizes the close relationship between ferroptosis and liver metabolic diseases, including MASLD [91]. MASLD progression is regulated by numerous ferroptosis-related genes. Among them, GPX4 and Nrf2 stand out as protective mechanisms that inhibit ferroptosis. GPX4 is an essential target in MASLD, and up-regulation of GPX4 expression can effectively alleviate hepatic metabolic injury. Thymosin beta 4 (Tβ4) protects against hepatocyte injury and upregulates GPX4, thereby inhibiting ferroptosis and optimizing lipid metabolism in mice with MASLD induced by a high-fat diet. Squalene is an essential metabolite that prevents ferroptosis in a subset of ALK1 anaplastic large-cell lymphoma cell lines that lack squalene epoxidase, the enzyme acting downstream of squalene; as such, these cells are enriched with squalene, while being auxotrophic for cholesterol [92]. Also, ablation of squalene epoxidase renders HT1080 cells resistant, whereas ablation of

squalene synthase has minimal effect on ferroptosis sensitivity. Furthermore, supplementation with exogenous squalene fails to prevent ferroptosis. In conclusion, the mechanism underlying the antiferroptotic effect of squalene remains unclear but appears to depend on its accumulation [92], also the role of ferroptosis in treating and preventing MASLD needs further study because of the many pathways involved and the ambiguity of the mechanisms of MASLD [91]. Necroptosis shares induction receptors with apoptosis but results in caspase-independent cell and organelle swelling; it can lead to cell death when apoptosis is inhibited. Finally, pyroptosis involves the activation of hepatocyte caspase 1 and Kupffer cells being mediated by the NLRP3 inflammasome (nucleotide oligomerization domain (NOD)-like receptor family, pyrin domain-containing 3) [93,94]. Mice lacking this inflammasome develop less severe liver injury while mice with a constitutively activated NLRP3 inflammasome showed pyroptosis-mediated cell death in their hepatocytes [93,94].

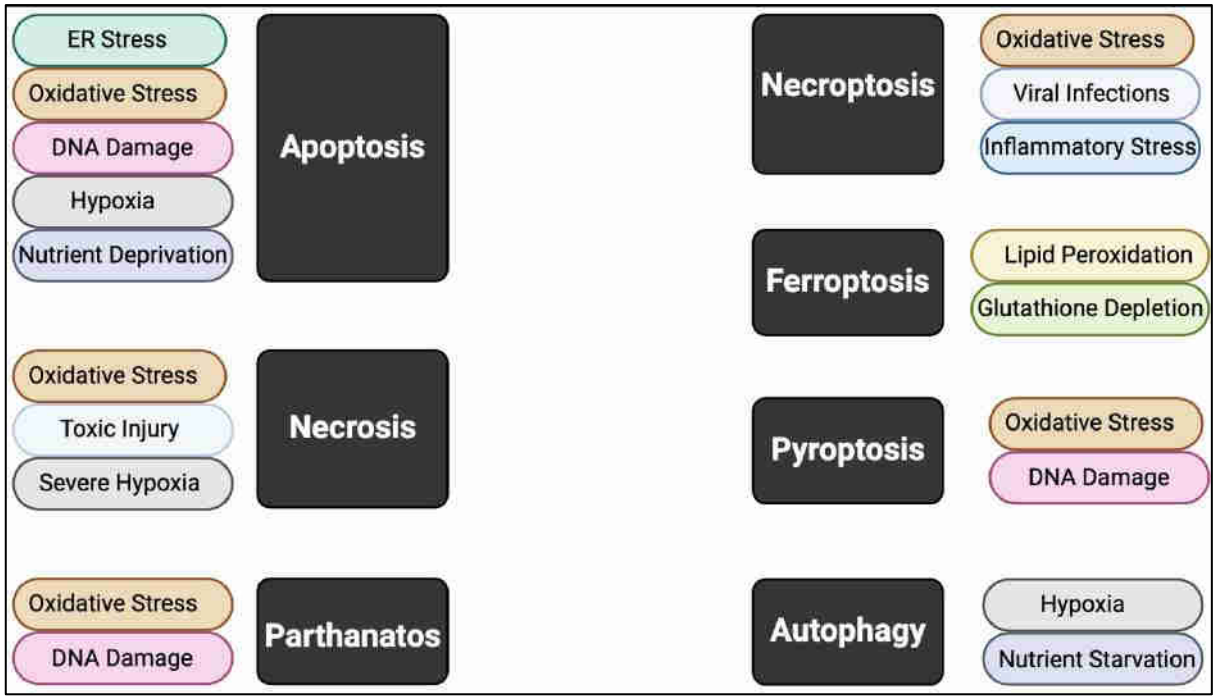

Figure 8. An overview of cell death mechanisms and their associated stressors. Created by BioRender.com, accessed on 26 September 2024. Adapted from ref [81,89,90,93,94].

4. Cellular Stress

4.1. Overview of Cellular Stress

The wide range of adverse conditions that challenge the integrity of cellular processes, upsetting the body's internal homeostasis and triggering either defensive or adaptive responses, is known as cellular stress. Oxidative stress, ER stress, thermal shock, DNA damage, nutritional deprivation, and hypoxia are a few examples of cellular stress (Figure 8) [95,96]. The malfunction of the mitochondria, which are the organelles that produce energy for the cell, is known as mitochondrial stress. Cells can efficiently regulate ROS levels when there is no mitochondrial malfunction. However, ROS generation rises when mitochondrial function is

impaired, resulting in oxidative stress and damage to proteins, lipids, and mitochondrial DNA. The mitochondrial unfolded protein response (UPRmt) is one of the cellular reactions that are triggered by this stress because it disrupts energy homeostasis and reduces ATP generation [95,97]. The heat shock response (HSR) constitutes a cellular defense mechanism that is triggered by exposure to elevated temperatures or other stressors [98,99]. Different stressors disrupt protein folding and are primarily facilitated by a family of proteins known as heat shock proteins (HSPs). JNK plays a key role in the HSR by activating transcription factors that upregulate HSPs, which help stabilize and refold damaged proteins (Figure 9) [98]. On the other side, nutrient stress occurs when cells experience an imbalance or shortage of vital nutrients, such as vitamins, fatty acids, amino acids, and glucose, which interferes with the regular operation of cellular metabolism. In times of nutritional scarcity, signaling pathways like AMPK and the mechanistic target of mTOR are activated to control metabolism and enhance survival (Figure 9) [96,100,101].

The condition known as hypoxia-induced stress occurs when cells are not given enough oxygen, which hinders their capacity to carry out their regular metabolic processes. A transcription factor called HIF controls gene expression to help cells survive in hypoxic environments. In order to save energy, this involves controlling genes that improve oxygen delivery (for example, through angiogenesis) and switching cellular metabolism from oxidative phosphorylation to anaerobic glycolysis [102]. In the event of deoxyribonucleic acid (DNA) damage by different stressors, whether resulting from single- or double-strand breaks, base modifications, or crosslinks, the cell initiates a sophisticated network of repair pathways, collectively known as the DNA damage response (DDR). Proteins such as ATM (ataxia-telangiectasia mutated) and ATR (ATM and Rad3-related) are instrumental in detecting DNA damage and initiating signaling cascades that halt the cell cycle. However, if the damage is too severe, cells may initiate apoptosis to prevent the propagation of mutations. p53 and BAX are crucial for the initiation of apoptosis in response to DNA damage (Figure 9) [103].

Oxidative stress refers to the state in which the generation of ROS is out of balance with the cell's capacity to detoxify them or repair the harm they cause. Superoxide anions, hydrogen peroxide, and hydroxyl radicals are examples of chemically reactive molecules that contain oxygen [104]. The latter are naturally produced during the regular metabolic processes, especially in the mitochondria during the creation of ATP. p53 triggers pro-apoptotic pathways in response to oxidative stress, which ultimately leads to cytochrome c release and mitochondrial permeabilization [105,106]. As a result, caspase-9 is activated, which in turn triggers caspase-3, completing apoptosis and destroying damaged cells while halting the growth of malignant changes [104,105]. ER stress is defined as the phenomenon whereby the ER, a vital organelle with functions including protein folding, lipid synthesis, and calcium storage, becomes overloaded as a result of the accumulation of unfolded or misfolded proteins. A number of factors, including nutrient deprivation, hypoxia, viral infection, oxidative stress and excessive protein synthesis, can impinge upon this process, resulting in a buildup of misfolded proteins. This imbalance results in the activation of the unfolded protein response (UPR), a cellular signaling pathway that is designed to restore ER homeostasis [95,107]. Key

types of cellular stress and their associated apoptosis activation mechanisms are summarized in Figure 9.

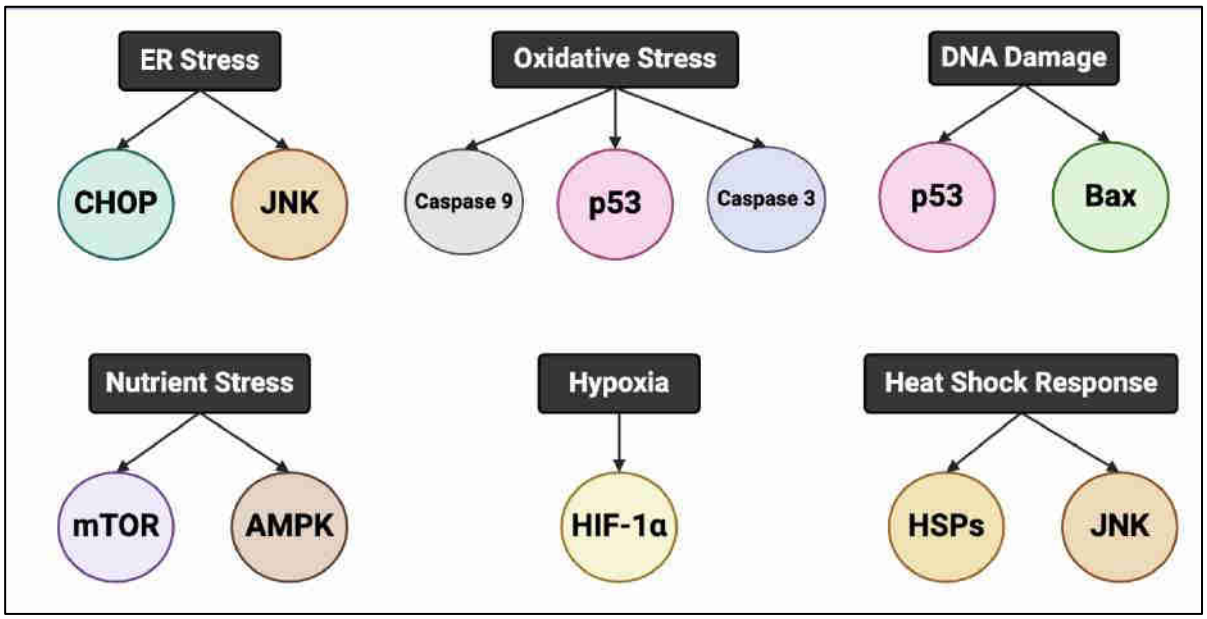

Figure 9. Key types of cellular stress and their associated apoptosis activation mechanisms. Created by BioRender.com, accessed on 26 September 2024. Adapted from ref [95–98,102,103,105].

4.2. Oxidative Stress in MASLD

The hepatocyte contains between 500-4000 mitochondria, occupying 18% of the cell volume. The synthesis of ATP, β-oxidation, ROS, inflammasome activation, and apoptosis, all depend on mitochondria. In general, oxidative stress is caused by an imbalance between ROS production and the scavenging capacity of the antioxidant defense system. Increased generation of pro-oxidant products, antioxidant system malfunction, and hepatocyte lipid buildup set off this cascade, which impacts metabolic organelles and results in lipotoxicity, lipid peroxidation, persistent ER stress, and mitochondrial impairment [105,106,108,109]. Elevated ROS levels lead to oxidative changes in proteins, lipids, and nucleic acids that are implicated in inflammation, insulin signaling, and lipid metabolism. The accumulation of these damaged macromolecules is a major factor leading to the inflammation and fibrogenesis involved in the progression of MASLD [108–110].

4.3. ER and its Stress in MASLD

4.3.1. ER

The ER is a central organelle of the eukaryotic cell, having multiple functions such as cellular transport, protein synthesis, and folding, among others. The ER is composed of a set of membrane sacs called cisterna, constituting more than half of the membranous content of the cell. The inner part or lumen of the membrane is a continuation of the perinuclear space, separating it from the outer part, the cytosol [111]. There are two types of ER: rough

endoplasmic reticulum (RER) and smooth endoplasmic reticulum (SER) whose proportions vary according to the function of the cell, sharing numerous proteins in common, as well as the synthesis of cholesterol and multiple lipids. The main difference is the ribosomes located in the cytosolic membrane of the RER, which makes it specialize in the synthesis and folding of proteins, being especially prominent in cells such as hepatocytes. The SER lacks ribosomes and is involved in the synthesis of lipids, phospholipids, and steroids, being especially abundant in liver and gonadal cells [111].

The surface of the RER is studded with protein synthesis complexes or ribosomes, which give it the rough appearance that gives it its name. The ribosome binding site is called a translocon, however, ribosomes are not a stable component of the ribosome as they are continuously being released and retained. A ribosome only binds to the RER when a nucleic acid-protein complex is formed in the cytosol. This special complex is formed when the ribosome begins to encode a signal peptide that redirects this new protein to the secretory pathway, which is recognized and bound by a signal recognition particle (SRP). Translocation pauses synthesis while the ribosome anchors to the membrane forming the complex by which translation continues with the synthesis of the nascent protein within the lumen or membrane of the reticulum. The protein is processed in the ER by a peptidase that removes the signal peptide, and the ribosomes are released back into the cytosol [112,113]. In many cell types, the smooth endoplasmic reticulum is sparse, with areas where the reticulum is part smooth, and part rough, called transitional ER because it contains exit domains. These are the areas where the transport of vesicles containing lipids and proteins from the ER are directed to the Golgi apparatus. Carbohydrate metabolism, detoxification of metabolic products, such as alcohol and drugs, the binding of cell membrane receptors, steroid metabolism and in muscle cells it regulates calcium concentration are also carried out [114,115]. Secreted proteins are marked by the reticulum with a signal peptide located at the N-terminal end of the polypeptide chain consisting of a few amino acids that are removed once they reach their destination. Proteins destined for other organelles are packaged and transported by a system of vesicles that move through the cytoskeleton to their final destination [114].

4.3.2. Protein synthesis and stress modulation

The ER functions as the cellular transport and distribution system. Most of the resident proteins of the reticulum are retained due to a four-amino acid motif at the end of the protein sequence. The most common retention motif is KDEL for lumen proteins and KKXX for transmembrane proteins. One of the main functions of the reticulum is the correct folding of proteins, including N-glycosylation, disulfide bond formation, and oligomerization. Chaperone proteins are involved in these processes, including protein disulfide isomerases, the HSP70 family, calnexin, and calreticulin (CALR). Only correctly folded proteins can be transported from the ER to the Golgi apparatus (Figure 10) [114,116,117]. When the number of unfolded proteins in the lumen of the reticulum is high, the adaptive stress signal known as the UPR is activated. Pathological situations, such as excess NEFA, alterations in redox regulation, glucose deprivation, viral infection, or protein overexpression, among others, can induce this stress and the subsequent UPR signal during which protein folding is slowed down, increasing

the number of unfolded proteins, which can cause damage due to hypoxia or ischemia, as well as insulin resistance. When the UPR occurs as a cellular response, signaling cascades are activated to increase the production of chaperones involved in cell folding [118,119]. Physiologically, UPR is essential to maintain homeostasis in hepatocytes during protein metabolism and secretion, however, this signal can lead to liver pathogenesis causing inflammatory responses, steatosis, hepatic apoptosis and fibrosis via HSC activation. UPR signaling is carried out through three main pathways carried by transmembrane proteins: ERN1 (Endoplasmic Reticulum to Nucleus Signaling 1), EIF2AK3 (Eukaryotic Translation Initiation Factor 2 Alpha Kinase 3) and ATF6 (Activating Transcription Factor 6) (Figure 10) [120,121].

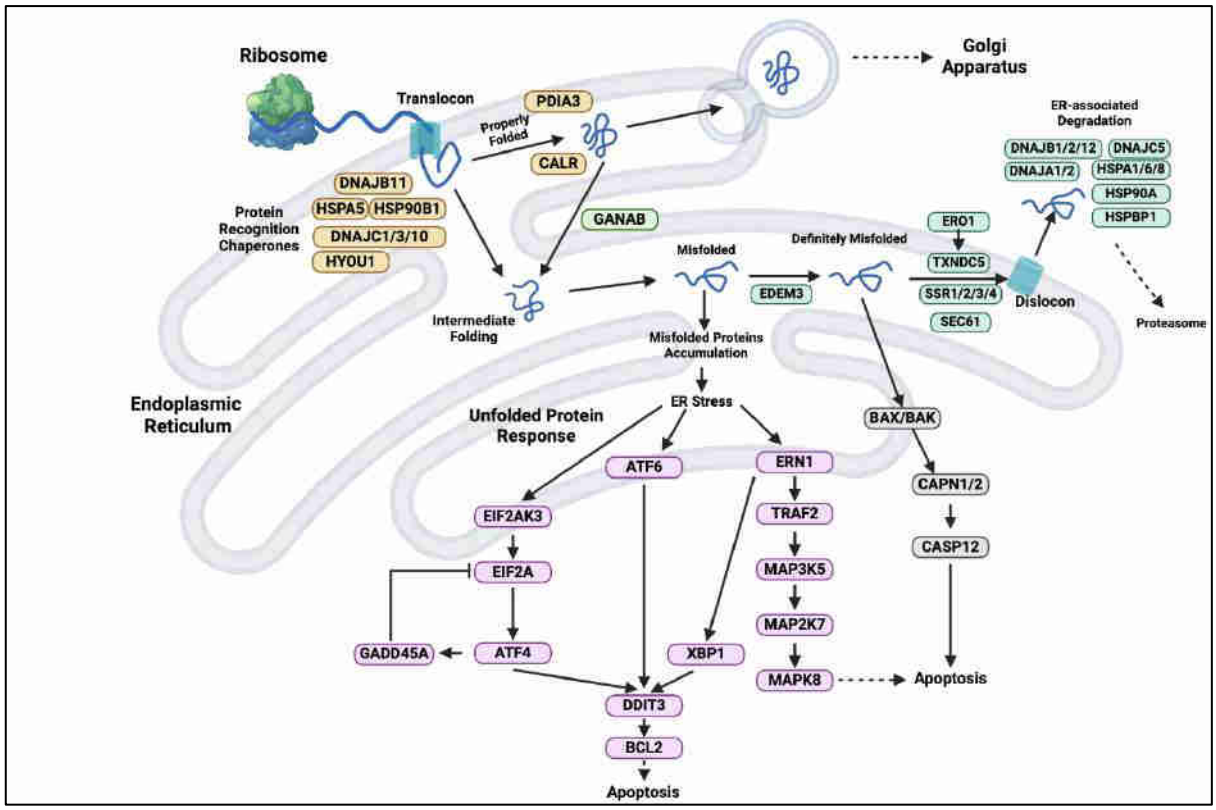

Figure 10. ER protein processing. Adapted from ref [122].

4.3.2.1. ERN1 (IRE1) Pathway

Signaling through ERN1 also known as a IRE1 (Inositol Requiring Enzyme 1) is the most conserved of the three pathways; under normal conditions, this protein is bound to chaperones in the lumen of the ER, preventing its signaling. When the capacity of the chaperones is exceeded, ERN1 oligomerizes and autophosphorylates, activating its signaling cascade that begins with the activation of its endoribonuclease domain. ERN1 acts on the splicing of XBP1 (Factor X-Box Binding Protein 1), releasing a 26-nucleotide fragment of the original mRNA that will encode its "splicing version" called XBP1s. XBP1s activates the transcription of several chaperones and components of the secretory pathway to relieve ER overload, as well as the ER-associated degradation (ERAD) machinery to facilitate the export of misfolded proteins for degradation (Figure 11). Another function of the endoribonuclease is

the limitation of mRNA and some non-essential microRNA translation through a process called RIDD (Regulated IRE1-Dependent Decay). However, the ERN1 domain has a different signaling pathway by recruiting the receptor-associated tumor necrosis factor 2 (TRAF2), which acts as an adaptor to activate the apoptotic signal-regulating kinase 1 (ASK1). ASK1 in turn phosphorylates JNK that promotes apoptosis and inflammation, the inhibition of NF-κB signaling and the production of ROS [123–126].

4.3.2.2. EIF2AK3 (PERK) Pathway

EIF2AK3 also known as a PERK (Protein Kinase RNA-Like ER Linase) is activated through the recruitment of chaperones, its activation causes the phosphorylation of several substrates including EIF2α (Eukaryotic Initiation Factor 2α) causing attenuation of global translation, but allowing the translation of several transcription factors such as ATF4 (Activating Transcription Factor 4). Subsequently, ATF4 initiates the expression of genes involved in stress responses, including DDIT3 (DNA Damage Inducible Transcript 3) also known as a CHOP, which plays a pivotal role in the pro-apoptotic response to prolonged ER stress (Figure 11) [127–129].

4.3.2.3. ATF6 Pathway

In the absence of stress, ATF6 is present in the ER membrane as an inactive transmembrane protein, where it is maintained in a folded state by chaperones. Upon the onset of ER stress, ATF6 undergoes a conformational change that facilitates its transport to the Golgi apparatus and when it is processed to its active form, it translocates to the nucleus to act as a transcription factor for several chaperones such as HSPA5 also known as a GRP78. This transport process entails the cleavage of ATF6 by site-1 and site-2 proteases within the Golgi apparatus, which results in the release of its cytosolic domain and its subsequent translocation to the nucleus. However, if ER stress persists and the protein folding capacity remains overwhelmed, ATF6 can also contribute to the induction of apoptosis. In conclusion, it heterodimerizes with XBP1s increasing the expression of the ERAD and DDIT3 machinery (Figure 11) [130–134].

4.3.3. ER Stress and lipid homeostasis

Hepatocytes are secretory cells responsible for synthesizing most plasma proteins except immunoglobulins, thanks to a very abundant ER through which it regulates the synthesis process, quality control and secretion. In addition, the ER is also the site where the biosynthesis of several lipids occurs, such as cholesterol, phospholipids or ceramides. As mentioned, VLDL begins its biogenesis here and apolipoprotein B100 is loaded with lipids by the MTTP protein while it is translocated through the ER [121,135,136]. Correct ER function is vital for hepatocyte functioning, for example, liver-specific deletion of the HSPA5 chaperone in mice causes ER disorganization and dilation, causing stress, steatosis, apoptosis, liver injury and fibrosis. Loss of function of Sec61α1, a component of the ER translocon, also causes hepatitis, hepatomegaly, and activation of the ER stress response. Pharmacological induction of ER

stress in animal models lacking UPR elements corroborated hepatic steatosis with the common factor of the existence of sustained, excessive, or unresolved stress. All these data indicate that hepatic steatosis is the most conserved response to unresolved ER stress and possibly the different UPR pathways prevent this lipid accumulation under physiological conditions [137–139].

The mouse lacking hepatic XBP1 showed profound hypocholesterolemia and hyperglycemia due to reduced *de novo* synthesis of FAs. In these mice, hyperactivity of ERN1 was found, whose silencing restored plasma lipid levels, suggesting a possible role for ERN1 through RIDD in maintaining lipid homeostasis in the liver. In obese mice, deletion of XBP1 caused the reduction of cholesterol and triglycerides in both plasma and liver, confirming that in the absence of XBP1, the RIDD response is the predominant one and the cause of this lipid reduction. Contrary to these results, overexpression of XBP1 had an anti-steatotic effect, reducing fatty acid synthesis due to a reduction of target genes. However, this is expected because a greater XBP1 response does not prevent the effect of ERN1 through the RIDD response [140–142]. Other studies have shown that ERN1 regulates other aspects of lipid homeostasis such as the suppression of lipogenic transcription factors and the correct maintenance of VLDL secretion by activating PDIs, a vital component for the correct function of MTTP activity. Also, other UPR sensors like ATF6, regulate lipid metabolism through binding to active SREBP-2, inhibiting it, and blocking the transcriptional activity of its target genes [143,144]. The crosstalk between UPR signaling pathways and lipogenesis is summarized in Figure 11.

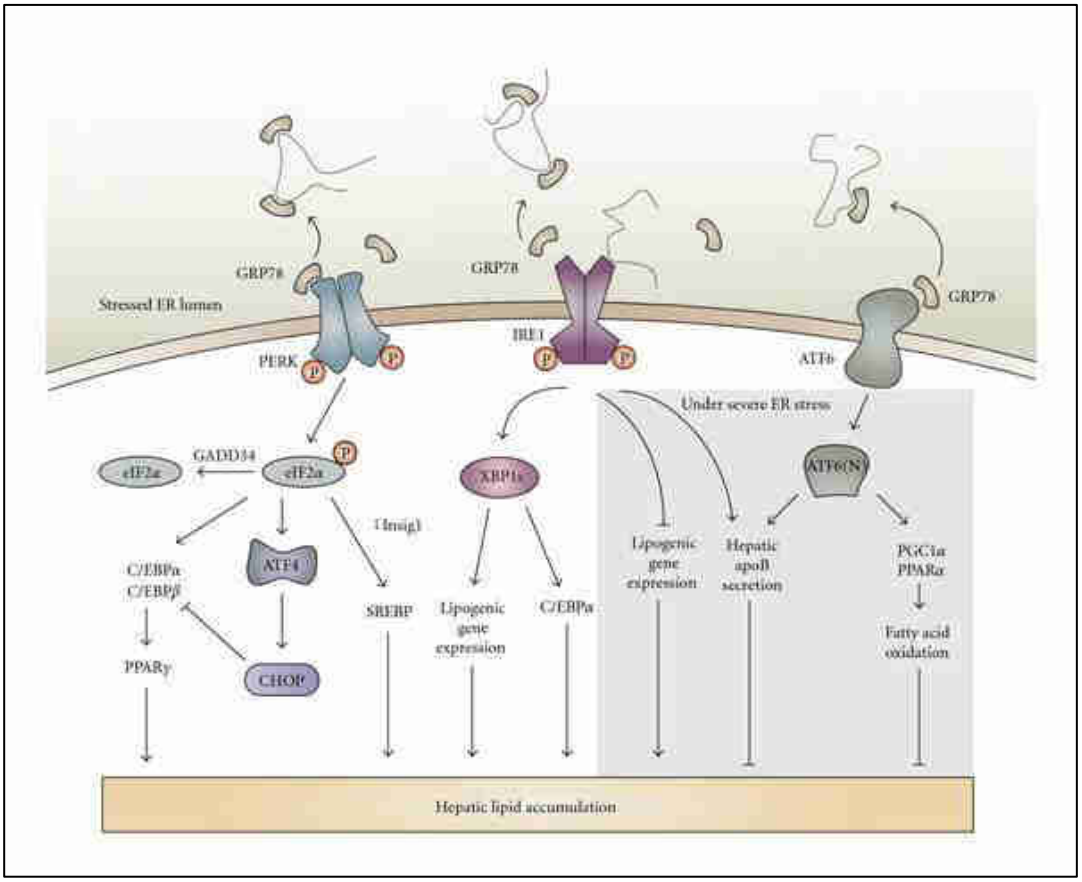

Figure 11. Crosstalk between UPR signaling pathways and lipogenesis. Adapted from ref [145].

4.3.4. ER Stress Inducers

For experimental reasons, chemicals like palmitic acid, thapsigargin, and tunicamycin are typically used to induce ER stress in animals or cultured cells [107,146]. Dietary fatty acids as the first category of ER stressors are important in the MASLD development, because the most abundant saturated fatty acid present in the diet and serum, palmitic acid, is capable of inducing lipotoxicity in hepatocytes. Elevated levels of palmitic acid have been demonstrated to increase ER stress, which contributes to the accumulation of misfolded proteins within the ER and resulting pyroptosis activation in hepatic cells [147,148]. Glycosylation inhibitors are part of the second category of ER stressors. The majority of proteins produced in the ER are N-glycosylated, and protein folding frequently depends on N-glycosylation. Therefore, substances that interfere with N-glycosylation may cause ER stress. *Streptomyces lysosuperificus* produces the antibiotic tunicamycin, which inhibits N-glycosylation by blocking the activity of the enzyme UDP-GlcNAc–dolichol phosphate GlcNAc-phosphate transferase [146,149]. Ca^{2+} metabolism disruptors are another category of ER stressors. Since the ER maintains a high concentration of Ca^{2+} ions and ER chaperones like HSPA5 depend on them, substances that interfere with the ER's Ca^{2+} metabolism cause ER stress. Thapsigargin and other Ca^{2+} ionophores are frequently used to induce ER stress [146,150,151].

5. TXNDC5

5.1. Overview of TXNDC5

TXNDC5, also known as endoplasmic reticulum protein 46 (ERp46), endothelial protein disulfide isomerase (EndoPDI), or protein disulfide isomerase family A member 15 (PDIA15), is a member of the protein disulfide isomerase (PDI) family [152,153]. It is predominantly expressed in endothelial cells, fibroblasts, pancreatic β-cells, liver cells, and hypoxic tissues, including cancerous endothelial cells and atherosclerotic plaques [152–154]. TXNDC5 is primarily localized in the ER and to a lesser extent in the cytoplasm, where it plays a crucial role in facilitating protein folding, preventing UPR-induced apoptosis, oxidative folding of secretory proteins, modulating adiponectin signaling and insulin production, stabilizing extracellular matrix (ECM) proteins, and participating in mannose trimming for glycoprotein substrates [152,154–156]. TXNDC5 regulates cell proliferation, apoptosis, migration and cellular response against oxidative stress. It contains three redox-active thioredoxin-like domains with CGHC active sites, facilitating the forming and rearrangement of native disulfide bonds and, consequently, modulating oxidative activity [152–154]. As a potent disulfide initiator, TXNDC5 is particularly active during the early stages of protein translation, where it introduces disulfide bonds into nascent polypeptides outside the ribosome exit site. This process occurs through a dithiol–disulfide exchange reaction, assisted by TXNDC5 and other oxidoreductases of the PDI family [157,158]. Abnormal expression of TXNDC5 and single nucleotide polymorphisms (SNPs) within the TXNDC5 gene have been

associated with an increased risk of a variety of diseases, including organ fibrosis, atherosclerosis, diabetes, liver disease, rheumatoid arthritis, cancer, neurodegenerative diseases, and vitiligo. TXNDC5 expression is increased under hypoxic conditions, as frequently occurring in rheumatoid arthritis, non-small cell lung cancer, and colorectal cancer. It favors redox-sensitive activation of cardiac fibroblasts, thus participating in the development of cardiac fibrosis. Moreover, TXNDC5 has the potential to serve as a diagnostic and therapeutic marker for those conditions, since it reduces oxidative stress and the levels of inflammatory cytokines, hence underlining its therapeutic value [152,153,156,159].

5.2. *TXNDC5* Gene and Protein Structure

The *TXNDC5* gene is conserved across a wide range of species, including humans, chimpanzees, mice, and rats. However, the majority of research conducted over the past decade has focused on human and mouse cell lines and tissues. The *TXNDC5* gene exhibits high structural conservation among vertebrates. A significant number of SNPs linked to pathology have been identified in non-coding regions of DNA, including introns, 5′-UTR, and 3′-UTR. This underscores the pivotal role of these regions in regulating *TXNDC5* gene expression [160,161]. The *TXNDC5* gene, as determined by the genomic sequence assembly (version GRCh38.p14 of the Homo sapiens, NCBI, National Center for Bioinformation of the United States), is located on chromosome 6p24.3 and spans a length of the gene spans 29,272 base pairs and contains ten exons and nine introns, encoding six transcripts. Two of these, TXNDC5-isoform 1 and TXNDC5-isoform 3, are translated into proteins. The TXNDC5-isoform 1 protein contains 432 amino acids, while TXNDC5-isoform 3 contains 324 amino acids. In accordance with the genomic sequence of the *Mus musculus* (version GRCm39 of strain C57BL/6J, NCBI), the *Txndc5* gene, located on chromosome 13 with a length of 28,559 bp, contains ten exons and the gene contains nine introns and encodes TXNDC5-isoform 1, TXNDC5-isoform 2, and TXNDC5-isoform 3, which can be translated into 417, 323, and 344 amino acid proteins, respectively [152,161]. Human 6p25.1p24.3 microdeletion has been reported and is associated with mild mental retardation, facial dysmorphisms, hypopigmentation of abdominal skin, cardiac defects, mild pontine hypoplasia, and hypotonia. TXNDC5 deletion alongside 13 other genes featured in this microdeletion [162].

A correct balance between a functional proteome through competitive and integrated biological pathways within cells has been described as proteostasis. Such pathways regulate protein biogenesis, folding, trafficking, and degradation of proteins inside and outside the cell. The ER is a subcellular organelle where proteins are folded with the assistance of lumenal chaperones. The newly synthesized peptides move across the pore into the ER, where they undergo glycosylation. The correctly folded proteins are then assembled into transport vesicles, which carry them to the Golgi complex. TXNDC5 is a 48 kDa protein that is predominantly expressed in the ER but also expressed in lysosomes, vacuoles, cytosol, Golgi apparatus, mitochondria, and the plasma membrane [152,153]. Additionally, TXNDC5 has the capacity to be exported to the extracellular medium. As a protein, TXNDC5 undergoes post-translational modifications, and through its function as a disulfide isomerase, catalyzes the rearrangement of disulfide bonds in other proteins. This process facilitates the correct folding

of proteins and prevents cells undergoing apoptosis. Furthermore, TXNDC5 exhibits chaperone activity that is independent of its isomerase activity. This activity contributes to the oxidative folding of newly synthesized membrane proteins in the ER, thereby providing further support for the antioxidative function of TXNDC5. Furthermore, TXNDC5 facilitates the accurate folding of proteins by engaging in electron transfer with other oxidoreductases during the oxidation process [161,163]. It is crucial to acknowledge the function of thioredoxins in bacteria and the potential for their morphological alterations to induce redox changes within the cell, which could ultimately result in disease [164,165]. TXNDC5 contains three Trx-like domains (a0, a, and a′) that all possess redox active sites, including the CGHC, CxxC, and CxxU motifs (Figure 12A). The protein folding process is accelerated by the three Trx-like domains of TXNDC5, which are linked by approximately 20 amino acid residues that can function independently. Studies using X-ray crystallography and small-angle X-ray scattering have revealed that these three Trx-like domains are connected by unusually long loops (Figure 12B). These loops exhibit minimal interdomain interactions and are arranged in an extended manner to form an open V-shape. The TXNDC5 protein displays a domain configuration analogous to that observed in TRX, a finding that, given the lack of analogous structures among other PDIs, suggests a distinctive molecular architecture. Furthermore, the three Trx-like domains appear to function independently within the intact TXNDC5, as no cooperative actions were observed [122,160,161]. The redox-active sites of TXNDC5 are located separately on the molecular surface, facilitating the introduction of disulfide bonds to unfolded substrates with greater rapidity and promiscuity than observed in other PDIs [154,166–168]. The three catalytic domains of TXNDC5 have the capacity to bind peptides that contain aromatic or basic residues. Moreover, it is postulated that the cysteine residues of the Trx-like domains, Cys88, 217, and 350, may possess protein binding functionality. The crystal interaction observed in TXNDC5 indicates that the third catalytic domain may bind to the substrate through small hydrophobic pockets on the surface of the Trx-like domain or by exposing the Trp349 residues. TXNDC5 exhibits a distinctive structural characteristic, namely the presence of a lysine residue (Lys344) in close proximity to the second cysteine within the CxxC motif. Moreover, it was demonstrated that the reactivity of Trx-like proteins is not solely contingent upon their CxxC motif. In the third Trx-like domain of TXNDC5, Arg415 establishes hydrogen bonds with the carbonyl oxygen of Pro397, rather than inserting into the hydrophobic nucleus. This prevents it from regulating the cysteine pKa value, which is in close spatial proximity to the CxxC motif and determines reactivity [122,152].

A)

B)

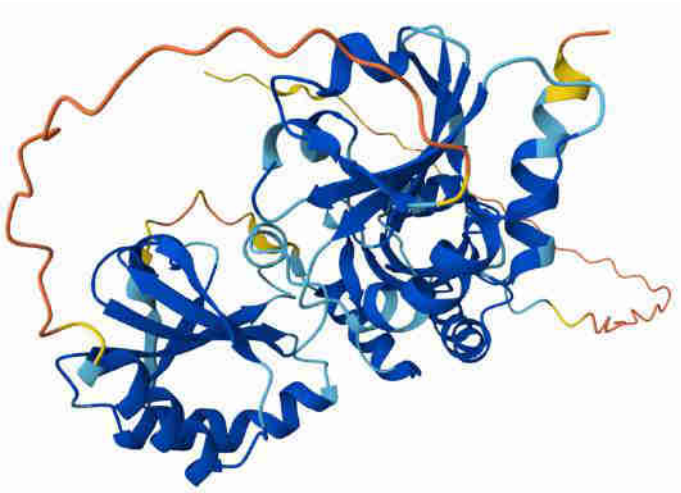

C)

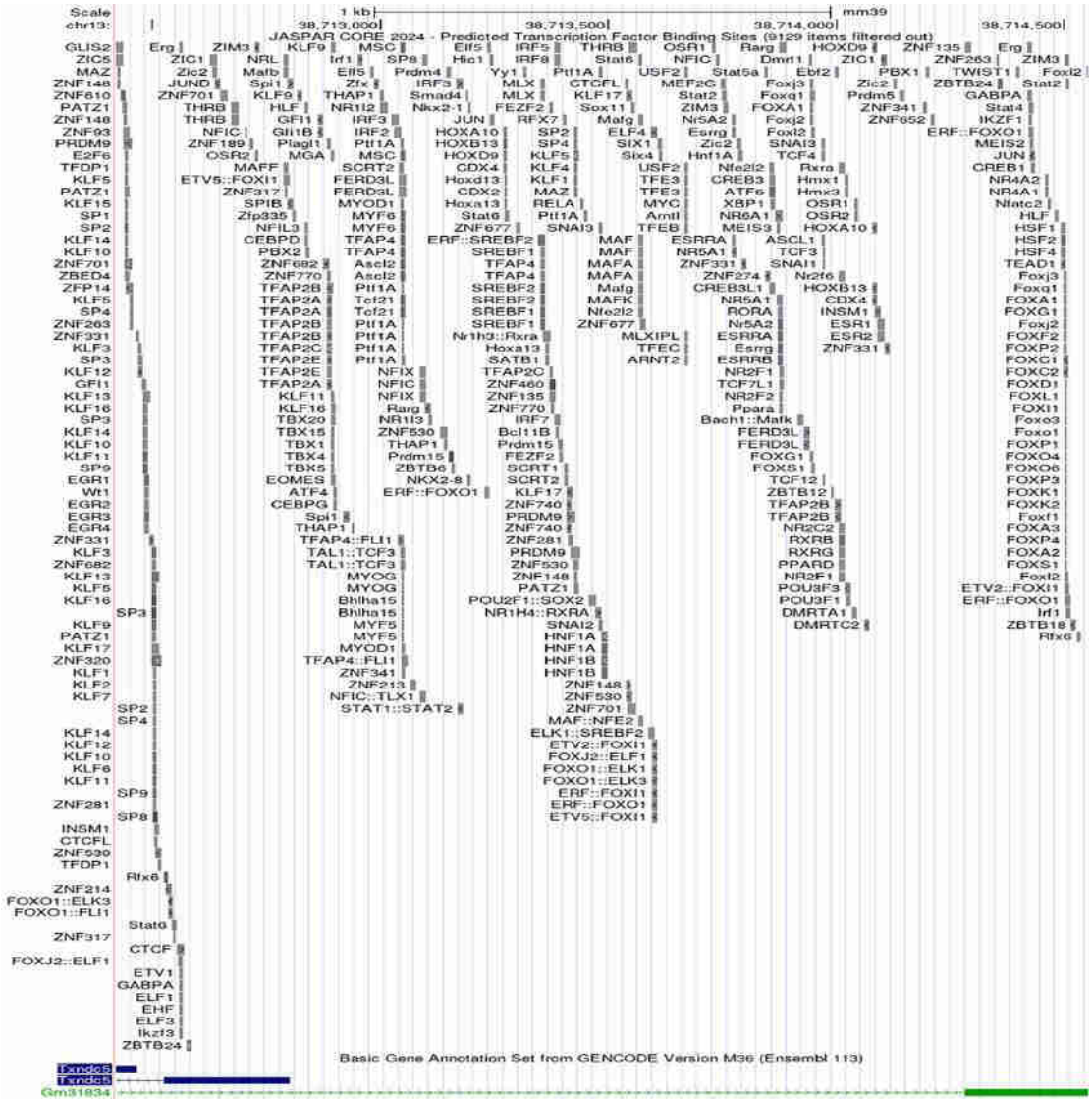

Figure 12. Schemes showing **(A)** TXNDC5 domains that show an N-terminal amino acid 1-35, followed by the three Trx domains located between amino acids 35-155, 156-281 and 289-417, ending with the endoplasmic retention sequence KDEL, adapted from ref [122,161]. **(B)** prediction of the 3D structure of mouse TXNDC5 by alphafold [169,170]. **(C)** Prediction of putative transcription

factors binding the 2-kb of mouse *Txndc5* promoter. Prediction carried out using JASPAR CORE 2024 at UCSC server [171].

A thorough analysis was conducted using the JASPAR CORE 2024 database to investigate the potential binding of transcription factors to the 2-kb region of the mouse *Txndc5* promoter (Figure 12C) [171]. The results of this analysis unveiled the intricate dynamics of transcription factors binding to the *Txndc5* promoter, thereby providing a comprehensive understanding of the complex regulatory mechanisms underlying gene expression. The majority of these factors are involved in general cell processes, modulating a wide range of the steps involved in gene transcription, and have ubiquitous expression. Most of them are involved in misfolding protein processes, ER stress, hypoxia, differentiation, proliferation, apoptosis, and cancer development [161]. The regulation of *Txndc5* gene expression, in particular about its promoter, enhancers or other known regulating sequences and factors revealed that *Txndc5* promoter is regulated by transcription factor(s) downstream of TGFβ1 signaling pathway, which deletion of the ATF6 binding site completely blocked TGFβ1-induced *Txndc5* transcriptional activation and indicating that ATF6 directly and specifically binds to *Txndc5* promoter. Collectively, these results demonstrate that TGFβ1 induces *Txndc5* expression through ER stress and ATF6-dependent transcriptional control [122]. Other studies have reported that NR4A1 binds to the promoter of *Txndc5*; additionally, elevated levels of *Txndc5* mRNA in PRDX4 ablation, which is a specific redox partner, lead to aberrant ER homeostasis. In contrast, NR4A1 antagonists result in decreased interactions of NR4A1, EP300, and POLR2A with the *Txndc5* and *Idh1* promoters and also some loss of SP1 from the *Txndc5* promoter [122]. Furthermore, the findings indicate that ER stress-associated apoptosis is a significant mechanism responsible for the apoptotic effect of cisplatin and cetuximab. Cetuximab enhances cisplatin-induced ER stress-associated apoptosis through DDIT3 and CASP3, mainly by inhibiting the expression of TXNDC5 via gene transcription/promoter level, thereby increasing ROS production [122]. Additionally, the reduction in TXNDC5 under high glucose conditions is restored by liraglutide, such as GLP-1. This suggests that ATF6 and XBP1, through consensus motifs of the *Txndc5* promoter that can be recognized by them, can contribute to UPR involved in the differential expression of TXNDC5 under high glucose conditions [122]. Also, KLF2 binding motif (CACCC) identified in both mouse and human *Txndc5*/TXNDC5 promoter sequences, that shows that TXNDC5 is transcriptionally repressed by KLF2 and TXNDC5 up-regulation is mediated by KLF2 reduction [172].

5.3. TXNDC5 and Fibrosis-Related Pathologies

TXNDC5 promotes fibrosis in multiple organs, including the heart, lung, kidney, and liver, by mediating TGFβ signaling. TGFβ increases TXNDC5 expression through ER stress and ATF6 activation. TXNDC5 aids in the proper folding of pro-fibrotic proteins and activates cardiac fibroblasts via its redox-sensitive PDI activity and JNK signaling. In mice, deletion of TXNDC5 protects against myocardial fibrosis and hypertrophy. Targeting TXNDC5 may offer a more specific and potentially less side-effect-prone approach to treating cardiac fibrosis compared to targeting TGFβ or RAAS [173,174]. TXNDC5 contributes to the progression of pulmonary fibrosis (PF) and renal fibrosis by modulating TGFβ signaling. In PF, TGFβ1

stimulates TXNDC5 upregulation in lung fibroblasts through ER stress and ATF6-mediated transcription. TXNDC5 exerts its effects by preventing TGFBR1 from degradation to reinforce TGFβ signaling in positive feedback for the exacerbation of lung scarring. These findings are reproduced by inducible fibroblast-specific TXNDC5 deletion. Similarly, TXNDC5 regulates the TGFβ/ATF6/TGFBR1 axis in renal fibrosis, with ATF6-dependent ER stress driving TXNDC5 expression. Depleting TXNDC5 reduces fibroblast activation, proliferation, and ECM production in human kidney cells and decreases scarring in these fibrotic mouse models [175,176]. TXNDC5 has been implicated in liver fibrosis (LF) progression, showing significant expression in activated hepatic stellate cells (HSCs) and fibrotic areas in the livers of both human and mouse models with liver fibrosis or cirrhosis. TXNDC5 promotes HSC activation through ROS-dependent JNK signaling and enhances HSC resistance to apoptosis via STAT3 signaling, leading to increased accumulation of activated HSCs and excessive liver fibrosis. Inhibiting TXNDC5's catalytic function blocks JNK and STAT3 activation, reducing fibrotic responses. Additionally, TXNDC5 contributes to TGFβ-induced ER stress, initiating TGFβ signaling and stabilizing ECM and TGFβR1 proteins, thus reinforcing a positive feedback loop in liver fibrosis. TXNDC5's role in organ fibrosis is multifaceted, involving ECM protein folding, TGFβR1 stabilization, fibroblast activation via JNK signaling, and resistance to apoptosis through STAT3 activation (Figure 13) [177].

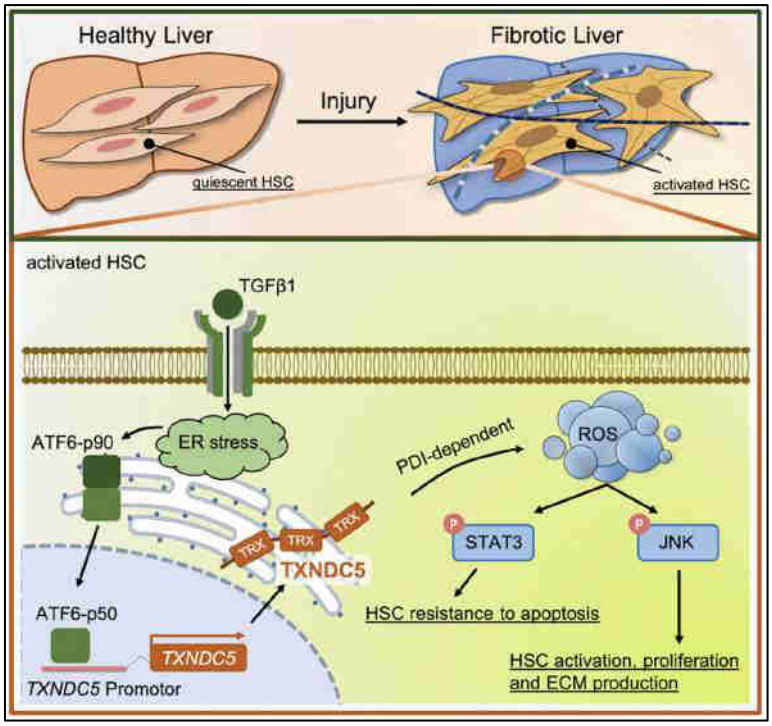

Figure 13. Summary of TXNDC5-mediated liver fibrogenesis schematic illustration of the mechanisms by which TXNDC5 contributes to liver fibrosis. Adapted from ref [177].

5.4. The Role of TXNDC5 in Chronic Diseases

5.4.1. TXNDC5 and Diabetes Mellitus

Diabetes mellitus (DM) is a metabolic disorder characterized by peripheral insulin resistance, hyperglycemia, and defective insulin secretion [178]. The insulin-producing pancreatic β-cells have a highly developed ER and are therefore susceptible to ER stress under hyperglycemic conditions. The gene TXNDC5 has long been considered a contributor to diabetes susceptibility. It plays a significant role in regulating insulin content and may also contribute to glucose toxicity by affecting insulin production [179]. Consequently, loss-of-function variations in TXNDC5 elevate fasting blood glucose levels. Conversely, casein, a dietary protein source for individuals with type 2 diabetes, has been demonstrated to downregulate TXNDC5 [180]. TXNDC5 is in close association with and interacts with proinsulin in pancreatic islets. The reduction in TXNDC5 under high glucose conditions is restored by liraglutide, a GLP-1 analogue. This indicates that ATF6 and XBP1, via consensus motifs within the TXNDC5 promoter that they can recognize, may contribute to UPR-mediated differential TXNDC5 expression under high glucose conditions. TXNDC5 plays a role in the formation of disulfides in proinsulin as a downstream target of the ERN1–XBP1 pathway. Consequently, ERN1 is necessary for the increased expression of TXNDC5 in pancreatic β cells. Furthermore, TXNDC5 can regulate the activity of IGF1. These findings indicate a novel pathogenetic mechanism of TXNDC5 triggered by glucotoxicity and provide new targets for future therapeutic interventions [122,123,178,179].

5.4.2. TXNDC5 and Heart Diseases

Heart failure (HF) represents a significant and expanding public health issue, with a primary etiology attributed to cardiac fibrosis (CF) and atherosclerosis [173]. Atherosclerosis is a progressive inflammatory disease characterized by the accumulation of lipids in the arterial intima and the development of atherosclerotic plaques. These are the major contributors to human morbidity and mortality. Moreover, atherosclerotic lesions often appear at preferred sites of arteries where disturbed flow stimulates the mechano-transduction and activation of endothelial cells, developing peripheral artery disease, carotid artery disease, and ischemic stroke [172,181]. TXNDC5 has been demonstrated to facilitate the folding of ECM proteins, thereby promoting cardiac fibrosis. Furthermore, it activates cardiac fibroblasts and stimulates their proliferation via JNK signaling, which is dependent on NOX4-derived ROS and independent of SMAD3. Cardiac TXNDC5 expression is observed to increase in hypertrophic and failing hearts, with this likely occurring under the control of a TGFβ1/ER stress/ATF6 signaling axis. This results in the excessive accumulation of myofibroblasts and ECM proteins, which in turn leads to cardiac fibrosis. A number of studies have demonstrated that both disturbed flow and hyperlipidemia have a considerable impact on the endothelial expression of TXNDC5. Moreover, TXNDC5 mediated TNF-α-induced activation of NOX in ECs. However, exposure of TXNDC5 to aeroplysinin-1—a modulator of the EC redox balance—reduced its protein level. In contrast, a chicory root diet up-regulated TXNDC5 protein level in the porcine aorta. TXNDC5 enhanced endothelial activation and the development of atherosclerosis induced by disturbed blood flow. It has been noted that TXNDC5 increases the ubiquitination and subsequent proteasome-mediated degradation of transcription factor HSF1; this, in turn, reduces the expression of HSP90AB1, which decreases the stability of NOS3 and KLF2 proteins [122,172,181]. Additional evidence indicates that TXNDC5 plays a role in

platelet function and arterial thrombosis through the enhanced activation of ITGA2B by targeting disulfide bonds, platelet aggregation, and ATP release. The expression of TXNDC5 on the platelet surface is increased by thrombin stimulation, whereas PGHG, which acts as an inhibitor of PDI reductase activity, has been shown to suppress TXNDC5. Moreover, platelets of PDIA6-deficient showed higher expression levels for HSPA5, CALR, and TXNDC5. Thus, selective interference with TXNDC5 might represent a novel treatment strategy to reduce excessive CF and related dysfunction, possibly affecting cardiac function and outcomes in heart failure patients and atherosclerotic cardiovascular diseases [122,172,173,181,182].

5.4.3. TXNDC5 and Liver Cancer

Liver cancer is one of the leading public health problems worldwide with a high-ranking number in terms of mortality rate among all cancers. Generally, this is a high-metastasis and high-recurrence malignant tumor. Hepatocellular carcinoma (HCC) is one of the principal liver cancers that most people develop in response to a chronic liver injury caused by viral infection, alcohol use, LF, NASH, and MASLD. The TXNDC5 (rs1225943) AA genotype was the most prevalent in HCC, and serum TXNDC5 levels were markedly elevated in patients with HCC [177,183]. TXNDC5 has been demonstrated to correlate with hepatic steatosis and redox control in the liver. This is evidenced by the observation of increased liver mass with higher fat content, which is associated with the expression of SAA1, SAA2, and APOA1 (Figure 14) [184]. Moreover, TXNDC5 may interact with the regulation of APOB levels via the oxidative stress pathway, thereby influencing subsequent hepatic lipid metabolism. TXNDC5 interacts with PRDX4, PRDX6, and HSPA9 to regulate glutathione metabolism and lipid peroxidation in liver cells. A deficiency of TXNDC5 was observed to result in a reduction in the levels of PRDX6 and HSPA9 proteins. Moreover, the activities of lipid peroxidation, glutathione, and iPLA2 were markedly diminished in TXNDC5-deficient cells [45]. Another study identified HSPA5, TXNDC5, and GSTM3 as specific and potent binding partners for CRELD2, which play a crucial role in maintaining hepatic metabolic homeostasis. High levels of TXNDC5 promote liver fibrogenesis by inducing HSC activation and proliferation and by producing ECM proteins. Furthermore, TXNDC5 has been found to confer resistance against apoptosis in activated HSCs via the redox-dependent activation of two downstream fibrogenic proteins from the non-canonical TGFβ pathway, namely JNK and STAT3. Furthermore, it was observed that TGFβ1 activation in HSCs resulted in the upregulation of TXNDC5, apparently dependent on the increase in ER stress levels and ATF6-dependent transcriptional regulation. [132,185]. The efficient elimination of TXNDC5 can be achieved through the addition of N-(2-hydroxy-5-methylphenyl)-3-phenylpropanolamine, which serves as an ATF6 activator [132]. TXNDC5 plays a role in reducing the efficacy of photothermal therapy, a minimally invasive and highly specific antineoplastic treatment, by resisting oxidative stress damage and promoting tumor growth and metastasis. Furthermore, glucagon-like peptide-1 has been demonstrated to safeguard liver cells against MASLD by markedly enhancing the expression of TXNDC5 and attenuating the expression of the ER stress marker [186]. Other studies have demonstrated that TXNDC5 is specifically upregulated by SERPINA1 and SREK1 in alpha1-antitrypsin deficiency liver and HCC, respectively (Figure 14). Furthermore, it plays a role in hepatitis C virus replication, potentially through its influence

on lipid metabolism or its involvement in translational control via RNA binding. In light of the aforementioned information, the selective targeting of TXNDC5 may represent a promising new avenue for the treatment of LF and the preservation of hepatic function in patients with HCC [122,177,186].

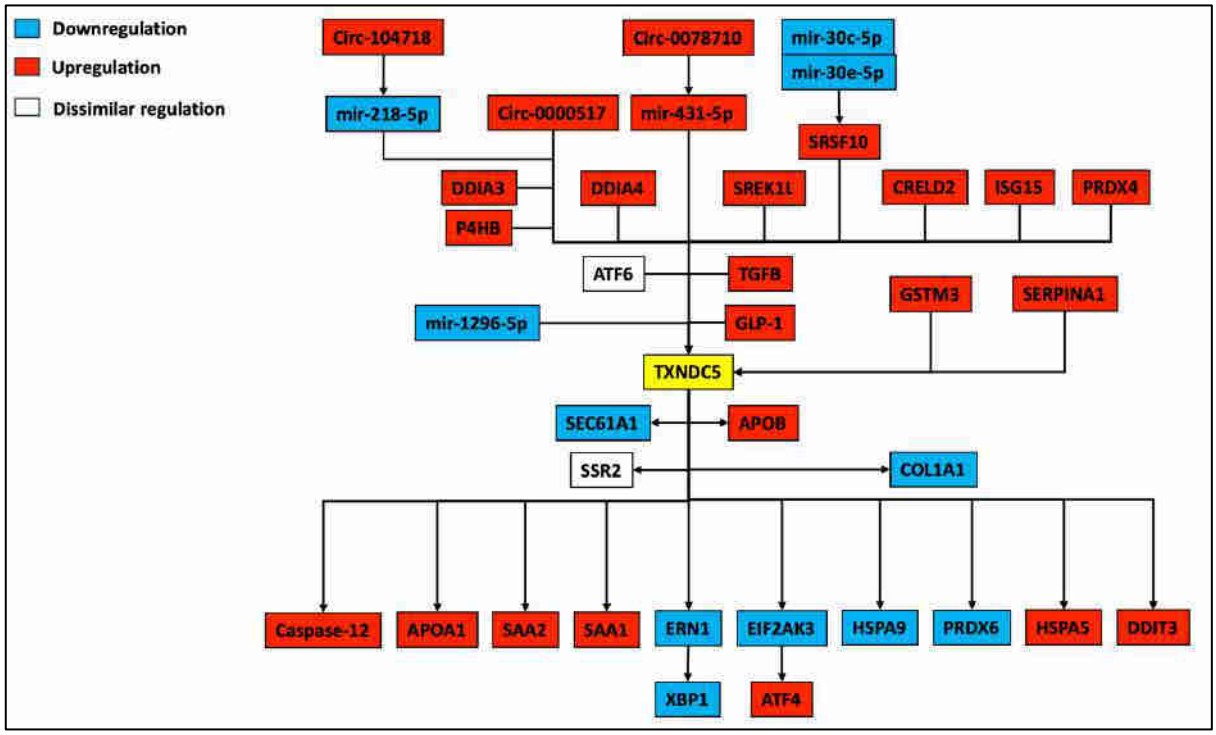

Figure 14. An overview of pathways that implicate markers related to TXNDC5 in liver. Each arrow indicates one marker's association with another. Blue indicates downregulation, while red indicates upregulation. White indicates that regulation of these markers differs between different studies. Adapted from ref [122].

5.5. TXNDC5 and Dietary Patterns

As previously stated, TXNDC5 is a protein that has been linked to oxidative stress, inflammation, and fibrosis. These factors are critical in the pathophysiology of various diseases, particularly MASLD. Research indicates that dietary patterns exert a significant influence on the expression of TXNDC5 in the liver [122]. A diet rich in saturated fat, refined carbohydrates, and sugars has been associated with inducing oxidative stress or inflammation, further inducing TXNDC5 and thus leading to liver injury. More salutary patterns of diet, as seen in the Mediterranean diet, plenty of antioxidants, healthy fats, and anti-inflammatory constituents have been represented and associated with reduced oxidative stress, leading to a lower expression of TXNDC5 along with reduced liver injury [46,184]. For example, squalene, a minor component of olive oil, has been demonstrated to effectively protect liver cells against oxidative and endoplasmic reticulum stress in a TXNDC5-dependent manner through ERN1 and EIF2AK3 downregulation [187]. Furthermore, CALR and APMAP are positively correlated with lipid droplets in the presence of squalene and are decreased in the absence of TXNDC5 [188]. This indicates that dietary changes modulate not only the fat content of the

liver but also the molecular pathways, including such proteins as TXNDC5, underlining the crucial role of diet in managing MASLD and limiting disease progression through its impact on oxidative stress and cellular stress responses [45,122,187,188].

6. Mediterranean Diet

6.1. Overview and Key Components of the Mediterranean Diet

The Mediterranean diet (MD) is a diet that started in ancient times around the Mediterranean Sea [189]. The MD is a plant-based diet rich in olive oil, especially virgin and extra virgin olive oil (EVOO), which is the main source of fat, along with nuts and fiber from vegetables, grains, legumes, and fruits [190,191]. It includes a lot of fish and seafood, and limited red meat, processed meat, dairy, sweets, and wine (Figure 15). The diet has been studied for its health benefits. One study showed that people in Greece and parts of Italy and Yugoslavia had a lower risk of heart disease than people in other countries. Many studies have shown that MD can help prevent and treat many chronic diseases, including type 2 diabetes, hypertension, obesity, MASLD, and cancer [189,192,193]. These effects are due to the anti-inflammatory, antioxidant, and cholesterol-lowering properties of the food. Collectively, these elements show a comprehensive approach to nutrition that promotes wellbeing. This approach highlights the value of a healthy diet in addition to lifestyle elements like social interaction and physical activity [191,193].

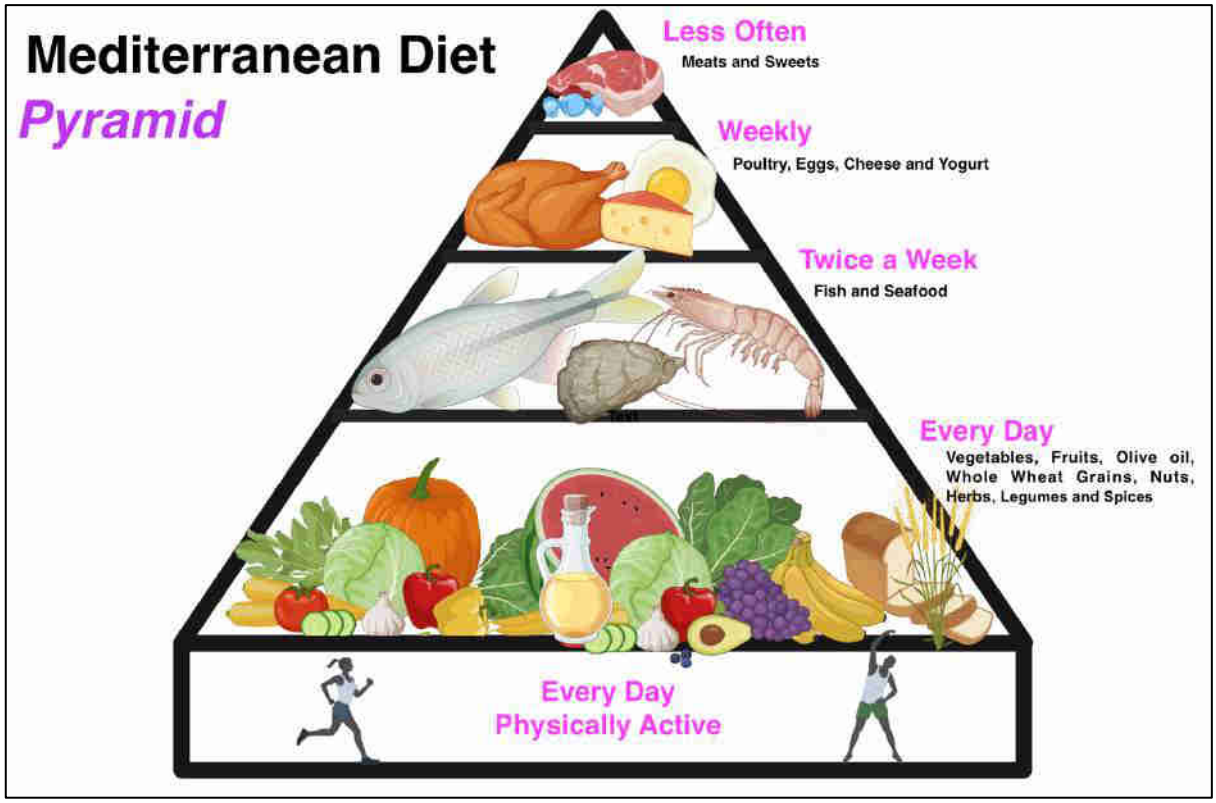

Figure 15. The Mediterranean diet pyramid. Created by BioRender.com, accessed on 30 September 2024. Adapted from ref [191].

6.2. The Role of Healthy Fats in the MD

MD is high in fat, with 36-40% of total energy intake (TEI) coming from lipids. These are mostly MUFA, with a small amount of SFA and a balanced amount of PUFA [194,195]. Carbohydrates and proteins, which make up 35-40% and 15-20% of the TEI respectively, and a high fiber content, together with a low intake of water, nitrogen and carbon. Low consumption of saturated fats lowers low-density lipoprotein (LDL), TGs, and plasma total cholesterol. The balanced omega-6/omega-3 (ω6/ω3) PUFA ratio and high MUFA content are predicated on eating more vegetables, legumes, nuts, olive oil, and fish rather than red meat. The primary source of MUFA is EVOO, while the primary source of ω-3 PUFA is fish [193–198]. By lowering lipid accumulation, including the percentage of lipids in MASLD, and postprandial adiponectin expression, which lowers hepatic glucose production, MUFA intake reduces metabolic risk factors [193,194,199]. PUFA controls important transcription factors in hepatic lipid and carbohydrate metabolism by inhibiting sterol regulatory element binding protein-1 (SREBP-1) and carbohydrate regulatory element binding protein (ChREBP)/Max-like factor X (MLX), which suppresses glycolysis and DNL, and activating hepatic PPARα, which is involved in fatty acids oxidation [193,195]. As a result, PUFA encourages a change in metabolism that moves FAs oxidation away from FAs production and storage. PUFA also suppresses TNFs and IL-6, which triggers an anti-inflammatory response. By controlling the synthesis of inflammatory cytokines, ω-6 PUFA, on the other hand, has pro-inflammatory properties. Vitamins and phenolic compounds found in whole grains, vegetables and fresh fruit, olive oil, nuts and red wine have anti- inflammatory and antioxidant effects. Water-soluble fiber, mainly from vegetables, whole grains and legumes, increases the rate of bile excretion and reduces serum total and LDL cholesterol. All of these effects work together to enhance the MD's overall health-promoting qualities, which makes it an effective strategy for preventing illness and improving long-term wellbeing [193–195,198].

6.3. EVOO

The olive tree (Olea europaea L.) is a small tree that was first cultivated in Asian countries 6000 years ago. Although it eventually extended to every continent, the Mediterranean region continued to be the primary producer of olives, with Spain, Italy, and Greece accounting for over 70% of global production. The mechanical extraction of EVOO involves centrifugation, filtration, decantation, and washing at thermal settings that do not alter the oil's composition [200]. The genotypic traits of the plant, the olive variety, the ripeness of the fruit, the harvest time, agricultural and environmental factors, and the extraction and storage conditions all affect the amount of EVOO. With an acidity of ≤ 0.8 g per 100 g, EVOO is regarded as the highest quality oil when it is pure fruit juice. EVOO's distinct lipid profile and bioactive components are the source of its health benefits. Olive pomace oil, commonly known as Orujo (pomace) olive oil (acidity ≤ 1 g per 100 g), is a combination of virgin olive oil and refined oil made from olive leftovers [200,201]. The oil has anti-inflammatory and lipid-lowering properties and is a good dietary source of triterpenic chemicals [202,203]. Triacylglycerols (TAGs) make up a high percentage of the saponifiable fraction of EVOO. Fatty acids make up 97-99% of lipids and 65.2-80.8% are MUFA, particularly oleic acid, which

makes up 49-83% of total FAs and is correlated with EVOO acidity when not esterified. Low acidity ensures a high-quality oil produced from healthy fruit under ideal conditions. PUFAs make up about 14% of the oil composition [200]. The PUFA content is mainly linoleic acid (18:2 ω-6) (6.6-14.8% total FAs) and α-linolenic acid (18:3 ω-3) (0.46-0.69% total FAs). DAGs (diacylglycerols) and MAGs (monoacylglycerols) are present in concentrations of 1-2.8% and 0.25% respectively.

The minor components of EVOO account for 1-3% of its composition. These include hydrocarbons, phytosterols, triterpenes, phenolic compounds and tocopherols, among others. With regard to hydrocarbons, squalene accounts for more than 90% of hydrocarbons and is the most abundant compound in the unsaponifiable matter, ranging from 200 to 7500 mg/kg of oil, while β-carotene pigment accounts for 0.15-0.67 mg/kg of oil. The total phytosterol content of EVOO varies between 1000 and 2000 mg/kg. Triterpenes represent a primary fraction and are divided into diol-alcohols and triterpenic acids. The most important terpenic alcohols are erythrodiol and uvaol. Triterpenic acids include oleanolic (17- 344 mg/kg) and maslinic (19-250 mg/kg), with traces of ursolic acid, compared to higher levels in olive pomace oil [201]. Phenols are hydrophilic compounds present in the range of 50-1000 mg/kg of oil and include hydroxytyrosol, oleuropein and tyrosol [195,200]. α-Tocopherols (vitamin E) are methylated phenols. α-tocopherol accounts for more than 90% of tocopherols, ranging from 191.5 to 292.7 mg/kg compared to 10 mg/kg, 20 mg/kg of β-tocopherol and γ-tocopherol [195,200]. Overall, EVOO is a versatile and vital part of the MD, with a flavor profile that ranges from mild to powerful. Because of its beneficial qualities, it is a good option for daily use (Figure 16) [204].

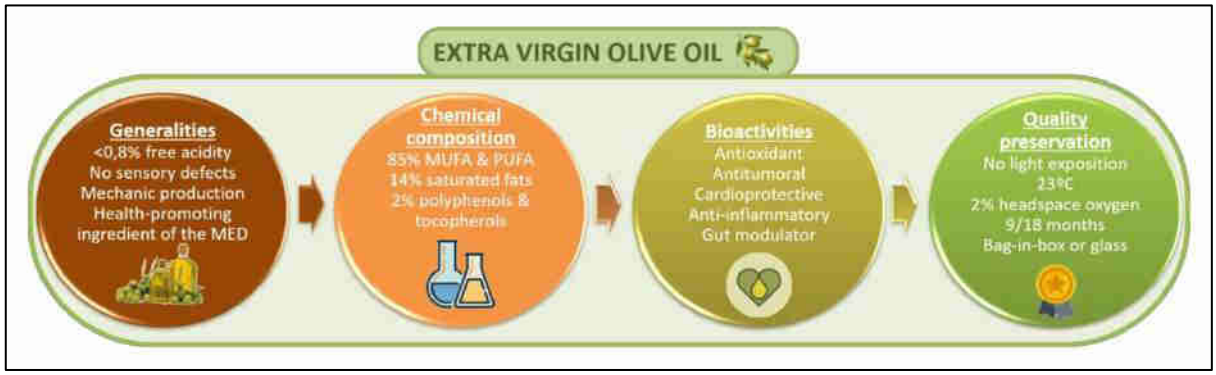

Figure 16. Bioactive Compounds and Quality of EVOO. Adapted from ref [200].

6.4. Bioactive Compounds in EVOO

EVOO reduces risk factors, including type 2 diabetes and MASLD, by suppressing lipogenic, ROS and pro-inflammatory genes and by reducing levels of IL-6, TNF-α and C-reactive protein (CRP). A dose of 20 g/d may reduce the degree of fatty liver. EVOO also has atheroprotective properties. Additionally, EVOO possesses atheroprotective qualities. Diastolic blood pressure can be lowered by up to 0.73 mm Hg with a daily dose of 10–50 ml. Besides the anti-tumor, anti-cancer, and antibacterial qualities [195,200,205]. Any pattern of carcinogenesis is inversely correlated with oil consumption (34% lower risk with EVOO

consumption). Squalene, another significant component, has been demonstrated to support skin health [206], act as an antioxidant, and may offer protective effects against cancer [203,207,208]. Oleic acid stimulates hepatocytes to secrete bile and pancreatic cells to secrete MUFAs. In addition, it possesses anticoagulant, anti-inflammatory, and antioxidant properties and enhances blood pressure, cholesterol, and glucose metabolism. Although linoleic acid lowers LDL, it is converted to arachidonic acid, which has prothrombotic, pro-inflammatory, and pro-aggregatory effects. The ω6/ω3 PUFA ratio tilts the scales in favor of hepatic DNL by protecting against inflammatory and autoimmune disorders as well as β-oxidation [195,200]. Furthermore, maslinic acid and oleanolic acid exhibit anti-inflammatory, anti-diabetic, hypolipidemic, hepatoprotective, anticancer, antiviral, antibacterial, and antifungal qualities. β-Sitosterols are useful for lowering LDL and total cholesterol levels as well as for promoting cancer cell death [195,200,209]. Tocopherols are significant lipophilic antioxidants found in nature. In addition to their antibacterial and anticancer properties, these chemicals alter the expression of homeostatic genes that prevent lipid peroxidation and offer protection against oxidative and inflammatory processes, such as cancer and degenerative disorders. Phenolic compounds have high antioxidant and free radical scavenging properties, and they also lower cholesterol, LDL, HDL, lipopolysaccharides, and pro-inflammatory markers including CRP and IL-6. The oxidative stability of olive oil is due to phenols and tocopherols. Carotenoid pigments contain anti-cancer and antioxidant qualities and are precursors to vitamin A [195,200,209]. These bioactive compounds act in concert to provide the distinctive health benefits associated with EVOO, thereby making it a vital component of the MD (Figure 16) [204].

6.5. Squalene

Mitsumaru Tsujimoto, a Japanese chemist, discovered squalene in 1916. He called it after the genus of sharks from which it was isolated (*Squallus spp., Centrophorus squamous*) and classified the molecule as extremely unsaturated. The polyunsaturated linear terpenoid squalene (2,6,10,15,19,23-hexamethyl-6,6,10,14,18,20-tetracosahexane, C30H50) (Figure 17) has six double bonds and a molecular mass of 410.3913 [210,211]. In addition to the sterol form, which enables it to be incorporated into membranes, the double bonds enable squalene to exist in symmetrical, stretched, and coiled forms [212]. Shark liver oil contains a significant amount of squalene (nearly 40–70% of the oil weight), but the intense fishing for this isoprenoid and the presence of organic pollutants such as organochlorine pesticides, polycyclic hydrocarbons, dioxins, and heavy metals have made it imperative to look for alternative sources of squalene, especially from the plant kingdom [210,211,213]. The following plant sources contain detectable levels of squalene: palm oil, soybean oil (9.9 mg/100 g), grape seed oil (14.1 mg/100 g), peanut (27.4 mg/100 g), maize, amaranth (5942 mg/100 g), olive oil (564 mg/100 g), and rice bran and wheat germ oils (100–700 mg/100 of oil content) [213]. In EVOO, squalene is present in a variable concentration from 1.5 to 10.1 g per kg, depending on the variety, and agronomic issues such as region, climate, crop, harvesting method and olive processing. Where consumption of EVOO is high, such as in Mediterranean countries, intake of squalene is increased to 200-400 mg/day [211,213].

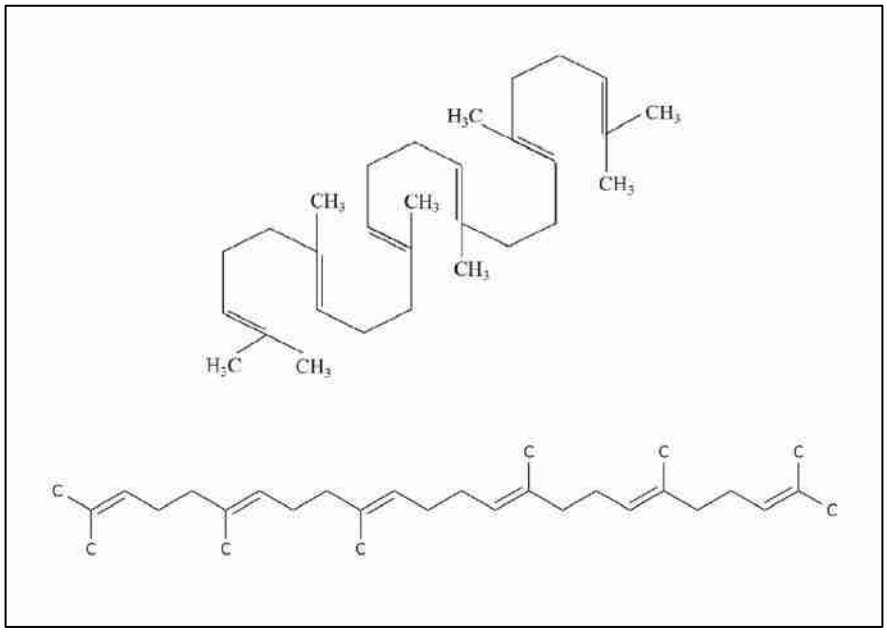

Figure 17. Squalene chemical structure. Adapted from ref [214].

6.5.1. Squalene and Biological Role

The sebaceous glands in humans secrete squalene, which accounts for 10–15% of lipids at 300–500 μg/g. A balance between dietary intake and endogenous synthesis in the intestinal and hepatocytes is represented by the squalene content. The various tissues absorb and distribute about 60–85% of the dietary squalene [215]. Chylomicrons carry intestinal and exogenous squalene into the bloodstream, where it is either re-secreted into VLDL and LDL along with hepatic-synthesized squalene for distribution to different organs or hepatic absorption for conversion to sterols and BAs [216]. The isoprenoid structure's six double bonds shield cells from microbial infection and oxidative damage. Squalene absorbs over 25% of the oxygen in the skin, preventing damage to nucleic acids from ultraviolet (UV) rays and shielding the skin from cutaneous bacteria and peroxidases [215,217–220]. Furthermore, squalene exhibits anti-cancer properties by inhibiting HMGR towards the synthesis of cholesterol and by suppressing intermediate steps via MVA, where FPP is involved in the geranylgeranylation and farnesylation of proteins, including small guanosine triphosphate (GTP)-binding proteins like Ras [220–222]. This suppression of these proteins, which in turn inhibit the signaling involved in the proliferation and differentiation of malignant cells, by controlling the metabolism of carcinogenic xenobiotics, or by scavenging free radicals and ROS to prevent mutagenesis and carcinogenesis brought on by nucleic acid oxidation [187,223,224]. Squalene may also inhibit NASH-related HCC, which is interrupted by elevated cholesteryl ester concentrations [215,216,219,222,223]. Squalene also retains detoxifying activities via stimulation of hepatic P450 enzymes, together with the non-polar nature of the triterpene which

provides an affinity for detoxification of non-ionized xenobiotics [212,213,217,218]. Another study in the context of diquat-induced oxidative stress revealed that the administration of a basal diet supplemented with squalene to broilers resulted in an enhanced oxidative status, characterized by elevated expression levels of Nrf2 and GPX1, and concurrently, the regulation of apoptosis-related genes (Bax and CASP3) led to a notable reduction in liver injury [225]. Two *in-silico* pharmacology studies provided a strong scientific framework for the idea that squalene plays a crucial role in the management of inflammation by regulating CRHR1, EGFR, ERBB2, HIF1A, SLC6A3, MAP2K1, and F2R [226], and antidiabetic activity by demonstrating its interaction with TRPV1 and KARS protein [227], also both squalene and its derivatives can promote the adipogenesis and ameliorate inflammatory response [228].

6.5.2. Squalene and Cholesterol Synthesis

As previously mentioned, endogenous squalene is synthesized via the cholesterol synthesis pathway, which is known as the mevalonate pathway (MVA pathway) (Figure 18) in which acetyl-CoA is converted to 3-hydroxy-3-methylglutaryl coenzyme A (HMG-CoA) by thiolases, also known as acetyl-coenzyme A acetyltransferases (ACAT), are the enzymes responsible for the conversion of 2 units of acetyl-CoA into acetoacetyl-CoA and HMG-CoA synthase (HMG-CoA-S, EC 2.3.3.10) as a 42 kDa homodimeric protein that catalyzes the irreversible condensation of acetyl-CoA and acetoacetyl-CoA to HMG-CoA and CoA. Then HMG-CoA reduced to MVA by 3-Hydroxy-3-methyl-glutaryl-CoA reductase or HMG-CoA reductase (HMG-CoA-R) catalyzes the NADP-dependent (in mammals) or NAD-dependent (in prokaryotes) synthesis of mevalonate from HMG-CoA. For this reason, the enzyme commission designated this enzyme as EC 1.1.1.34 for the NADPH-dependent enzyme, whereas EC 1.1.1.88 links to the NADH-dependent enzyme. In animal cells, the cholesterol biosynthetic pathway contains a unique series of three sequential ATP-dependent enzymes that convert mevalonate to isopentenyl diphosphate: mevalonate kinase (MK), phosphomevalonate kinase (PMK), and mevalonate 5-diphosphate decarboxylase (MDD). Diphosphomevalonate decarboxylase, also known as mevalonate diphosphate decarboxylase (MDD, EC 4.1.1.33), catalyzes the final step of the mevalonate pathway, i.e., the divalent cation-dependent decarboxylation of MVAPP to isopentenyl diphosphate [or isopentenyl pyrophosphate (IPP)], with concurrent hydrolysis of ATP to form ADP and inorganic phosphate. This reaction is required for the production of polyisoprenoids and sterols from acetyl-CoA [212,229–231]. Isopentenyl-diphosphate δ-isomerase [or isopentenyl pyrophosphate isomerase, IPP isomerase (EC 5.3.3.2)] catalyzes the conversion of the relatively unreactive IPP to the more reactive electrophile dimethylallyl pyrophosphate (DMAPP). Both reactants and products of this reaction are substrates for the successive reaction that results in the synthesis of farnesyl diphosphate (FPP) and, ultimately, cholesterol. This isomerization is therefore a key step in the biosynthesis of isoprenoids through the mevalonate pathway. Farnesyl diphosphate synthase also known as farnesyl pyrophosphate synthase (FDPS, EC 2.5.1.10) is a Mg^{2+}-dependent homodimeric enzyme, localized in peroxisomes, which catalyzes a chain elongation reaction and controls the first branching point of the mevalonate pathway [232,233]. Squalene synthase (SQS, EC 2.5.1.21) catalyzes an unusual head-to-head reductive dimerization of two molecules of FPP to form squalene. This enzyme is of particular importance as it is the first enzyme in

the pathway responsible for the production of a metabolite that is solely committed to cholesterol synthesis. Squalene monooxygenase (SM, EC 1.14.13.132), also known as squalene epoxidase, is a 64 kDa flavin adenine dinucleotide (FAD)-containing enzyme that catalyzes the first oxygenation step of cholesterol synthesis [233]. The reaction requires NADPH and molecular oxygen to oxidize squalene to 2,3-oxidosqualene (squalene epoxide). 2,3-Oxidosqualene cyclase-lanosterol synthase (OSC, EC 5.4.99.7) is a 78 kDa membrane-bound enzyme that catalyzes the conversion of the acyclic compound 2,3-oxidosqualene (OS) to the cyclic lanosterol. Both oxidosqualene and lanosterol are mostly hydrocarbons and thus are not very soluble in water [233]. The enzyme solves this problem by sticking to the membrane in peroxisomes. It then can pull oxidosqualene directly out of the membrane and release lanosterol back there [233]. The conversion of lanosterol into cholesterol is a very complex and multistep pathway, which involves several enzymes. After squalene is transformed into lanosterol, this molecule can follow two different routes, both of which end with a cholesterol molecule. They are termed the Bloch pathway and the Kandutsch–Russell pathway (K-R pathway). The difference between them is that the first uses Δ^{24}-unsaturated sterols while in the second the intermediates have their side chain saturated (Figure 18). While the K-R pathway uses the same enzymes as the Bloch pathway to reduce the Δ^{24} bond of lanosterol and convert dihydrolanosterol to cholesterol via 7-dehydrocholesterol reductase (DHCR7), the Bloch pathway consists of a subsequent side-chain of unsaturated intermediates ending in desmosterol, which is subsequently reduced to cholesterol via 24- dehydrocholesterol reductase (DHCR24) [212,229–231]. Overall, squalene plays a variety of roles in the route that go beyond its structural role [229,233,234].

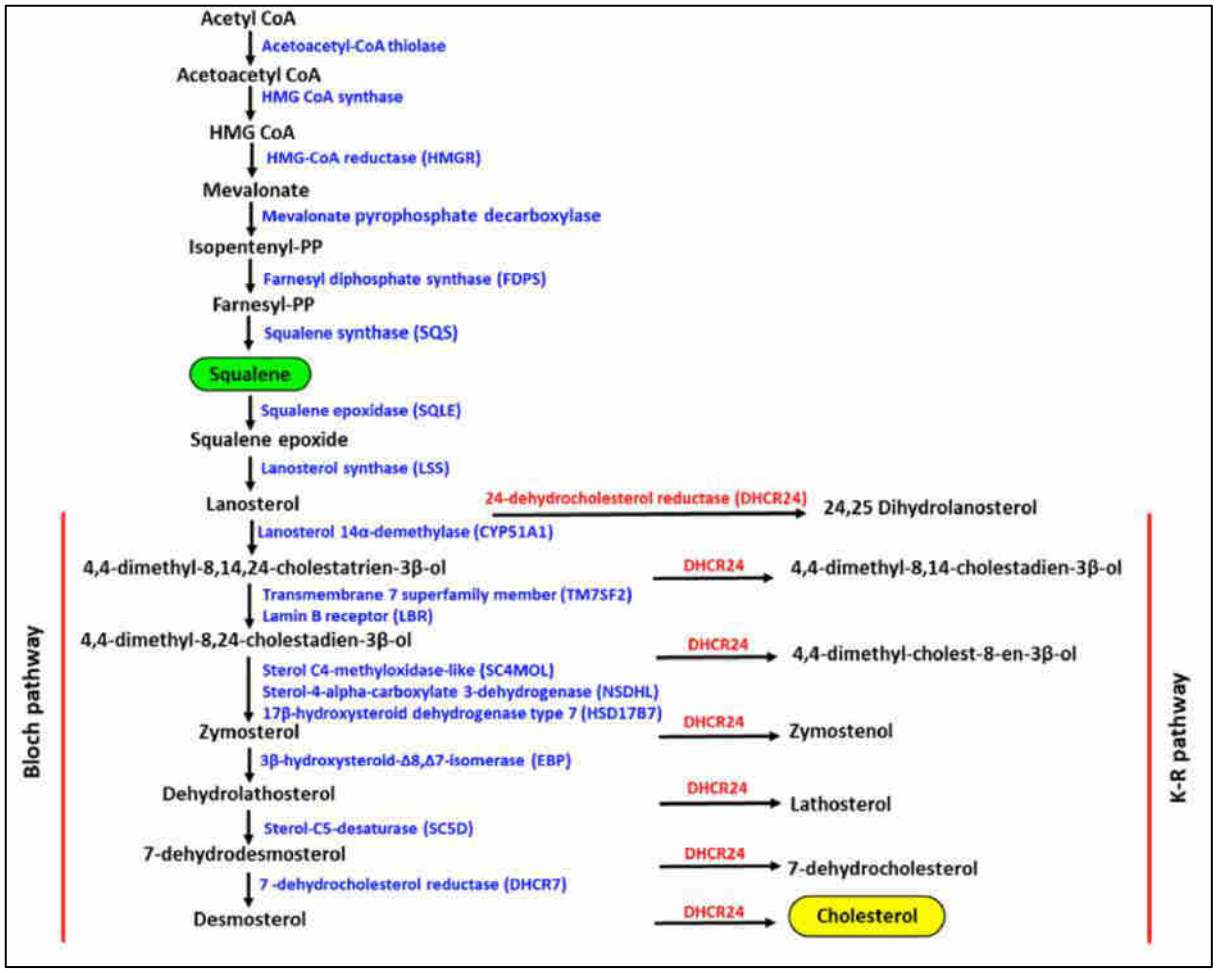

Figure 18. The cholesterol biosynthetic pathway. Include: pre-squalene cholesterol synthetic pathway, post-squalene cholesterol synthetic pathway (Bloch pathway and Kandutsch-Russel pathway). Adapted from ref [230,233].

7. Nanoparticles

7.1. Definition and Characteristics

Being the fundamental component of nanotechnology, nanoparticles (NPs) have a wide spectrum of applications in both commercial and domestic aspects. They are being extensively investigated by researchers as they occupy a big region in the length scale between the macro- and molecular levels. NPs are defined as particles that are in the nanometer (nm) size range (less than 1 μm) [235]. However, the definitions of the term "NPs" currently in use in the literature vary. For example, NPs are sometimes used to describe particles with a size of less than 100 nm (irrespective of the mode of measurement), sometimes with a size of less than 50 nm, at times for particles with a size of 10 nm or less, and occasionally with a size of less than 1 μm [235,236]. The significance of NPs in technological advancements can be attributed to their adaptable characteristics and enhanced performance relative to their parent material. The synthesis of NPs frequently involves the reduction of metal ions into uncharged NPs using reducing agents that are potentially hazardous. Nevertheless, in recent years, there have been

several efforts to develop environmentally friendly technology that utilizes natural resources in place of hazardous chemicals for the production of NPs. In green synthesis, biological methods are employed for the synthesis of NPs due to their environmentally friendly, clean, safe, cost-effective, straightforward, and highly productive nature. A multitude of biological organisms, including bacteria, actinomycetes, fungi, algae, yeast, and plants, are employed in the green synthesis of NPs. The NPs have significant applications in a number of sectors, including the environment, agriculture, food, biotechnology, biomedical, and medicines. For instance, they can be used for the treatment of wastewater, environmental monitoring, functional food additives, and antimicrobial agents. The cutting-edge properties of NPs, including their natural, biocompatible, anti-inflammatory, and antibacterial characteristics, effective drug delivery, bioactivity, bioavailability, tumor targeting, and bio-absorption, have contributed to a notable expansion in the biotechnological and applied microbiological applications of NPs [237].

7.2. Classification Based on Composition

7.2.1. Metal Nanoparticles

Metal NPs are composed exclusively of metal precursors. These NPs possess unique optoelectrical properties due to their well-known localized surface plasmon resonance (LSPR) characteristics. NPs of the alkali and noble metals, specifically copper, silver, and gold, exhibit a broad absorption band within the visible range of the solar electromagnetic spectrum [237,238]. The synthesis of metal NPs with controlled facets, sizes, and shapes is a crucial aspect of modern materials science. Silver NPs (AgNPs) are particles with a size range of 1–100 nanometers, composed of silver. Their unique physical and chemical properties are a consequence of their small size, high surface area-to-volume ratio, and ability to absorb and scatter light in the visible and near-infrared range. Furthermore, they may exhibit additional antimicrobial capabilities. Zinc oxide (ZnO) NPs are particles with a size range of 1–100 nm, composed of zinc. ZnONPs are a wide band gap semiconductor with a room temperature energy gap of 3.37 eV. Its catalytic, electrical, optoelectronic, and photochemical capabilities have rendered it a valuable and widely utilized material. Copper NPs (CuNPs) are particles comprising a size range of 1–100 nm, based on copper. Gold NPs (AuNPs) are nanoparticles composed of gold. These particles possess distinctive physical and chemical characteristics, enabling them to absorb and scatter light within the visible and near-infrared regions. The fluorescence of copper and gold metals has been documented for a considerable period of time [237,239,240]. NPs composed of aluminum are referred to as aluminum NPs (AlNPs). The strong reactivity of aluminum NPs makes them promising for use in high-energy compositions, hydrogen generation in water processes, and the synthesis of alumina 2D and 3D structures. Iron NPs (FeNPs) are particles with a size range of 1–100 nanometers, composed of iron. FeNPs have several potential applications, including their use as catalysts, drug delivery systems, sensors, and energy storage and conversion. FeNPs are employed for the targeted delivery of drugs to specific sites within the body, including cancer cells. Additionally, they are utilized in MRI and for the removal of contaminants from water [237]. Overall, metal NPs represent a field in continuous evolution, and current efforts are toward the optimization of

their synthesis and extension of their application in many fields, from medicine to electronics and material sciences [239].

7.2.2. Ceramic Nanoparticles

Ceramic NPs constitute an inorganic nanostructure, typically measuring between 1 and 100 nm in size. They are distinguished by their stability, elevated strength, and resilience to heat and corrosion. The most commonly used materials are silica (SiO_2), titanium (TiO_2), and zirconium dioxides (ZrO_2), each of which possesses distinctive properties that render them appropriate for a variety of applications [241]. Silica nanoparticles, for instance, are widely employed as drug delivery carriers due to their extensive surface area and capacity for straightforward functionalization, which enhances drug loading and release profiles. TiO_2 NPs exhibit excellent photocatalytic properties, rendering them valuable for environmental applications in water purification and air treatment, as well as in cosmetics for UV protection. Zirconium dioxide NPs are renowned for their elevated mechanical strength and biocompatibility, rendering them optimal for dental and orthopedic applications [241,242]. The synthesis of ceramic NPs can be achieved through a number of different methods, including sol-gel processes, hydrothermal synthesis, and spray pyrolysis. In general, ceramic NPs are inorganic, non-metallic material particles subjected to heat and cooling processes in a way as to endow them with specific properties. They may be amorphous or polycrystalline, dense or porous, or hollow shapes; and they resist heat, durable properties. Ceramic NPs are utilized in coating, catalysts, batteries, and drug delivery [237,243,244].

7.2.3. Carbon-based Nanoparticles

The discovery of carbon NPs was first documented in 1991, while the synthesis of single-wall carbon nanotubes with a diameter of 1 nm was first announced by Iijima and Ichihashi in 1993 [237]. Nanomaterials comprising carbon atoms and arranged in distinctive structural configurations, including fullerenes, carbon nanotubes (CNTs), graphene, and carbon dots, are versatile in nature [245,246]. CNTs, also referred to as Bucky tubes, are a category of nanomaterial constituted by a two-dimensional hexagonal lattice of carbon atoms. The individual units are bent in a single direction and subsequently joined to form a hollow cylinder. Carbon nanotubes represent a class of carbon allotropes situated between fullerenes and graphenes. NPs of globular hollow cages, which are allotropic forms of carbon, are found in fullerenes. Due to their electrical conductivity, high strength, structure, electron affinity, and adaptability, they have attracted significant economic interest [237]. Carbon dots are fluorescent, biocompatible nanoparticles being applied in bioimaging and sensing. Chemical vapor deposition and laser ablation stand out among the methods investigated to synthesize such kinds of NPs. Yet toxicity, environmental impact, and scalability remain under deliberation. The applications of carbon-based NPs remain one of the drivers of the current development in the said area, from medicine up to electronics and material sciences [245–248].

7.2.4. Polymeric Nanoparticles

Polymeric NPs with a diameter between 1 and 1,000 nm can be functionalized with active substances on the surface of the polymeric core or within the polymeric body. The term "polymer NPs" is frequently employed in the literature to refer to them. They are most often described as nanospheres or nano-capsules (Figure 19) [237]. Polymeric NPs are significantly advancing the field of nanomedicine due to their capacity for targeted and regulated drug release. Polymeric NPs are formed from two principal types of material: natural or synthetic. Synthetic polymers are more homogenous in composition and therefore have a higher purity than natural polymers. However, it should be noted that not all synthetic polymers are suitable for drug delivery as they need to be biodegradable and should have low cytotoxic effects. Examples of NPs made from synthetic polymers are polyesters which include poly(lactic acid) (PLA), poly(glycolic acid) (PGA), their co-polymer: poly(lactide-co-glycolic acid) (PLGA) (Figure 20), as well as polyalkyl(cyano)acrylates (PCA) [249–251]. All of these are not newcomers to the medical field and have been extensively used in clinical settings. For example, PLA is used for surgical stitches and implants. PCAs are used to seal wounds. Thus, the degradation kinetics of such polymers are well understood which allows for the preparation of better formulations for better controlled release [252]. In contrast, natural polymeric NPs exhibit considerable variability in purity, necessitating cross-linking and additional modifications that could potentially impact the stability of the associated drug. Natural polymers are typically derived from proteins and obtained from a range of sources. Gelatin is derived from collagen, which is found in the bones. Since they are isolated from natural sources, they should be biocompatible and display low cytotoxic effects [253]. The use of proteins allows for the possibility of modifications to the N-terminus, C-terminus, and the various associated amino acid side groups for specific tasks [251]. Another natural polymer is chitosan, a polysaccharide, utilized for the purpose of drug delivery. The PCA NPs have demonstrated considerable efficacy in drug delivery applications [251,254,255]. Overall, polymeric nanoparticles represent a promising and evolving platform in nanomedicine, driving innovations in targeted therapy and personalized medicine [249,250].

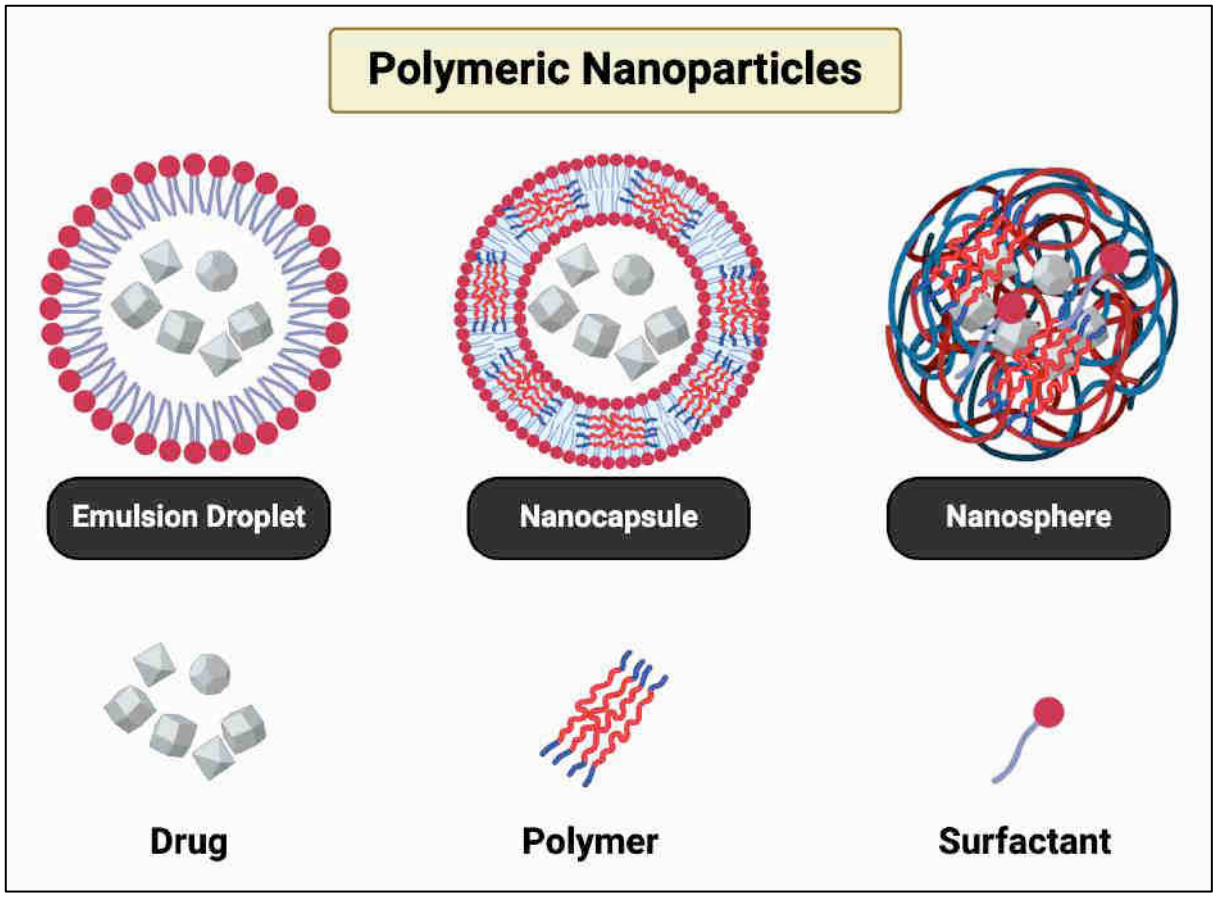

Figure 19. An overview of polymeric nanoparticles for drug delivery. Created by BioRender.com, accessed on 29 September 2024. Adapted from ref [256].

7.2.4.1. PLGA

PLA and PGA polymers are copolymerized to create PLGA NPs. The FDA and European Medicine Agency have approved their usage for human therapy, and they belong to the polyester family [251,252,257,258]. Because PLGA NPs are synthetic, they provide a number of benefits. The production of PLGA NPs is more repeatable due to the high purity of synthetic polymers. Compared to each polymer alone, the copolymer particle is more resistant to hydrolytic cleavage. Moreover, it is simple to alter the surface characteristics to suit a preferred purpose or targeting choices [251,254,255]. Because PLGA NPs hydrolyze to produce lactic and glycolic acids, which are the body's natural metabolites, they also have the advantage of being highly biodegradable [187,251,259]. The target organs and the drug's hydrophilic or hydrophobic nature determine how effective the production method is. For PLGA NPs, numerous formulation procedures have been created. Every strategy has benefits and drawbacks, which led to the optimization of particular protocols, such as those for drug encapsulation or drug surface adsorption [254,257]. In addition, the nature of the drug, their size and size distribution are other important physical parameters for PLGA NPs and also dictate the most suitable preparation method. In terms of drug release from PLGA NP, Sang

Yoo et al. reported that doxorubicin conjugated to PLGA NPs exhibited a loading efficiency of 96.6% and sustained release for over 25 days. In contrast, unconjugated doxorubicin in PLGA NPs had a loading efficiency of 6.7% and a release rate of around 5 days. Thus, the method used to prepare the NP has a great impact on drug release [251]. In conclusion, PLGA is one of the most studied and used polymers in biomedicine because to its combination of biodegradability, biocompatibility, tunable characteristics, and ease of formulation [252,257–260].

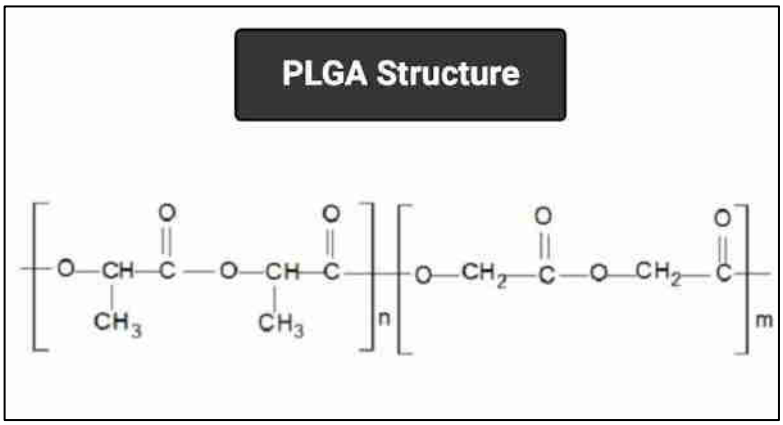

Figure 20. PLGA chemical structure. Adapted from [251,261] and created by BioRender.com, accessed on 29 September 2024.

7.2.4.2. Chitosan

Chitosan with the molecular structure shown in Figure 21 is the most important derivative of chitin, produced by removing the acetate moiety from chitin. Chitosan is obtained by the chemical modification of chitin in basic solutions at very high temperatures of 80–140 °C for prolonged periods of time [251]. Chitosan is mainly composed of β(1-4)-linked glucosamine units, with varying amounts of N-acetylglucosamine units depending on the degree of deacetylation [253,262]. It is derived from crustacean shells such as shrimp, crabs, and insects, as well as from the cell walls of fungi (Figure 21). It is a naturally occurring polysaccharide, cationic, highly basic, mucoadhesive biocompatible polymer and approved by the U.S. FDA for tissue engineering and drug delivery [251,263,264]. This polymer is soluble in weak acidic environments but insoluble in water. The products of the breakdown of chitosan are entirely safe. Various deacetylation techniques are used to create water-soluble chitosan, which is vulnerable to lipases, lysozymes, and other enzymes [251,264]. By releasing the epithelium's tight connections, chitosan improves penetration. Both the paracellular and transcellular transport of medications are facilitated by chitosan. Chitosan forms a compound with negatively charged mucus through hydrophobic and ionic interactions as well as hydrogen bonding [264]. In addition to being a mucoadhesive, this polymer has been demonstrated to possess antibacterial and anticancer characteristics in its particles. Because of its high mucus-binding properties as an adhesive, it increases adsorption into intestinal epithelial cells. Its total cationic charge, which produces electrostatic interactions with the negatively charged bacterial cell surface, is the source of its antibacterial effect [262–265]. The impacts on apoptosis, cell

cycle regulation, and metabolic pathways are what give it its anticancer effects. A variety of synthesis procedures for NPs made from chitosan or hybrid particles containing chitosan are being developed for a multitude of uses [264]. In conclusion, chitosan's intrinsic properties render it a highly valuable biomaterial with broad potential applications in medicine and biotechnology [253,263,266].

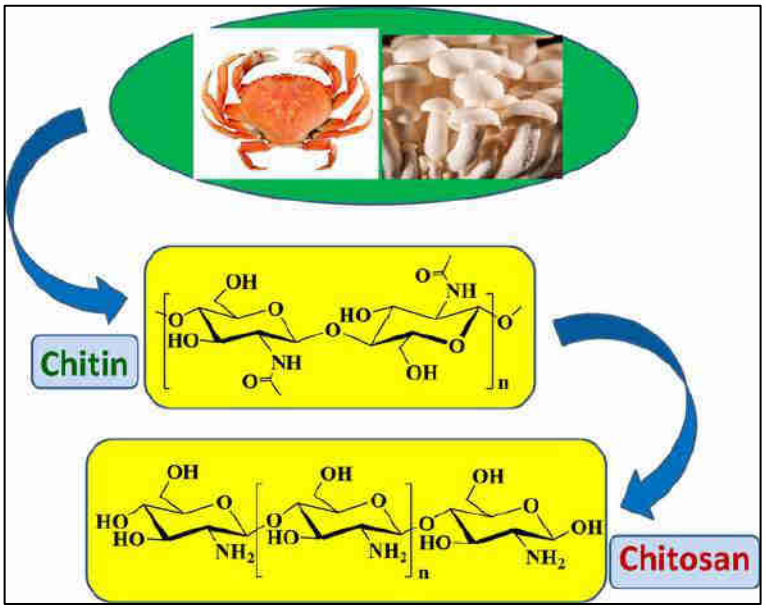

Figure 21. Natural sources of chitin and chitosan derived from the N-deacetylation of chitin. Adapted from ref [267].

8. Role of AML12 Cell Line in Hepatic Research

The development of *in vitro* cell models has been a great contribution to science because it allows cells derived from various organisms and tissues to be maintained in an environment with precise and absolute control. Moreover, cell culture allows studies to be conducted with the same cell population for both the control and treatment groups. In the present study, the AML12 cell line (alpha mouse liver 12) was used, which was chosen because of its suitability for the intended purpose. This cell line is derived from genetically modified mouse hepatocytes, strain CD1, line MT42, which expresses human transforming growth factor alpha (TGFα) [268]. These cells contain peroxisomes and are capable of forming structures that are morphologically similar to bile canaliculi. AML12 cells retain the ability to express serum proteins including albumin, alpha1 antitrypsin, transferrin, and GAP-binding proteins like connexins 26 and 32. The production of liver-specific proteins diminishes with time but can be reinstated by culturing them in serum-free conditions [268,269]. This cell line has been used in the study of many aspects of hepatic physiology, including lipid metabolism and mechanisms of action of drug delivery systems. All of these features, make AML12 cells an important cell line in the study of hepatic mechanisms and the development of new treatments against liver diseases [270].

III. OBJECTIVES

OBJECTIVES (ENGLISH)

It is thought that squalene, in conjunction with TXNDC5, exerts considerable biological effects *in vitro*. In order to gain further insight into this phenomenon, the following objectives have been established for a detailed characterization.

1. To identify novel protein interactions involving TXNDC5 in the liver and to assess the impact of TXNDC5 deficiency on these interactions.

2. Determining the influence of TXNDC5 on the gene and protein expressions associated with the ER stress pathways.

3. To explore the influence of squalene, loaded into PLGA nanoparticles on oxidative and ER stress in a mouse hepatic cell line.

4. To investigate the therapeutic effect of squalene by using chitosan as a novel drug delivery system for hepatocytes.

OBJETIVOS (ESPAÑOL)

Se cree que el escualeno, en combinación con TXNDC5, ejerce efectos biológicos considerables *in vitro*. Con el fin de obtener más información sobre este fenómeno, se han establecido los siguientes objetivos para una caracterización detallada.

1. Identificar nuevas interacciones proteicas que impliquen a TXNDC5 en el hígado y evaluar el impacto de la deficiencia de TXNDC5 en estas interacciones.

2. Determinar la influencia de TXNDC5 en las expresiones de genes y proteínas asociadas con las vías de estrés del RE.

3. Explorar la influencia del escualeno, cargado en nanopartículas de PLGA, en el estrés oxidativo y del RE en una línea celular hepática de ratón.

4. Investigar el efecto terapéutico del escualeno mediante el uso de quitosano como un nuevo sistema de administración de fármacos para los hepatocitos.

IV. PUBLICATIONS

List of publications

1. Endoplasmic Reticulum Protein TXNDC5 Interacts with PRDX6 and HSPA9 to Regulate Glutathione Metabolism and Lipid Peroxidation in the Hepatic AML12 Cell Line

This article was published in Int J Mol Sci in 2023 (5;24(24):17131 with. doi: 10.3390/ijms242417131)

2. TXNDC5 Plays a Crucial Role in Regulating Endoplasmic Reticulum Activity through Different ER Stress Signaling Pathways in Hepatic Cells

This article was published in Int J Mol Sci in 2024 (28;25(13):7128 with doi: 10.3390/ijms25137128)

3. Squalene Loaded Nanoparticles Effectively Protect Hepatic AML12 Cell Lines against Oxidative and Endoplasmic Reticulum Stress in a TXNDC5-Dependent Way

This article was published in Antioxidants in 2022 (18;11(3):581 with doi: 10.3390/antiox11030581)

4. Chitosan Nanoparticles, a Novel Drug Delivery System to Transfer Squalene for Hepatocyte Stress Protection

This article was published in ACS Omega in 2024 (9;52:51379 with doi: 10.1021/acsomega.4c08258)

International Journal of
Molecular Sciences

MDPI

Article

Endoplasmic Reticulum Protein TXNDC5 Interacts with PRDX6 and HSPA9 to Regulate Glutathione Metabolism and Lipid Peroxidation in the Hepatic AML12 Cell Line

Seyed Hesamoddin Bidooki [1,2,3], Javier Sánchez-Marco [1], Roberto Martínez-Beamonte [1,4,5], Tania Herrero-Continente [1], María A. Navarro [1,4,5], María J. Rodríguez-Yoldi [4,5,6] and Jesús Osada [1,4,5,*]

[1] Departamento de Bioquímica y Biología Molecular y Celular, Facultad de Veterinaria, Instituto de Investigación Sanitaria de Aragón, Universidad de Zaragoza, E-50013 Zaragoza, Spain; h.bidooki94@gmail.com (S.H.B.); javiersanchezmarc@gmail.com (J.S.-M.); romartin@unizar.es (R.M.-B.); taniaherrero1992@gmail.com (T.H.-C.); angelesn@unizar.es (M.A.N.)
[2] CNRS, IPREM, Universite de Pau et des Pays de l'Adour, E2S UPPA, 64 000 Pau, France
[3] MANTA—Marine Materials Research Group, Universite de Pau et des Pays de l'Adour, E2S UPPA, 64 600 Anglet, France
[4] Instituto Agroalimentario de Aragón, CITA-Universidad de Zaragoza, E-50013 Zaragoza, Spain; mjrodyol@unizar.es
[5] Centro de Investigación Biomédica en Red de Fisiopatología de la Obesidad y Nutrición (CIBEROBN), Instituto de Salud Carlos III, E-28029 Madrid, Spain
[6] Departamento de Farmacología, Fisiología, Medicina Legal y Forense, Facultad de Veterinaria, Instituto de Investigación Sanitaria de Aragón, Universidad de Zaragoza, E-50013 Zaragoza, Spain
* Correspondence: josada@unizar.es; Tel.: +34-976-761-644; Fax: +34-976-761-612

Abstract: Non-alcoholic fatty liver disease or steatosis is an accumulation of fat in the liver. Increased amounts of non-esterified fatty acids, calcium deficiency, or insulin resistance may disturb endoplasmic reticulum (ER) homeostasis, which leads to the abnormal accumulation of misfolded proteins, activating the unfolded protein response. The ER is the primary location site for chaperones like thioredoxin domain-containing 5 (TXNDC5). Glutathione participates in cellular oxidative stress, and its interaction with TXNDC5 in the ER may decrease the disulfide bonds of this protein. In addition, glutathione is utilized by glutathione peroxidases to inactivate oxidized lipids. To characterize proteins interacting with TXNDC5, immunoprecipitation and liquid chromatography–mass spectrometry were used. Lipid peroxidation, reduced glutathione, inducible phospholipase A_2 ($iPLA_2$) and hepatic transcriptome were assessed in the AML12 and TXNDC5-deficient AML12 cell lines. The results showed that HSPA9 and PRDX6 interact with TXNDC5 in AML12 cells. In addition, TXNDC5 deficiency reduced the protein levels of PRDX6 and HSPA9 in AML12. Moreover, lipid peroxidation, glutathione and $iPLA_2$ activities were significantly decreased in TXNDC5-deficient cells, and to find the cause of the PRDX6 protein reduction, proteasome suppression revealed no considerable effect on it. Finally, hepatic transcripts connected to PRDX6 and HSPA9 indicated an increase in the *Dnaja3*, *Mfn2* and *Prdx5* and a decrease in *Npm1*, *Oplah*, *Gstp3*, *Gstm6*, *Gstt1*, *Serpina1a*, *Serpina1b*, *Serpina3m*, *Hsp90aa1* and *Rps14* mRNA levels in AML12 KO cells. In conclusion, the lipid peroxidation system and glutathione mechanism in AML12 cells may be disrupted by the absence of TXNDC5, a novel protein–protein interacting partner of PRDX6 and HSPA9.

Keywords: protein interaction; TXNDC5; endoplasmic reticulum; PRDX6; HSPA9; glutathione; lipid peroxidation; liver

Citation: Bidooki, S.H.; Sánchez-Marco, J.; Martínez-Beamonte, R.; Herrero-Continente, T.; Navarro, M.A.; Rodríguez-Yoldi, M.J.; Osada, J. Endoplasmic Reticulum Protein TXNDC5 Interacts with PRDX6 and HSPA9 to Regulate Glutathione Metabolism and Lipid Peroxidation in the Hepatic AML12 Cell Line. *Int. J. Mol. Sci.* **2023**, *24*, 17131. https://doi.org/10.3390/ijms242417131

Academic Editor: Jessica Holien

Received: 15 November 2023
Revised: 29 November 2023
Accepted: 3 December 2023
Published: 5 December 2023

1. Introduction

Non-alcoholic fatty liver disease (NAFLD) or steatosis, an accumulation of fat in the liver independently of alcohol abuse, has come to be a burgeoning hassle due to its prevalence in the standard population [1,2]. NAFLD may evolve into a variety of

pathological conditions, such as steatohepatitis, cirrhosis and hepatocellular cancer [3]. In addition to impairing lipid metabolism [4,5], hepatic steatosis also causes profound changes in whole-genome expression [2].

Lipid metabolism, calcium homeostasis, protein synthesis, post-translational modification, and trafficking are all regulated by the cellular organelle known as the endoplasmic reticulum (ER) [6,7]. In fact, one-third of proteins are transported through the ER, where the correct formation of disulfide bonds depends on the oxidative environment that is kept by the glutathione balance [8,9]. Disturbed homeostasis within the ER, resulting from excessive levels of free fatty acid, depletion of calcium, or insulin resistance, can disturb ER functions and induce the pathological accumulation of misfolded proteins, commonly called the unfolded protein response (UPR) [10–13].

Thioredoxin domain-containing 5 (TXNDC5) has three thioredoxin-like domains, is a member of the nineteen existing protein disulfide isomerase (PDI) families of oxidoreductases, is predominantly expressed in the ER, and plays a critical role in signal transduction and cancer development [2,14,15]. PDIs are widely distributed proteins whose activity promotes a cysteine–disulfide–thiol exchange that reduces disulfides in other proteins. Protein stability, damage resistance, and half-lives can all be improved by PDIs, which are crucial in determining the structure and function of proteins [16–18]. TXNDC5 helps proteins fold appropriately by forming disulfide connections through its thioredoxin domains and is particularly abundant in liver and endothelial tissues [13]. Induced expression of TXNDC5 has been observed in a number of cancers, including of the cervix, colon, stomach, prostate, liver, and lung [19,20]. TXNDC5 has been linked to a number of biological processes, including antioxidation, promotion of angiogenesis, energy metabolism, involvement in cellular inflammation and the function of reduced glutathione [1,9]. The interaction of TXNDC5 with glutathione in the ER may reduce the disulfide bonds of this protein [21]. In addition, numerous processes use glutathione, and it is consumed by glutathione peroxidases to decrease oxidized lipids [22,23]. Recently, the absence of TXNDC5 under fasting stress led to a prodromal stage of sterile inflammation and increased lipid peroxidation. This could be due to the antioxidant characteristics of TXNDC5 and its involvement in several cellular processes [9,24]. However, the molecular mechanisms of TXNDC5 have not been well studied, including its role in liver metabolism. In this study, we found that TXNDC5 is a novel protein–protein interaction partner of PRDX6 and HSPA9, and their lack of interaction in mouse hepatocytes may contribute to the impairment of the glutathione mechanism and lipid peroxidation in the development of liver disease and its possible repercussions.

2. Results

2.1. Identification of PRDX6 and HSPA9 as Novel TXNDC5-Interacting Proteins in the AML12 Cell Line

In the AML12 cell line, due to its relevance to hepatic functions and ER processes, a study aimed at elucidating novel interacting partners of TXNDC5, a protein involved in redox regulation and protein folding [15], is crucial for understanding the proper functioning of TXNDC5 in the ER proteostasis network and cellular processes and signaling pathways. In order to find out the putative TXNDC5 interacting proteins, co-immunoprecipitation (Co-IP) and mass spectrometry were used. In Supplementary Table S2 are listed the identified proteins in the wild-type (WT) AML12 and absent in the TXNDC5 knockout cell lines. A total of 24 proteins were differentially immunoprecipitated in the presence or absence of TXNDC5 using an anti-TXNDC5 antibody. Considering the percentage of the protein sequence covered by the peptides (coverage > 10%), the presence of the number of distinct and unique peptides, and the total number of identified peptide sequences (peptide spectrum matches, (PSMs)), two proteins were clearly identified: HSPA9 and PRDX6. These findings were confirmed using Western blot analysis (Figure 1). To validate the immunoprecipitation, Western blot detection of TXNDC5 in immunoprecipitated WT and TXNDC5-KO AML12 cells was carried out using an anti-TXNDC5 antibody (Figure 1A).

As expected, the band corresponding to TXNDC5 was not observed in the TXNDC5-KO AML12 cells. When the same preparations were revealed using an anti-HSPA9 antibody, no band was observed in the TXNDC5-KO AML12 cells (Figure 1B). Using an anti-PRDX6 for immunoprecipitation (Figure 1C), no TXNDC5 band was detected in the cells lacking TXNDC5 (Figure 1D). These results confirm the interaction of TXNDC5 with HSPA9 and PRDX6 in the AML12 cell line. The identification of PRDX6 and HSPA9 as novel interacting partners of TXNDC5 in the AML12 cell line expands our understanding of the protein's cellular context, shedding light on its potential roles in redox regulation, lipid peroxidation, and ER–mitochondrial crosstalk.

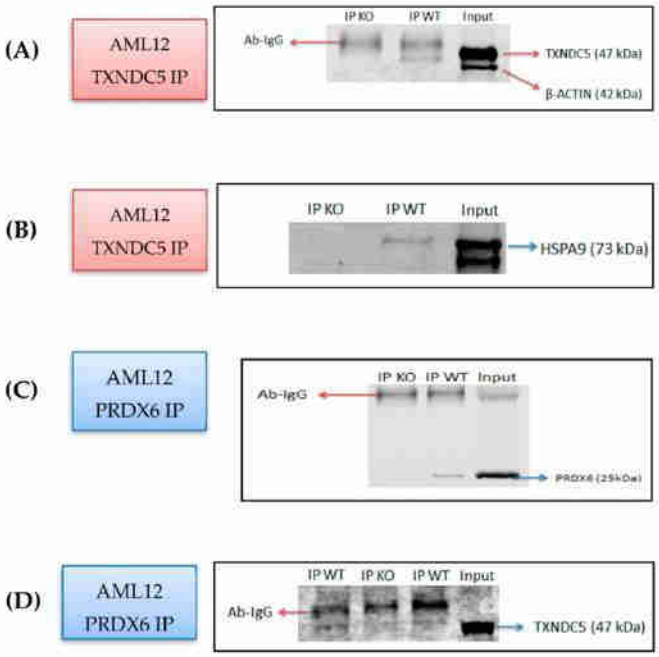

Figure 1. Confirmation of proteins interacting with TXNDC5 observed via Co-IP and mass spectrometry. Co-immunoprecipitation assays of AML12 WT and KO were immunoprecipitated with the TXNDC5 antibody, and the precipitates were analyzed by means of Western blot using an antibody against (**A**) TXNDC5 and (**B**) HSPA9. (**C**) AML12 WT and KO were co-immunoprecipitated with the PRDX6 antibody, and (**D**) the precipitates were examined via Western blotting with the anti-TXNDC5 antibody. Description of the lanes from left to right (**A–C**): first lane: co-immunoprecipitation in KO AML12 cells sample, second lane: co-immunoprecipitation in WT AML12 cells sample, third lane: WT AML12 cells sample without co-immunoprecipitation as input. (**D**) First and third lanes: co-immunoprecipitation in WT AML12 cells sample, second lane: co-immunoprecipitation in KO AML12 cells sample; fourth lane: WT AML12 cells sample without co-immunoprecipitation as input.

2.2. HSPA9 mRNA and Protein Levels Are Differentially Influenced by the Absence of TXNDC5

HSPA9 is a mitochondrial chaperone protein involved in protein folding and transport [25]. Its interaction with TXNDC5 suggests possible crosstalk between ER and mitochondrial protein-folding mechanisms. To understand the effect of TXNDC5 deficiency on hepatic cells, we investigated whether the HSPA9 mRNA and protein expressions were altered by the absence of TXNDC5 and the lack of its interaction. Elimination of TXNDC5 significantly reduced the *Hspa9* mRNA expression in the AML12 cell line (Figure 2A).

As shown in Figure 2B, the protein level of HSPA9 significantly decreased in response to the lack of TXNDC5 in hepatic cells. Due to our results, TXNDC5 and HSPA9 have protein–protein interactions that stabilize or regulate each other's expression. The loss of TXNDC5 could disrupt this interaction, leading to the degradation or altered stability of HSPA9, and it also might disrupt a cellular pathway or mechanism that indirectly affects HSPA9 expression. This could be due to a regulatory feedback loop or crosstalk between pathways. In addition, the absence of TXNDC5 might trigger a stress response that influences HSPA9 expression as part of an adaptive cellular mechanism or as an alteration in cellular redox status can impact the gene and protein expression. The mRNA level of *Hspa9* was reduced by 16% and could be the cause of the 20% reduction in the HSPA9 protein level; therefore, there was no evidence or indication of huge degradation due to post-translational modification and the reason for the HSPA9 protein reduction could be the mRNA changes. These could be the reasons that the downregulations were observed in the mRNA and protein levels of HSPA9 in the absence of TXNDC5.

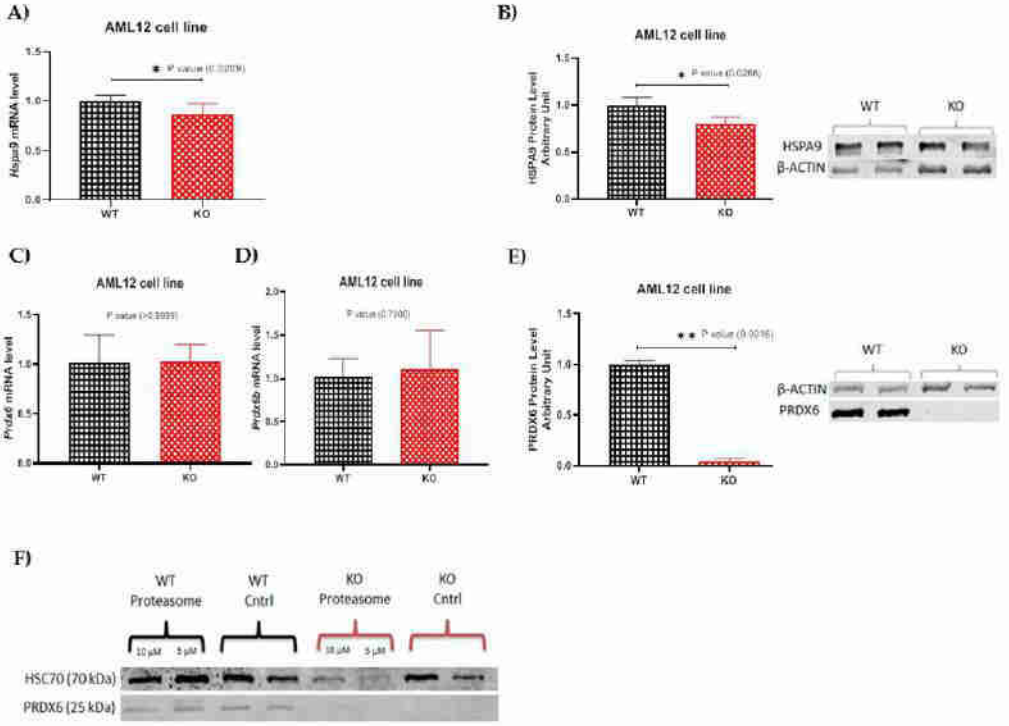

Figure 2. (**A**,**B**) Expression pattern of HSPA9. mRNA level of *Hspa9* in the (**A**) AML12 cell line. (**B**) Protein level of HSPA9 and its Western blot in the hepatic cell line. (**C**–**E**) Expression pattern of PRDX6. The RNA expression level of *Prdx6* (**C**) in the AML12 cell line and (**D**) the mRNA level of *Prdx6b* is shown in the AML12 cell line. (**E**) The protein level of PRDX6 was analyzed using Western blot in the hepatic cell lines. The Mann–Whitney U test for pairwise comparisons was used for statistical analysis; * $p < 0.05$, ** $p < 0.01$. (**F**) Effect of a proteasome inhibitor on the PRDX6 protein levels in the AML12 WT and KO cell lines. Cells were exposed to 5 and 10 μM MG-132 as a proteasome inhibitor for 24 h; then, the proteins were extracted and analyzed via Western blot. The MG-132-exposed WT cells displayed the same PRDX6 bands as the control group; even so, the KO cells did not show any bands. (HSC70 was used as a control protein.)

2.3. TXNDC5 Absence Reduces PRDX6 Protein Levels

Both TXNDC5 and PRDX6 are involved in redox regulation. TXNDC5, with its thioredoxin domain, participates in thiol–disulfide exchange reactions [21], while PRDX6 directly scavenges ROS [26]. Their functions in redox regulation suggest a potential interplay. Furthermore, TXNDC5 is implicated in protein folding within the ER. If it interacts with PRDX6, this interaction might contribute to the coordination of protein-folding processes and the maintenance of ER proteostasis. The interplay between TXNDC5 and PRDX6 could be part of a broader mechanism to maintain cellular homeostasis, balancing redox status, protein folding, and antioxidant defense [27]. To examine the effect of TXNDC5 deficiency on PRDX6 expression at the mRNA and protein levels. TXNDC5 deletion was incapable of influencing *Prdx6* mRNA expression in the AML12 cell line (Figure 2C). Hence, according to the NCBI blast analysis, which found 86% comparable identities between PRDX6 and PRDX6b, the expression level of *Prdx6b* was also studied, and Figure 2D shows no alteration. Interestingly, the absence of TXNDC5 resulted in a significant reduction in the protein level of PRDX6 in the liver cell line, as shown in Figure 2E. The discordance between the lack of change in the *Prdx6* mRNA expression and the downregulation of the PRDX6 protein levels following TXNDC5 knockout could be attributed to various post-transcriptional and post-translational regulatory mechanisms. Since the *Prdx6* mRNA levels remain constant, changes in the RNA-binding proteins or microRNAs might influence *Prdx6* mRNA translation. On the other hand, it is possible that TXNDC5 plays a role in the folding of PRDX6 by catalyzing thiol–disulfide exchange reactions and helping to maintain the correct redox state of cysteine residues for the formation of its three-dimensional structure and stability, and as a consequence of TXNDC5 deficiency, the degradation rate of the PRDX6 protein might be affected and influence the proper folding of PRDX6 or its interaction with chaperone proteins and be targeted for degradation, leading to a decrease in the PRDX6 protein levels.

2.4. Proteasomes Are Not Involved in the Reduction of PRDX6 Protein Induced by the Absence of TXNDC5

The ubiquitin–proteasome system (UPS) represents the main pathway for proteolysis in eukaryotic cells. Given that many cancer cells have increased proteasome activity and a malfunctioning UPS, inhibition of proteasomes in tumor cells results in apoptosis and cell cycle arrest [25]. TXNDC5 knockout could trigger ubiquitination of PRDX6, marking it for proteasomal degradation. This post-translational modification could impact the protein levels without affecting mRNA expression. To address proteasome involvement in PRDX6 protein reduction in the TXNDC5-deficient AML12 cells, cells were incubated in the presence of 5 and 10 µM MG-132 as a proteasome inhibitor for 24 h. The PRDX6 protein levels were assessed via Western blot. As shown in Figure 2F, the WT cells treated with the proteasome inhibitor at both concentrations exhibited PRDX6 bands compared to the control group. This suggests that the proteasome is not involved in the degradation of this protein. This was reinforced in the KO cells, where there was a lack of PRDX6 protein in the presence of proteasome inhibitor.

2.5. Lipid Peroxidation Was Decreased in the Absence of TXNDC5

PRDX6 is a multi-functional protein with peroxidase activity. Its involvement in redox signaling and lipid peroxidation suggests a potential connection to TXNDC5's role in redox regulation in the ER [28]. It also plays a crucial role in protecting cells from oxidative stress by scavenging reactive oxygen species and reducing lipid peroxides [29]. An MDA assay was used to compare the levels of lipid peroxidation in the AML12 cell lines (Figure 3A). As shown, the malondialdehyde (MDA) in the AML12 KO cells was significantly decreased compared to the WT cells. TXNDC5's absence may affect the cellular redox balance through other antioxidant enzymes or pathways that compensate for the loss of this protein, or it may lead to changes in lipid composition due to the phospholipase A_2 activity of PRDX6, potentially reducing oxidative stress and resulting in a cellular environment less prone to

lipid peroxidation and MDA formation. In conclusion, it is possible that TXNDC5 and its interacting protein PRDX6 are involved in the lipid peroxidation processes in AML12 cells.

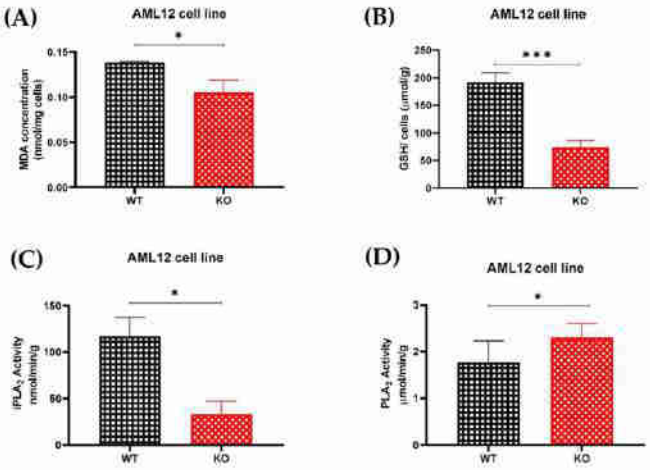

Figure 3. (**A**) Lipid peroxidation analysis. Significant MDA reduction in the KO cells is shown. (**B**–**D**) Assessment of glutathione and $iPLA_2$ activities. Considerable decrements of (**B**) GSH and (**C**) $iPLA_2$ activity in the KO cells are indicated. (**D**) AML12 KO cells display a remarkable increment in the total PLA_2. Statistical analysis was carried out according to the Mann–Whitney U test for pairwise comparisons; * $p < 0.05$, *** $p < 0.001$.

2.6. TXNDC5 Deficiency Decreases Reduced Glutathione and IPLA$_2$ Activity

The relationship of TXNDC5 and PRDX6 with glutathione and PLA_2 involves their interconnected roles in redox regulation, antioxidant defense, and lipid metabolism. PRDX6 interacts directly with glutathione during its peroxidase activity, and it also has phospholipase A_2 activity, contributing to the remodeling of cellular membranes by releasing fatty acids. This activity is crucial for maintaining lipid homeostasis [30]. As previously described, the elimination of TXNDC5 reduced the protein expression of PRDX6 in the AML12 cell line. To examine the redox status of the cell in relation to the glutathione peroxidase and calcium-independent phospholipase A_2 ($iPLA_2$) activity in the AML12 cell line, GSH, a marker of redox status, and $iPLA_2$ activity assays were carried out (Figure 3). As shown in Figure 3B,C, the GSH concentration and $iPLA_2$ activity in the AML12 KO cells were significantly decreased compared to the WT cells. Additionally, Figure 3D reveals that the AML12 KO cells had more total PLA_2 than the WT cells. The knockout of TXNDC5 might trigger compensatory mechanisms to maintain the overall phospholipase activity. When $iPLA_2$ is reduced, other PLA_2 isoforms might be upregulated to compensate for the loss and maintain essential lipid metabolism. As a result, TXNDC5, by interacting with PRDX6, could be a potential mediator in maintaining the overall phospholipase activity.

2.7. HSPA9 and PRDX6 Target Genes

TXNDC5 knockout might influence transcription factors or regulatory elements that control PRDX6 and HSPA9 gene expression. The absence of TXNDC5 may lead to changes in the transcriptional landscape, affecting the expression of downstream genes related to HSPA9 and PRDX6. Using different databases, 67 genes were identified as PRDX6 and HSPA9 targets (Supplementary Table S3). Based on the RNAseq data, 38 genes associated with PRDX6 and HSPA9 showed substantial changes in the transcript levels $SL_2R > \pm 2$ and $SL2R > \pm 1$, respectively, between the AML12 WT and KO cell lines (Figure 4D). The PAXdb database was used as a final filter to select 13 genes based on the liver protein abundance

(parts per million (PPM)). PPM > 100 and PPM > 300 were also chosen to filter the HSPA9 and PRDX6 datasets, respectively.

RNAseq data obtained from normal and TXNDC5-deficient AML12 cell lines were analyzed, and the represented data were summarized according to transcripts in the liver based on the described databases (Figure 4). This analysis was performed to find the most important genes and modifications based on the absence of TXNDC5 (Supplementary Table S3). The HSBP and MAPK gene families showed the majority of the changes connected to HSPA9, whereas the CHAC, GGT, GSTA, GSTT, PRXL2, RRM and SERPINA gene families indicated the most changes linked to PRDX6. As a result, 13 genes were found to be up- or downregulated in the AML12 cell line (Tables 1 and 2).

Table 1. Hepatic transcripts associated with HSPA9.

Gene Symbol	Gene ID (NCBI)	SL_2R RNAseq (AML12)	Regulation (AML12) KO/WT
Dnaja3 [31]	83945	1.2331	UP
Hsp90aa1 [32]	15519	−1.2332	DOWN
Mfn2 [33]	170731	1.6794	UP
Rps14 [31]	20044	−1.6093	DOWN

Abbreviations: *Dnaja3*, Dna] heat shock protein family (Hsp40) member A3; *Hsp90aa1*, heat shock protein 90, alpha (cytosolic), class A member 1; *Mfn2*, mitofusin 2; *Rps14*, ribosomal protein S14.

Table 2. Hepatic transcripts linked to PRDX6.

Gene Symbol	Gene ID (NCBI)	SL_2R RNAseq (AML12)	Regulation (AML12) KO/WT
Gstm6	14867	−2.1758	DOWN
Gstp3	225884	−2.6291	DOWN
Gstt1	14871	−3.3955	DOWN
Npm1 [34]	18148	−2.3854	DOWN
Oplah	75475	−2.5423	DOWN
Prdx5 [35]	54683	−2.0351	DOWN
Serpina1a [36]	20700	−3.8105	DOWN
Serpina1b [36]	20701	−2.5978	DOWN
Serpina3m [37]	20717	−6.7645	DOWN

Abbreviations: *Gstm6*, glutathione S-transferase, mu 6; *Gstp3*, glutathione S-transferase pi 3; *Gstt1*, glutathione S-transferase, theta 1; *Npm1*, nucleophosmin 1; *Oplah*, 5-oxoprolinase (ATP-hydrolysing); *Prdx5*, peroxiredoxin 5; *Serpina1a*, serine (or cysteine) peptidase inhibitor, clade A, member 1A; *Serpina1b*, serine (or cysteine) peptidase inhibitor, clade A, member 1B; *Serpina3m*, serine (or cysteine) peptidase inhibitor, clade A, member 3M.

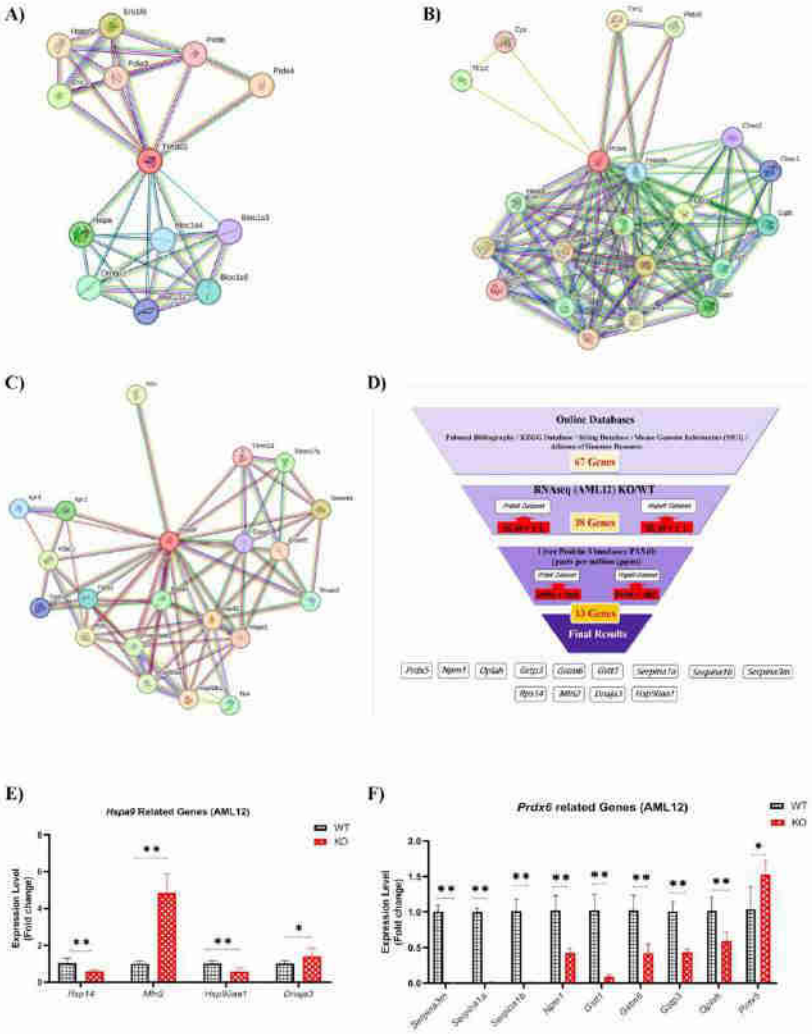

Figure 4. (**A**–**C**) Possible protein–protein interactions of mouse (**A**) TXNDC5, (**B**) PRDX6 and (**C**) HSPA9 generated by the String database. High confidence of 0.7 and not more than 20 interactors are shown. Nodes: network nodes represent proteins; red nodes: query proteins, colored nodes: the first shell of interactors, white nodes: the second shell of interactors. Edges represent protein–protein associations; blue and purple edges: known interactions, green, red and dark-blue edges: predicted interactions, yellow, black and light-blue: others. (**D**) Identification algorithm of genes associated with PRDX6 and HSPA9 based on the PubMed, KEGG, String, Mouse Genome Informatics, and Alliance of Genome Resource databases. Identification was based on mRNA changes according to the RNAseq analysis of the AML12 WT and KO cell lines ($SL_2R > \pm 2$ in the *Prdx6* dataset and $SL_2R > \pm 1$ in the *Hspa9* dataset). The liver protein abundance (parts per million (ppm)) based on the PAX database was considered as a final step (PPM > 300 in the *Prdx6* dataset and PPM > 100 in the *Hspa9* dataset). Expression of (**E**) *Hspa9*- and (**F**) *Prdx6*-associated genes in the AML12 cell line. Data are mean ± SD. Statistical analysis was performed according to the Mann–Whitney U test. * $p < 0.05$, ** $p < 0.01$.

2.8. Hepatic Gene Expression

The effect of TXNDC5 on hepatic transcripts linked to *Prdx6* and *Hspa9* was examined using RNA analysis in the AML12 WT and KO cell lines. To confirm the RNAseq data, 13 transcripts were selected from Tables 1 and 2, including *Dnaja3*, *Hsp90aa1*, *Mfn2*, *Rps14*, *Gstm6*, *Gstp3*, *Gstt1*, *Npm1*, *Oplah*, *Prdx5*, *Serpina1a*, *Serpina1b* and *Serpina3m*. Cell samples were used to set up and validate their RT-qPCR assays. According to the proposed *Hspa9* interactions, TXNDC5 deletion cells exhibit significantly downregulated levels of *Hsp90aa1* and *Rsp14* and significantly upregulated levels of *Dnaja3* and *Mfn2* (Figure 4E). Figure 4F displays the results for all the genes selected to interact with *Prdx6* in the AML12 cell lines. *Prdx5* exhibited a significant increase, whereas *Oplah*, *Gstm6*, *Gstt1* and *Npm1* showed decreased expression in the KO cells. Surprisingly, the SERPINA gene family, including *Serpina1a*, *Serpina1b*, and *Serpina3m*, showed a strong reduction in mRNA levels in the KO cells compared to WT cells.

A correlation study performed between the RNAseq and RT-qPCR by evaluating the $\log_2$ fold change values of the transcripts showed a significant agreement ($r = 0.91$, $p < 0.0001$) in the AML12 cells (Supplementary Figure S3A1), and all the genes were correctly categorized (Supplementary Figure S3A1). However, there were some differences between the signal-$\log_2$ ratios of the qPCR and RNAseq for *Prdx5* in the AML12 cells. These outcomes reveal that TXNDC5 deficiency and the elimination of its interaction with PRDX6 and HSPA9 can alter the transcriptional landscape, affecting the expression of their downstream genes and multiple cellular processes (Figure 5).

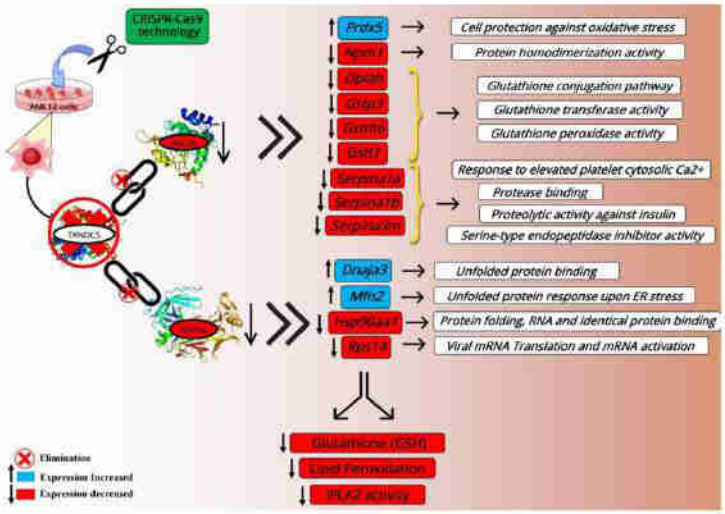

Figure 5. Diagram illustrating the interactions of the TXNDC5 protein with HSPA9 and PRDX6 as well as the impact of TXNDC5 deficiency in AML12 KO cells on different transcriptomes and their functions. Microsoft Publisher Document Version 2010 was used to create this schematic. ↑ Significantly increased, ↓ Significantly decreased. Red circle and cross: Elimination.

3. Discussion

The purpose of this study was to identify novel protein interactions involving TXNDC5 in the liver and the impact that TXNDC5 deficiency on those interactions. We also explored how these interactions affected the activities of $iPLA_2$, glutathione (GSH), and lipid peroxidation. Finally, we investigated the mRNA levels of the most significant HSPA9-, PRDX6-, and TXNDC5-related genes. TXNDC5 interacts with a plethora of various proteins and

is crucial for numerous cell functions. Histone modification, DNA transcription, mRNA splicing, cell cycle regulation, cell signaling, mobility and transport, metabolism, and protein degradation are among the processes in which it may play a role [1]. Some of these interactions may be important in the progression of certain diseases, including diabetes, neurological diseases, vitiligo, arthritis, and liver cancer [3]. For instance, TXNDC5's interactions with NENF, PPP1R2, ALDOC, LDH, or PGD may help explain its relevance in diabetes. TXNDC5 dysregulation may influence the cell cycle through cyclin CDK5, histones, or transcription factors like ATF2 or ZNHIT2, which have been implicated as potential carcinogens [38,39]. Moreover, hepatic fat influences TXNDC5, which has been linked to the regulation of ER stress, and may be crucial for the control of apolipoprotein B (APOB) and the development of steatosis [5].

The co-immunoprecipitation (co-IP) and mass spectrometry results identified HSPA9 and PRDX6 as novel TXNDC5-interacting proteins in the AML12 cell line (Figure 1). HSPA9, a member of the heat shock protein 70 family and a ubiquitous molecular chaperone in mammalian cells, has been linked to a variety of biological processes, including protein folding, the assembly of multi-protein complexes, protein trafficking [25], stress responses [40], mitochondrial biogenesis [41], and differentiation [42]. Numerous malignancies, including leukemia, brain cancer, colorectal adenocarcinoma and hepatocellular carcinoma, have been linked to increased expression of *Hspa9* [43–46]. Metastasis and early tumor recurrence have been associated with *Hspa9* overexpression in liver cancer [47]. Additionally, it has been demonstrated that overexpressing *Hspa9* is adequate to induce breast cancer cells to be more aggressive [46]. These findings suggest that HSPA9 is a promising target for cancer therapy [46]. Also, numerous studies link TXNDC5's high expression with cancer, and there may be a possible connection between that and HSPA9. According to the results revealed in Figure 2A–C, TXNDC5 inactivation can decrease the expression of HSPA9 mRNA and protein levels, which can induce cell growth arrest and enhance cell apoptosis. These findings are comparable to those of the RNA interference-based selective knockdown of *Hspa9* expression [48].

The reduction in a variety of cellular peroxides is catalyzed by the peroxiredoxin family of proteins, an evolutionarily conserved group of antioxidants that protect cells from oxidative damage [49,50]. The oxidative stress response, cell proliferation, and differentiation are just a few of the biological activities that peroxiredoxins have been linked to collectively [26,27]. H_2O_2 and a number of phospholipid peroxides can be reduced by PRDX6, which is cytosolically localized and capable of performing this function [51]. It is highly expressed in several organs, including the liver, lung, and keratinocytes [52–56]. The present study demonstrates that TXNDC5 deficiency does not influence the mRNA level of *Prdx6* in the AML12 cell line, although it induces a remarkable reduction in the protein level (Figure 3C–E). Pathological situations indicate that it may be impacted by *Prdx6* differential expression. According to recent studies, *Prdx6* mRNA levels decrease upon serum deprivation, and keratinocyte growth factor (KGF) is a strong inducer of *Prdx6* expression in both liver cells and keratinocytes. Results also showed that H_2O_2 upregulated *Prdx6* in mouse liver cells [29]. Basic biological processes such as cell growth, proliferation, cell cycle, and apoptosis are regulated by the ubiquitin/proteasome system (UPS), and when these activities are dysregulated, malignant transformation results [57]. Since many cancer cells, such as colon and breast cancer, have a defective UPS and elevated proteasome activity, proteasome inhibition in tumor cells has been shown to enhance the accumulation of inhibitors of cyclin-dependent kinases, pro-apoptotic, and tumor suppressor proteins, leading to cell cycle arrest and apoptosis [58–60]. To examine whether TXNDC5 could interact with the proteasome and thereby inhibit PRDX6 protein expression, we performed proteasome inhibition via MG-132 in the WT and KO AML12 cell lines; however, the results did not reveal any significant effect on PRDX6 protein expression in the cells, suggesting that the proteasome is not the cellular target of these complexes (Figure 2F).

Recent research has demonstrated that *Prdx6* overexpression can protect lung cells from oxidative stress-induced membrane lipid peroxidation and apoptosis in transfected

cells and adenovirus-mediated transfer in mice, whereas *Prdx6* antisense suppression increases oxidative stress susceptibility and cell death [61,62]. However, our results illustrate a significant decrease in lipid peroxidation in the AML12 cell line following the lack of TXNDC5 and reduction in PRDX6 protein (Figure 3A). Alongside lipid peroxidase activity, PRDX6 has been shown to possess glutathione peroxidase and phospholipase A_2 activities, which are concomitantly increased with *Prdx6* expression. Therefore, this protein plays an important role in membrane phospholipid metabolism [30,63]. The present study, as shown in Figure 3B–D, confirmed that the glutathione (GSH) and $iPLA_2$ activities were reduced in the AML12 knockout cells, which is consistent with the study of PRDX6 knockdown in A549, NCI-H460 and H1299 cell lines via siRNA, in which a reduction in the $iPLA_2$ and glutathione peroxidase activities was found [30,64].

To assess the impact of *Txndc5* in vivo, RNAseq was previously performed [9], but to determine it in vitro, a next-generation transcriptomic assay was performed. After analysis of RNAseq data from both normal and TXNDC5-deficient AML12 cell lines, the data presented were summarized based on the liver transcripts using the described databases (Figure 4D). In the AML12 cell line, the effect of TXNDC5 on the hepatic transcripts associated with *Hspa9* was examined. From Table 1, the transcripts *Dnaja3*, *Hsp90aa1*, *Mfn2* and *Rps14* were chosen. Our findings show that there is in vitro excessive *Dnaja3* expression. The J-protein *Dnaja3* is in charge of attracting substrates to *Hspa9* and is connected to the non-mitochondrial import functions of *Hspa9* [65]. In two IL-7 responsive B-cell lines (human 697 pre-B and mouse mIL-7R expressing Ba/F3 cells), overexpression of *Dnaja3* inhibits Stat5 phosphorylation and cell proliferation. Reducing the abundance of *Hspa9* may increase the amount of *Dnaja3* in hematopoietic and mouse β-cell lines; however, *Hspa9* and *Dnaja3* have also been established as regulators of *p53* via a similar mechanism [31,66]. However, in liver cells, the absence of TXNDC5 results in a reduction in *Hspa9* and *Dnaja3*. It has been shown that overexpression of *Hsp90* in cancer tissues, particularly in hepatocellular carcinoma, is associated with a poor prognosis and poor therapeutic outcomes [67,68]. *Hsp90*'s prevention of cancer cell proliferation mostly occurs through the degradation of client proteins, including AKT and P53, which in turn causes cancer cells to undergo apoptosis. According to these findings, the combined inhibition of *Hsp90* and *Hspa9* was found to dramatically reduce tumor growth in a liver cancer xenograft model, and the *Hsp90* inhibitor was also found to promote the expression of *Hspa9* [32]. According to the present study, *Hsp90aa1* is downregulated in the absence of TXNDC5 and *Hspa9* is downregulated, which is consistent with previous studies in the liver. Contact points between the endoplasmic reticulum (ER) and mitochondria (referred to as MAMs) in the liver may serve as important nodes for the control of lipid metabolism. However, ER stress was directly associated with altered triglyceride metabolism after *Hspa9* or *Mfn2* overexpression in Huh7 cells, highlighting the importance of the two key partners in establishing MAM integrity and activity [33,69], although *Mfn2* overexpression is present in vitro when *Hspa9* expression is reduced and TXNDC5 is deleted. HSPA9 deletion has been linked to enhanced reactive oxygen species formation in other biological systems. As a consequence, cellular stress is caused by the deletion of RPS14, a gene that is frequently deleted alongside HSPA9 on deletion (5q) as a result of ribosomal insufficiency and P53 activation [31], and haploinsufficiency of deletion genes, such as RPS14 and HSPA9, may play a role in bone marrow failure and inadequate hematopoiesis in hematopoietic cells by activating wild-type TP53 and inducing apoptosis [70]. Nevertheless, TXNDC5 deletion can induce the mRNA activation failure of *Hspa9* and *Rps14* in hepatic cells (Figure 4E).

Accordingly, our results in Figure 4F show that downregulation of TXNDC5 decreased the protein level of PRDX6 in the AML12 cell line, which may alter the expression of several hepatic genes associated with PRDX6 (Table 2). In the AML12 KO cells, *Oplah*, *Gstm6*, *Gstt1*, and *Gstp3*, which play a roles in glutathione metabolism [71], displayed decreased expression. Glutathione synthase deficiency is known to cause oxidative damage to the red blood cell membrane, and another known metabolic defect of the gamma–glutamyl cycle affects an ATP hydrolyzing enzyme (5-oxo-L-prolinase) encoded by the OPLAH gene [72].

Additionally, under oxidative stress, the expression of *Gstm6*, *Gstt1*, and *Gstp3* is decreased in glial cells of the retina, liver, and hepatocytes of rats, respectively [73–75]. Our results showed that *Prdx5* was upregulated in the AML12 cells in the absence of TXNDC5, whereas *Prdx5* was downregulated in the PRDX6 knockout HepG2 cells [35]. Recently, it has been shown that *Npm1*, a DNA/RNA chaperone, stimulates *Prdx6* expression and also *Npm1* gene knockdown, suppresses *Prdx6* expression, and on the contrary, an increase in the *Npm1* level can provide an increase in the *Prdx6* level. Furthermore, they are involved in the ROS-P53 pathway and their downregulation can improve the expression level of phosphorylated *p53* and ROS content in HepG2 cells [34,63]. Consequently, our study confirms the *Npm1* decrease in AML12 cells while the PRDX6 protein level is down-expressed. Finally, the mRNA patterns of the predominantly liver-produced *Serpina1a*, *Serpina1b* and *Serpina3m* showed a substantial down-expression in vitro when lacking TXNDC5. Proteins associated with inflammation, such as the SERPINA1 family and TXNDC5, are differentially positively altered in cutaneous squamous cell carcinoma and hepatocytes [36,76]. While the *Serpina3m* transcript levels decreased dramatically in the liver cells, adenomas and carcinomas, they tended to decrease in the non-neoplastic liver cells [37]. Serpin peptidase inhibitor, clade A (alpha-1 antiproteinase, antitrypsin) is the *Serpina3m* gene product that inhibits neutrophil elastase [77]. Due to its tissue-damaging effect, it has been suggested that enhanced neutrophil elastase activity is connected to the generation of carcinogenic responses [37]. These findings imply that the TXNDC5 and PRDX6 complex in the current study may be related to the decreased neutrophil elastase activity caused by *Serpina3m* deficiency. Consistent with these results, perhaps TXNDC5 and its function to fold the proteins and SERPINA family has an unknown interaction through the PRDX6 mediator in the liver.

4. Materials and Methods

4.1. AML12 Cell Culture

The ATCC collection (Manassas, VA, USA) provided the mouse hepatocyte cell line (AML12), which was cultured in 25 cm^2 plastic flasks at a density of 5×10^5 cells/cm^2 (in duplicate) at 37 °C in a humidified atmosphere of 5% CO_2 in Dulbecco's modified Eagle's minimum essential medium (DMEM; Thermo Fisher Scientific, Waltham, MA, USA): F-12-Ham's medium (GE Healthcare Life Science, South Logan, UT, USA) at a 1:1 ratio supplemented with 10% fetal bovine serum (Thermo Fisher Scientific, Waltham, MA, USA), 1:500 insulin–transferrin–selenium (Corning, Bedford, MA, USA), 40 ng/mL dexamethasone (Sigma-Aldrich; Merck Millipore, Darmstadt, Germany), 1% non-essential amino acids (Thermo Fisher Scientific, Waltham, MA, USA), 1% amphotericin B (1000 mg/mL; Thermo Fisher Scientific, Waltham, MA, USA), 1% penicillin (1000 U/mL; Thermo Fisher Scientific, Waltham, MA, USA), and 1% streptomycin (1000 mg/mL; Thermo Fisher Scientific, Waltham, MA, USA). Every two days, the culture medium was replaced. After the AML12 cells had achieved 90–100% confluence, the medium was removed and the cells were washed with PBS and trypsinized with 0.25% trypsin (DMEM; Thermo Fisher Scientific, Waltham, MA, USA) and 1 mM EDTA (DMEM; Thermo Fisher Scientific, Waltham, MA, USA). After centrifugation, the cell pellet was stored at −70 °C for RNA and protein extraction.

4.2. Creation of a Stable TXNDC5 Knockout AML12 Cell Line

The AML12 cell line was expanded, as previously described [24] Briefly, in order to generate stable clones lacking TXNDC5, the culture medium was removed after one week, the cells were transfected with TXNDC5/ERp46 HDR and TXNDC5 CRISPR/Cas9 KO plasmids (Santa Cruz Biotechnology, Dallas, TX, USA) using Lipofectamine 2000 (Thermo Fisher Scientific, Waltham, MA, USA). The gRNA sequence 5′-TTATCAAGTTCTTCGCTCCG-3′ in the TXNDC5 CRISPR/Cas9 KO plasmid caused a double-strand break (DSB) in the fifth exon of *Txndc5*. The TXNDC5/ERp46 HDR recombined the *Txndc5* gene with a puromycin resistance gene to facilitate the selection of stable knockout AML12 cells [39] AML12 KO cells that were puromycin resistant were selected after repeated puromycin incubations. Western blot confirmed the absence of TXNDC5 (Supplementary Figure S1).

4.3. Co-Immunoprecipitation (Co-IP) Assay

Cells were lysed using radioimmunoprecipitation assay (RIPA) lysis buffer for protein extraction, as previously described [78]. Immunoprecipitation was carried out using 1 mg SureBeads ™ Protein A-Magnetic Beads (BioRad, Hercules, CA, USA) in 1.5 mL tubes coupled with 7.5 µg rabbit anti-TXNDC5 (Proteintech, Manchester, UK). Unbound antibody was washed three times with PBS-T (PBS + 0.1% Tween 20). After the sample lysis, the supernatants were incubated with protein A-magnetic beads conjugated to rabbit anti-TXNDC5 overnight at 4 °C. The beads were washed three times with PBS-T. To break the conjugation between the beads and proteins, 20 µL of 20 mM glycine pH 2.0 was added and incubated for 10 min at room temperature. The magnetic beads were captured and the eluent was transferred to a new vial and neutralized with 2 µL (10% eluent volume) of 1 M phosphate buffer pH 7.4. The eluents were analyzed via Western blot analysis.

4.4. Protein Identification via LC-MS/MS

Proteomic analysis of the immunoprecipitation from the wild-type and TXNDC5 knockout AML12 cell lines was performed at the Proteomics Unit of the Complutense University of Madrid. Protein samples were boiled for 5 min in loading buffer (6 mM Tris, 2% SDS, 10% glycerol, 0. 5 M beta-mercaptoethanol, traces of bromo-phenol blue) and cooled for 5 min at 4 °C, and they were then loaded on a 4 cm separating gel at 10% acrylamide (acrylamide:bisacrylamide, 19:1) in 1.5 M Tris, pH 8.8, and a 4 cm concentrating gel at 4% acrylamide in 0.5 M Tris, pH 6.5. Electrophoresis was performed in Laemmli buffer at 100 V in a mini-protean system (Bio-Rad, Hercules, CA, USA) until the electrophoretic front (bromophenol blue) had advanced approximately 2 cm in the concentrating gel. The protein bands were visualized by means of staining with colloidal Coomassie (G-250). The bands of the concentrating gel were excised and digested with trypsin. The Coomassie residues and equilibration buffer were removed via two washes with acetonitrile (ACN) alternating with rehydration of the gel with 25 mM ammonium bicarbonate. The disulfide bridges were reduced with 10 mM DTT in 25 mM AMBI at 56 °C for 30 min and blocked with 22.5 mM iodoacetamide in 25 mM AMBI for 15 min in the dark. After removing any traces of the reagents with two ACN washes, the gel was completely dehydrated in a Speed-Vac (Thermo-Savant, Waltham, MA, USA) for 30 min, followed by 0.5 µg of proteomics grade recombinant trypsin (Roche, Madrid, Spain) in 20 µL of 25 mM AMBI and allowed to act overnight at 37 °C. The peptides were collected in the supernatant from the digestion and extraction of the gel with 20 µL acetonitrile. The resulting liquid was blotted dry in a Speed-Vac and reconstituted in 20 µL 2% ACN, 0.1% formic acid. For the peptide separation via reversed-phase chromatography, 10 µL of the digested peptide mixture was injected into the Easy-nLC 1000 nano-HPLC (Thermo), concentrated on a PEPMAP100 C18 NanoViper Trap precolumn (Thermo Fisher Scientific, Waltham, MA, USA), and separated on a 50 cm PEPMAP RSLC C18 column (Thermo) with a gradient of 5% to 40% acetonitrile and 0.1% formic acid in 90 min before loading into the mass spectrometer for analysis. The peptides separated via chromatography were ionized using an electrospray in positive mode and analyzed in a Q Exactive HF (Thermo Fisher Scientific, Waltham, MA, USA) mass spectrometer in DDA (data-dependent acquisition) mode. From each MS scan (between 350 and 1700 Da), the 10 most intense precursors (charge between 2+ and 5+) were selected for their high collision energy dissociation (HCD) fragmentation and the corresponding MSMS spectra were acquired. The data files generated in the shotgun analysis were transferred to Proteome Discoverer 2.4 software (Thermo Fisher Scientific, Waltham, MA, USA), where the PSMs (peptide spectrum matches) of each MSMS spectrum were identified through comparison with the lists of theoretical masses corresponding to the mass of the precursor of origin extracted from the UniProt database (https://www.uniprot.org/) (accessed on 1 November 2020) taxonomically bound to *Mus musculus* and UniProt–Swiss-Prot (all entries) using the Sequest search engine. The identified peptides were assigned to their corresponding proteins.

4.5. Western Blot

Proteins were extracted from the AML12 cells, quantified, and transferred to a PVDF membrane, as previously published [24,78]. The membranes were blocked with PBS buffer containing 5% BSA for 1 h at room temperature. After blocking, the membranes were incubated overnight at 4 °C with rabbit primary polyclonal antibodies against mouse TXNDC5 (1:1000, Proteintech, Manchester, UK), PRDX6 (1:1000, Proteintech, Manchester, UK), HSPA9 (1:1000, Proteintech, Manchester, UK), mouse monoclonal anti-HSC70 (1:1000, Proteintech, Manchester, UK) and mouse monoclonal anti-β-ACTIN (1:1000, Sigma, St. Louis, MO, USA). The membranes were washed with PBS solution containing 0.1% Tween 20 before incubation for 1 h at room temperature with conjugated goat anti-rabbit IgG (H&L) DyLight 800 secondary antibody (1:60,000, Thermo-Scientific, Waltham, MA, USA) or goat anti-mouse IgG (H&L) DyLight 680 secondary antibody (1:30,000, Thermo-Scientific, Waltham, MA, USA). The blots were captured using Odyssey® Clx (LI-COR, Bad Hamburg, Germany). The blots were quantified using Image Studio Lite Version 5.2 software (LI-COR Biosciences—GmbH, Bad Homburg, Germany). We expressed the densitometric values normalized to the housekeeping antibodies in arbitrary units.

4.6. Bioinformatic Analyses

Data from online bioinformatics databases and a PubMed search were used to confirm and identify the most relevant genes associated with TXNDC5, PRDX6, and HSPA9. In November 2022, 115 and 70 genes were extracted from the PubMed publication date since 2007 using the keywords TXNDC5 and PRDX6, TXNDC5 and HSPA9, respectively. The String database (Figure 4A–C) (https://string-db.org accessed on 20 July 2023) with the criteria of high confidence (0.7) and no more than 20 interactions was used to extract 21 genes per each search, and the KEGG database (https://www.genome.jp/kegg/pathway.html accessed on 20 March 2023) was used to find the 77 and 33 possible genes interacting with the potential biochemical pathways related to PRDX6 and HSPA9 target genes, respectively (Supplementary Figure S2). Then, a total of 67 genes were selected for filtering based on the different databases, including Mouse Genome Informatics (MGI) (http://www.informatics.jax.org accessed on 20 July 2023), PAXdb (https://pax-db.org accessed on 10 September 2023), and Alliance of Genome Resource (https://www.alliancegenome.org accessed on 20 July 2023). The combined information was considered to evaluate the gene and protein expression of their potential target genes in liver.

4.7. RNA Extraction

The total cellular RNA was extracted according to the manufacturer's instructions using a Quick-RNA™ MiniPrep kit (Zymo Research, CA, USA). A spectrophotometer (SPECTROstar®, Omega, BMG Labtech, Ortenberg, Germany) was used to measure the amount of RNA based on the absorbance ratio at a wavelength of 260/280 nm. The 28S/18S ratio was greater than 2, which was determined via electrophoresis on a 1% agarose gel, followed by ethidium bromide staining to validate the integrity of the 28S and 18S ribosomal RNAs.

4.8. RNAseq Analyses

For the RNA sequencing, the total RNA of the wild-type AML12 (WT) and TXNDC5-knockout AML12 cell lines was prepared. The RNA samples were sequenced at the Beijing Genomics Institute (BGI Genomics, Shenzhen, China). As previously mentioned [79], the following steps were completed: RNA quality testing, library creation, sequencing reads and posterior clean, genome mapping, analysis, identification, and quantification. The average genome mapping rate was 95.95% for the AML12 cells and the full datasets were deposit at GEO (Accession number GSE242049).

4.9. Reverse Transcription and Quantitative Real-Time PCR

Quantitative reverse transcriptase PCR assays of these transcripts were optimized for the primer and input cDNA amounts to achieve similar efficiencies. According to the manufacturer's instructions, 500 ng of extracted total RNA was reverse-transcribed into complementary deoxyribonucleic acid using the PrimeScript RT Reagent Kit (TaKaRa Biotechnology, Kusatsu, Shiga, Japan) in the presence of random and oligo (dT) primers. The primers for each gene were designed using Primer Express (Applied Biosystems, Foster City, CA, USA) (Supplementary Table S1), which were then validated for gene specificity and amplification of cDNA rather than genomic DNA using BLAST analysis (NCBI). Finally, the primers were selected based on the primer efficiency. Quantitative real-time PCR was performed on a StepOnePlus Real-Time PCR System (Applied Biosystems, Foster City, CA, USA) according to the manufacturer's instructions (SYBR Green PCR Master Mix, Applied Biosystems, Foster City, CA, USA). The relative ratio of the transcript expression level of each gene to the mean values of the control samples was calculated using the comparative $2^{-\Delta\Delta CT}$ method, normalized to the endogenous control genes *Ppib* and *Tbp*.

4.10. Proteasome Inhibition in AML12 WT and KO Cells

The AML12 WT and KO cells, as previously described, were cultured in 25 cm^2 plastic flasks at a density of 5×10^5 cells/cm^2 (in duplicate). Afterwards, the medium was removed once the AML12 cells had reached 90–100% confluence, and the cells were washed once with PBS before being incubated in fetal bovine serum-free medium, 5 µM amphotericin B, with 5 µM and 10 µM of MG-132 (Sigma, St Louis, MO, USA) [60] dissolved in DMSO as a proteasome inhibitor. After 24 h of exposure to the proteasome inhibitor, the cells were trypsinized and stored at −20 °C for protein extraction.

4.11. Determination of Cellular Lipid Peroxidation via MDA Assay

Malondialdehyde (MDA), an end product of lipid peroxidation, was measured in the AML12 cells using a commercially available MDA assay kit (MAK085, Sigma, Saint Louis, MO, USA).

4.12. Total Phospholipase A_2 (PLA_2) and Calcium-Independent Phospholipase A_2 ($iPLA_2$) Activity Assays

The PLA_2 and $iPLA_2$ activities were assayed according to the manufacturer's instructions (Cayman Chemicals, Ann Arbor, MI, USA). Briefly, the cells were homogenized and the supernatants obtained via centrifugation at 10,000× *g* for 15 min at 4 °C. Supernatants containing 50 µg protein in a total volume of 45 µL were added to microplate wells containing 5 µL of assay buffer with ($iPLA_2$ activity) or without 10 µM bromoenol lactone (total PLA_2 activity). The reaction was initiated via the addition of 200 µL of arachidonoyl thio-phosphatidylcholine and was incubated at room temperature for 60 min. By adding 10 µL of 25 mM 5,5′-dithiobis-(2-nitrobenzoic acid), the reaction was stopped, and the absorbance was measured at 405 nm using a microplate reader (SPECTROstar®, Omega, BMG Labtech, Ortenberg, Germany). The manufacturer's recommendations were followed for the calculation of $iPLA_2$ activity.

4.13. Intracellular Reduced Glutathione (GSH) Concentration Determination

According to the instructions provided by the manufacturer, a kit (38185, Merk KGaA, Darmstadt, Germany) was used to measure the intracellular GSH concentrations in the cells. A kinetic assay was utilized to detect the GSH levels by continuously monitoring the conversion of 5,5′-dithiobis-(2-nitrobenzoic acid) into 5-thio-2-nitrobenzoic acid at 420 nm.

4.14. Statistical Analysis

GraphPad Prism 8 (GraphPad, S. Diego, CA, USA) for Windows was used for statistical purposes. The Shapiro–Wilk test and Bartlett's or Levene's test were used to assess the homology of variance between the groups and the normal distribution of the data,

respectively. Factors meeting both criteria were examined using two-way ANOVA with Dunnett's multiple comparison test and a two-tailed Student's *t*-test. If any of the hypotheses failed, statistical analysis was performed using the Mann–Whitney U test. The means and standard deviations of the results are presented. A *p*-value of less than 0.05 was used to indicate statistical significance.

5. Conclusions

As a conclusion, our research showed that the HSPA9 and PRDX6 proteins interact with TXNDC5 in AML12 cells. TXNDC5 deficiency reduced the PRDX6 protein levels without altering its transcripts, while the HSPA9 protein and mRNA expression decreased. Lipid peroxidation, reduced-form glutathione (GSH) and $iPLA_2$ activity were significantly decreased in the TXNDC5-deficient cells, while the total PLA_2 was increased. Proteasome suppression via MG-132 in the WT and KO AML12 cell lines revealed no considerable effect on PRDX6 protein expression in the cells, suggesting that the proteasome is not the biological target of the TXNDC5–PRDX6 complex. The effect of TXNDC5 on the hepatic transcripts associated with PRDX6 and HSPA9 revealed that in the AML12 KO cells, *Dnaja3*, *Mfn2*, and *Prdx5* were overexpressed while *Hsp90aa1*, *Rsp14*, *Oplah*, *Gstp3*, *Gstm6*, *Gstt1*, *Serpina1a*, *Serpina1b*, and *Serpina3m* were downregulated (Figure 5).

Limitations and Future Research

While gene knockdown or knockout experiments can provide valuable insights into the impact of TXNDC5 deficiency on HSPA9 and PRDX6 levels and cell growth, there are some limitations and considerations to be aware of. Cells may activate compensatory mechanisms in response to gene knockout or knockdown, potentially masking the true impact on the HSPA9 and PRDX6 levels and cell growth. Therefore, these results should be validated by using other approaches to knockdown these genes, especially if the study aims to understand the role of TXNDC5 deficiency. The effects of TXNDC5 gene knockout may follow temporal dynamics. Investigating the short- and long-term effects of the temporal dynamics of TXNDC5 deficiency and interaction with PRDX6 and HSPA9 by assessing the early, intermediate and late responses under oxidative stress conditions may be another aspect of future research. This may reveal how cellular responses evolve over time. By addressing these limitations and expanding the research in these suggested directions, future studies can provide a more nuanced understanding of the impact of TXNDC5 deficiency on cellular processes and potentially identify novel therapeutic targets.

Supplementary Materials: The following supporting information can be downloaded at https://www.mdpi.com/article/10.3390/ijms242417131/s1.

Author Contributions: Conceptualization, S.H.B., J.S.-M., R.M.-B., T.H.-C., M.A.N., M.J.R.-Y. and J.O.; methodology, S.H.B., J.S.-M., R.M.-B. and T.H.-C.; software, S.H.B. and J.S.-M.; validation, S.H.B. and J.S.-M.; formal analysis, S.H.B., J.S.-M. and R.M.-B.; investigation, S.H.B.; resources, M.J.R.-Y. and J.O.; data curation, S.H.B. and J.O.; writing—original draft preparation, S.H.B.; writing—review and editing, S.H.B., J.S.-M., R.M.-B., T.H.-C., M.A.N., M.J.R.-Y. and J.O.; visualization, S.H.B.; supervision, R.M.-B., M.A.N. and J.O.; project administration, M.J.R.-Y. and J.O.; funding acquisition, M.J.R.-Y. and J.O. All authors have read and agreed to the published version of the manuscript.

Funding: This research was supported by grants (CIBEROBN, CB06/03/1012) from CIBER Fisiopatología de la Obesidad y Nutrición as an initiative of FEDER-ISCIII, Ministerio de Ciencia e Innovación-Fondo Europeo de Desarrollo Regional (PID2019-104915RB-I00 and PID2022-104915RB-I00) and Fondo Social Europeo-Gobierno de Aragón (B16_23R). S.H.B. was recipient of a joint fellowship from the Universities of Zaragoza and Pau, and J.S.-M. was recipient of a Fundación Cuenca Villoro fellowship. The proteomic analysis was performed in the Proteomics Unit of Complutense University of Madrid, a member of ProteoRed, and supported by grant PT17/0019, of the PE I+D+i 2013-2016, funded by ISCIII and ERDF or "Grant PRB3 (IPT17/0019-ISCIII-SGEFI/ERDF)".

Institutional Review Board Statement: Not applicable.

Informed Consent Statement: Not applicable.

Data Availability Statement: All data are contained within the article and Supplementary Material.

Acknowledgments: We thank Cristina Barranquero for her help in maintaining the lab.

Conflicts of Interest: The authors declare no conflict of interest.

References

1. Horna-Terrón, E.; Pradilla-Dieste, A.; Sánchez-de-Diego, C.; Osada, J. TXNDC5, a newly discovered disulfide isomerase with a key role in cell physiology and pathology. *Int. J. Mol. Sci.* **2014**, *15*, 23501–23518. [CrossRef] [PubMed]
2. Loomba, R.; Friedman, S.L.; Shulman, G.I. Mechanisms and disease consequences of nonalcoholic fatty liver disease. *Cell* **2021**, *184*, 2537–2564. [CrossRef]
3. Ao, N.; Yang, J.; Wang, X.; Du, J. Glucagon-like peptide-1 preserves non-alcoholic fatty liver disease through inhibition of the endoplasmic reticulum stress-associated pathway. *Hepatol. Res.* **2016**, *46*, 343–353. [CrossRef] [PubMed]
4. Musso, G.; Gambino, R.; Cassader, M. Recent insights into hepatic lipid metabolism in non-alcoholic fatty liver disease (NAFLD). *Prog. Lipid Res.* **2009**, *48*, 1–26. [CrossRef] [PubMed]
5. Ramirez-Torres, A.; Barceló-Batllori, S.; Martínez-Beamonte, R.; Navarro, M.A.; Surra, J.C.; Arnal, C.; Guillén, N.; Acín, S.; Osada, J. Proteomics and gene expression analyses of squalene-supplemented mice identify microsomal thioredoxin domain-containing protein 5 changes associated with hepatic steatosis. *J. Proteom.* **2012**, *77*, 27–39. [CrossRef] [PubMed]
6. Han, J.; Kaufman, R.J. The role of ER stress in lipid metabolism and lipotoxicity. *J. Lipid Res.* **2016**, *57*, 1329–1338. [CrossRef]
7. Hama, Y.; Morishita, H.; Mizushima, N. Regulation of ER-derived membrane dynamics by the DedA domain-containing proteins VMP1 and TMEM41B. *EMBO Rep.* **2022**, *23*, e53894. [CrossRef]
8. Hwang, C.; Sinskey, A.J.; Lodish, H.F. Oxidized redox state of glutathione in the endoplasmic reticulum. *Science* **1992**, *257*, 1496–1502. [CrossRef]
9. Sánchez-Marco, J.; Martínez-Beamonte, R.; Diego, A.D.; Herrero-Continente, T.; Barranquero, C.; Arnal, C.; Surra, J.; Navarro, M.A.; Osada, J. Thioredoxin Domain Containing 5 Suppression Elicits Serum Amyloid A-Containing High-Density Lipoproteins. *Biomedicines* **2022**, *10*, 709. [CrossRef]
10. Cnop, M.; Foufelle, F.; Velloso, L.A. Endoplasmic reticulum stress, obesity and diabetes. *Trends Mol. Med.* **2012**, *18*, 59–68. [CrossRef]
11. Fu, S.; Yang, L.; Li, P.; Hofmann, O.; Dicker, L.; Hide, W.; Lin, X.; Watkins, S.M.; Ivanov, A.R.; Hotamisligil, G.S. Aberrant lipid metabolism disrupts calcium homeostasis causing liver endoplasmic reticulum stress in obesity. *Nature* **2011**, *473*, 528–531. [CrossRef] [PubMed]
12. Fu, S.; Watkins, S.M.; Hotamisligil, G.S. The role of endoplasmic reticulum in hepatic lipid homeostasis and stress signaling. *Cell Metab.* **2012**, *15*, 623–634. [CrossRef] [PubMed]
13. Tan, F.; Zhu, H.; He, X.; Yu, N.; Zhang, X.; Xu, H.; Pei, H. Role of TXNDC5 in tumorigenesis of colorectal cancer cells: In vivo and in vitro evidence. *Int. J. Mol. Med.* **2018**, *42*, 935–945. [CrossRef] [PubMed]
14. Alberti, A.; Karamessinis, P.; Peroulis, M.; Kypreou, K.; Kavvadas, P.; Pagakis, S.; Politis, P.K.; Charonis, A. ERp46 is reduced by high glucose and regulates insulin content in pancreatic β-cells. *Am. J. Physiol.-Endocrinol. Metab.* **2009**, *297*, E812–E821. [CrossRef] [PubMed]
15. Chawsheen, H.A.; Jiang, H.; Ying, Q.; Ding, N.; Thapa, P.; Wei, Q. The redox regulator sulfiredoxin forms a complex with thioredoxin domain–containing 5 protein in response to ER stress in lung cancer cells. *J. Biol. Chem.* **2019**, *294*, 8991–9006. [CrossRef] [PubMed]
16. Hatahet, F.; Ruddock, L.W. Protein disulfide isomerase: A critical evaluation of its function in disulfide bond formation. *Antioxid. Redox Signal.* **2009**, *11*, 2807–2850. [CrossRef]
17. Benham, A.M. The protein disulfide isomerase family: Key players in health and disease. *Antioxid. Redox Signal.* **2012**, *16*, 781–789. [CrossRef] [PubMed]
18. Duivenvoorden, W.; Hopmans, S.N.; Austin, R.C.; Pinthus, J.H. Endoplasmic reticulum protein ERp46 in prostate adenocarcinoma. *Oncol. Lett.* **2017**, *13*, 3624–3630. [CrossRef]
19. Mo, R.; Peng, J.; Xiao, J.; Ma, J.; Li, W.; Wang, J.; Ruan, Y.; Ma, S.; Hong, Y.; Wang, C. High TXNDC5 expression predicts poor prognosis in renal cell carcinoma. *Tumor Biol.* **2016**, *37*, 9797–9806. [CrossRef]
20. Wang, L.; Song, G.; Chang, X.; Tan, W.; Pan, J.; Zhu, X.; Liu, Z.; Qi, M.; Yu, J.; Han, B. The role of TXNDC5 in castration-resistant prostate cancer—Involvement of androgen receptor signaling pathway. *Oncogene* **2015**, *34*, 4735–4745. [CrossRef]
21. Chawsheen, H.A.; Ying, Q.; Jiang, H.; Wei, Q. A critical role of the thioredoxin domain containing protein 5 (TXNDC5) in redox homeostasis and cancer development. *Genes Dis.* **2018**, *5*, 312–322. [CrossRef] [PubMed]
22. Maiorino, M.; Bosello, V.; Cozza, G.; Roveri, A.; Toppo, S.; Ursini, F. Glutathione peroxidase-4. In *Selenium*; Springer: Berlin/Heidelberg, Germany, 2011; pp. 181–195.
23. Janssen-Heininger, Y.; Reynaert, N.L.; van der Vliet, A.; Anathy, V. Endoplasmic reticulum stress and glutathione therapeutics in chronic lung diseases. *Redox Biol.* **2020**, *33*, 101516. [CrossRef] [PubMed]
24. Bidooki, S.H.; Alejo, T.; Sánchez-Marco, J.; Martínez-Beamonte, R.; Abuobeid, R.; Burillo, J.C.; Lasheras, R.; Sebastian, V.; Rodriguez-Yoldi, M.J.; Arruebo, M. Squalene Loaded Nanoparticles Effectively Protect Hepatic AML12 Cell Lines against Oxidative and Endoplasmic Reticulum Stress in a TXNDC5-Dependent Way. *Antioxidants* **2022**, *11*, 581. [CrossRef] [PubMed]

25. Dores-Silva, P.R.; Cauvi, D.M.; Kiraly, V.T.; Borges, J.C.; De Maio, A. Human HSPA9 (mtHsp70, mortalin) interacts with lipid bilayers containing cardiolipin, a major component of the inner mitochondrial membrane. *Biochim. Et Biophys. Acta BBA-Biomembr.* **2020**, *1862*, 183436. [CrossRef] [PubMed]
26. Fujii, J.; Ikeda, Y. Advances in our understanding of peroxiredoxin, a multifunctional, mammalian redox protein. *Redox Rep.* **2002**, *7*, 123–130. [CrossRef] [PubMed]
27. Immenschuh, S.; Baumgart-Vogt, E. Peroxiredoxins, oxidative stress, and cell proliferation. *Antioxid. Redox Signal.* **2005**, *7*, 768–777. [CrossRef] [PubMed]
28. Fujii, S.; Ushioda, R.; Nagata, K. Redox states in the endoplasmic reticulum directly regulate the activity of calcium channel, inositol 1, 4, 5-trisphosphate receptors. *Proc. Natl. Acad. Sci. USA* **2023**, *120*, e2216857120. [CrossRef]
29. Gallagher, B.M.; Phelan, S.A. Investigating transcriptional regulation of Prdx6 in mouse liver cells. *Free Radic. Biol. Med.* **2007**, *42*, 1270–1277. [CrossRef]
30. Yun, H.-M.; Park, K.-R.; Lee, H.P.; Lee, D.H.; Jo, M.; Shin, D.H.; Yoon, D.-Y.; Han, S.B.; Hong, J.T. PRDX6 promotes lung tumor progression via its GPx and iPLA2 activities. *Free Radic. Biol. Med.* **2014**, *69*, 367–376. [CrossRef]
31. Krysiak, K.; Tibbitts, J.F.; Shao, J.; Liu, T.; Ndonwi, M.; Walter, M.J. Reduced levels of Hspa9 attenuate Stat5 activation in mouse B cells. *Exp. Hematol.* **2015**, *43*, 319–330.e310. [CrossRef]
32. Guo, W.; Yan, L.; Yang, L.; Liu, X.; E, Q.; Gao, P.; Ye, X.; Liu, W.; Zuo, J. Targeting GRP75 improves HSP90 inhibitor efficacy by enhancing p53-mediated apoptosis in hepatocellular carcinoma. *PLoS ONE* **2014**, *9*, e85766. [CrossRef] [PubMed]
33. Bassot, A.; Prip-Buus, C.; Alves, A.; Berdeaux, O.; Perrier, J.; Lenoir, V.; Ji-Cao, J.; Berger, M.-A.; Loizon, E.; Cabaret, S. Loss and gain of function of Grp75 or mitofusin 2 distinctly alter cholesterol metabolism, but all promote triglyceride accumulation in hepatocytes. *Biochim. Et Biophys. Acta BBA-Mol. Cell Biol. Lipids* **2021**, *1866*, 159030. [CrossRef] [PubMed]
34. Chen, J.; Cao, X.; Qin, X.; Liu, H.; Chen, S.; Zhong, S.; Li, Y. Proteomic analysis of the molecular mechanism of curcumin/β-cyclodextrin polymer inclusion complex inhibiting HepG2 cells growth. *J. Food Biochem.* **2020**, *44*, e13119. [CrossRef]
35. López-Grueso, M.J.; Lagal, D.J.; García-Jiménez, Á.F.; Tarradas, R.M.; Carmona-Hidalgo, B.; Peinado, J.; Requejo-Aguilar, R.; Bárcena, J.A.; Padilla, C.A. Knockout of PRDX6 induces mitochondrial dysfunction and cell cycle arrest at G2/M in HepG2 hepatocarcinoma cells. *Redox Biol.* **2020**, *37*, 101737. [CrossRef] [PubMed]
36. Azimi, A.; Kaufman, K.L.; Ali, M.; Arthur, J.; Kossard, S.; Fernandez-Penas, P. Differential proteomic analysis of actinic keratosis, Bowen's disease and cutaneous squamous cell carcinoma by label-free LC–MS/MS. *J. Dermatol. Sci.* **2018**, *91*, 69–78. [CrossRef] [PubMed]
37. Yafune, A.; Kawai, M.; Itahashi, M.; Kimura, M.; Nakane, F.; Mitsumori, K.; Shibutani, M. Global DNA methylation screening of liver in piperonyl butoxide-treated mice in a two-stage hepatocarcinogenesis model. *Toxicol. Lett.* **2013**, *222*, 295–302. [CrossRef]
38. Charlton, H.K.; Webster, J.; Kruger, S.; Simpson, F.; Richards, A.A.; Whitehead, J.P. ERp46 binds to AdipoR1, but not AdipoR2, and modulates adiponectin signalling. *Biochem. Biophys. Res. Commun.* **2010**, *392*, 234–239. [CrossRef]
39. Heiker, J.T.; Kosel, D.; Beck-Sickinger, A.G. Molecular Mechanisms of Signal Transduction via Adiponectin and Adiponectin Receptors. *Biol. Chem.* **2010**, *391*. [CrossRef]
40. Lu, W.; Lee, N.; Kaul, S.; Lan, F.; Poon, R.; Wadhwa, R.; Luk, J. Mortalin–p53 interaction in cancer cells is stress dependent and constitutes a selective target for cancer therapy. *Cell Death Differ.* **2011**, *18*, 1046–1056. [CrossRef]
41. Ornatsky, O.; Connor, M.; Hood, D. Expression of stress proteins and mitochondrial chaperonins in chronically stimulated skeletal muscle. *Biochem. J.* **1995**, *311*, 119–123. [CrossRef]
42. Xu, J.; Xiao, H.H.; Sartorelli, A.C. Attenuation of the induced differentiation of HL-60 leukemia cells by mitochondrial chaperone HSP70. *Oncol. Res.* **1999**, *11*, 429–435. [PubMed]
43. Pizzatti, L.; Sá, L.A.; de Souza, J.M.; Bisch, P.M.; Abdelhay, E. Altered protein profile in chronic myeloid leukemia chronic phase identified by a comparative proteomic study. *Biochim. Et Biophys. Acta BBA-Proteins Proteom.* **2006**, *1764*, 929–942. [CrossRef] [PubMed]
44. Takano, S.; Wadhwa, R.; Yoshii, Y.; Nose, T.; Kaul, S.C.; Mitsui, Y. Elevated levels of mortalin expression in human brain tumors. *Exp. Cell Res.* **1997**, *237*, 38–45. [CrossRef]
45. Rozenberg, P.; Kocsis, J.; Saar, M.; Prohászka, Z.; Füst, G.; Fishelson, Z. Elevated levels of mitochondrial mortalin and cytosolic HSP70 in blood as risk factors in patients with colorectal cancer. *Int. J. Cancer* **2013**, *133*, 514–518. [CrossRef] [PubMed]
46. Wadhwa, R.; Takano, S.; Kaur, K.; Deocaris, C.C.; Pereira-Smith, O.M.; Reddel, R.R.; Kaul, S.C. Upregulation of mortalin/mthsp70/Grp75 contributes to human carcinogenesis. *Int. J. Cancer* **2006**, *118*, 2973–2980. [CrossRef] [PubMed]
47. Yi, X.; Luk, J.M.; Lee, N.P.; Peng, J.; Leng, X.; Guan, X.-Y.; Lau, G.K.; Beretta, L.; Fan, S.-T. Association of mortalin (HSPA9) with liver cancer metastasis and prediction for early tumor recurrence. *Mol. Cell. Proteom.* **2008**, *7*, 315–325. [CrossRef] [PubMed]
48. Wadhwa, R.; Takano, S.; Taira, K.; Kaul, S.C. Reduction in mortalin level by its antisense expression causes senescence-like growth arrest in human immortalized cells. *J. Gene Med. A Cross-Discip. J. Res. Sci. Gene Transf. Its Clin. Appl.* **2004**, *6*, 439–444. [CrossRef]
49. Hofmann, B.; Hecht, H.-J.; Flohé, L. Peroxiredoxins. *Biol. Chem.* **2002**, *383*. [CrossRef]
50. Rhee, S.G.; Chae, H.Z.; Kim, K. Peroxiredoxins: A historical overview and speculative preview of novel mechanisms and emerging concepts in cell signaling. *Free Radic. Biol. Med.* **2005**, *38*, 1543–1552. [CrossRef]
51. Fisher, A.B.; Dodia, C.; Manevich, Y.; Chen, J.-W.; Feinstein, S.I. Phospholipid hydroperoxides are substrates for non-selenium glutathione peroxidase. *J. Biol. Chem.* **1999**, *274*, 21326–21334. [CrossRef]

52. Sparling, N.E.; Phelan, S.A. Identification of multiple transcripts for antioxidant protein 2 (Aop2): Differential regulation by oxidative stress and growth factors. *Redox Rep.* **2003**, *8*, 87–94. [CrossRef] [PubMed]
53. Wang, X.; Phelan, S.A.; Forsman-Semb, K.; Taylor, E.F.; Petros, C.; Brown, A.; Lerner, C.P.; Paigen, B. Mice with targeted mutation of peroxiredoxin 6 develop normally but are susceptible to oxidative stress. *J. Biol. Chem.* **2003**, *278*, 25179–25190. [CrossRef] [PubMed]
54. Kim, T.-S.; Dodia, C.; Chen, X.; Hennigan, B.B.; Jain, M.; Feinstein, S.I.; Fisher, A.B. Cloning and expression of rat lung acidic Ca2+-independent PLA2 and its organ distribution. *Am. J. Physiol.-Lung Cell. Mol. Physiol.* **1998**, *274*, L750–L761. [CrossRef] [PubMed]
55. Frank, S.; Munz, B.; Werner, S. The human homologue of a bovine non-selenium glutathione peroxidase is a novel keratinocyte growth factor-regulated gene. *Oncogene* **1997**, *14*, 915–921. [CrossRef] [PubMed]
56. Munz, B.; FRANK, S.; HÜBNER, G.; OLSEN, E.; WERNER, S. A novel type of glutathione peroxidase: Expression and regulation during wound repair. *Biochem. J.* **1997**, *326*, 579–585. [CrossRef] [PubMed]
57. Avram, H.; Aaron, C.; Alexander, V. The ubiquitin system. *Annu. Rev. Biochem.* **1998**, *67*, 425–479.
58. Chen, L.; Madura, K. Increased proteasome activity, ubiquitin-conjugating enzymes, and eEF1A translation factor detected in breast cancer tissue. *Cancer Res.* **2005**, *65*, 5599–5606. [CrossRef]
59. Arlt, A.; Bauer, I.; Schafmayer, C.; Tepel, J.; Müerköster, S.S.; Brosch, M.; Röder, C.; Kalthoff, H.; Hampe, J.; Moyer, M. Increased proteasome subunit protein expression and proteasome activity in colon cancer relate to an enhanced activation of nuclear factor E2-related factor 2 (Nrf2). *Oncogene* **2009**, *28*, 3983–3996. [CrossRef]
60. Quero, J.; Cabello, S.; Fuertes, T.; Mármol, I.; Laplaza, R.; Polo, V.; Gimeno, M.C.; Rodriguez-Yoldi, M.J.; Cerrada, E. Proteasome versus thioredoxin reductase competition as possible biological targets in antitumor mixed thiolate-dithiocarbamate gold (III) complexes. *Inorg. Chem.* **2018**, *57*, 10832–10845. [CrossRef]
61. Manevich, Y.; Sweitzer, T.; Pak, J.H.; Feinstein, S.I.; Muzykantov, V.; Fisher, A.B. 1-Cys peroxiredoxin overexpression protects cells against phospholipid peroxidation-mediated membrane damage. *Proc. Natl. Acad. Sci. USA* **2002**, *99*, 11599–11604. [CrossRef]
62. Pak, J.H.; Manevich, Y.; Kim, H.S.; Feinstein, S.I.; Fisher, A.B. An antisense oligonucleotide to 1-cys peroxiredoxin causes lipid peroxidation and apoptosis in lung epithelial cells. *J. Biol. Chem.* **2002**, *277*, 49927–49934. [CrossRef] [PubMed]
63. Sharapov, M.G.; Novoselov, V.I.; Gudkov, S.V. Radioprotective role of peroxiredoxin 6. *Antioxidants* **2019**, *8*, 15. [CrossRef] [PubMed]
64. Lu, B.; Chen, X.-B.; Hong, Y.-C.; Zhu, H.; He, Q.-J.; Yang, B.; Ying, M.-D.; Cao, J. Identification of PRDX6 as a regulator of ferroptosis. *Acta Pharmacol. Sin.* **2019**, *40*, 1334–1342. [CrossRef] [PubMed]
65. Goswami, A.V.; Chittoor, B.; D'Silva, P. Understanding the functional interplay between mammalian mitochondrial Hsp70 chaperone machine components. *J. Biol. Chem.* **2010**, *285*, 19472–19482. [CrossRef] [PubMed]
66. Dhennin-Duthille, I.; Nyga, R.; Yahiaoui, S.; Gouilleux-Gruart, V.; Régnier, A.; Lassoued, K.; Gouilleux, F. The tumor suppressor hTid1 inhibits STAT5b activity via functional interaction. *J. Biol. Chem.* **2011**, *286*, 5034–5042. [CrossRef] [PubMed]
67. Gooljarsingh, L.T.; Fernandes, C.; Yan, K.; Zhang, H.; Grooms, M.; Johanson, K.; Sinnamon, R.H.; Kirkpatrick, R.B.; Kerrigan, J.; Lewis, T. A biochemical rationale for the anticancer effects of Hsp90 inhibitors: Slow, tight binding inhibition by geldanamycin and its analogues. *Proc. Natl. Acad. Sci. USA* **2006**, *103*, 7625–7630. [CrossRef]
68. Pascale, R.M.; Simile, M.M.; Calvisi, D.F.; Frau, M.; Muroni, M.R.; Seddaiu, M.A.; Daino, L.; Muntoni, M.D.; De Miglio, M.R.; Thorgeirsson, S.S. Role of HSP90, CDC37, and CRM1 as modulators of P16INK4A activity in rat liver carcinogenesis and human liver cancer. *Hepatology* **2005**, *42*, 1310–1319. [CrossRef]
69. Muñoz, J.P.; Ivanova, S.; Sánchez-Wandelmer, J.; Martínez-Cristóbal, P.; Noguera, E.; Sancho, A.; Díaz-Ramos, A.; Hernández-Alvarez, M.I.; Sebastián, D.; Mauvezin, C. Mfn2 modulates the UPR and mitochondrial function via repression of PERK. *EMBO J.* **2013**, *32*, 2348–2361. [CrossRef]
70. Liu, T.; Krysiak, K.; Shirai, C.L.; Kim, S.; Shao, J.; Ndonwi, M.; Walter, M.J. Knockdown of HSPA9 induces TP53-dependent apoptosis in human hematopoietic progenitor cells. *PLoS ONE* **2017**, *12*, e0170470. [CrossRef]
71. Kanehisa, M. Toward understanding the origin and evolution of cellular organisms. *Protein Sci.* **2019**, *28*, 1947–1951. [CrossRef]
72. Almaghlouth, I.; Mohamed, J.; Al-Amoudi, M.; Al-Ahaidib, L.; Al-Odaib, A.; Alkuraya, F. 5-Oxoprolinase deficiency: Report of the first human OPLAH mutation. *Clin. Genet.* **2012**, *82*, 193–196. [CrossRef] [PubMed]
73. Wang, J.; Shanmugam, A.; Markand, S.; Zorrilla, E.; Ganapathy, V.; Smith, S.B. Sigma 1 receptor regulates the oxidative stress response in primary retinal Müller glial cells via NRF2 signaling and system xc−, the Na+-independent glutamate–cystine exchanger. *Free Radic. Biol. Med.* **2015**, *86*, 25–36. [CrossRef] [PubMed]
74. Parl, F.F. Glutathione S-transferase genotypes and cancer risk. *Cancer Lett.* **2005**, *221*, 123–129. [CrossRef] [PubMed]
75. Wiegand, H.; Boesch-Saadatmandi, C.; Regos, I.; Treutter, D.; Wolffram, S.; Rimbach, G. Effects of quercetin and catechin on hepatic glutathione-S transferase (GST), NAD (P) H quinone oxidoreductase 1 (NQO1), and antioxidant enzyme activity levels in rats. *Nutr. Cancer* **2009**, *61*, 717–722. [CrossRef] [PubMed]
76. Karatas, E.; Raymond, A.-A.; Leon, C.; Dupuy, J.-W.; Di-Tommaso, S.; Senant, N.; Collardeau-Frachon, S.; Ruiz, M.; Lachaux, A.; Saltel, F. Hepatocyte proteomes reveal the role of protein disulfide isomerase 4 in alpha 1-antitrypsin deficiency. *JHEP Rep.* **2021**, *3*, 100297. [CrossRef]

77. Francavilla, R.; Castellaneta, S.P.; Hadzic, N.; Chambers, S.M.; Portmann, B.; Tung, J.; Cheeseman, P.; Rela, M.; Heaton, N.D.; Mieli-Vergani, G. Prognosis of alpha-1-antitrypsin deficiency-related liver disease in the era of paediatric liver transplantion. *J. Hepatol.* **2000**, *32*, 986–992. [CrossRef]
78. Herrera-Marcos, L.V.; Martínez-Beamonte, R.; Macías-Herranz, M.; Arnal, C.; Barranquero, C.; Puente-Lanzarote, J.J.; Gascón, S.; Herrero-Continente, T.; Gonzalo-Romeo, G.; Alastrué-Vera, V. Hepatic galectin-3 is associated with lipid droplet area in non-alcoholic steatohepatitis in a new swine model. *Sci. Rep.* **2022**, *12*, 1–17. [CrossRef]
79. Abuobeid, R.; Herrera-Marcos, L.; Navarro, M.A.; Arnal, C.; Martínez-Beamonte, R.; Surra, J.; Osada, J. Dietary erythrodiol modifies hepatic transcriptome in mice in a sex and dose-dependent way. *Int. J. Mol. Sci.* **2020**, *21*, 7331. [CrossRef]

Supplementary Table S1. Sequences of the real-time PCR primers according to the MIQE guidelines

Gene symbol	Primer sequence, sense/antisense (5'->3')	Amplicon length	Accession	Exon	Concentration	Efficiency
Dnaja3	CCCGGCTTACAGCTTCAGAT TGGTCCTAGACAAGAGCCGT	123	NM_001135112.1, NM_023646.4	12	0.2 µM	99%
Hsp90aa1	CCTGACGGACCCCAGTAAAC TCCACAATGGTCAGGGTTCG	90	NM_010480.5	3	0.2 µM	104%
Mfn2	ATTCACTTCAGAGCAGAGCCA CAGGGTGCCATTCTGAGGAA	379	XM_036163781.1, XM_036163780.1, XM_036163779.1, XM_036163778.1, XM_006538609.5, NM_001355590.1, NM_001355591.1, NM_001285922.1, NM_001285920.1, NM_001285921.1, NM_133201.3, NM_001285923.1	18/19	0.2 µM	96%
Rps14	GGGATGAAGATTGGGCGGAT ACGACCCCCTTTTCTTCGAG	72	NM_020600.4	4/5	0.2 µM	95%
Gstm6	CACGTGGGGCAATGAGTAAG TGGAGGCTTGAGTGAAAGGG	207	XM_036162903.1, XM_006501025.4, NM_001379505.1, NM_001379507.1, NM_001379504.1, XM_006501023.1, NM_001379509.1, NM_008184.4, NM_001379506.1, NM_001379510.1, NM_001379508.1	6	0.2 µM	93%
Gstp3	ACCAGATCTCTTTCGCGGAC ATAGGCGGAGAACAGGGGAA	101	XM_006531725.4, XM_011248620.3, XM_030250873.2, XM_030250874.1, NM_144869.3, NM_001362043.1	2	0.4 µM	87%
Gstt1	CACCTCAGCGATGCGTTTG GGTGAAGCCACCATCCATCA	72	NM_008185.3, NM_001358778.1	2	0.2 µM	94%
Npm1	TTCCCAAAGTGGAAGCCAAGT TCTTGGCAAGTGAACCTGGAC	240	NM_001252260.1, NM_008722.3	10/11	0.2 µM	101%
Oplah	CTTCCATTTTGCCATCGACCG GAGCAGCTTCAGGACACGTA	88	XM_006521509.3, XM_030248806.2, XM_006521508.5, XM_006521507.5, XM_030248807.2, NM_153122.3	2	0.2 µM	98%
Prdx5	AGGCACCTCTTTCTGCGATT GATGCACGGAGCACAGAAC	253	NM_012021.3, NM_001358444.1	1	0.2 µM	99%
Serpina1a	GTCTATGCCCCCTATCCTGC CTATTTGCATGGCTGGAGGAG	369	NM_009243.4, NM_001252569.1	5	0.2 µM	98%
Serpina1b	AGAAGGTTAGTCCAGATCCATATCC GGGCATAGACATAGGAACGGC	246	NM_009244.4	4/5	0.2 µM	94%
Serpina3m	GAAGTTTCTGACCACACGCC CAGGTTGTAGTCAGTAGAGATGGAG	235	XM_006515637.2, NM_009253.2	3/4	0.2 µM	96%
Tbp	GTGAGTTGCTTGCTCTGTGC GCTGCGTTTTTGTGCAGAGT	359	NM_013684.3	8	0.2 µM	104%
Ppib	GGAGATGGCACAGGAGGAA TAGTGCTTCAGCTTGAAGTTCTCAT	71	NM_011149.2	3/4	0.2 µM	99%
Txndc5	CAGGCTTGTCAGATGTCACCAT TAACCTCGTACCGAGTACTTGCTG	82	NM_001289599.1, NM_001289598.1, NM_145367.4	9/10	0.2 µM	92%
Prdx6	CAGCAAACAAGGTAGTGTCAGTG AGGCTTTCTGAGCCCACTTC	218	NM_007453.4, NM_001303408.1, XM_030243163.1	7	0.2 µM	95%
Prdx6B	TATGTCACCAACGATGCCGT CCTTTGACAACAGCAGGCAA	134	NM_177256.5	1	0.2 µM	102%
Hspa9	AAAGTGTGTCAGGGGGAACG TCTGTTGCTCACGACCAGTG	181	NM_010481.2	12/13	0.2 µM	93%

Abbreviations: *Dnaja3*, DnaJ heat shock protein family (Hsp40) member A3; *Hsp90aa1*, heat shock protein 90, alpha (cytosolic), class A member 1; *Mfn2*, mitofusin 2; *Rps14*, ribosomal protein S14; *Gstm6*, glutathione S-transferase, mu 6; *Gstp3*, glutathione S-transferase pi 3; *Gstt1*, glutathione S-transferase, theta 1; *Npm1*, nucleophosmin 1; *Oplah*, 5-oxoprolinase (ATP-hydrolysing); *Prdx5*, peroxiredoxin 5; *Serpina1a*, serine (or cysteine) peptidase inhibitor, clade A, member 1A; *Serpina1b*, serine (or cysteine) preptidase inhibitor, clade A, member 1B; *Serpina3m*,

serine (or cysteine) peptidase inhibitor, clade A, member 3M; *Tbp*, TATA-box binding protein; *Ppib*, peptidylprolyl isomerase B; *Txndc5*, thioredoxin domain contalning 5; *Prdx6*, peroxiredoxin 6; *Prdx6B*, peroxiredoxin 6B; *Hspa9*, heat shock protein 9

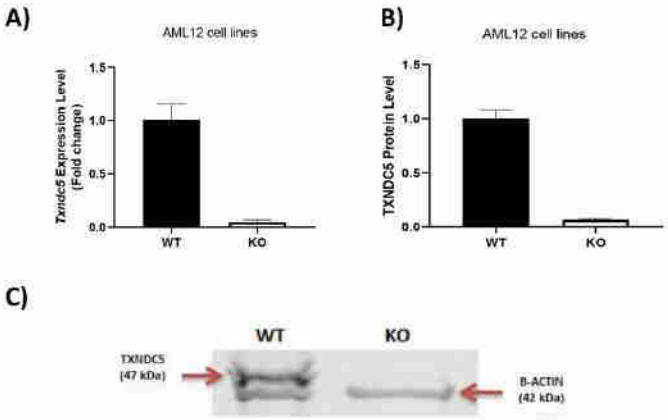

Supplementary Figure S1. Characterization of the AML12 cell lines. **(A)** *Txndc5* mRNA , (**B**) protein levels and (**C**) Western Blot in wildtype (WT) AML12 cells and TXNDC5- knockout (KO) AML12 cells

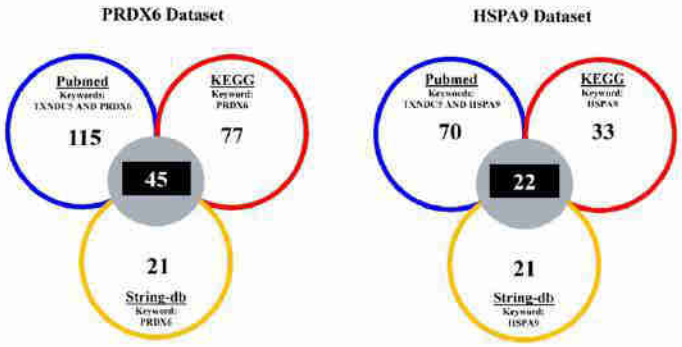

Supplementary Figure S2. Online bioinformatics databases and a PubMed search to confirm and identify the most pertinent genes with TXNDC5, PRDX6, and HSPA9.

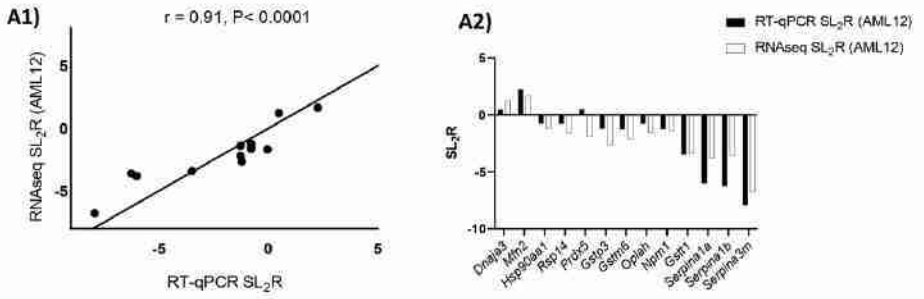

Supplementary Figure S3. Compatibility of RNA analysis techniques. (**A1**) Correlation analysis of 13 selected genes between RNAseq and RT-qPCR normalized to the invariant *Ppib* and *Tbp* genes. The mean values obtained for signal $\log_2$ ratio (SL_2R) from individual analyses in the AML12 cell line. Good agreement between the procedures was observed ($r = 0.91$, $p < 0.0001$). (**A2**) The difference in results of SL_2R expression of both procedures of the 13 selected genes in the AML12 cell line.

International Journal of
Molecular Sciences

MDPI

Article

TXNDC5 Plays a Crucial Role in Regulating Endoplasmic Reticulum Activity through Different ER Stress Signaling Pathways in Hepatic Cells

Seyed Hesamoddin Bidooki [1,2,3,4], Cristina Barranquero [2,5], Javier Sánchez-Marco [1], Roberto Martínez-Beamonte [1,2,5], María J. Rodríguez-Yoldi [2,5,6], María A. Navarro [1,2,5], Susana C. M. Fernandes [3,4] and Jesús Osada [1,2,5,*]

1 Departamento de Bioquímica y Biología Molecular y Celular, Facultad de Veterinaria, Instituto de Investigación Sanitaria de Aragón, Universidad de Zaragoza, E-50013 Zaragoza, Spain; h.bidooki94@gmail.com (S.H.B.); javiersanchezmarc@gmail.com (J.S.-M.); romartin@unizar.es (R.M.-B.); angelesn@unizar.es (M.A.N.)
2 Instituto Agroalimentario de Aragón, CITA, Universidad de Zaragoza, E-50013 Zaragoza, Spain; cbarranq@unizar.es (C.B.); mjrodyol@unizar.es (M.J.R.-Y.)
3 Institute of Analytical Sciences and Physico-Chemistry for Environment and Materials (IPREM), Universite de Pau et des Pays de l'Adour, E2S UPPA, CNRS, 64 000 Pau, France; susana.fernandes@univ-pau.fr
4 MANTA—Marine Materials Research Group, Universite de Pau et des Pays de l'Adour, E2S UPPA, 64 600 Anglet, France
5 Centro de Investigación Biomédica en Red de Fisiopatología de la Obesidad y Nutrición (CIBEROBN), Instituto de Salud Carlos III, E-28029 Madrid, Spain
6 Departamento de Farmacología, Fisiología, Medicina Legal y Forense, Facultad de Veterinaria, Instituto de Investigación Sanitaria de Aragón, Universidad de Zaragoza, E-50013 Zaragoza, Spain
* Correspondence: josada@unizar.es; Tel.: +34-976-761-644; Fax: +34-976-761-612

check for updates

Citation: Bidooki, S.H.; Barranquero, C.; Sánchez-Marco, J.; Martínez-Beamonte, R.; Rodríguez-Yoldi, M.J.; Navarro, M.A.; Fernandes, S.C.M.; Osada, J. TXNDC5 Plays a Crucial Role in Regulating Endoplasmic Reticulum Activity through Different ER Stress Signaling Pathways in Hepatic Cells. *Int. J. Mol. Sci.* **2024**, *25*, 7128. https://doi.org/10.3390/ijms25137128

Academic Editors: Orsolya Kapuy and Beáta Lizák

Received: 31 May 2024
Revised: 27 June 2024
Accepted: 27 June 2024
Published: 28 June 2024

Abstract: The pathogenesis of non-alcoholic fatty liver disease (NAFLD) is influenced by a number of variables, including endoplasmic reticulum stress (ER). Thioredoxin domain-containing 5 (TXNDC5) is a member of the protein disulfide isomerase family and acts as an endoplasmic reticulum (ER) chaperone. Nevertheless, the function of TXNDC5 in hepatocytes under ER stress remains largely uncharacterized. In order to identify the role of TXNDC5 in hepatic wild-type (WT) and TXNDC5-deficient (KO) AML12 cell lines, tunicamycin, palmitic acid, and thapsigargin were employed as stressors. Cell viability, mRNA, protein levels, and mRNA splicing were then assayed. The protein expression results of prominent ER stress markers indicated that the ERN1 and EIF2AK3 proteins were downregulated, while the HSPA5 protein was upregulated. Furthermore, the ATF6 protein demonstrated no significant alterations in the absence of TXNDC5 at the protein level. The knockout of TXNDC5 has been demonstrated to increase cellular ROS production and its activity is required to maintain normal mitochondrial function during tunicamycin-induced ER stress. Tunicamycin has been observed to disrupt the protein levels of HSPA5, ERN1, and EIF2AK3 in TXNDC5-deficient cells. However, palmitic acid has been observed to disrupt the protein levels of ATF6, HSPA5, and EIF2AK3. In conclusion, TXNDC5 can selectively activate distinct ER stress pathways via HSPA5, contingent on the origin of ER stress. Conversely, the absence of TXNDC5 can disrupt the EIF2AK3 cascade.

Keywords: NAFLD; liver; endoplasmic reticulum stress; TXNDC5; ATF6; EIF2AK3; PERK; ERN1; IRE1a; HSPA5; tunicamycin; palmitic acid; thapsigargin; hepatocytes

1. Introduction

Non-alcoholic fatty liver disease (NAFLD) is highly prevalent in the general population [1] and is now the most common liver pathology in Western countries, posing a significant public health concern [2]. NAFLD develops naturally without alcohol abuse, but its precise pathophysiology is still unknown [3,4]. The pathogenic conditions associated

with NAFLD range from simple steatosis to steatohepatitis (NASH) and cirrhosis, which can ultimately result in hepatocellular cancer [5,6]. According to the 'two hits' hypothesis, fat accumulation is the initial step. This accumulation makes the liver more susceptible to the damaging effects of one or more additional factors, leading to the development of steatohepatitis and fibrosis [7]. Multiple factors are believed to contribute to the pathogenesis of NAFLD, including hepatic lipid buildup, insulin resistance, oxidative stress, apoptotic pathways, and adipocytokine production [8].

The endoplasmic reticulum (ER) is the primary organelle for secretory pathways in all eukaryotic cells [9,10]. The ER serves as the entry point into the secretory system and plays a crucial role in maintaining cellular calcium homeostasis, lipid production, and transmembrane protein folding. Therefore, preserving ER homeostasis is a crucial element of cellular physiology [11]. ER processes can be impaired by various factors, leading to the accumulation of unfolded proteins and activation of the unfolded protein response (UPR). The UPR is responsible for restoring ER balance and promoting survival [12–14]. ER stress has been associated with various disorders, such as cardiovascular, endocrine, and nervous system disorders [15,16]. Under sustained and severe ER stress, the UPR can become cytotoxic, leading to apoptosis, instead of being cytoprotective. The UPR signaling pathways involve three distinctive signaling transduction mechanisms: activating transcription factor 6 (ATF6), eukaryotic translation initiation factor 2 alpha kinase 3 (EIF2AK3, also known as protein kinase RNA-like ER kinase, PERK), and endoplasmic reticulum to nucleus signaling 1 (ERN1) [15]. ATF6 is a type II transmembrane protein that serves as an ER stress sensor. It activates chaperones and elements of the endoplasmic reticulum-associated protein degradation (ERAD) pathway [17]. Furthermore, it can activate the target genes DNA-damage inducible transcript 3 (DDIT3), glucose-regulated protein 94 (GRP94), and heat shock protein family A member 5 (HSPA5)/BIP [18]. EIF2AK3 reduces the workload of misfolded proteins by inhibiting mRNA translation during ER stress and limiting further synthesis [19]. To translate activating transcription factor 4 (ATF4), one of the UPR-dependent signaling proteins, EIF2AK3, phosphorylates eukaryotic initiation factor 2 (EIF2α). This process also activates DDIT3, which leads to the production of reactive oxygen species [20,21]. The transmembrane protein ERN1 regulates its own expression and functions as an endoribonuclease and protein kinase. It produces a potent transcription activator called X-box binding protein 1 (XBP1). ERN1 is related to different translocon proteins such as signal sequence receptor, beta (SSR2) and SEC61 translocon subunit alpha 1 (SEC61A1) [22], which may improve the ER's ability to fold proteins [23–25]. HSPA5 detects these proteins and plays a crucial role in managing accumulated proteins [26].

As mentioned, the ER is the site where nascent peptides are correctly folded. A number of redox proteins, including members of the protein disulfide isomerase (PDI) family, interact to coordinate this complex process. TXNDC5, an essential member of the PDI family, participates in a series of disulfide bond exchange events that converge in folding newly synthesized polypeptides into their mature form [27–29]. TXNDC5 protects liver cells from stress-induced apoptosis and is essential for signal transduction and cancer development [30,31]. The aim of this research was to investigate how the TXNDC5 protein interacts in the context of ER stress. Specifically, we aim to examine its role through the three key signaling pathways involved in ER stress: ATF6, EIF2AK3, and ERN1. To this end, mouse hepatocytes with and without TXNDC5 will be exposed to known inducers of ER stress, and the key molecular mechanisms will be investigated. This experimental setup will provide a comprehensive understanding of the functional significance of TXNDC5 in maintaining cellular homeostasis under ER stress conditions.

2. Results

2.1. TXNDC5 Deletion Alters ER Stress-Related Expressions

TXNDC5 was completely knocked out in AML12 cells (KO), as evidenced by significantly decreased mRNA and protein expression levels compared to wild-type AML12 cells (WT) (Supplementary Figure S1). To investigate the role of TXNDC5 in regulating ER stress

markers in AML12 cells, RT-qPCR was performed to assess the mRNA expression of *Atf6*, *Ern1*, *Xbp1*, *Eif2ak3*, *Atf4*, and *Ddit3*; as primary genes involved in the three different ER stress cascades, *Ssr2* and *Sec61a1*; as translocon genes and *Hspa5*; as an ER protein recognition chaperon in WT and TXNDC5-KO AML12 cells. Table 1 shows that the knockout of TXNDC5 in AML12 cells resulted in downregulation of ER genes *Ern1*, *Eif2ak3*, *Xbp1*, and *Sec61α1* compared to WT cells. Additionally, TXNDC5 inactivation significantly increased the mRNA levels of *Hspa5*, *Atf4*, and *Ddit3*. However, the absence of TXNDC5 did not cause any significant change in the mRNA levels of *Atf6* and *Ssr2*. To confirm these results at the protein level, the most prominent ER stress markers were selected for Western blot analysis. The results indicated that the ERN1 and EIF2AK3 proteins were downregulated, while the HSPA5 protein was upregulated. However, the ATF6 protein did not exhibit any significant changes in the absence of TXNDC5 at the protein level. These results are fully compatible with the mRNA expression outcomes and suggest that TXNDC5 plays a critical role in maintaining the stability of ER genes in mouse hepatocytes.

Table 1. The mRNA and protein expression of ER indicators in the absence of TXNDC5 in basal conditions.

Gene or Protein Symbol	mRNA Expression (Fold Change)		Protein Expression (Arbitrary Units)		Changes
	Wild-Type	TXNDC5-KO	Wild-Type	TXNDC5-KO	KO/WT
ATF6	1.0 ± 0.1	1.1 ± 0.2	105 ± 17	87 ± 36	No change
ERN1	1.0 ± 0.1	0.7 ± 0.1	100 ± 11	41 ± 20	Downregulation *
EIF2AK3	1.0 ± 0.1	0.8 ± 0.1	100 ± 9	18 ± 11	Downregulation *
HSPA5	1.0 ± 0.1	1.3 ± 0.2	100 ± 7	131 ± 34	Upregulation *
Xbp1	1.0 ± 0.2	0.4 ± 0.2	NA	NA	Downregulation **
Sec61α1	1.0 ± 0.1	0.7 ± 0.1	NA	NA	Downregulation **
Atf4	1.0 ± 0.2	1.4 ± 0.3	NA	NA	Upregulation **
Ddit3	1.0 ± 0.2	2.4 ± 0.5	NA	NA	Upregulation **
Ssr2	1.0 ± 0.1	0.9 ± 0.1	NA	NA	No change

Data are means and standard deviations. The Mann–Whitney's U-tests were used in the data analyses. * $p < 0.05$, ** $p < 0.01$.

2.2. Effect of ER Stressors (Tunicamycin, Palmitic Acid, or Thapsigargin) on the Survival Rate of AML12 Cell Lines

Both WT and TXNDC5-KO cells were incubated in the presence of pharmacological inducers of the UPR and ER stress: thapsigargin, an inhibitor of the ER calcium pump, tunicamycin, an inhibitor of N-linked glycosylation, and palmitic acid, an inhibitor of thapsigargin-sensitive calcium stores and a representative saturated fatty acid [22,32]. Figure 1 shows the cell viability of WT and TXNDC5-KO cells. After 24 h of exposure to different stressor concentrations, the cell viability of TXNDC5-KO cells was found to be the same as that of WT cells. Based on these results, we selected 12.5 nM of thapsigargin as an inducer of severe stress, with a viability rate of approximately 40% (Figure 1A). We also selected 1 and 20 μg/mL of tunicamycin as conditions of slight and moderate stress, respectively, with viability rates of 90% and 75%, respectively (Figure 1B). Additionally, 600 μM palmitic acid was selected as a representative of substantial stress, with a viability rate of 55% (Figure 1C), to assess the expression patterns of ER stress genes.

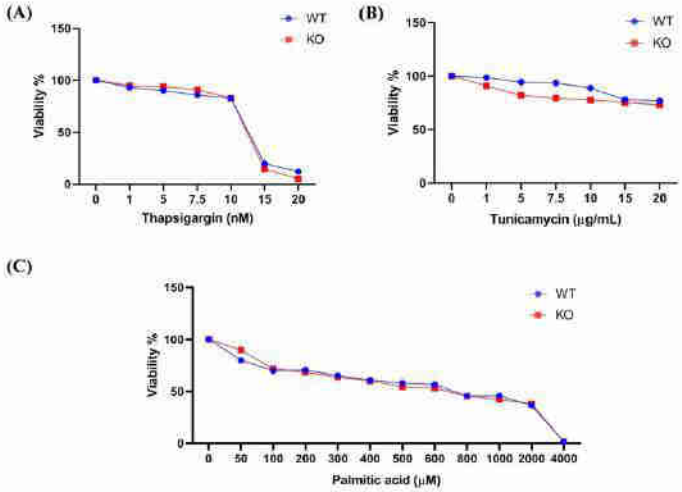

Figure 1. The cell viability evaluation of mouse hepatocytes upon ER stress. After 24 h, treated with different concentrations of thapsigargin, tunicamycin, and palmitic acid, TXNDC5 absence did not produce a substantial difference in cell viability of WT compared to KO cells. Viability rates were indicated in the exposure of (**A**) thapsigargin, (**B**) tunicamycin, and (**C**) palmitic acid. WT: normal mouse hepatocyte AML12 cells, KO: TXNDC5-deficient AML12 cells.

2.3. The Knockout of TXNDC5 Increases Reactive Oxygen Species in Hepatic Cells

The intracellular ROS levels were determined by measuring the dichlorodihydrofluorescein (DCF) production in WT and TXNDC5-KO-AML12 cells. The results, as shown in Figure 2, indicate that TXNDC5-KO cells exhibited a significant increase in ROS production compared to WT cells. This suggests that TXNDC5 regulates ROS production in AML12 cells and its absence leads to an increase in ROS levels. Furthermore, to determine whether ER stressors can induce oxidative stress, WT and TXNDC5-KO cells were incubated with different concentrations of thapsigargin, palmitic acid, and tunicamycin for 24 h. However, no significant increase in intracellular ROS was detected in either group (Figure S2). These results suggest that the concentration used for inducing ER stress did not enhance further ROS production and indicate that these ER stressors may affect different pathways than oxidative stress.

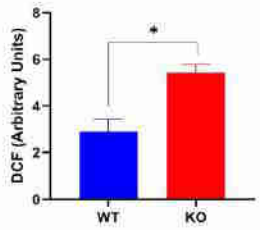

Figure 2. The impact of TXNDC5 deficiency on ROS production. WT: normal mouse hepatocyte AML12 cells, KO: TXNDC5-deficient AML12 cells. Statistical analyses were conducted according to Mann–Whitney's U-test; * $p < 0.05$.

2.4. TXNDC5 Activity Is Required to Maintain Normal Mitochondrial Function during Tunicamycin-Induced ER Stress

As the canonical function of TXNDC5 is to assist protein folding in the ER, we investigated whether depletion of TXNDC5 or induction of ER stress could potentially damage mitochondria. Therefore, we used the loss of mitochondrial membrane potential (MMP) as a biomarker of effect. The tetramethylrhodamine, methyl ester (TMRM) assay was utilized to evaluate the loss of MMP in hepatic cells either by fluorimetric or microscopic procedures. The knockout of TXNDC5 did not significantly affect the mitochondrial function of the cells, as evidenced by the lack of decrease in MMP values (Figure 3A). Additionally, the results indicate a different response to ER stressors. Whereas 6.25 nM thapsigargin (Figure 3B) or 300 µM palmitic acid (Figure 3C) caused a decrease in MMP values, this was not the case for tunicamycin at the tested concentrations of 1 and 20 µg/mL (Figure 3D)) in AML12 WT cells after 24 h. In contrast, TXNDC5-KO cells exhibited altered MMP levels when exposed to tunicamycin at those concentrations, like the other ER stressors, after 24 h of exposure. The results of both procedures in WT cells indicate that tunicamycin did not decrease MMP levels (Figure 3E,F). However, in the absence of TXNDC5, tunicamycin at 20 µg/mL significantly reduced MMP levels. The lack of effect in WT cells may be due to tunicamycin's non-interaction with the mitochondria of AML12 cells. However, in TXNDC5-KO cells, the absence of TXNDC5 may cause damage to the mitochondrial membrane when exposed to tunicamycin. These results suggest that TXNDC5 activity is necessary to maintain normal mitochondrial function during tunicamycin–ER stress.

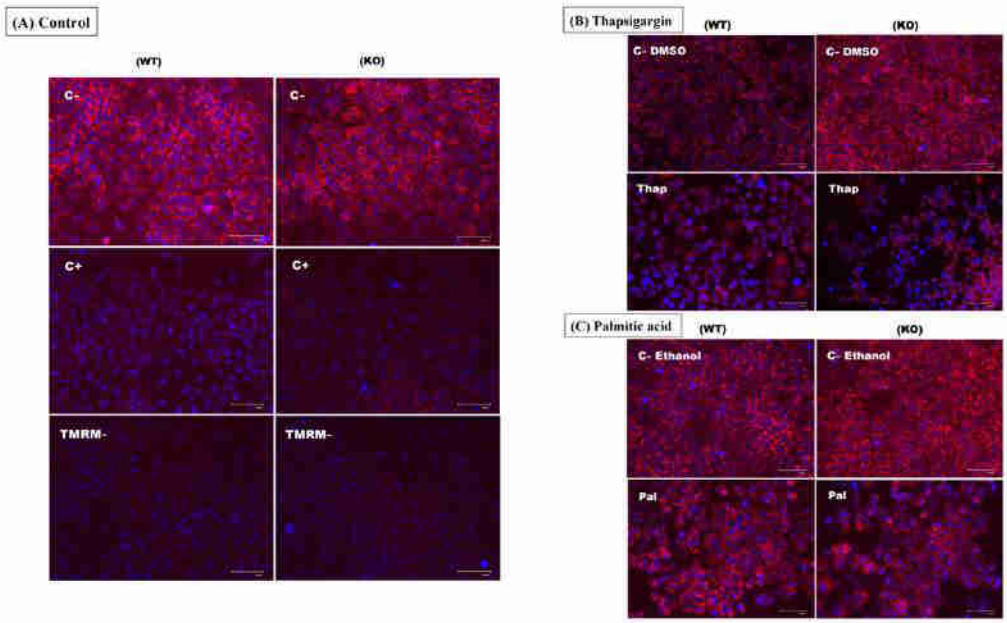

Figure 3. *Cont.*

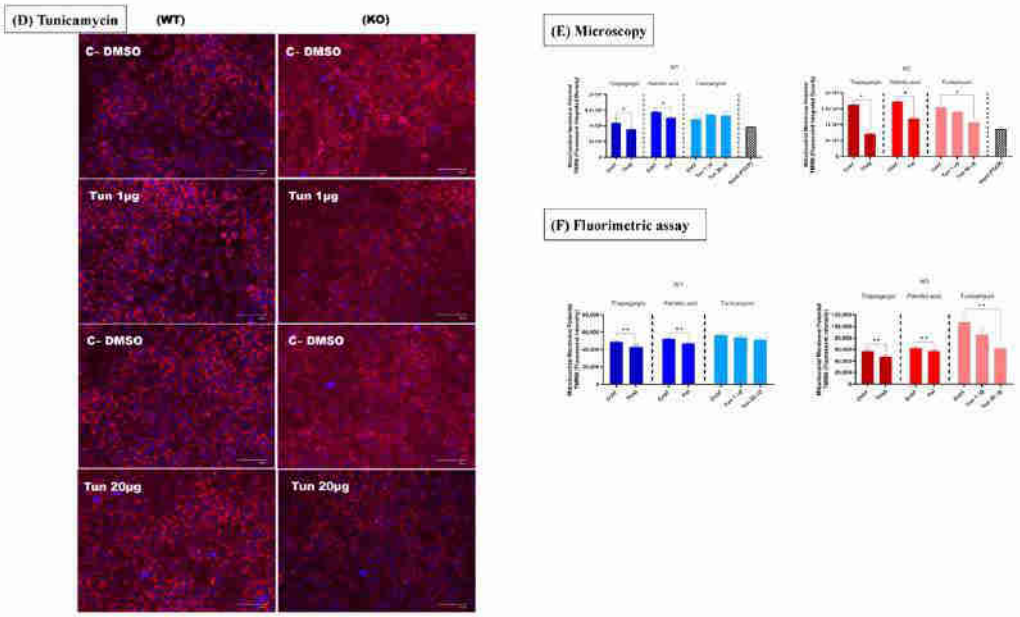

Figure 3. The mitochondrial membrane potential was evaluated using the TMRM assay in the following conditions: (**A**) Control negative (C−) refers to cells that were not subjected to any treatment. Control positive (C+) refers to cells that were treated with carbonylcyanide 4-(trifluoromethoxy)phenylhydrazone (FCCP), an uncoupler that will reduce the mitochondrial membrane potential and prevent staining by TMRM. TMRM negative (TMRM−) refers to cells that were not stained by TMRM. (**B**) (C− DMSO) refers to the cells that were treated with DMSO as a control negative and (Thap) refers to the cells that were treated with 6.25 nM thapsigargin. (**C**) (C− Ethanol) refers to the cells that were treated with ethanol as a control negative and (Pal) refers to the cells that were treated with 300 µM palmitic acid. (**D**) (C− DMSO) refers to the cells that were treated with DMSO as a control negative, (Tun 1 µg) refers to the cells that were treated with 1 µg/mL tunicamycin, and (Tun 20 µg) refers to the cells that were treated with 20 µg/mL tunicamycin. (**A**–**D**) The red-fluorescent probe (TMRM) localizes in mitochondria and detects mitochondrial membrane depolarization. The blue-fluorescent probe (NucBlue) detects the cellular nucleus. (**E**) The fluorescent integrated density of the red probe in the aforementioned conditions was evaluated through fluorescent microscopy, with the resulting data subsequently analyzed using the ImageJ (Fiji) software version windows 64-bit Java 8. (**F**) The fluorescent intensity of TMRM was assessed using a microplate fluorimeter at excitation/emission of 548/575 nm to corroborate the microscopic visualization results. WT: normal mouse hepatocyte AML12 cells, KO: TXNDC5-deficient AML12 cells. The statistical analyses were conducted in accordance with the Mann–Whitney U-test, with the following significance levels: * $p < 0.05$, ** $p < 0.01$.

2.5. The Upregulation of TXNDC5 in Hepatic Cells Is Dependent on Increased ER Stress Induced by Thapsigargin, Palmitic Acid, and Tunicamycin

To investigate whether ER stressors regulate the TXNDC5 promoter through distinct cascades, we transfected mouse TXNDC5 promoter–luciferase constructs into AML12 hepatic cells. AML12 WT cells were treated with thapsigargin, palmitic acid, and tunicamycin, and TXNDC5 promoter–luciferase ratios were quantified. The experiments demonstrated that the TXNDC5 promoter was induced by all stressors (Figure 4A). These data indicate that the upregulation of TXNDC5 in hepatic cells is dependent on increased ER stress in-

duced by thapsigargin, palmitic acid, or tunicamycin. To confirm the results of the TXNDC5 promoter, assays were conducted to quantify Txndc5 mRNA expression and protein level under different stressors. In accordance with the profibrotic effects of TXNDC5 signaling previously described [27], tested stressors were observed to increase the expression and protein level of TXNDC5 in WT cells (Figure 4B,C).

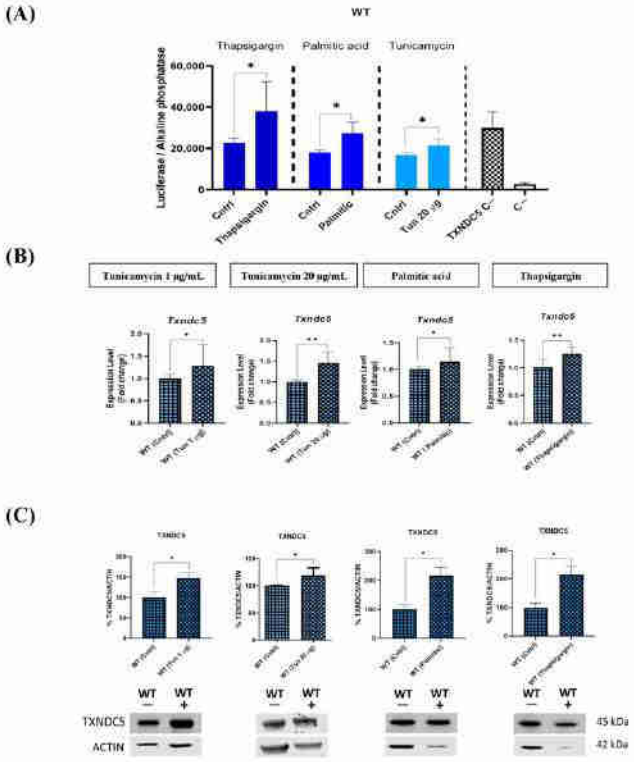

Figure 4. Transcriptional, mRNA, and protein responses of TXNDC5 to different stressors. (**A**) The influence of tunicamycin, palmitic acid, or thapsigargin stressors on the TXNDC5 promoter. The TXNDC5 C− and C− labels represent cells that have been transfected or cells that have not been transfected with the TXNDC5 promoter, respectively, in the absence of stressors. (**B**) mRNA levels of *Txndc5* and (**C**) protein level of TXNDC5 in WT and TXNDC5-KO cells exposed to 1 µg/mL (first column), or 20 µg/mL of tunicamycin (second column), 600 µM palmitic acid (third column), and 12.5 nM thapsigargin (fourth column). Significant augments were observed in TXNDC5 protein and mRNA expression for all stressors. WT: normal mouse hepatocyte AML12 cells, KO: TXNDC5-deficient AML12 cells. The statistical tests were conducted using the Mann–Whitney U-test. The significance levels were: * $p < 0.05$, ** $p < 0.01$.

2.6. Absence of TXNDC5 Abolishes the Induction of ATF6 and HSPA5 Expressions following Palmitic Acid Incubation

As illustrated in Figure 5A, the mRNA expression of *Atf6* was elevated in a variety of ER stress conditions in WT cells. The elimination of TXNDC5 in cells resulted in the abolition of the induction of *Atf6* by palmitic acid, while the changes observed in the presence of tunicamycin or thapsigargin remained unaffected. These results were corroborated at the protein level, although no significant difference was observed in ATF6 protein

expression in WT and TXNDC5-KO cells following tunicamycin exposure. These results demonstrate that tunicamycin can alter the expression of ATF6 at the mRNA level, but not at the protein level. A similar pattern was observed in the case of *Hspa5* mRNA levels (Figure 5B). The deletion of TXNDC5 in cells resulted in the disruption of the induction of *Hspa5* by palmitic acid, while the changes observed in the presence of tunicamycin or thapsigargin remained unaffected. However, the HSPA5 protein level revealed that the absence of TXNDC5 abolished the HSPA5 expression induced by tunicamycin and palmitic acid. Consequently, TXNDC5 plays a pivotal role in the regulation of ATF6 and HSPA5 expression in response to palmitic acid-induced ER stress.

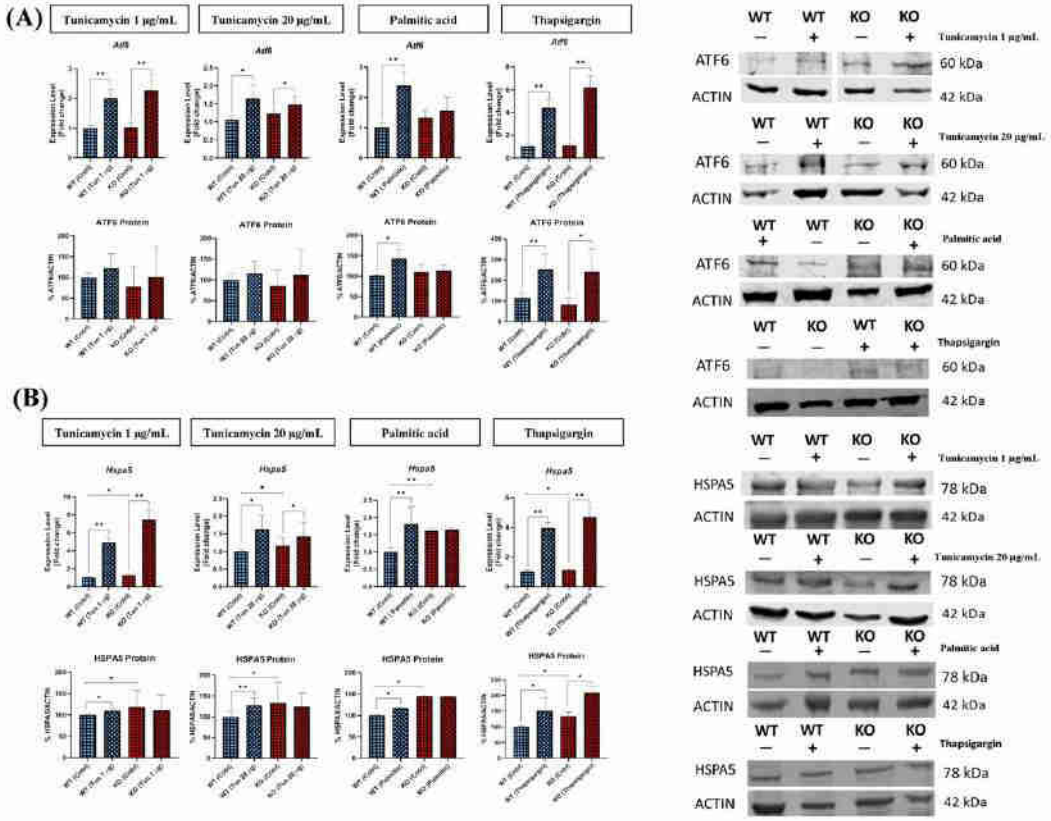

Figure 5. The mRNA and protein levels of (**A**) ATF6 and (**B**) HSPA5 in WT and TXNDC5-KO cells exposed to 1 (first column) or 20 μg/mL (second column) tunicamycin, 600 μM palmitic acid (third column), and 12.5 nM thapsigargin (fourth column). A notable induction was observed for ATF6 and HSPA5 mRNA and protein levels in WT cells under ER stress conditions. In the presence of palmitic acid, ATF6 levels remained unaltered in TXNDC5-KO cells. TXNDC5-KO cells demonstrated no alterations in HSPA5 expression in the presence of palmitic acid and tunicamycin. WT: normal mouse hepatocyte AML12 cells, KO: TXNDC5-deficient AML12 cells. Statistical analyses were conducted according to Mann–Whitney's U-test; * $p < 0.05$, ** $p < 0.01$.

2.7. EIF2AK3 Cascade Is Disrupted in TXNDC5 Knockout Cells Exposed to Tunicamycin and Palmitic Acid

To ascertain the impact of TXNDC5 depletion on the EIF2AK3 cascade, previously designated as PERK, the mRNA and protein expression levels of EIF2AK3 were quantified. Following incubation with the three stressors, elevated *Eif2ak3* expressions were observed in WT cells (Figure 6A). However, the protein levels of EIF2AK3 showed a different pattern and displayed decreases following tunicamycin and palmitic acid, respectively. Conversely, the absence of TXNDC5 abolished the observed changes. Of note, thapsigargin induced the EIF2AK3 in both WT and TXNDC5-KO cells despite the profound decrease in EIF2AK3 expression in TXNDC5-KO cells (Figure 6A).

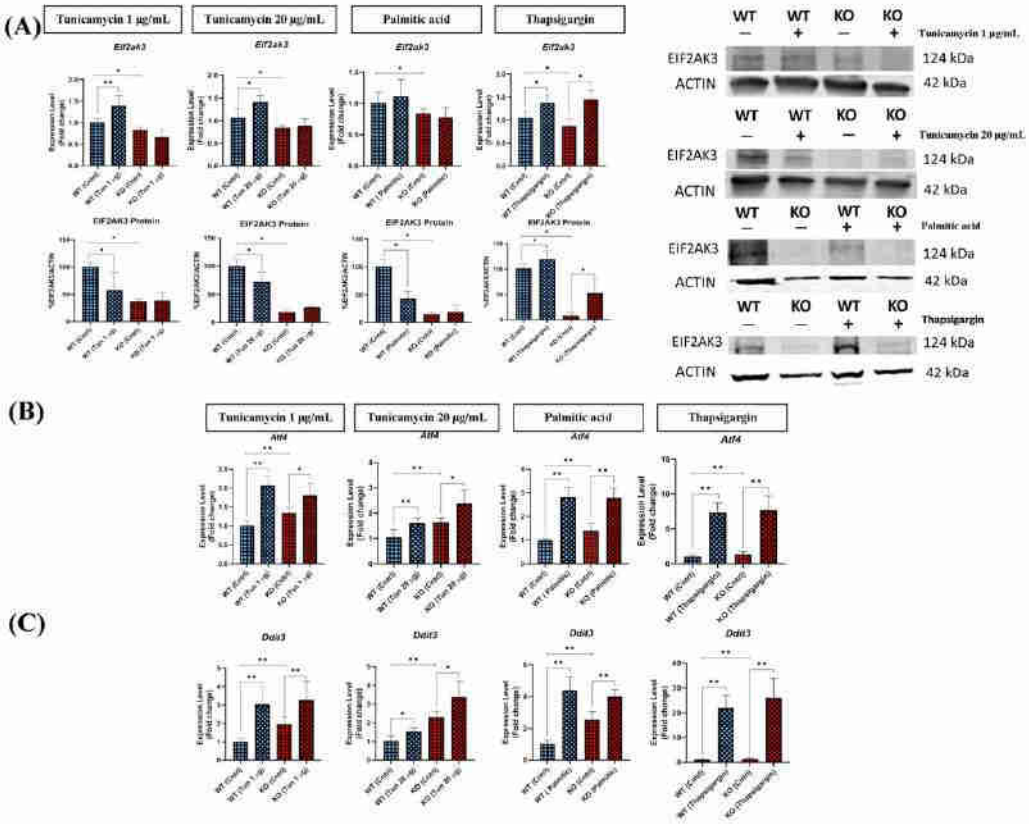

Figure 6. Expression level of (**A**) EIF2AK3, (**B**) *Atf4*, and (**C**) *Ddit3* in WT and TXNDC5-KO cells subjected to the 1 μg/mL tunicamycin (first column), 20 μg/mL tunicamycin (second column), palmitic acid (600 μM) (third column), and thapsigargin (12.5 nM) (fourth column). All WT cells exhibited *Eif2ak3* expression changes, whereas TXNDC5-KO cells demonstrated no alterations in ER stress, with the exception of thapsigargin. The EIF2AK3 protein levels were downregulated in WT cells in the presence of tunicamycin and palmitic acid. However, this downregulation was not observed in TXNDC5-KO cells. The mRNA levels of *Atf4* and *Ddit3* in WT and TXNDC5-KO cells exhibited a significant induction under conditions of ER stress. WT: normal mouse hepatocyte AML12 cells, KO: TXNDC5-deficient AML12 cells. Mann–Whitney's U-test was used for statistical analysis; * $p < 0.05$, ** $p < 0.01$.

To evaluate the effect of EIF2AK3 disruption, the mRNA expression of other members of the EIF2AK3 cascade, including *Atf4* (Figure 6B) and *Ddit3* (Figure 6C), was assessed. There were significant increases in the mRNA levels of these genes in both WT and TXNDC5-KO cells exposed to ER stressors. Furthermore, the absence of TXNDC5 did not result in a decrement in mRNA levels of *Atf4* and *Ddit3* in TXNDC5-KO cells compared to WT cells. Consequently, TXNDC5 plays a prominent role in the stability of the EIF2AK3 cascade in tunicamycin and palmitic acid conditions, although it did not affect the *Atf4* and *Ddit3* mRNA expressions in hepatic cells.

2.8. TXNDC5 Deficiency Alters the ERN1 Pathway in Tunicamycin ER Stress

To evaluate the effects of TXNDC5 on the ERN1 cascade, previously known as IRE1, the mRNA levels of key members of this ER pathway were examined. In fact, *Ern1* exhibited elevated mRNA levels in WT and TXNDC5-KO hepatic cells following treatment with various ER stress inducers (Figure 7A). Nevertheless, this increase was not observed in WT cells in the tunicamycin condition at the protein level. The data indicated that TXNDC5 deficiency resulted in changes in ERN1 protein levels in tunicamycin stress and the ERN1 protein expression was not affected by the absence of TXNDC5 in the context of palmitic and thapsigargin stress. To elucidate the role of XBP1 in this pathway in AML12 cells, as shown in Figure 7B, *Xbp1* expression was significantly induced in tunicamycin ER stress circumstances in both WT and TXNDC5-KO cells. However, there was not a significant induction in thapsigargin and palmitic conditions. These findings demonstrate that the absence of TXNDC5 does not alter the expression of *Xbp1*, and that palmitic acid and thapsigargin are unable to induce the mRNA expression of *Xbp1*. To directly observe the activation of the ERN1–XBP1 pathway in mouse hepatic cells, estimation of *Xbp1* mRNA splicing intensity was employed. This analysis revealed that *Xbp1* mRNA splicing was significantly elevated in the ER stress induced by thapsigargin compared to the control group (Figure 7C). In accordance with the level of *Xbp1* mRNA splicing observed in the thapsigargin condition, TXNDC5-KO cells exhibited a higher spliced form than WT cells (Figure 7D). In conclusion, these findings indicate that the ERN1–XBP1 pathway is activated under conditions of thapsigargin ER stress in this hepatic cell line, and that the absence of TXNDC5 can induce the *Xbp1* spliced form. Moreover, the upregulation of ERN1 may alter the splicing pattern of *Xbp1*, rather than merely influencing its mRNA expression.

2.9. Expression of Ssr2 and Sec61α1 ER Protein-Translocon Channels Are Selectively Influenced by the Absence of TXNDC5

A significant proportion of the most robust and selective ERN1 transcriptional targets identified in the UPR experiments were ER protein-translocon channels or their associated proteins [22]. As illustrated in Figure 8A, all stressors tested failed to induce the *Ssr2* gene in WT and TXNDC5-KO cells, with the exception of palmitic acid, which induced *Ssr2* mRNA expression in WT cells. This result indicates that the absence of TXNDC5 can impede the activation of *Ssr2* in response to palmitic acid exposure. However, when *Sec61α1* mRNA expression was assayed, it was observed that the different ER stressors induced its expression in WT and TXNDC5-KO cells, with the exception of the tunicamycin condition. In the presence of tunicamycin (Figure 8B), the induction of this gene was particularly dependent on TXNDC5, such that *Sec61α1* mRNA levels could not be induced in TXNDC5-KO hepatic cells. The outcomes demonstrated that the expression of *Ssr2* and *Sec61α1* ER protein-translocon channels is selectively influenced by the absence of TXNDC5 depending on the used stressor.

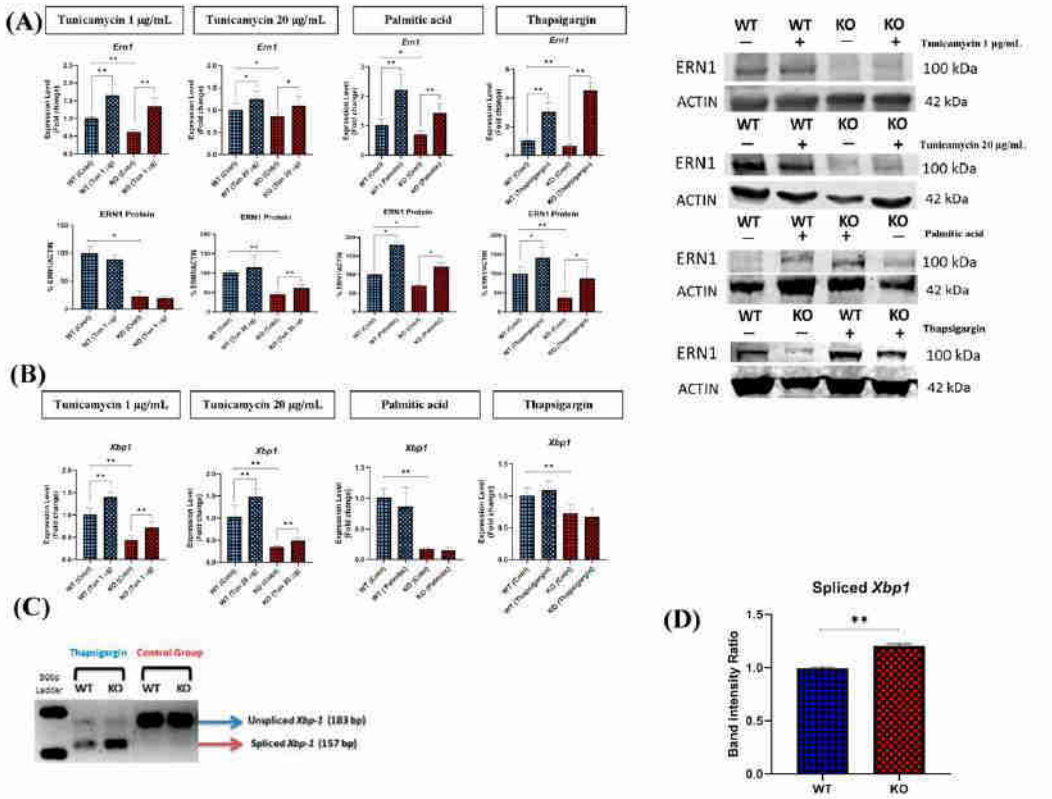

Figure 7. (**A**) Protein and mRNA levels of ERN1 and (**B**) *Xbp1* transcripts in WT and TXNDC5-KO cells exposed to the 1 μg/mL tunicamycin (first column), 20 μg/mL tunicamycin (second column), palmitic acid (600 μM) (third column), and thapsigargin (12.5 nM) (fourth column). A notable elevation in the level of *Ern1* mRNA was observed in both TXNDC5-KO and WT cells in response to all stressors. However, WT cells exhibited no discernible increase in the level of ERN1 protein compared to TXNDC5-KO cells in the presence of tunicamycin. In both WT and TXNDC5-KO cells, there were no changes in *Xbp1* mRNA levels in response to palmitic acid or thapsigargin. (**C**) Cells revealed a substantial spliced form of *Xbp1* mRNA in stress induced by thapsigargin. (**D**) The band intensity ratio of TXNDC5-KO cells showed significant induction of spliced form of *Xbp1* under ER stress conditions compared to the WT cells. WT: normal mouse hepatocyte AML12 cells, KO: TXNDC5-deficient AML12 cells. Statistical analysis was carried out by Mann–Whitney U-test; * $p < 0.05$, ** $p < 0.01$.

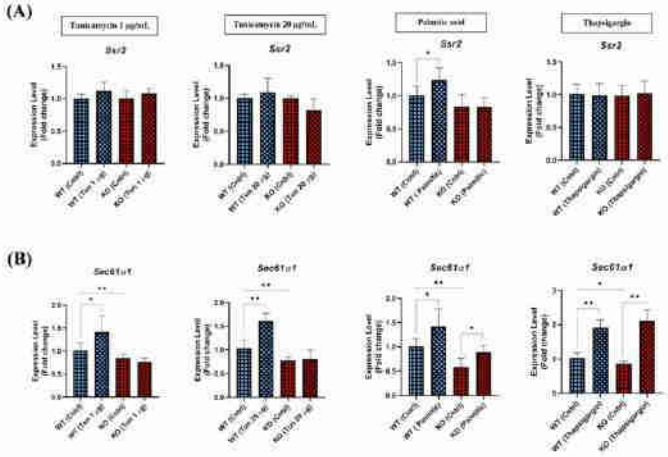

Figure 8. The mRNA levels of the (**A**) *Ssr2* and (**B**) *Sec61α1* genes were quantified in WT and TXNDC5-KO cells exposed to the following treatments: 1 µg/mL tunicamycin, 20 µg/mL tunicamycin, 600 µM palmitic acid, and 12.5 nM thapsigargin. The expression level of *Ssr2* was found to be increased only in WT cells exposed to palmitic acid. The expression of *Sec61α1* was elevated in WT and TXNDC5-KO cells subjected to palmitic acid and thapsigargin stress, and there was a disruption in TXNDC5-KO cells relative to WT cells in the presence of tunicamycin. WT: normal mouse hepatocyte AML12 cells, KO: TXNDC5-deficient AML12 cells. Mann–Whitney U-test was used for statistical analysis; * $p < 0.05$, ** $p < 0.01$ were considered significant.

3. Discussion

The objective of this work was to investigate the influence of TXNDC5 on gene and protein expressions associated with ER stress pathways. To this end, a hepatic cell line lacking TXNDC5 was generated. The results demonstrated that TXNDC5 deficiency resulted in reduced *Ern1*, *Xbp1*, *Eif2ak3*, and *Sec61a1* expression, increased *Hspa5*, *Atf4*, and *Ddit3* expression, and did not change *Atf6* and *Ssr2* expressions. At the protein level, the absence of TXNDC5 was associated with a reduction in ERN1 and EIF2AK3 expression, while the HSPA5 protein was upregulated. Nevertheless, the ATF6 protein did not exhibit any change. The absence of TXNDC5 did not alter the pattern of mortality induced by the three known ER stressors, tunicamycin, palmitic acid, and thapsigargin, in the AML12 cell line, despite the observed enhancement of cellular ROS levels in TXNDC5-deficient cells. Nevertheless, it is evident that TXNDC5 is solely responsible for the maintenance of mitochondrial ROS levels during tunicamycin-induced ER stress. The use of these three agents resulted in elevated *Atf6*, *Hspa5*, *Atf4*, *Ddit3*, *Ern1*, and *Sec61a1* expressions in WT AML12 cells, with the exception of a lack of induction of *Eif2ak3*, *Xbp1*, and *Ssr2* in the presence of palmitic acid, thapsigargin, and tunicamycin, respectively.

A more complex outcome was observed in TXNDC5-deficient cells. In this context, while ATF6, HSPA5, and EIF2AK3 demonstrated no induction of expression in the presence of palmitic acid and tunicamycin, induction was observed in ERN1. *Xbp1* and *Ssr2* exhibited similar expression patterns to those observed in WT cells. However, in the presence of thapsigargin, the absence of TXNDC5 facilitated the splicing of *Xbp1*. Nevertheless, the expression of *Sec61a1* was disrupted by the lack of TXNDC5 in the presence of tunicamycin. Overall, TXNDC5 may regulate ER activity and is particularly involved in the palmitic acid-induced response of ATF6 and HSPA5 genes, as well as an attenuated response of EIF2AK3 signaling.

TXNDC5 has been linked to a multitude of cellular processes as an ER molecular chaperone, as evidenced by previous research [29]. As illustrated in Table 1, TXNDC5

deficiency was associated with reduced expression of ERN1, EIF2AK3, *Xbp1*, and *Sec61a1*, while expressions of HSPA5, *Atf4*, and *Ddit3* were elevated. Other studies have also demonstrated a correlation between TXNDC5 and these proteins. In this context, the fragmentation of the ER and the altered expression of numerous ER proteins, including ATF6, HSPA5, ATF4, and CCAAT/enhancer-binding protein homologous protein, are caused by the downregulation of TXNDC5 in pancreatic β-cells [33–35]. In addition, low TXNDC5 levels have been observed to result in increased expression levels of HSPA5, *Ddit3*, and *eIF2a*, which collectively lead to ER stress and an increase in misfolded proteins in pancreatic β-cells [34]. In summary, TXNDC5 can activate ER stress cascades via HSPA5, either directly or indirectly.

In this report, three stressors have been utilized: tunicamycin, an inhibitor of GlcNAc phosphotransferase, causes a significant accumulation of unfolded proteins, activates the UPR, increases *Txndc5*, and ultimately results in cell death by apoptosis in human head-and-neck carcinoma cells [36]. Palmitic acid is a saturated fatty acid that causes ER stress and increases the UPR in well-differentiated hepatocyte cell lines [37,38]. Thapsigargin, an inhibitor of Ca^{2+} ATPase, alters the concentration of Ca2+ within the ER lumen of mouse hepatocytes [39]. In the current study, all of the agents induced dose-dependent mortality in AML12 cells (Figure 1) and promoted TXNDC5 expression (Figure 4). It has been demonstrated in various studies that *Txndc5* is overexpressed in laryngeal squamous carcinoma cells, colorectal cancer cells, and liver and kidney cells under circumstances of ER stress [40–42]. In light of these observations, it can be postulated that TXNDC5 plays a role in the ER stress response induced by these agents and may act as a protective factor. However, the absence of TXNDC5 did not result in any alterations to the survival patterns, in stark contrast with other agents such as H_2O_2 [28]. Consequently, the absence of TXNDC5 is insufficient to alter cell survival in response to these ER stressors.

Our findings indicate that the deficiency of TXNDC5 can markedly induce cellular ROS in hepatocytes (Figure 2). These data corroborate the previous results demonstrating the enhancement of ROS in the absence of TXNDC5 in endometrial, ovarian, and colorectal tissues. In endometrial cancer cells where NR4A1 is silenced, the major source of ROS is associated with the downregulation of TXNDC5 and IDH1. This is supported by a significant increase in ROS and oxidative/ER stress after the silencing of TXNDC5 [43]. The ER has dynamic membrane contact with mitochondria, which are referred to as mitochondria–ER contacts. This contact plays an important role in regulating mitochondrial function. For instance, calcium transfer at these sites could cause calcium overload in mitochondria and initiate apoptosis. The malfunction of mitochondria and the disruption of protein translocation, translation, and folding within this organelle may result in the phenomenon of "mitochondrial stress". ER stress and mitochondrial stress initiate a shared downstream signaling pathway that represses global translation through phosphorylation of eIF2a [44]. The results demonstrated that the absence of TXNDC5 was unable to induce mitochondrial ROS in hepatocytes. Notwithstanding, these results diverge in the context of ER stress. All ER stressors reduced mitochondrial membrane potential in TXNDC5-KO cells. In WT cells, the presence of tunicamycin resulted in TXNDC5 maintaining mitochondrial stability, with no reduction in mitochondrial membrane potential observed (Figure 3). In this context, our previous findings indicate that TXNDC5 directly interacts with HSPA9 as a mitochondrial chaperone protein involved in protein folding and transport. The downregulation of HSPA9 in hepatocytes following the knockdown of TXNDC5 suggests that this protein may play a significant role in protecting mitochondria against tunicamycin [45].

The absence of TXNDC5 did not influence the expression of ATF6 in the presence of tunicamycin and thapsigargin (Figure 5A), but did suppress the induction raised by palmitic acid. Prior research has identified a unique positive feedback loop of the TGF1–ATF6–TXNDC5–TGFBR1 signaling axis in kidney, heart, and lung fibroblasts. This loop begins with TGF1, which causes the induction of TXNDC5 through ER stress and ATF6-mediated transcriptional control [46–50]. Our findings indicate that TXNDC5 may play a role in certain circumstances. Two ER stressors (tunicamycin and thapsigargin) do not

appear to influence ATF6 levels, whereas palmitic acid appears to require TXNDC5 to induce this ATF6 effect (Figure 9).

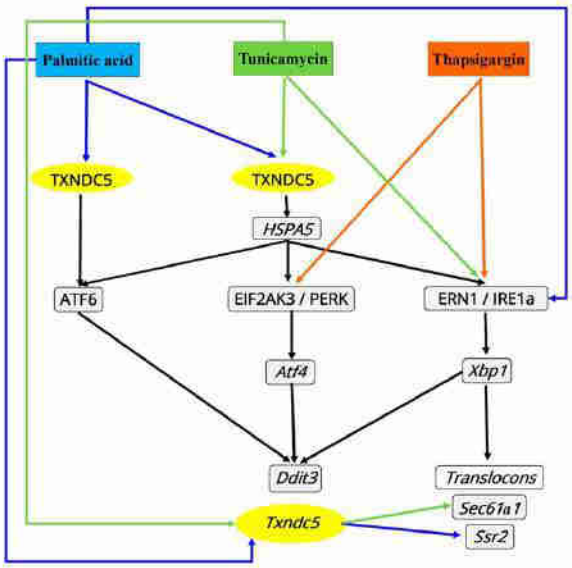

Figure 9. Putative involvement of TXNDC5 on the effect of ER stress triggers in the three different ER stress cascades.

The detachment of the chaperone HSPA5 from the luminal portion of the ER integral membrane proteins EIF2AK3, ERN1, and ATF6 is a crucial process in the activation of ER stress in human leukemia and bladder carcinoma cell lines [51]. Lee et al. demonstrated that the orphan nuclear receptor 4A1 (NR4A1) is tightly linked to *Txndc5*-induced transcriptional activity, and that defragmentation of the ER and altered expression of *Hspa5* are outcomes of *Txndc5* downregulation in pancreatic malignant cells [35]. The results obtained from the hepatic AML12 cell line indicate that the expression of HSPA5 is altered by the absence of TXNDC5 (Table 1). Furthermore, our results demonstrate that, in the absence of TXNDC5, ER stressors modify the protein level of HSPA5, with the exception of palmitic acid as a saturated fatty acid (Figure 5B). This observation provides evidence that HSPA5 may be involved in lipid metabolism, in addition to TXNDC5 [52]. In this context, HSPA5 exhibited elevated protein and mRNA levels in the group of rats fed a high-fat diet [53]. Furthermore, obese mice exhibited elevated hepatic levels of *Hspa5* mRNA in response to ATF6 and EIF2AK3 activation. In addition, *Hspa5* overexpression in hepatocytes reduces ER stress indicators, inhibits SREBP1c cleavage, and suppresses the transcription of SREBP1c and SREBP2 target genes, resulting in a significant reduction in hepatic cholesterol levels [54]. Furthermore, the activation of JNK as a central mediator of palmitic acid-induced hepatic lipoapoptosis causes the suppression of *Hspa5* in this cell line [55,56]. This saturated fatty acid has been demonstrated to induce lipotoxicity and insulin resistance in both mouse and human hepatocytes [32]. On the other side, our previous findings indicate that TXNDC5 is directly involved in the regulation of PRDX6 and the absence of TXNDC5 results in the downregulation of PRDX6 [45]. Therefore, the results of this study provide further evidence to support the link between TXNDC5 and the HSPA5 response to palmitic acid and it is possible that PRDX6 is involved in this pathway through a protein depalmitoylation [57].

The impact of TXNDC5 depletion on the EIF2AK3 cascade, previously designated as PERK, was also investigated. In the wild-type cell line, the mRNA expression levels of

ER stress-related markers, including *Eif2ak3*, *Atf4*, and *Ddit3*, were found to be elevated in response to various ER stressors. The protein expression of EIF2AK3 exhibited a disparate pattern in tunicamycin and palmitic acid exposure, indicating that these stressors are involved in post-transcriptional regulation. However, TXNDC5-deficient AML12 hepatocytes exhibited a disruption in EIF2AK3 expression in the presence of tunicamycin and palmitic acid (Figure 6A). Negative feedback loops within the UPR result in a rapid downregulation of EIF2AK3-EIF2α signaling in CHO cells, due to the upregulation of *Ddit3* and its targets [58]. Furthermore, the reduction of EIF2AK3-EIF2α signaling has been observed to result in the development of diabetes phenotypes in mouse models of EIF2AK3 deficiency [59]. Conversely, the disruption of the EIF2AK3 pathway has been observed to result in the enhanced production of ROS [3] during ER stress in mouse fibroblasts [60]. The expression levels of *Eif2ak3* and *Txndc5* in NIH-3T3 fibroblasts exhibited a gradual increase over time under stressful conditions [48], suggesting a coordinated regulatory mechanism. On the other side, thapsigargin was found to promote the phosphorylation of EIF2AK3, which was markedly reduced by overexpression of *Hspa5* in hepatic steatosis in mice [39]. Thapsigargin was an exception in our experimental setting. In fact, the expression of EIF2AK3 in the presence of thapsigargin could be effectively stimulated in the absence of TXNDC5. Consequently, our findings indicate that TXNDC5 is essential for the induction of EIF2AK3 expression under specific stressful conditions in hepatocytes (Figure 10).

The absence of TXNDC5 had no effect on the expression of *Atf4* and *Ddit3* in AML12 cells under ER stress, as demonstrated in Figure 6B,C. Recent studies have demonstrated that the expression of *Atf4*, *Ddit3*, and apoptosis induced by NR4A1 (a modulator of TXNDC5) silencing regulates ER stress in MCF-7, RKO, MDA-MB-231, and Jurkat cell lines [35]. DDIT3 deletion has been observed to partially protect both cells and animals from ER stress-induced cell death, in contrast to overexpression of *Ddit3*, which has been shown to trigger cell death in the absence of other stimuli [61]. DDIT3 has been linked to the overexpression of death receptor 5 (DR5) and the downregulation of the anti-apoptotic protein BCL2 [62,63]. In contrast, DNA damage-inducible 34 protein (GADD34) has recently been identified in mouse fibroblasts as a target of DDIT3. Consequently, deletion of either DDIT3 or GADD34 protects cells against acute ER stress-induced cell death [64]. Consequently, the absence of TXNDC5 does not appear to suppress *Atf4* and *Ddit3* expression in AML12 cells under ER stress, suggesting that these cells may be induced to apoptosis. Our findings also indicate that TXNDC5 is not directly involved in the upregulation of *Atf4* and *Ddit3* expression in hepatocytes under ER stress conditions.

The reduction in one of the three ER stress markers frequently results in the activation of other ER stress markers in secretory goblet cells [65]. Both the EIF2AK3 and ERN1 pathways are implicated in the control of ER chaperones, ER-associated degradation, and other protective activities in mouse embryonic cells, NIH-3T3 fibroblasts, human embryonic kidney 293, and Phoenix-Eco cells [60,66–69]. Tsuchiya et al. also observed an increase in *Eif2ak3* expression in MIN6 cells lacking ERN1 protein [70]. Consequently, the disruption of EIF2AK3 in TXNDC5-deficient AML12 cells may result in increased ER stress and the activation of other ER stress sensors (Figure 10), such as ERN1. Indeed, the expression patterns of hepatocytes indicated that the expression of ERN1 could be increased in the context of ER stress when the expression of EIF2AK3 is disturbed in the absence of TXNDC5, as compared to the WT cells (Figures 6A and 7A). It can be postulated that TXNDC5 plays a dynamic role in ER stress protection between the EIF2AK3 and ERN1 pathways in mouse hepatocytes, which is independent of the proapoptotic Bax (BCL2-associated X protein) and Bak (BCL2 antagonist of cell death) proteins, which have the potential to enhance ERN1 signaling [71,72]. This could explain why, despite the observed enhancement of ERN1 expression and EIF2AK3 disturbance, no changes in cell mortality were observed in TXNDC5-deficient hepatocytes.

X-box binding protein 1 (*Xbp1*) mRNA is the substrate of the endoribonuclease ERN1, which removes a 26-base intron [73]. It has been demonstrated that mice lacking ERN1 and XBP1 exhibit embryonic defects in liver formation and B lymphocyte differentiation [74,75].

The ERN1–XBP-1 signaling pathway has been linked to TXNDC5, as evidenced by the observation that the pharmacological inhibition of ERN1 and knockdown of XBP1 resulted in a reduction in TXNDC5 expression in pulmonary fibroblasts [48]. However, the present study in mouse hepatocytes indicates that the absence of TXNDC5 is associated with a reduction in *Xbp1* expression compared to the WT cells (Figure 7B). Moreover, it was observed that the absence or presence of TXNDC5 did not result in the induction of *Xbp1* by palmitic acid and thapsigargin.

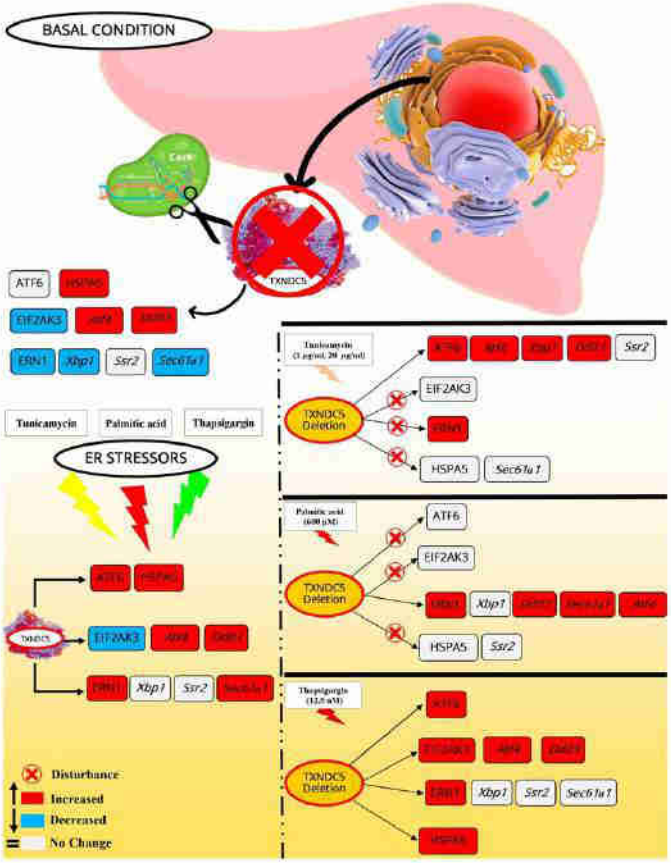

Figure 10. A summary of the findings of mRNA and protein expressions of ER stress sensors and their associated genes in response to different ER stressors, with and without TXNDC5. The scheme was created using Microsoft Publisher 2010. The symbols used to indicate the effects of ER stress on the expression of genes are as follows: red cross, disturbance in cascade; red color, increased expression; blue color, decreased expression; and white color, no changes.

Chen et al. proposed that ERN1 may regulate TXNDC5 through *Xbp1* mRNA splicing in lung fibroblasts [48] and that it plays a role in NAFLD, in which DDIT3, caspase-12, and JNK participate in ER stress by enhancing its activities [76]. In contrast, autophosphorylation of ERN1 may activate downstream genes without causing the *Xbp1* mRNA splicing, suggesting that ERN1 can exist in more states than just "on" and "off" in mouse embryonic fibroblasts and human pancreatic beta cells [77,78]. It has been postulated

that XBP1 may interact with TXNDC5 indirectly [29], through binding to the promoter regions of downstream target genes, including HSPA5 in C2C12 myoblasts and MIN6 cells. This interaction may modulate *Txndc5* expression [79]. Our findings demonstrate that thapsigargin is an effective agent for converting *Xbp1* from its unspliced form to the spliced variant. Furthermore, the absence of TXNDC5 results in an increase in the latter form in AML12 cells (Figure 7C,D). In conclusion, the absence of TXNDC5 in hepatocytes modulates the splicing process of *Xbp1* in the context of thapsigargin exposure in the ERN1 cascade, which points to the role of TXNDC5 and its mRNA expression in this particular splicing process, and it is possible that ERN1 affects *Xbp1* splicing, not just its mRNA.

ERN1 and XBP1 target the translocon and translocon auxiliary components in mouse embryonic fibroblasts and HEK293T cells [66,80]. Studies in HeLa and Cos-7 cells have shown that XBP1 splicing is maximized when ERN1 binds to the translocons and SRP recruits unspliced XBP1 (XBP1u) to the ER [81,82]. This suggests that ERN1 may act in physical association with the translocons, unlike ATF6 or EIF2AK3 [82]. SEC61A1, which encodes an ER protein–translocation channel, and SSR2, a translocon auxiliary protein, are involved in SRP-mediated protein targeting to the ER [22]. Furthermore, repression of the SEC61A1 translocon subunits appeared to exclusively and specifically activate the ERN1 branch and also upregulated the SSR2 in human embryonic kidney cells and mouse embryonic fibroblasts [22,83]. The present report indicates that the *Ssr2* expression was not significantly induced by ER stress in TXNDC5 knockout cells (Figure 8A), although it was only induced by palmitic acid in WT cells. In contrast, the expression of *Sec61a1* was augmented in WT cells via all ER stressors. However, its expression exhibited no alterations in tunicamycin exposure in TXNDC5-KO cells (Figure 8B). This observation corroborates previous findings indicating that *Sec61a1* expression is uniquely regulated by the ERN1 cascade [80]. Moreover, translocons may also be regulated by other mediators, such as DDIT3 and HSPA5. The suppression of SEC61A1 and SEC61B has been observed to stimulate *Ddit3* expression in myelogenous leukemia cells [84]. However, DDIT3 was upregulated in SEC61A1-induced HeLa cells [85], which is consistent with our findings. In addition, *Txndc5*, *Sec61a1*, and *Ssr2* are upregulated in XBP-1-transduced NIH-3T3 fibroblasts and murine macrophage cells [86,87]. However, another study indicated that in the presence of sertraline as an anti-stress drug in HepG2 cells, the mRNA level of *Txndc5* decreased and *Ssr2* and *Ern1* increased [88]. Consequently, it is plausible that the regulation of translocons by DDIT3 and HSPA5 is contingent upon the specific tissue in question. These results indicate a feedback paradigm where TXNDC5 can regulate translocon expression by modulating the expression of the ERN1 cascade via the XBP1 mediator in ER stress conditions. Additionally, ERN1 may be utilized to monitor the status of the translocon in mouse hepatocytes. Furthermore, the expression of *Ssr2* and *Sec61a1* ER protein–translocon channels is selectively influenced by the absence of TXNDC5, with the influence dependent on the source of ER stress.

4. Materials and Methods

4.1. Generation of TXNDC5 Knockout AML12 Cells

The Alpha mouse liver (AML12) cell line with a stable knockout of TXNDC5 was generated as previously described [28]. The cells were transfected with TXNDC5/ERp46 HDR and TXNDC5 CRISPR/Cas9 KO plasmids (Santa Cruz Biotechnology, Dallas, TX, USA) using lipofectamine 3000 (Thermo Fisher Scientific, Waltham, MA, USA). The TXNDC5 CRISPR/Cas9 KO plasmid contains a gRNA sequence, 5′-TTATCAAGTTCTTCGCTCCG-3′, which generates a double-stranded break (DSB) specifically in the fifth exon of the *Txndc5* gene. After multiple rounds of puromycin incubation, puromycin-resistant AML12 TXNDC5-KO cells were selected. RNA and Western blot analyses confirmed the deletion of TXNDC5 (Supplementary Figure S1).

4.2. Cell Culture and Treatment

The AML12 cell line (WT) was obtained from the ATCC collection (Manassas, VA, USA) and generated TXNDC5-KO AML12 cells (KO) cultured in a 6-well plate (in duplicate) at 37 °C in a humidified atmosphere of 5% CO_2 in Dulbecco's modified Eagle's minimum essential medium (DMEM; Thermo Fisher Scientific, Waltham, MA, USA): F-12-Ham's medium (GE Healthcare Life Science, South Logan, UT, USA) at a 1:1 ratio supplemented with 10% fetal bovine serum (Thermo Fisher Scientific, Waltham, MA, USA), 1:500 insulin-transferrin-selenium (Corning, Bedford, MA, USA), 40 ng/mL dexamethasone (Sigma-Aldrich; Merck Millipore, Darmstadt, Germany), 1% nonessential amino acids (Thermo Fisher Scientific, Waltham, MA, USA), 1% amphotericin B (1000 mg/mL; Thermo Fisher Scientific, Waltham, MA, USA), 1% penicillin (1000 U/mL; Thermo Fisher Scientific), and 1% streptomycin (1000 mg/mL; Thermo Fisher Scientific, Waltham, MA, USA). After reaching 90–100% confluence, the AML12 cells were given fresh medium without fetal bovine serum and amphotericin B. For RNA isolation, the cells were treated with 1 and 20 μg/mL of tunicamycin (Sigma-Aldrich, Merck Millipore, Darmstadt, Germany), 12.5 nM of thapsigargin (Sigma-Aldrich, Merck Millipore, Darmstadt, Germany), and 600 μM of palmitic acid (Sigma-Aldrich, Merck Millipore, Darmstadt, Germany) for 24 h.

4.3. MTT Assay

Cell viability was assessed using the 3-(4,5-dimethylthiazol-2-yl)-2,5-diphenyltetrazolium bromide test (MTT; Sigma-Aldrich, Merck Millipore, Darmstadt, Germany). The cells were seeded at a density of 5000 cells/well on a 96-well plate and exposed to a range of 1 to 20 nM of thapsigargin (Sigma-Aldrich, Merck Millipore, Darmstadt, Germany) for 24 h. Tunicamycin (Sigma-Aldrich, Merck Millipore, Darmstadt, Germany) was dissolved in 0.1% DMSO to a concentration of 1 to 20 μg/mL, while palmitic acid (Sigma-Aldrich, Merck Millipore, Darmstadt, Germany) was dissolved in ethanol to a concentration of 50 to 4000 μM. The culture medium was then supplemented with 1 mg/mL of MTT. After a 3-h incubation, the cell growth medium was replaced with DMSO and the absorbance was measured at 570 nm using a SPECTROstar® Nano Microplate Reader (Omega, BMG Labtech, Ortenberg, Germany). The IC50 survival rates of AML12 WT and TXNDC5-KO cells in ER stress circumstances were obtained using this method.

4.4. TXNDC5 Promoter Plasmid Construction and Transfection

To investigate the activity of the *Txndc5* promoter, we constructed expression plasmids by inserting PCR-amplified 2024 bp length *Txndc5* promoter (nucleotides 38,527,915 to 38,529,935 of GRCm38.p6 *Mus musculus* assembly) into the EcoRI site of the pEZX-GA01 expression vector (GeneCopoeia, Rockville, MD, USA) following the CloneAmp™ HiFi PCR Premix and In-Fusion® HD Cloning Kit Protocols (Takara Bio, San Jose, CA, USA). AML12 cells were plated at a density of 1×10^4 cells/well in 96-well plates containing Dulbecco's modified Eagle's medium supplemented with 10% fetal bovine serum. After 24 h, LipofectAMINE 3000 reagent (Invitrogen, Carlsbad, CA, USA) was used to transfect the cells with 100 ng of the constructed plasmid, following the manufacturer's protocol. The cells were then treated with thapsigargin (6.25 nM), palmitic acid (300 μM), and tunicamycin (20 μg/mL) for 24 h.

4.5. Alkaline Phosphatase Assay

The transfected cell culture medium was collected and heated at 65 °C for 15 min. Then, 100 μL of 4-nitrophenyl phosphate disodium salt hexahydrate (1 mg/mL) dissolved in deionized water (Sigma-Aldrich, Merck Millipore, Darmstadt, Germany) was added to 10 μL of each sample in a microplate. Absorbance was measured at a wavelength of 405 nm using a SPECTROstar® Nano microplate reader (Omega, BMG Labtech, Ortenberg, Germany).

4.6. Luciferase Activity Assay

The luciferase assay was conducted based on the ratio of luciferase to alkaline phosphatase units. Coelenterazine (6 µM) dissolved in deionized water (Sigma-Aldrich, Merck Millipore, Darmstadt, Germany) was added to 10 µL of culture medium of transfected cells in a microplate. The intensity of luminescence was measured with a microplate reader (FLUOstar®, Omega, BMG Labtech, Ortenberg, Germany) using an emission filter with a gain of 3600.

4.7. RNA Extraction

Total cellular RNA was extracted using a Quick-RNA™ MiniPrep kit (Zymo Research, Tustin, CA, USA) following the manufacturer's instructions. RNA concentration was measured at 260/280 nm wavelengths using a SPECTROstar® Nano microplate reader (Omega, BMG Labtech, Ortenberg, Germany). The integrity of the 28S and 18S ribosomal RNAs was confirmed by electrophoresis on a 1% agarose gel followed by ethidium bromide staining (Sigma-Aldrich, Merck Millipore, Darmstadt, Germany), and the 28S/18S ratio was greater than 2.

4.8. Quantitation of mRNA by RT-qPCR

To measure gene RNA expression, cDNA was prepared from 500 ng of total RNA using the PrimeScript RT reagent kit (TaKaRa Biotechnology, Kusatsu, Shiga, Japan) following the manufacturer's instructions. The cDNA was then analyzed using a Step One Plus Real-Time PCR System (Applied Biosystems, Foster City, CA, USA) with SYBR Green PCR Master Mix (Applied Biosystems, Foster City, CA, USA) according to the manufacturer's guidelines. The primers for RT-qPCR were designed using Primer Express (Applied Biosystems, Foster City, CA, USA). They were then validated for gene specificity and amplification of cDNA rather than genomic DNA using BLAST analysis (NCBI). Finally, the primers were selected based on their efficiency (Table S1). The comparative $2^{-\Delta\Delta CT}$ method was used to calculate the relative ratio of each gene's transcript expression level to the mean values of control samples. The results were normalized to the reference genes *Ppib* and *Tbp*.

4.9. Estimation of Xbp1 mRNA Splicing

To estimate the extent of *Xbp1* mRNA splicing, 500 ng of cDNA was amplified with specific primers using CloneAmp™ HiFi PCR Premix (TaKaRa Biotechnology, Kusatsu, Shiga, Japan) in a standard thermocycler. The primers used were Mouse *Xbp1* forward, 5′-GAG AAC CAG GAG TTA AGA ACA CG-3′ and reverse, 5′-GAA GAT GTT CTG GGG AGG TGA C-3′ [70]. To evaluate the spliced and unspliced forms of *Xbp1* mRNA, the PCR products were separated by electrophoresis on 4% agarose gels and visualized by ethidium bromide staining (Sigma-Aldrich, Merck Millipore, Darmstadt, Germany). The intensities of the bands were then measured to determine the extent of *Xbp1* splicing by Quantity One software version 4.6.8 (Bio-Rad, Hercules, CA, USA).

4.10. Western Blot

Proteins were extracted from AML12 WT and TXNDC5-KO cells that were treated with stressors, as explained above. The proteins were quantified and transferred to a polyvinylidene difluoride (PVDF) membrane (Bio-Rad, Hercules, CA, USA)., following the methodology described in previous publications [28,89]. The membranes were then blocked with phosphate-buffered saline (PBS) containing 5% bovine serum albumin (BSA) for 1 h at room temperature. Following blocking, the membranes were incubated overnight at 4 °C with rabbit primary polyclonal antibody against mouse TXNDC5 (1:1000, Proteintech, Manchester, UK), mouse monoclonal anti-HSPA5 (1:1000, Proteintech, Manchester, UK), mouse monoclonal anti-ATF6 (1:500, Proteintech, Manchester, UK), rabbit monoclonal anti-EIF2AK3 (1:500, Cell Signaling Technology, Danvers, MA, USA), rabbit monoclonal anti-ERN1 (1:500, Thermo Fisher Scientific, Waltham, MA, USA), rabbit monoclonal anti-β-ACTIN (1:2000, Sigma, St. Louis, MO, USA), and mouse monoclonal anti-β-ACTIN (1:2500,

Sigma, St. Louis, MO, USA). The membranes were washed with a PBS solution containing 0.1% Tween 20 before incubation for 1 h at room temperature with a conjugated goat anti-rabbit IgG (H&L) DyLight 800 secondary antibody (1:15,000, Thermo-Scientific, Waltham, MA, USA) or a goat anti-mouse IgG (H&L) DyLight 680 secondary antibody (1:30,000, Thermo-Scientific, Waltham, MA, USA). The blots were captured using the Odyssey® Clx (LI-COR, Bad Hamburg, Germany). The blots were quantified using Image Studio Lite Version 5.2 software from LI-COR Biosciences GmbH in Bad Homburg, Germany. The densitometric values were normalized to the housekeeping antibodies and expressed in arbitrary units.

4.11. ROS Assessment with Flow Cytometry

To quantify cellular ROS, flow cytometry was used to assess AML12 WT and TXNDC5-KO cell lines. The cells were treated with 10 µL of 2.0 mg/mL 2,7-dichlorofluorescein diacetate (DCFH-DA; Sigma-Aldrich, Merck Millipore, Darmstadt, Germany) dissolved in fresh PBS for 30 min at 37 °C. After exposure, the cells were trypsinized, washed, collected, centrifuged, and resuspended to 7.5×10^5 cells/mL in PBS. The fluorescence within the cells was measured using flow cytometry (Beckman Coulter, Brea, CA, USA) with excitation/emission spectra of 485/520 nm, respectively. A total of 30,000 cells were analyzed for all conditions, and the data were processed using Kaluza Analysis Version 1.5a software.

4.12. Intracellular ROS Production

AML12 WT and TXNDC5-KO cells were seeded at a density of 5000 cells per well in a 96-well plate and cultured for 72 h at 37 °C. The cells were treated with thapsigargin, palmitic acid, and two different concentrations of tunicamycin for 24 h. The treatments were administered in medium free of fetal bovine serum and amphotericin B at a concentration of 6.25 nM, 300 µM, 1 and 20 µg/mL of the respective substances. Subsequently, 10 µL of 2.0 mg/mL DCFH-DA (Sigma-Aldrich, Merck Millipore, Darmstadt, Germany) dissolved in fresh PBS was added to the cells. After 30 min at 37 °C, the medium was removed, and the presence of reactive oxygen species was assessed by measuring the conversion of DCFH-DA into fluorescent DCF using a microplate reader (FLUOstar®, Omega, BMG Labtech, Ortenberg, Germany) at excitation and emission wavelengths of 485 and 520 nm, respectively.

4.13. Mitochondrial Membrane Potential Assay

The mitochondrial membrane potential assay (Ab228569 TMRM assay kit, Abcam, Waltham, MA, USA) was used to determine potential mitochondrial damage caused by different ER stressors in AML12 WT and TXNDC5-KO cells. The cells were seeded in 96-well plates at a concentration of 5×10^5 cells/mL and exposed to thapsigargin, palmitic acid, and tunicamycin at concentrations of 6.25 nM, 300 µM, and 1 and 20 µg/mL, respectively, for 24 h. After exposure, the cells were washed with PBS and 1µM TMRM was added. After 30 min incubation in 37 °C, the cells were washed twice with PBS/0.2% BSA. Then, 1X live cell imaging buffer was added. The fluorescence intensity was measured using a microplate reader (FLUOstar®, Omega, BMG Labtech, Ortenberg, Germany) with an excitation/emission of 548/575 nm.

4.14. TMRM Microscopy Procedure

To confirm the TMRM results, the microscopy procedure was also performed with 200 nM of TMRM (Ab228569 TMRM assay kit, Abcam, Waltham, MA, USA). Additionally, we used 20 µM carbonylcyanide 4-(trifluoromethoxy)phenylhydrazone (FCCP) as a positive control for 10 min prior to staining with TMRM. The cell's nucleus was stained using NucBlue Live Ready Probes Reagent (Invitrogen, Thermo-Scientific, Waltham, MA, USA) and incubated for 20 min at 25 °C. The cells were evaluated using a FLoid Cell Imaging Station (Life Technologies, Invitrogen, Thermo-Scientific, Waltham, MA, USA) that was

equipped with bandpass filters capable of visualizing EX/EM = 548/573. The data were analyzed using ImageJ (Fiji) software version windows 64-bit Java 8.

4.15. Statistical Analysis

The figures display means ± standard deviations. Statistical significance was calculated using GraphPad Prism 8 for Windows (GraphPad, San Diego, CA, USA). The normal distribution of the data and homogeneity of variance among groups were assessed using the Shapiro–Wilk test and Bartlett's or Levene's tests, respectively. Statistical differences were calculated using the one-tailed Mann–Whitney's U- or Student's *t*-tests. The figure legends indicate the *p*-values, denoted as *, $p < 0.05$; **, $p < 0.01$; ***, $p < 0.001$, and ****, $p < 0.0001$.

5. Conclusions

The results of the current study indicate that TXNDC5 deficiency is associated with a reduction in mRNA expression of *Ern1*, *Xbp1*, *Eif2ak3*, and *Sec61a1* and an increase in those of *Atf4*, *Hspa5*, and *Ddit3* in mouse hepatocytes. The expression of *Atf6* and *Ssr2* was not significantly altered in the absence of TXNDC5. The protein expression results of prominent ER stress markers indicated that the ERN1 and EIF2AK3 proteins were downregulated, while the HSPA5 protein was upregulated. Moreover, the ATF6 protein did not exhibit any significant changes in the absence of TXNDC5 at the protein level. The knockout of TXNDC5 has been demonstrated to increase cellular ROS production in AML12 cells. Furthermore, TXNDC5 activity is required to maintain normal mitochondrial function during tunicamycin-induced ER stress. The enhancement of TXNDC5 in AML12 cells is dependent on the induction of ER stress by thapsigargin, palmitic acid, and tunicamycin. Tunicamycin, an inhibitor of glycosylation, has been observed to disrupt the protein levels of HSPA5, ERN1, and EIF2AK3 in TXNDC5-deficient cells. Additionally, tunicamycin has been shown to affect the mRNA levels of *Eif2ak3* and *Sec61a1* in TXNDC5-deficient cells. However, palmitic acid, which is an inducer of excessive saturated fatty acids, can disarrange ATF6, HSPA5, and EIF2AK3 at the protein level and *Atf6*, *Hspa5*, *Eif2ak3*, and *Ssr2* at the gene expression level in TXNDC5 knockout cells. The absence of TXNDC5 did not affect any ER stress cascades in thapsigargin-induced ER stress in hepatocytes, despite the activation of the ERN1–XBP1 pathway under these conditions. Furthermore, the absence of TXNDC5 can induce the Xbp1 spliced form. Moreover, it is conceivable that the upregulation of ERN1 may alter the splicing pattern of Xbp1, rather than merely influencing its mRNA expression. In summary, TXNDC5 can selectively activate different ER stress cascades via HSPA5, depending on the source of ER stress. Conversely, the absence of TXNDC5 can disrupt the EIF2AK3 cascade.

Limitations and Future Research

To address the potential limitations of cell viability as an endpoint, we plan to include a broader range of functional assays in future experiments. These could include assessments of lipid accumulation, inflammatory cytokine production, and markers of liver injury and fibrosis. Such approaches would provide a more comprehensive understanding of the impact of TXDNC5 on liver health under stress conditions. In addition, it is important to consider the long-term effects of TXDNC5 deficiency. Chronic stress conditions or prolonged exposure to ER stress inducers may reveal cumulative effects on cell viability and function that are not apparent in short-term assays. Finally, future studies could examine the effects of TXDNC5 KO on the expression of proteins involved in lipid metabolism, inflammation, and fibrosis, which are key components of NAFLD progression.

Supplementary Materials: The following supporting information can be downloaded at: https://www.mdpi.com/article/10.3390/ijms25137128/s1.

Author Contributions: Conceptualization, S.H.B., C.B., J.S.-M., R.M.-B., M.A.N., M.J.R.-Y., S.C.M.F. and J.O.; methodology, S.H.B., C.B., J.S.-M. and R.M.-B.; software, S.H.B., C.B. and J.S.-M.; validation, S.H.B., C.B. and J.S.-M.; formal analysis, S.H.B., C.B., J.S.-M. and R.M.-B.; investigation, S.H.B.;

resources, M.J.R.-Y. and J.O.; data curation, S.H.B. and J.O.; writing—original draft preparation, S.H.B.; writing—review and editing, S.H.B., C.B., J.S.-M., R.M.-B., M.A.N., M.J.R.-Y., S.C.M.F. and J.O.; visualization, S.H.B.; supervision, M.A.N., S.C.M.F. and J.O.; project administration, M.J.R.-Y. and J.O.; funding acquisition, M.J.R.-Y. and J.O. All authors have read and agreed to the published version of the manuscript.

Funding: This research was supported by grants (CIBEROBN, CB06/03/1012, 1 January 2008) from CIBER Fisiopatología de la Obesidad y Nutrición as an initiative of FEDER-ISCIII, Ministerio de Ciencia e Innovación-Fondo Europeo de Desarrollo Regional (PID2022-136414OB-I00, 1 June 2023), SUDOE (Manpower, S1/1.1/E0116), Plan de Recuperación, Transformación y Resiliencia-MRR, and Fondo Social Europeo-Gobierno de Aragón (B16_23R, 26 March 2023). S.H.B. was a recipient of a joint fellowship from the Universities of Zaragoza and Pau and short-term fellowship from Universidad de Zaragoza, Fundación Bancaria Ibercaja, and Fundación CAI (CM 7/22, 4 October 2022), and J.S.-M. was a recipient of a Fundación Cuenca Villoro fellowship.

Institutional Review Board Statement: Not applicable.

Informed Consent Statement: Not applicable.

Data Availability Statement: Data are contained within the article and Supplementary Material.

Acknowledgments: We extend our gratitude to the flow cytometry service at Centro de Investigación Biomédica de Aragón (CIBA) and Tania Herrero Continente for their invaluable assistance in maintaining the laboratory.

Conflicts of Interest: The authors declare no conflicts of interest.

Abbreviations

NAFLD	Non-alcoholic fatty liver disease
NASH	Non-alcoholic steatohepatitis
ATF6	Activating transcription factor 6
HSPA5	Heat shock protein 5
EIF2AK3	Eukaryotic translation initiation factor 2 alpha kinase 3
ATF4	Activating transcription factor 4
DDIT3	DNA-damage inducible transcript 3
ERN1	Endoplasmic reticulum (ER) to nucleus signaling 1
XBP1	X-box binding protein 1
SSR2	Signal sequence receptor, beta
SEC61A1	Sec61 alpha 1 subunit
Tbp	TATA-box binding protein
Ppib	Peptidylprolyl isomerase B
TXNDC5	Thioredoxin domain containing 5
WT	Wild-type AML12
KO	TXNDC5-Knockout AML12
ER	Endoplasmic reticulum
CRISPR	Clustered regularly interspaced short palindromic repeats
UPR	Unfolded protein response
PDI	Protein disulfide isomerase
MTT	3-(4 5-dimethylthiazol-2-yl)-2 5-diphenyltetrazolium bromide
ROS	Reactive oxygen species
AML12	Alpha mouse liver cell line
NIH-3T3	Mouse NIH/Swiss embryo fibroblasts
MCF-7	Michigan Cancer Foundation-7
RKO	Human colon carcinoma cell line
MDA-MB-231	M.D. Anderson-metastatic breast 231
Jurkat	Immortalized line of human T lymphocyte cells
L3.6pL	L3.6 pancreas-liver cell line
MIN6	Mouse insulinoma cell line 6
C2C12	C2C12 mouse myoblast cell line

HEK293T	Human embryonic kidney cells 293T
HeLa	Henrietta Lacks cancer cells
COS-7	Monkey African green kidney fibroblasts

References

1. Page, A.B.J. Nonalcoholic fatty liver disease: The hepatic metabolic syndrome. *J. Am. Acad. Nurse Pract.* **2012**, *24*, 345–351. [CrossRef] [PubMed]
2. Loomba, R.; Friedman, S.L.; Shulman, G.I. Mechanisms and disease consequences of nonalcoholic fatty liver disease. *Cell* **2021**, *184*, 2537–2564. [CrossRef] [PubMed]
3. Charlton, M.R.; Burns, J.M.; Pedersen, R.A.; Watt, K.D.; Heimbach, J.K.; Dierkhising, R.A. Frequency and outcomes of liver transplantation for nonalcoholic steatohepatitis in the United States. *Gastroenterology* **2011**, *141*, 1249–1253. [CrossRef] [PubMed]
4. Harrison, S.A.; Allen, A.M.; Dubourg, J.; Noureddin, M.; Alkhouri, N. Challenges and opportunities in NASH drug development. *Nat. Med.* **2023**, *29*, 562–573. [CrossRef] [PubMed]
5. Schuppan, D.; Gorrell, M.D.; Klein, T.; Mark, M.; Afdhal, N.H. The challenge of developing novel pharmacological therapies for non-alcoholic steatohepatitis. *Liver Int.* **2010**, *30*, 795–808. [CrossRef]
6. Schuppan, D.; Afdhal, N.H. Liver cirrhosis. *Lancet* **2008**, *371*, 838–851. [CrossRef] [PubMed]
7. Younossi, Z.; Tacke, F.; Arrese, M.; Chander Sharma, B.; Mostafa, I.; Bugianesi, E.; Wai-Sun Wong, V.; Yilmaz, Y.; George, J.; Fan, J. Global perspectives on nonalcoholic fatty liver disease and nonalcoholic steatohepatitis. *Hepatology* **2019**, *69*, 2672–2682. [CrossRef] [PubMed]
8. Younossi, Z. Current management of non-alcoholic fatty liver disease and non-alcoholic steatohepatitis. *Aliment. Pharmacol. Ther.* **2008**, *28*, 2–12. [CrossRef] [PubMed]
9. Schröder, M.; Kaufman, R.J. The mammalian unfolded protein response. *Annu. Rev. Biochem.* **2005**, *74*, 739–789. [CrossRef]
10. Chang, T.-Y.; Chang, C.C.; Ohgami, N.; Yamauchi, Y. Cholesterol sensing, trafficking, and esterification. *Annu. Rev. Cell Dev. Biol.* **2006**, *22*, 129–157. [CrossRef]
11. Hetz, C. The unfolded protein response: Controlling cell fate decisions under ER stress and beyond. *Nat. Rev. Mol. Cell Biol.* **2012**, *13*, 89–102. [CrossRef] [PubMed]
12. Szegezdi, E.; Logue, S.E.; Gorman, A.M.; Samali, A. Mediators of endoplasmic reticulum stress-induced apoptosis. *EMBO Rep.* **2006**, *7*, 880–885. [CrossRef] [PubMed]
13. Kim, I.; Xu, W.; Reed, J.C. Cell death and endoplasmic reticulum stress: Disease relevance and therapeutic opportunities. *Nat. Rev. Drug Discov.* **2008**, *7*, 1013–1030. [CrossRef] [PubMed]
14. Metcalf, M.G.; Higuchi-Sanabria, R.; Garcia, G.; Tsui, C.K.; Dillin, A. Beyond the cell factory: Homeostatic regulation of and by the UPRER. *Sci. Adv.* **2020**, *6*, eabb9614. [CrossRef] [PubMed]
15. Walter, P.; Ron, D. The unfolded protein response: From stress pathway to homeostatic regulation. *Science* **2011**, *334*, 1081–1086. [CrossRef] [PubMed]
16. Marciniak, S.J.; Ron, D. Endoplasmic reticulum stress signaling in disease. *Physiol. Rev.* **2006**, *86*, 1133–1149. [CrossRef] [PubMed]
17. Schuck, S.; Prinz, W.A.; Thorn, K.S.; Voss, C.; Walter, P. Membrane expansion alleviates endoplasmic reticulum stress independently of the unfolded protein response. *J. Cell Biol.* **2009**, *187*, 525–536. [CrossRef] [PubMed]
18. Bailey, D.; O'Hare, P. Transmembrane bZIP transcription factors in ER stress signaling and the unfolded protein response. *Antioxid. Redox Signal.* **2007**, *9*, 2305–2322. [CrossRef]
19. Zeeshan, H.M.A.; Lee, G.H.; Kim, H.-R.; Chae, H.-J. Endoplasmic reticulum stress and associated ROS. *Int. J. Mol. Sci.* **2016**, *17*, 327. [CrossRef]
20. Zhong, F.; Xie, J.; Zhang, D.; Han, Y.; Wang, C. Polypeptide from Chlamys farreri suppresses ultraviolet-B irradiation-induced apoptosis through restoring ER redox homeostasis, scavenging ROS generation, and suppressing the PERK-eIF2a-CHOP pathway in HaCaT cells. *J. Photochem. Photobiol. B Biol.* **2015**, *151*, 10–16. [CrossRef]
21. Harding, H.P.; Zhang, Y.; Bertolotti, A.; Zeng, H.; Ron, D. Perk is essential for translational regulation and cell survival during the unfolded protein response. *Mol. Cell* **2000**, *5*, 897–904. [CrossRef]
22. Adamson, B.; Norman, T.M.; Jost, M.; Cho, M.Y.; Nuñez, J.K.; Chen, Y.; Villalta, J.E.; Gilbert, L.A.; Horlbeck, M.A.; Hein, M.Y. A multiplexed single-cell CRISPR screening platform enables systematic dissection of the unfolded protein response. *Cell* **2016**, *167*, 1867–1882.e21. [CrossRef]
23. Shamu, C.E.; Walter, P. Oligomerization and phosphorylation of the Ire1p kinase during intracellular signaling from the endoplasmic reticulum to the nucleus. *EMBO J.* **1996**, *15*, 3028–3039. [CrossRef] [PubMed]
24. Hassler, J.; Cao, S.S.; Kaufman, R.J. IRE1, a double-edged sword in pre-miRNA slicing and cell death. *Dev. Cell* **2012**, *23*, 921–923. [CrossRef]
25. Gardner, B.M.; Pincus, D.; Gotthardt, K.; Gallagher, C.M.; Walter, P. Endoplasmic reticulum stress sensing in the unfolded protein response. *Cold Spring Harb. Perspect. Biol.* **2013**, *5*, a013169. [CrossRef]
26. Zhao, L.; Ackerman, S.L. Endoplasmic reticulum stress in health and disease. *Curr. Opin. Cell Biol.* **2006**, *18*, 444–452. [CrossRef]
27. Chawsheen, H.A.; Ying, Q.; Jiang, H.; Wei, Q. A critical role of the thioredoxin domain containing protein 5 (TXNDC5) in redox homeostasis and cancer development. *Genes Dis.* **2018**, *5*, 312–322. [CrossRef]

28. Bidooki, S.H.; Alejo, T.; Sánchez-Marco, J.; Martínez-Beamonte, R.; Abuobeid, R.; Burillo, J.C.; Lasheras, R.; Sebastian, V.; Rodríguez-Yoldi, M.J.; Arruebo, M. Squalene Loaded Nanoparticles Effectively Protect Hepatic AML12 Cell Lines against Oxidative and Endoplasmic Reticulum Stress in a TXNDC5-Dependent Way. *Antioxidants* **2022**, *11*, 581. [CrossRef]
29. Horna-Terrón, E.; Pradilla-Dieste, A.; Sánchez-de-Diego, C.; Osada, J. TXNDC5, a newly discovered disulfide isomerase with a key role in cell physiology and pathology. *Int. J. Mol. Sci.* **2014**, *15*, 23501–23518. [CrossRef]
30. Sullivan, D.C.; Huminiecki, L.; Moore, J.W.; Boyle, J.J.; Poulsom, R.; Creamer, D.; Barker, J.; Bicknell, R. EndoPDI, a novel protein-disulfide isomerase-like protein that is preferentially expressed in endothelial cells acts as a stress survival factor. *J. Biol. Chem.* **2003**, *278*, 47079–47088. [CrossRef] [PubMed]
31. Chawsheen, H.A.; Jiang, H.; Ying, Q.; Ding, N.; Thapa, P.; Wei, Q. The redox regulator sulfiredoxin forms a complex with thioredoxin domain–containing 5 protein in response to ER stress in lung cancer cells. *J. Biol. Chem.* **2019**, *294*, 8991–9006. [CrossRef]
32. Pardo, V.; González-Rodríguez, Á.; Muntané, J.; Kozma, S.C.; Valverde, Á.M. Role of hepatocyte S6K1 in palmitic acid-induced endoplasmic reticulum stress, lipotoxicity, insulin resistance and in oleic acid-induced protection. *Food Chem. Toxicol.* **2015**, *80*, 298–309. [CrossRef]
33. Chen, D.-L.; Xiang, J.-N.; Yang, L.-Y. Role of ERp46 in β-cell lipoapoptosis through endoplasmic reticulum stress pathway as well as the protective effect of exendin-4. *Biochem. Biophys. Res. Commun.* **2012**, *426*, 324–329. [CrossRef]
34. Alberti, A.; Karamessinis, P.; Peroulis, M.; Kypreou, K.; Kavvadas, P.; Pagakis, S.; Politis, P.K.; Charonis, A. ERp46 is reduced by high glucose and regulates insulin content in pancreatic β-cells. *Am. J. Physiol.-Endocrinol. Metab.* **2009**, *297*, E812–E821. [CrossRef]
35. Lee, S.-O.; Jin, U.-H.; Kang, J.H.; Kim, S.B.; Guthrie, A.S.; Sreevalsan, S.; Lee, J.-S.; Safe, S. The orphan nuclear receptor NR4A1 (Nur77) regulates oxidative and endoplasmic reticulum stress in pancreatic cancer cells. *Mol. Cancer Res.* **2014**, *12*, 527–538. [CrossRef]
36. Noda, I.; Fujieda, S.; Seki, M.; Tanaka, N.; Sunaga, H.; Ohtsubo, T.; Tsuzuki, H.; Fan, G.K.; Saito, H. Inhibition of N-linked glycosylation by tunicamycin enhances sensitivity to cisplatin in human head-and-neck carcinoma cells. *Int. J. Cancer* **1999**, *80*, 279–284. [CrossRef]
37. Zhou, L.; Zhang, J.; Fang, Q.; Liu, M.; Liu, X.; Jia, W.; Dong, L.Q.; Liu, F. Autophagy-mediated insulin receptor down-regulation contributes to endoplasmic reticulum stress-induced insulin resistance. *Mol. Pharmacol.* **2009**, *76*, 596–603. [CrossRef]
38. Ruddock, M.W.; Stein, A.; Landaker, E.; Park, J.; Cooksey, R.C.; McClain, D.; Patti, M.-E. Saturated fatty acids inhibit hepatic insulin action by modulating insulin receptor expression and post-receptor signalling. *J. Biochem.* **2008**, *144*, 599–607. [CrossRef]
39. Kammoun, H.L.; Chabanon, H.; Hainault, I.; Luquet, S.; Magnan, C.; Koike, T.; Ferré, P.; Foufelle, F. GRP78 expression inhibits insulin and ER stress–induced SREBP-1c activation and reduces hepatic steatosis in mice. *J. Clin. Investig.* **2009**, *119*, 1201–1215. [CrossRef] [PubMed]
40. Tan, F.; Zhu, H.; He, X.; Yu, N.; Zhang, X.; Xu, H.; Pei, H. Role of TXNDC5 in tumorigenesis of colorectal cancer cells: In vivo and in vitro evidence. *Int. J. Mol. Med.* **2018**, *42*, 935–945. [CrossRef] [PubMed]
41. Peng, F.; Zhang, H.; Du, Y.; Tan, P. Cetuximab enhances cisplatin-induced endoplasmic reticulum stress-associated apoptosis in laryngeal squamous cell carcinoma cells by inhibiting expression of TXNDC5. *Mol. Med. Rep.* **2018**, *17*, 4767–4776. [CrossRef]
42. DeZwaan-McCabe, D.; Sheldon, R.D.; Gorecki, M.C.; Guo, D.-F.; Gansemer, E.R.; Kaufman, R.J.; Rahmouni, K.; Gillum, M.P.; Taylor, E.B.; Teesch, L.M. ER stress inhibits liver fatty acid oxidation while unmitigated stress leads to anorexia-induced lipolysis and both liver and kidney steatosis. *Cell Rep.* **2017**, *19*, 1794–1806. [CrossRef]
43. Bidooki, S.H.; Navarro, M.A.; Fernandes, S.C.; Osada, J. Thioredoxin Domain Containing 5 (TXNDC5): Friend or Foe? *Curr. Issues Mol. Biol.* **2024**, *46*, 3134–3163. [CrossRef]
44. Li, T.; Zhao, H.; Guo, G.; Xia, S.; Wang, L. VMP1 affects endoplasmic reticulum stress sensitivity via differential modulation of the three unfolded protein response arms. *Cell Rep.* **2023**, *42*, 112209. [CrossRef]
45. Bidooki, S.H.; Sánchez-Marco, J.; Martínez-Beamonte, R.; Herrero-Continente, T.; Navarro, M.A.; Rodríguez-Yoldi, M.J.; Osada, J. Endoplasmic Reticulum Protein TXNDC5 Interacts with PRDX6 and HSPA9 to Regulate Glutathione Metabolism and Lipid Peroxidation in the Hepatic AML12 Cell Line. *Int. J. Mol. Sci.* **2023**, *24*, 17131. [CrossRef] [PubMed]
46. Chen, Y.-T.; Jhao, P.-Y.; Hung, C.-T.; Wu, Y.-F.; Lin, S.-J.; Chiang, W.-C.; Lin, S.-L.; Yang, K.-C. Endoplasmic reticulum protein TXNDC5 promotes renal fibrosis by enforcing TGF-β signaling in kidney fibroblasts. *J. Clin. Investig.* **2021**, *131*, e143645. [CrossRef]
47. Lee, T.-H.; Yeh, C.-F.; Lee, Y.-T.; Shih, Y.-C.; Chen, Y.-T.; Hung, C.-T.; You, M.-Y.; Wu, P.-C.; Shentu, T.-P.; Huang, R.-T. Fibroblast-enriched endoplasmic reticulum protein TXNDC5 promotes pulmonary fibrosis by augmenting TGFβ signaling through TGFBR1 stabilization. *Nat. Commun.* **2020**, *11*, 4254. [CrossRef]
48. Chen, X.; Li, C.; Liu, J.; He, Y.; Wei, Y.; Chen, J. Inhibition of ER stress by targeting the IRE1α–TXNDC5 pathway alleviates crystalline silica-induced pulmonary fibrosis. *Int. Immunopharmacol.* **2021**, *95*, 107519. [CrossRef]
49. Bidoki, S.H.; Bayatani, A.; Sarlak, M.; Rasouli, M.; Mostafaie, P.; Saghafi, M.; Negari, A.T. Assessing Expression of TGF-B2 and PCDH9 Genes in Breast Cancer Patients. *Age* **2018**, *7*, 20.
50. Hashemi, M.; Arani, H.Z.; Orouei, S.; Fallah, S.; Ghorbani, A.; Khaledabadi, M.; Kakavand, A.; Tavakolpournegari, A.; Saebfar, H.; Heidari, H. EMT mechanism in breast cancer metastasis and drug resistance: Revisiting molecular interactions and biological functions. *Biomed. Pharmacother.* **2022**, *155*, 113774. [CrossRef]

51. Reddy, R.K.; Mao, C.; Baumeister, P.; Austin, R.C.; Kaufman, R.J.; Lee, A.S. Endoplasmic reticulum chaperone protein GRP78 protects cells from apoptosis induced by topoisomerase inhibitors: Role of ATP binding site in suppression of caspase-7 activation. *J. Biol. Chem.* **2003**, *278*, 20915–20924. [CrossRef] [PubMed]
52. Sánchez-Marco, J.; Bidooki, S.H.; Abuobeid, R.; Barranquero, C.; Herrero-Continente, T.; Arnal, C.; Martínez-Beamonte, R.; Lasheras, R.; Surra, J.C.; Navarro, M.A. Thioredoxin domain containing 5 is involved in the hepatic storage of squalene into lipid droplets in a sex-specific way. *J. Nutr. Biochem.* **2024**, *124*, 109503. [CrossRef] [PubMed]
53. Ao, N.; Yang, J.; Wang, X.; Du, J. Glucagon-like peptide-1 preserves non-alcoholic fatty liver disease through inhibition of the endoplasmic reticulum stress-associated pathway. *Hepatol. Res.* **2016**, *46*, 343–353. [CrossRef] [PubMed]
54. Werstuck, G.H.; Lentz, S.R.; Dayal, S.; Hossain, G.S.; Sood, S.K.; Shi, Y.Y.; Zhou, J.; Maeda, N.; Krisans, S.K.; Malinow, M.R. Homocysteine-induced endoplasmic reticulum stress causes dysregulation of the cholesterol and triglyceride biosynthetic pathways. *J. Clin. Investig.* **2001**, *107*, 1263–1273. [CrossRef]
55. Cazanave, S.C.; Mott, J.L.; Elmi, N.A.; Bronk, S.F.; Werneburg, N.W.; Akazawa, Y.; Kahraman, A.; Garrison, S.P.; Zambetti, G.P.; Charlton, M.R. JNK1-dependent PUMA expression contributes to hepatocyte lipoapoptosis. *J. Biol. Chem.* **2009**, *284*, 26591–26602. [CrossRef] [PubMed]
56. Schattenberg, J.M.; Singh, R.; Wang, Y.; Lefkowitch, J.H.; Rigoli, R.M.; Scherer, P.E.; Czaja, M.J. JNK1 but not JNK2 promotes the development of steatohepatitis in mice. *Hepatology* **2006**, *43*, 163–172. [CrossRef]
57. Howie, J.; Tulloch, L.B.; Brown, E.; Reilly, L.; Ashford, F.B.; Kennedy, J.; Wypijewski, K.J.; Aughton, K.L.; Mak, J.K.; Shattock, M.J. Glutathione-dependent depalmitoylation of phospholemman by peroxiredoxin 6. *Cell Rep.* **2024**, *43*, 113679. [CrossRef]
58. Novoa, I.; Zeng, H.; Harding, H.P.; Ron, D. Feedback inhibition of the unfolded protein response by GADD34-mediated dephosphorylation of eIF2α. *J. Cell Biol.* **2001**, *153*, 1011–1022. [CrossRef]
59. Harding, H.P.; Zeng, H.; Zhang, Y.; Jungries, R.; Chung, P.; Plesken, H.; Sabatini, D.D.; Ron, D. Diabetes mellitus and exocrine pancreatic dysfunction in perk−/− mice reveals a role for translational control in secretory cell survival. *Mol. Cell* **2001**, *7*, 1153–1163. [CrossRef]
60. Harding, H.P.; Zhang, Y.; Zeng, H.; Novoa, I.; Lu, P.D.; Calfon, M.; Sadri, N.; Yun, C.; Popko, B.; Paules, R. An integrated stress response regulates amino acid metabolism and resistance to oxidative stress. *Mol. Cell* **2003**, *11*, 619–633. [CrossRef]
61. Oyadomari, S.; Mori, M. Roles of CHOP/GADD153 in endoplasmic reticulum stress. *Cell Death Differ.* **2004**, *11*, 381–389. [CrossRef] [PubMed]
62. McCullough, K.D.; Martindale, J.L.; Klotz, L.-O.; Aw, T.-Y.; Holbrook, N.J. Gadd153 sensitizes cells to endoplasmic reticulum stress by down-regulating Bcl2 and perturbing the cellular redox state. *Mol. Cell. Biol.* **2001**, *21*, 1249–1259. [CrossRef] [PubMed]
63. Yamaguchi, H.; Wang, H.-G. CHOP is involved in endoplasmic reticulum stress-induced apoptosis by enhancing DR5 expression in human carcinoma cells. *J. Biol. Chem.* **2004**, *279*, 45495–45502. [CrossRef] [PubMed]
64. Marciniak, S.J.; Yun, C.Y.; Oyadomari, S.; Novoa, I.; Zhang, Y.; Jungreis, R.; Nagata, K.; Harding, H.P.; Ron, D. CHOP induces death by promoting protein synthesis and oxidation in the stressed endoplasmic reticulum. *Genes Dev.* **2004**, *18*, 3066–3077. [CrossRef]
65. Tsuru, A.; Fujimoto, N.; Takahashi, S.; Saito, M.; Nakamura, D.; Iwano, M.; Iwawaki, T.; Kadokura, H.; Ron, D.; Kohno, K. Negative feedback by IRE1β optimizes mucin production in goblet cells. *Proc. Natl. Acad. Sci. USA* **2013**, *110*, 2864–2869. [CrossRef] [PubMed]
66. Yamamoto, K.; Sato, T.; Matsui, T.; Sato, M.; Okada, T.; Yoshida, H.; Harada, A.; Mori, K. Transcriptional induction of mammalian ER quality control proteins is mediated by single or combined action of ATF6α and XBP1. *Dev. Cell* **2007**, *13*, 365–376. [CrossRef] [PubMed]
67. Novoa, I.; Zhang, Y.; Zeng, H.; Jungreis, R.; Harding, H.P.; Ron, D. Stress-induced gene expression requires programmed recovery from translational repression. *EMBO J.* **2003**, *22*, 1180–1187. [CrossRef] [PubMed]
68. Lee, A.-H.; Iwakoshi, N.N.; Glimcher, L.H. XBP-1 regulates a subset of endoplasmic reticulum resident chaperone genes in the unfolded protein response. *Mol. Cell. Biol.* **2003**, *23*, 7448–7459. [CrossRef] [PubMed]
69. Sriburi, R.; Jackowski, S.; Mori, K.; Brewer, J.W. XBP1: A link between the unfolded protein response, lipid biosynthesis, and biogenesis of the endoplasmic reticulum. *J. Cell Biol.* **2004**, *167*, 35–41. [CrossRef]
70. Tsuchiya, Y.; Saito, M.; Kadokura, H.; Miyazaki, J.-i.; Tashiro, F.; Imagawa, Y.; Iwawaki, T.; Kohno, K. IRE1–XBP1 pathway regulates oxidative proinsulin folding in pancreatic β cells. *J. Cell Biol.* **2018**, *217*, 1287–1301. [CrossRef]
71. Lisbona, F.; Rojas-Rivera, D.; Thielen, P.; Zamorano, S.; Todd, D.; Martinon, F.; Glavic, A.; Kress, C.; Lin, J.H.; Walter, P.; et al. BAX inhibitor-1 is a negative regulator of the ER stress sensor IRE1α. *Mol. Cell* **2009**, *33*, 679–691. [CrossRef] [PubMed]
72. Mirzaei, S.; Paskeh, M.D.A.; Entezari, M.; Bidooki, S.H.; Ghaleh, V.J.; Hejazi, E.S.; Kakavand, A.; Behroozaghdam, M.; Movafagh, A.; Taheriazam, A. siRNA and targeted delivery systems in breast cancer therapy. *Clin. Transl. Oncol.* **2022**, *25*, 1167–1188. [CrossRef] [PubMed]
73. Yoshida, H.; Matsui, T.; Yamamoto, A.; Okada, T.; Mori, K. XBP1 mRNA is induced by ATF6 and spliced by IRE1 in response to ER stress to produce a highly active transcription factor. *Cell* **2001**, *107*, 881–891. [CrossRef] [PubMed]
74. Reimold, A.M.; Etkin, A.; Clauss, I.; Perkins, A.; Friend, D.S.; Zhang, J.; Horton, H.F.; Scott, A.; Orkin, S.H.; Byrne, M.C. An essential role in liver development for transcription factor XBP-1. *Genes Dev.* **2000**, *14*, 152–157. [CrossRef] [PubMed]
75. Zhang, K.; Wong, H.N.; Song, B.; Miller, C.N.; Scheuner, D.; Kaufman, R.J. The unfolded protein response sensor IRE1α is required at 2 distinct steps in B cell lymphopoiesis. *J. Cnical Investig.* **2005**, *115*, 268–281. [CrossRef]

76. Loeuillard, E.; El Mourabit, H.; Lei, L.; Lemoinne, S.; Housset, C.; Cadoret, A. Endoplasmic reticulum stress induces inverse regulations of major functions in portal myofibroblasts during liver fibrosis progression. *Biochim. Biophys. Acta (BBA)-Mol. Basis Dis.* **2018**, *1864*, 3688–3696. [CrossRef] [PubMed]
77. Lipson, K.L.; Fonseca, S.G.; Ishigaki, S.; Nguyen, L.X.; Foss, E.; Bortell, R.; Rossini, A.A.; Urano, F. Regulation of insulin biosynthesis in pancreatic beta cells by an endoplasmic reticulum-resident protein kinase IRE1. *Cell Metab.* **2006**, *4*, 245–254. [CrossRef] [PubMed]
78. Zhou, J.; Liu, C.Y.; Back, S.H.; Clark, R.L.; Peisach, D.; Xu, Z.; Kaufman, R.J. The crystal structure of human IRE1 luminal domain reveals a conserved dimerization interface required for activation of the unfolded protein response. *Proc. Natl. Acad. Sci. USA* **2006**, *103*, 14343–14348. [CrossRef] [PubMed]
79. Acosta-Alvear, D.; Zhou, Y.; Blais, A.; Tsikitis, M.; Lents, N.H.; Arias, C.; Lennon, C.J.; Kluger, Y.; Dynlacht, B.D. XBP1 controls diverse cell type-and condition-specific transcriptional regulatory networks. *Mol. Cell* **2007**, *27*, 53–66. [CrossRef]
80. Shoulders, M.D.; Ryno, L.M.; Genereux, J.C.; Moresco, J.J.; Tu, P.G.; Wu, C.; Yates III, J.R.; Su, A.I.; Kelly, J.W.; Wiseman, R.L. Stress-independent activation of XBP1s and/or ATF6 reveals three functionally diverse ER proteostasis environments. *Cell Rep.* **2013**, *3*, 1279–1292. [CrossRef]
81. Kanda, S.; Yanagitani, K.; Yokota, Y.; Esaki, Y.; Kohno, K. Autonomous translational pausing is required for XBP1u mRNA recruitment to the ER via the SRP pathway. *Proc. Natl. Acad. Sci. USA* **2016**, *113*, E5886–E5895. [CrossRef] [PubMed]
82. Plumb, R.; Zhang, Z.-R.; Appathurai, S.; Mariappan, M. A functional link between the co-translational protein translocation pathway and the UPR. *Elife* **2015**, *4*, e07426. [CrossRef]
83. Lin, J.H.; Li, H.; Yasumura, D.; Cohen, H.R.; Zhang, C.; Panning, B.; Shokat, K.M.; LaVail, M.M.; Walter, P. IRE1 signaling affects cell fate during the unfolded protein response. *Science* **2007**, *318*, 944–949. [CrossRef] [PubMed]
84. Gilbert, L.A.; Horlbeck, M.A.; Adamson, B.; Villalta, J.E.; Chen, Y.; Whitehead, E.H.; Guimaraes, C.; Panning, B.; Ploegh, H.L.; Bassik, M.C. Genome-scale CRISPR-mediated control of gene repression and activation. *Cell* **2014**, *159*, 647–661. [CrossRef] [PubMed]
85. Wang, Y.; Shen, J.; Arenzana, N.; Tirasophon, W.; Kaufman, R.J.; Prywes, R. Activation of ATF6 and an ATF6 DNA binding site by the endoplasmic reticulum stress response. *J. Biol. Chem.* **2000**, *275*, 27013–27020. [CrossRef] [PubMed]
86. Sriburi, R.; Bommiasamy, H.; Buldak, G.L.; Robbins, G.R.; Frank, M.; Jackowski, S.; Brewer, J.W. Coordinate regulation of phospholipid biosynthesis and secretory pathway gene expression in XBP-1 (S)-induced endoplasmic reticulum biogenesis. *J. Biol. Chem.* **2007**, *282*, 7024–7034. [CrossRef] [PubMed]
87. Chen, H.; Zhang, Y.; Li, X.; Zhang, W.; He, H.; Du, B.; Li, T.; Tang, H.; Liu, Y.; Li, L. Transcriptome Changes and Potential Immunotoxicity Analysis in RAW264. 7 Macrophages Caused by Bisphenol F. *Front. Pharmacol.* **2022**, *13*, 846562.
88. Chen, S.; Xuan, J.; Couch, L.; Iyer, A.; Wu, Y.; Li, Q.-Z.; Guo, L. Sertraline induces endoplasmic reticulum stress in hepatic cells. *Toxicology* **2014**, *322*, 78–88. [CrossRef]
89. Herrera-Marcos, L.V.; Martínez-Beamonte, R.; Macías-Herranz, M.; Arnal, C.; Barranquero, C.; Puente-Lanzarote, J.J.; Gascón, S.; Herrero-Continente, T.; Gonzalo-Romeo, G.; Alastrué-Vera, V. Hepatic galectin-3 is associated with lipid droplet area in non-alcoholic steatohepatitis in a new swine model. *Sci. Rep.* **2022**, *12*, 1024. [CrossRef]

Supplementary Table S1. Sequences of real-time PCR primers according to MIQE guidelines

Gene symbol	Primer sequence, sense/antisense (5'->3')	Amplicon length	Accession	Exon	Biological Process	Concentration	Efficiency
Atf6	AGAGTCTGCTTGTCAGTCGC GGTTCTCTGACACCACCTCG	149	NM_001081304.1 , XM_030253420.2, XM_011238796.4, XM_006496792.5	8/9	Unfolded protein response (UPR) during ER stress	0.2 µM	99%
Hspa5	CTTGCCATTCAAGGTGGTTG TGCATGGGTAACCTTCTTTCCC	163	NM_022310.3, NM_001163434.1	3/5	Folding and assembly of proteins in the ER and ER homeostasis	0.2 µM	98%
Eif2ak3	TATGTTGGAAGGCTTGAGGTCC GTACATTCAGATGCAGCTGTGC	178	NM_010121.3, XM_011241202.3, XM_006505501.2	13/ 14	Unfolded protein response (UPR) and integrated stress response (ISR) during ER stress	0.2 µM	96%
Atf4	CAGCAGTGTTGCTGTAACGG ATCTCGGTCATGTTGTGGGG	85	NM_009716.3, NM_001287180.1	2/3	Integrated stress response (ISR)	0.2 µM	97%
Ddit3	GCGACAGAGCCAGAATAACA GATGCACTTCCTTCTGGAACA	168	NM_007837.4, XM_006513197.4	1/2	Adipogenesis and erythropoiesis in ER stress response	0.2 µM	95%
Ern1	AACAACCTGCCCAAACATCG TGGTCGGTGTGTTGTCTGAA	109	NM_023913.2	11/ 12	Unfolded protein response (UPR) during ER stress	0.2 µM	93%
Xbp1	GAGAACCAGGAGTTAAGAACACG GAAGATGTTCTGGGGAGGTGAC	157 & 183	NM_001271730.1, NM_013842.3	3/5	Unfolded protein response (UPR) during ER stress	0.4 µM	94%
Ssr2	TTGGCTCTGTTAGCCGTCAG TTGAGAGGACGCAGGACAAC	272	NM_001356316.1, NM_001356317.1, NM_025448.4, NM_001356319.1, NM_001356318.1	2/4	Protein translocation across the ER membrane	0.2 µM	96%
Sec61a1	TCTGCAAAAAGGGTACGGCT GTTCTGGCGGTAGAATGCCT	211	NM_016906.4	7/8	Transport of signal peptide-containing precursor polypeptides across the ER	0.2 µM	99%
Tbp	GTGAGTTGCTTGCTCTGTGC GCTGCGTTTTTGTGCAGAGT	359	NM_013684.3	8	Housekeeping gene	0.2 µM	98%
Ppib	GGAGATGGCACAGGAGGAA TAGTGCTTCAGCTTGAAGTTCTCAT	71	NM_011149.2	3/4	Housekeeping gene	0.2 µM	99%
Txndc5	CAGGCTTGTCAGATGTCACCAT TAACCTCGTACCGAGTACTTGCTG	82	NM_001289599.1, NM_001289598.1, NM_145367.4	9/1 0	Formation of disulfide bonds in proteins	0.2 µM	92%

Abbreviations: *Atf6*, activating transcription factor 6; *Hspa5*, heat shock protein 5; *Eif2ak3*, eukaryotic translation initiation factor 2 alpha kinase 3; *Atf4*, activating transcription factor 4; *Ddit3*, DNA-damage inducible transcript 3; *Ern1*, endoplasmic reticulum (ER) to nucleus signalling 1; *Xbp1*, X-box binding protein 1; *Ssr2*, signal sequence receptor, beta; *Sec61a1*, Sec61 alpha 1 subunit; *Tbp*, TATA-box binding protein; *Ppib*, peptidylprolyl isomerase B; *Txndc5*, thioredoxin domain containing 5

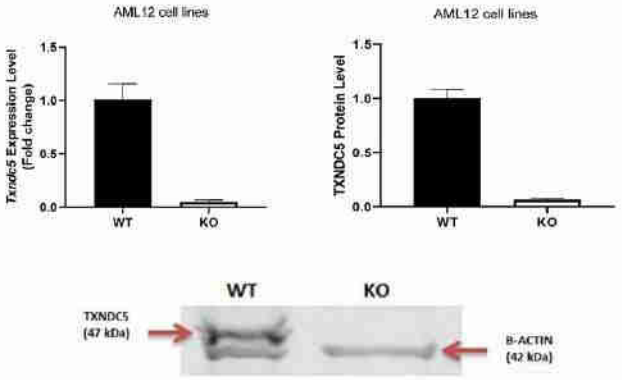

Supplementary Figure S1. Characterization of AML12 cell lines. *Txndc5* mRNA and protein levels in normal mouse hepatocyte AML12 cells (wildtype (WT)) and TXNDC5-deficient AML12 cells (knockout (KO))

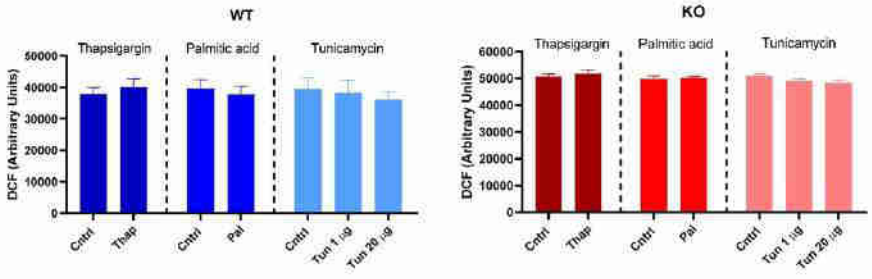

Supplementary Figure S2. ROS assessment of WT and KO AML12 cell lines under thapsigargin, palmitic acid, and tunicamycin stress.

antioxidants

MDPI

Article

Squalene Loaded Nanoparticles Effectively Protect Hepatic AML12 Cell Lines against Oxidative and Endoplasmic Reticulum Stress in a TXNDC5-Dependent Way

Seyed Hesamoddin Bidooki [1], Teresa Alejo [2,3], Javier Sánchez-Marco [1], Roberto Martínez-Beamonte [1,4,5], Roubi Abuobeid [1], Juan Carlos Burillo [6], Roberto Lasheras [6], Victor Sebastian [2,3,7], María J. Rodríguez-Yoldi [4,5,8], Manuel Arruebo [2,3,7] and Jesús Osada [1,4,8,*]

1 Departamento de Bioquímica y Biología Molecular y Celular, Facultad de Veterinaria, Instituto de Investigación Sanitaria de Aragón-Universidad de Zaragoza, E-50013 Zaragoza, Spain; h.bidooki94@gmail.com (S.H.B.); javiersanchezmarc@gmail.com (J.S.-M.); romartin@unizar.es (R.M.-B.); roubi.a.obeid@gmail.com (R.A.)
2 Departamento de Ingeniería Química y Tecnologías del Medio Ambiente, Universidad de Zaragoza, E-50018 Zaragoza, Spain; teresaal@unizar.es (T.A.); victorse@unizar.es (V.S.); arruebom@unizar.es (M.A.)
3 Instituto de Nanociencia y Materiales de Aragón (INMA), CSIC-Universidad de Zaragoza, E-50009 Zaragoza, Spain
4 Instituto Agroalimentario de Aragón, CITA-Universidad de Zaragoza, E-50013 Zaragoza, Spain; mjrodyol@unizar.es
5 Centro de Investigación Biomédica en Red de Fisiopatología de la Obesidad y Nutrición (CIBEROBN), Instituto de Salud Carlos III, E-28029 Madrid, Spain
6 Laboratorio Agroambiental, Servicio de Seguridad Agroalimentaria de la Dirección General de Alimentación y Fomento Agroalimentario, Gobierno de Aragón, E-50059 Zaragoza, Spain; jcburillo@aragon.es (J.C.B.); rjlasheras@aragon.es (R.L.)
7 Centro de Investigación Biomédica en Red de Bioingeniería, Biomateriales y Nanomedicina (CIBER-BBN), Instituto de Salud Carlos III, E-28029 Madrid, Spain
8 Departamento de Farmacología, Fisiología, Medicina Legal y Forense, Facultad de Veterinaria, Instituto de Investigación Sanitaria de Aragón-Universidad de Zaragoza, E-50013 Zaragoza, Spain
* Correspondence: josada@unizar.es; Tel.: +34-976-761-644; Fax: +34-976-761-612

check for updates

Citation: Bidooki, S.H.; Alejo, T.; Sánchez-Marco, J.; Martínez-Beamonte, R.; Abuobeid, R.; Burillo, J.C.; Lasheras, R.; Sebastian, V.; Rodríguez-Yoldi, M.J.; Arruebo, M.; et al. Squalene Loaded Nanoparticles Effectively Protect Hepatic AML12 Cell Lines against Oxidative and Endoplasmic Reticulum Stress in a TXNDC5-Dependent Way. *Antioxidants* **2022**, *11*, 581. https://doi.org/10.3390/antiox11030581

Academic Editor: Catalina Alarcón de-la-Lastra

Received: 28 February 2022
Accepted: 16 March 2022
Published: 18 March 2022

Publisher's Note: MDPI stays neutral with regard to jurisdictional claims in published maps and institutional affiliations.

Abstract: Virgin olive oil, the main source of fat in the Mediterranean diet, contains a substantial amount of squalene which possesses natural antioxidant properties. Due to its highly hydrophobic nature, its bioavailability is reduced. In order to increase its delivery and potentiate its actions, squalene has been loaded into PLGA nanoparticles (NPs). The characterization of the resulting nanoparticles was assessed by electron microscopy, dynamic light scattering, zeta potential and high-performance liquid chromatography. Reactive oxygen species (ROS) generation and cell viability assays were carried out in AML12 (alpha mouse liver cell line) and a TXNDC5-deficient AML12 cell line (KO), which was generated by CRISPR/cas9 technology. According to the results, squalene was successfully encapsulated in PLGA NPs, and had rapid and efficient cellular uptake at 30 μM squalene concentration. Squalene reduced ROS in AML12, whereas ROS levels increased in KO cells and improved cell viability in both when subjected to oxidative stress by significant induction of *Gpx4*. Squalene enhanced cell viability in ER-induced stress by decreasing *Ern1* or *Eif2ak3* expressions. In conclusion, TXNDC5 shows a crucial role in regulating ER-induced stress through different signaling pathways, and squalene protects mouse hepatocytes from oxidative and endoplasmic reticulum stresses by several molecular mechanisms depending on TXNDC5.

Keywords: olive oil; liver; squalene; PLGA; oxidative stress; endoplasmic reticulum stress; TXNDC5; *Gpx4*; *Ern1*; *Eif2ak3*

1. Introduction

The Mediterranean diet, also known as the Med diet, has been associated with a variety of health benefits on cardiovascular diseases, including a reduction in the frequency of

cardiovascular events as well as their risk factors, including obesity and metabolic disorders such as diabetes, hypertension and dyslipidemia [1]. This diet pattern consists of varying plant-based food sources such as fruits, vegetables, olive oil and nuts [2]. Virgin olive oil, the main source of fat in this diet, has been linked to a reduced risk of general and cause-specific mortality [3]. It is composed of an oily matrix of triglycerides containing monounsaturated fatty acids and a minor fraction dubbed unsaponifiable [4,5]. The biological effects of the latter compounds have recently been the focus of attention [6].

Squalene accounts for almost 90% of the hydrocarbons present in the unsaponifiable fraction of virgin olive oil [7]. Squalene is a terpenoid-like natural lipid with an isoprenoid structure that is used as an intermediary in the biosynthesis of phytosterols and terpenes in plants and cholesterol in animals [8]. Squalene has a number of demonstrated therapeutic features, including being a natural antioxidant, lowering blood cholesterol levels and having tumor-protective properties [9]. For instance, squalene inhibited aberrant hyperproliferation in a non-tumorigenic mammary epithelial cell line in vitro, according to Katdare et al. [10]. Squalene suppressed cell proliferation in an invasive MDA-MB-231 breast cancer cell line by triggering apoptosis and DNA damage [11]. Murakoshi et al. found that topically applied squalene significantly reduced mice skin tumors [12].

Several compounds encapsulated in nanoparticles for anti-cancer therapy and other disorders have been extensively studied with the goal of protecting sensitive chemicals from degradation, increasing their solubility and therefore favoring their bioavailability [13,14]. Nanoparticles have also been used for targeting and crossing biological barriers, lessening irritation or facilitating the bioavailability of different drugs while minimizing side effects [15,16]. As a result, a wide range of naturally derived and biodegradable particles, such as chitosan, poly (lactic-co-glycolic acid) (PLGA) and protein-based particles have been developed [17]. PLGA is one of the most effectively used biodegradable polymers due to the fact that its hydrolysis results in endogenous metabolite monomers, lactic acid and glycolic acid, which can easily be degraded in the body by the Krebs cycle. Therefore, because the body can adequately metabolize these two monomers, the use of PLGA for drug delivery or tissue engineering applications has a low risk of systemic toxicity [18]. Many routes have been reported to be involved in PLGA nanoparticle cellular uptake and penetration into the cytoplasm [19,20].

Protein synthesis, processing, and folding; intracellular transport and calcium signaling; drug detoxification; and lipid metabolism are all performed in the endoplasmic reticulum (ER), which is a multifunctional organelle [21]. ER homeostasis alterations are caused by high levels of free fatty acids, calcium depletion or insulin resistance and lead to an accumulation of misfolded proteins, which triggers the unfolded protein response (UPR) [22–24]. Grp78 releases Ern1, Eif2ak3 and Atf6 as a result of the presence of unfolded proteins in the ER [25,26]. Squalene reduces hepatic fat content and induces the expression of proteins involved in the lipidic metabolism [27]. Our hypothesis is that the restoring of those critical proteins by administering bioavailable squalene may result in reduced ER stress.

The imbalance between the excessive generation of cellular reactive oxygen species (ROS) [26] and the reduced ability of live organisms to counteract ROS through antioxidant system response is commonly referred to as oxidative stress [28–30]. Research from animal models suggests that oxidative stress plays a role in steatohepatitis [31]. Squalene's function has been studied in a variety of cell lines and appears to be linked to quenching oxidative stress. In mouse peritoneal macrophages and human promyelocytic leukemia cell lines (HL-60), respectively, squalene reduced the intracellular ROS content caused by lipopolysaccharide incubation and also suppressed hydrogen peroxide-induced protein carbonylation [32,33]. Squalene reduced intracellular ROS levels, inhibited H_2O_2-induced oxidative injury and protected human mammary epithelial cells (MCF10A) against oxidative DNA damage [34]. The liver is the most commonly affected organ by oxidative stress, owing to its constant exposure to oxidative stimuli and its high mitochondrial

activity [30,35]; dietary squalene administration could reduce oxidative stress in several mice models as well [36].

Thioredoxin domain-containing 5 (TXNDC5) protects hepatic cells from stress-induced apoptosis [37,38]. TXNDC5 is situated in the ER and, as a member of the protein disulfide isomerase (PDI) family, is implicated in protein modification and folding [39]. During hypoxic situations, TXNDC5 is abundantly expressed in the liver and endothelial cells and performs vital roles in anti-oxidative harm, anti-anoxia-induced apoptosis and cellular proliferation [40,41]. Hence, this present study describes the protection function of PLGA-based squalene nanoparticles on oxidative and ER stress in mouse hepatocytes. To address these issues and acquire a better understanding of the mechanisms involved in the putative role of squalene, the function of TXNDC5 and the main ER molecular mechanisms in stress circumstances were explored.

2. Materials and Methods

2.1. Preparation of PLGA-Based Squalene-Loaded Nanoparticles

Squalene–PLGA polymeric nanoparticles were synthesized by the single-emulsion solvent evaporation technique [42,43] using Resomer® RG 503H poly(D,L-lactide-co-glycolide) (PLGA-COOH, Mw 24–38 kDa) (Sigma-Aldrich; Merck Millipore, Darmstadt, Germany), Pluronic F68 (Panreac Quimica S.L.U; Barcelona, Spain) and ethyl acetate 99.6% ACS (Sigma-Aldrich, Merck Millipore, Darmstadt, Germany) in the presence of 100, 75, 50, 25 µL of squalene (2.05 M, ≥98%, liquid) (Sigma-Aldrich, Merck Millipore, Darmstadt, Germany). Briefly, PLGA (50 mg) and Pluronic (150 mg) were dissolved in ethyl acetate (5 mL). Different concentrations of squalene were added to the solution together with 10 mL of Milli-Q water and sonicated (Branson Digital Sonifier 450, Danbury, CT, USA) in an ice bath for 25 s and at 40% amplitude using a probe of 0.13 inches in diameter. Then, the organic solvent was evaporated under sterile conditions for 3 h with stirring at 600 rpm. Finally, the nanoparticles were collected by centrifugation (Thermo Fisher Scientific, Waltham, MA, USA) at 12,350× *g* and then at 15,000× *g* for 15 min at 10 °C and dispersed in fresh PBS for the subsequent cellular experiments.

2.2. Physicochemical Characterization of the Nanoparticles

A scanning electron microscope (SEM, FEG INSPECT-F50, Eindhoven, Netherlands) was used to determine the morphology of the resulting nanoparticles. For sample preparation, a drop of the NP dispersion (10 µL, 1 mg/mL) was placed on a glass slide, fixed with carbon tape to a holder, air-dried overnight and sputtered with a very thin, fine-grained Palladium coating to facilitate electron conduction (Leica EM ACE200, Wetzlar, Germany). In order to determine the resulting particle size, particles were also analyzed using transmission electron microscopy (TEM) (Tecnai T20, FEI Company, Hillsboro, OR, USA, operating at 200 kV). This microscope is equipped with a thermionic gun (LaB6) and a SuperTwin® objective lens that allows a 0.24 nm spatial resolution. The CCD camera selected to take the TEM Images was a Veleta CCD 2k × 2k, for fast acquisition and a wide field of view. Squalene–PLGA NPs were negatively stained using phosphotungstic acid dissolved in Milli-Q water (30 mg/mL). TEM samples were prepared on Forward Cu-200 mesh TEM grids by depositing 100 µL (1 mg/mL) of NP dispersion onto the grid, then squalene–PLGA NPs were stained with a phosphotungstic acid solution, washed with water to remove salts in excess and finally dried overnight. For each sample, four different areas of the grid were examined to obtain representative results, obtaining at least 15 images per sample. At least 150 nanoparticles were measured from TEM images using ImageJ software version 3.5 to plot the particle size histogram and determine mean diameter and standard deviation. A Brookhaven 90 Plus (Holtsville, NY, USA) (90° scattering angle, 25 °C) was used to assess the hydrodynamic particle size and zeta potential of the nanoparticles in water at neutral pH. When suspending 20 µL of NPs in 3 mL of distilled water for size measurements by dynamic light scattering (DLS), a good attenuator value (7–9) was procured. The average of five 180 s measurements yielded the mean hydrodynamic diameter for each prepara-

tion. PLGA-squalene NPs (70 µL) were dispersed in 2 mL of 1 mM KCl before filling the measurement cell for zeta potential measurements at neutral pH and 25 °C. The average of five independent measurements in automated mode, followed by the application of the Smoluchowski equation, yielded the mean zeta potential for each preparation. The findings were standardized using blank PLGA nanoparticles without squalene as a reference.

2.3. PLGA Encapsulation Efficiency Experiment

In a 5% dextrose solution, PLGA NPs with different initial squalene contents (100, 75, 50, 25 µL of 2.05 M of squalene) were formulated and then washed twice with water using an ultrafiltration device (Amicon, molecular weight cut-off, 100,000 Da). Squalene was extracted from the NPs using ethanol and quantified by high-performance liquid chromatography (HPLC). The HPLC Waters Alliance 1695 (Waters, Milford, MA, USA) was used, which was retrofitted with a Waters DAD 2996 photodiode array detector, a Hewlett-Packard computer running Waters Empower 3 software and a Waters autosampler with a 50 µL loop. Synchronous spectra detection wavelengths ranging from 200 to 600 nm were recorded for all peaks. A non-gradient mobile phase of acetonitrile and methanol (50:50, *v*/*v*) was adopted at a constant flow rate of 1 mL/min on a Waters XSelect LC-18 column (2.1 mm by 150 mm, 3.5 µm). The squalene peak was calculated quantitatively by comparing it to a standard curve at a wavelength of 216 nm. The absorbance of the organic solvents in the selected wavelength of 216 nm was subtracted by the autozero.

2.4. Squalene Extraction

Following cell harvest and squalene being loaded into PLGA NPs, squalene was extracted and analyzed by gas chromatography and mass spectrometry (GC/MS), as previously described [44].

2.5. AML12 Cell Culture

The mouse hepatocyte cell line (AML12) was obtained from the ATCC collection (Manassas, VA, USA) and cultured in a 6-well plate (in duplicate) at 37 °C in a humidified atmosphere of 5% CO_2 in Dulbecco's modified Eagle's minimum essential medium (DMEM; Thermo Fisher Scientific, Waltham, MA, USA): F-12-Ham's medium (GE Healthcare Life Science, South Logan, UT, USA) at a 1:1 ratio supplemented with 10% fetal bovine serum (Thermo Fisher Scientific, Waltham, MA, USA), 1:500 insulin-transferrin-selenium (Corning, Bedford, MA, USA), 40 ng/mL dexamethasone (Sigma-Aldrich; Merck Millipore, Darmstadt, Germany), 1% nonessential amino acids (Thermo Fisher Scientific, Waltham, MA, USA), 1% amphotericin B (1000 mg/mL; Thermo Fisher Scientific, Waltham, MA, USA), 1% penicillin (1000 U/mL; Thermo Fisher Scientific) and 1% streptomycin (1000 mg/mL; Thermo Fisher Scientific, Waltham, MA, USA). This medium was removed after the AML12 cells reached 90–100% confluence, and the cells were washed once with PBS before being given the medium free of fetal bovine serum and amphotericin B. For RNA isolation and cDNA synthesis, performed as described below, cells were treated with 12.5 nM of thapsigargin (Sigma-Aldrich, Merck Millipore, Darmstadt, Germany) or 25 mM of H_2O_2 (Sigma-Aldrich, Merck Millipore, Darmstadt, Germany) for 24 h and 30 min, respectively, after 72 h of exposure to 30 µM of squalene loaded PLGA nanoparticles.

2.6. Characterization of Cell Morphology in Presence of PLGA-Squalene Nanoparticles

AML12 cells (2000 cells per well) were cultured in a 24-well plate (in duplicate). Cells were incubated for 72 h in the presence of 150, 60, 30 and 15 µM squalene loaded in PLGA nanoparticles and non-loaded PLGA nanoparticles as control. After washing 2 times with PBS, cells were mixed with 4% formaldehyde (Panreac Química S.L.U., Barcelona, Catalonia, Spain) and dissolved in PBS for 30 min at room temperature. Cells were washed with 60% isopropanol (Panreac Química S.L.U., Barcelona, Catalonia, Spain) and PBS, respectively, afterward, stained with 1% Nile Red (Thermo Fisher Scientific, Waltham, MA, USA) and dissolved in PBS for 15 min in the dark. After PBS wash, an epifluorescence microscope

(Floid Cell Imaging System; Thermo Fisher Scientific, Waltham, MA, USA) with excitation and emission wavelengths of 552/636 nm was utilized for detecting the influence of several PLGA NPs concentrations on the AML12 cell line.

2.7. Generation of a Stable TXNDC5 Knockout AML12 Cell Line

The AML12 cell line was grown as erstwhile explained to create stable clones without TXNDC5. The culture medium was withdrawn after one week of development, and the cells were washed twice with PBS before being transfected with TXNDC5/ERp46 HDR and TXNDC5 CRISPR/Cas9 KO plasmids (Santa Cruz Biotechnology, Dallas, TX, USA) using lipofectamine 2000 (Thermo Fisher Scientific, Waltham, MA, USA). TXNDC5 CRISPR/Cas9 KO plasmid possesses gRNA sequence; 5′-TTATCAAGTTCTTCGCTCCG-3′ to generate a double-stranded break (DSB) specifically in the fifth exon of *Txndc5*. To provide the selection of constant knockout (KO) AML12 cells, the TXNDC5/ERp46 HDR recombined the *Txndc5* gene containing a puromycin resistance gene. Puromycin-resistant AML12 KO cells were selected after several rounds of puromycin incubations. TXNDC5 absence was confirmed by Western blot (Supplementary Figure S1).

2.8. RNA Extraction

Total cellular RNA was extracted according to the manufacturer's instructions by using a Quick-RNA^{TM} MiniPrep kit (Zymo Research, CA, USA). RNA was quantified based on the absorbance ratio at 260/280 nm wavelength using a Nanodrop 2000c Spectrophotometer (Thermo Fisher Scientific, Waltham, MA, USA). The integrity of the 28S and 18S ribosomal RNAs was confirmed by electrophoresis on a 1% agarose gel followed by ethidium bromide staining, and the 28S/18S ratio was larger than 2.

2.9. Quantitative Real-Time PCR (RT-qPCR)

To achieve equivalent efficiencies, the reverse transcriptase quantitative PCR tests of these transcripts were optimized in terms of primer and input cDNA concentrations. The PrimeScript RT reagent kit (TaKaRa Biotechnology, Kusatsu, Shiga, Japan) was used to reverse transcribe 500 ng of extracted total RNA into the supplementary deoxyribonucleic acid in the presence of random and oligo (dT) primers, following the manufacturer's instructions. Primer Express (Applied Biosystems, Foster City, CA, USA) was used to design the primers for each gene, as mentioned in Supplementary Table S1, which were then validated for gene specificity and amplification of cDNA rather than genomic DNA using BLAST analysis (NCBI); eventually, the primers were selected based on the primer efficiency. On a Step One Plus Real-Time PCR System (Applied Biosystem, Foster City, CA, USA), quantitative real-time PCR was performed according to the manufacturer's guidelines (SYBR Green PCR Master Mix, Applied Biosystems, Foster City, CA, USA). Each gene's transcript expression level was estimated using the comparative $2^{-\Delta\Delta CT}$ method, normalized to the endogenous control genes *Ppib* and *Tbp* and expressed as a relative ratio to the mean values of control samples.

2.10. Western Blot

The Bradford reagent (Bio-Rad, Hercules, CA, USA) was used to assess the total protein concentration in AML12 WT and KO cells after they were lysed. Then, 10 µg of proteins were separated on a 10% sodium dodecyl sulfate-polyacrylamide gel electrophoresis and transferred to polyvinylidene difluoride filter membranes (Bio-Rad, Hercules, CA, USA). The membrane was blocked for 1 h at room temperature using a PBS buffer containing 5% BSA. After blocking, the membrane was incubated at 4 °C overnight with a primary rabbit polyclonal antibody against mouse TXNDC5 (1:1000, Proteintech, Manchester, UK) and mouse monoclonal anti-β-ACTIN (1:1000, Sigma, St Louis, MO, USA). The membrane was washed three times with a PBS buffer containing 0.1% Tween 20 and incubated for 1 h at room temperature with conjugated goat anti-rabbit IgG (H&L) DyLight 800 secondary antibody (1: 60,000, Thermo-scientific, Waltham, MA, USA) and goat anti-mouse IgG (H&L)

DyLight 680 secondary antibody (1: 30,000, Thermo-scientific, Waltham, MA, USA). Blot was visualized by Odyssey®Clx (LI-COR, Bad Homburg, Germany).

2.11. Cell Viability Assay

Cell viability was determined using 3-(4 5-dimethylthiazol-2-yl)-2 5-diphenyltetrazolium bromide assay (MTT; Sigma-Aldrich, Merck Millipore, Darmstadt, Germany). Cells were seeded on a 96-well plate at 5000 cells/well and exposed for 24 h to 18 nM of thapsigargin (Sigma-Aldrich, Merck Millipore, Darmstadt, Germany) dissolved in 0.1% DMSO for ER stress and 30 min of 20, 25 and 30 mM of H_2O_2 (Sigma-Aldrich, Merck Millipore, Darmstadt, Germany) for oxidative stress in presence of 30 µM of nanoencapsulated squalene for 72 h, thereupon 1 mg/mL of MTT was added to the culture medium. Following 3 h incubation, cell growth medium was replaced by DMSO and absorbance measurements were assessed with a 96-well plate reader at 570 nm.

2.12. Reactive Oxygen Species Assay

AML12 cells (5000 cells per well) were seeded in a 96-well plate and cultured for 72 h at 37 °C. The cells were treated for 72 h with PLGA-squalene NPs or control NPs diluted in the medium free of fetal bovine serum and amphotericin B at a concentration of 30 µM; afterward, 10 µL of 2.0 mg/mL 2,7-dichlorofluorescein diacetate (DCFH-DA; Sigma-Aldrich, Merck Millipore, Darmstadt, Germany) dissolved in fresh PBS were added to the cells. After 3 h, the medium was removed, and cells were incubated with a medium containing hydrogen peroxide (H_2O_2; final concentration, 25 mM; Sigma-Aldrich, Merck Millipore, Darmstadt, Germany). After 3 h, the presence of ROS was assessed by measuring the conversion of DCFH-DA into fluorescent dichlorofluorescein (DCF) at excitation and emission wavelengths of 485 and 520 nm in a microplate reader (FLUOstar®, Omega, BMG Labtech, Ortenberg, Germany), respectively.

2.13. Statistical Analysis

Statistical analyses were carried out using the GraphPad Prism 8 for Windows (GraphPad, S. Diego, CA, USA). Statistical significance was defined as a p-value of less than 0.05. The Mann–Whitney U test was used to conduct the statistical analysis. The Shapiro–Wilk test was used to determine the normal distribution of data and Bartlett's or Levene's tests were used to determine the homology of variance among groups. A 2-tailed Student's t-test and two-way ANOVA with Dunnett's multiple comparisons test were used to investigate parameters that matched both criteria. The means and standard deviations of the results are shown.

3. Results

3.1. Synthesis and Physicochemical Characterization of Squalene Loaded PLGA Nanoparticles

To examine the synthesis and physicochemical characterization of the nanoparticles prepared using the single emulsion approach, the squalene encapsulation ability of PLGA was characterized by HPLC (Table 1). The maximum squalene loading in PLGA-based nanoparticles was found when using 50 µL initial squalene (2.05 M, ≥98%, liquid) volume that reached 8122 ± 735 µM of squalene loading. This represented 77.8 ± 5.1% encapsulation efficiency, and the highest ratio of squalene referred to PLGA of the ones tested. The encapsulation efficiency reported in the literature for squalene loaded nanoparticles was variable depending on the nanoparticle type and the synthetic method ranging from 26 to 82% [45–47]. These nanoparticles were selected to carry out the experimental work. Nanoparticles were characterized by scanning electron microscopy (SEM) to determine their morphology and size (Figure 1). PLGA NPs devoid of squalene were spherical in shape, in contrast to NPs loaded with squalene that showed a larger size an oval shape (Figure 1). Transmission electron microscopy (TEM) analysis confirmed a general trend toward size increase when squalene was loaded in PLGA (Figure 1). Particle size histograms determined from TEM images revealed that the mean size of PLGA nanoparticles increased

from 90.5 ± 13.3 to 167.9 ± 31.3 when squalene was encapsulated (Figure 1). Then, it seems that squalene affects both the micelle shape and size during the emulsification process. This observation is in agreement with previous results where the presence of lipids such as cholesterol can increase the PLGA size [48]. The hydrodynamic diameter of the nanoparticles in water at neutral pH, estimated by dynamic light scattering (DLS), was 259 ± 107 nm for squalene loaded PLGA NPs and their dispersion was higher than that of empty NPs (Table 2). The analysis on the particle size between TEM and DLS demonstrated the same trend, confirming the size enlargement when squalene is encapsulated. The nanoparticle mean diameters from TEM image-based measurements were smaller than the ones obtained from hydrodynamic size measurement. However, these differences can be explained by the technique differences—in TEM, the nanoparticles are dried, and the size should be smaller after shrinking [49–52]. The presence of squalene also had a clear impact on the zeta potential values. In this sense, the negative values (−46.8 ± 0.6 mV) of PLGA nanoparticles without squalene significantly decreased in PLGA-based squalene nanoparticles (−36.2 ± 0.3 mV) at neutral pH. The negative charge of PLGA NPs without squalene could be attributed to the presence of ionized carboxyl groups in the acid terminated PLGA (PLGA-COOH), whereas the less negative charge of PLGA-based squalene nanoparticles might be due to the presence of squalene on the surface of the nanoparticles, as described previously for other nanoparticles [53].

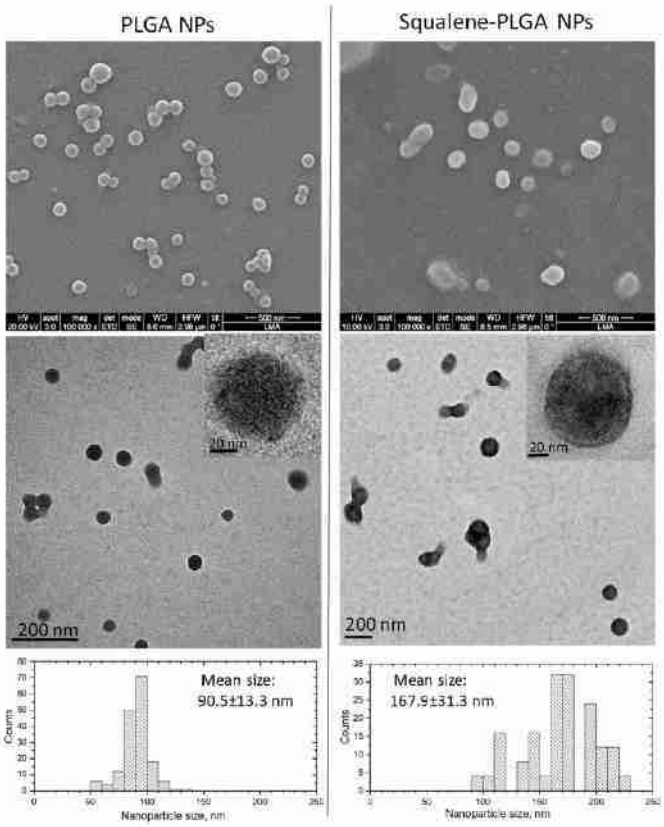

Figure 1. Electron microscopy analysis, SEM, TEM and particle size histograms of PLGA nanoparticles with and without squalene.

Table 1. Squalene content and encapsulation based on the squalene initial volume in PLGA nanoparticles.

Squalene Initial Volume	Squalene Concentration (μM)	Squalene Encapsulation (%)	Squalene/PLGA (*w*/*w*)
100 μL	7472 ± 530	35.8 ± 3.8	0.614
75 μL	5417 ± 474	34.6 ± 3.0	0.445
50 μL	8122 ± 735	77.8 ± 5.1	0.667
25 μL	4842 ± 671	92.7 ± 12.9	0.398

Table 2. Physicochemical characterization of PLGA nanoparticles.

Polymer	Diameter (nm)	Dispersion	Zeta Potential (mV)
PLGA NPs with squalene	259 ± 107	0.173	−36.2 ± 0.3
PLGA NPs without squalene	129 ± 37	0.083	−46.8 ± 0.6

3.2. *Influence of Several PLGA NPs Concentrations on the Morphology of AML12 Cell Line*

After squalene extraction and GC/MS analysis, the squalene concentration loaded into PLGA nanoparticles was determined to be 3.05 mM. The influence of various concentrations of PLGA nanoparticles was qualitatively examined by microscopy after 72 h of incubation with AML12 cells. Hence, four different concentrations were investigated. Figure 2 shows the AML12 cell line after exposure to 150, 60, 30 and 15 μM doses of squalene loaded into PLGA nanoparticles and to the PLGA nanoparticles without squalene. The 150 μM PLGA NPs caused the cell to completely shrink (Figure 2A), but the shrinkage was mitigated by lowering the nanoparticle dosage (Figure 2B–D). Due to the observed morphological impact of the highest doses, the 30 μM of squalene loaded in the PLGA nanoparticles was selected to carry out the subsequent studies on AML12 cells.

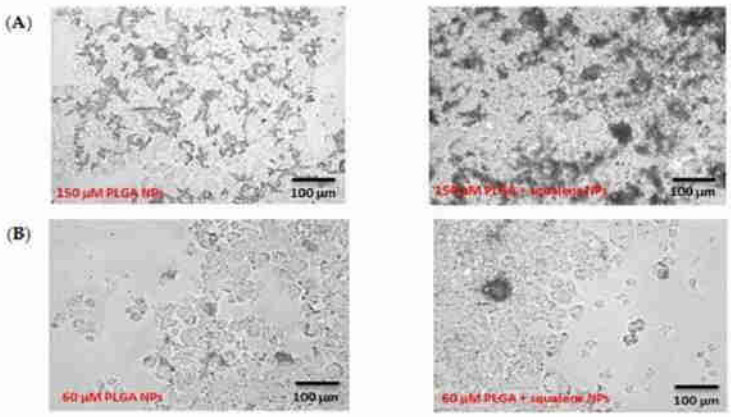

Figure 2. *Cont.*

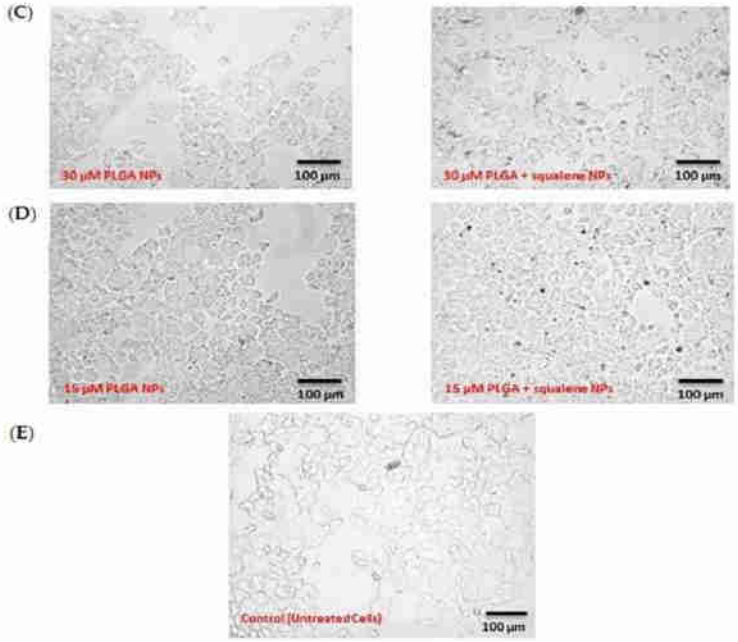

Figure 2. Detection of the effect of different PLGA nanoparticles concentrations (with and without squalene) on the AML12 cell line. (**A**) 150 μM, (**B**) 60 μM, (**C**) 30 μM, (**D**) 15 μM and (**E**) untreated cells.

3.3. AML12 Cellular Uptake of Squalene

To study the capability of PLGA-based squalene NPs to be uptaken by the AML12 hepatocyte cell line, these cells were incubated in the presence of 30 μM of PLGA-based squalene NPs and empty PLGA NPs for 72 h, and cellular squalene content was measured (Figure 3). As shown, the cellular uptake of squalene increased significantly when the NPs were loaded with squalene, indicating that this is an efficient vehicle to deliver this compound in this cell line.

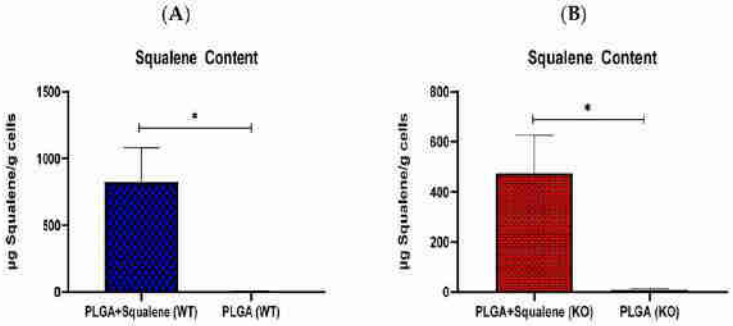

Figure 3. In vitro cellular uptake of squalene. Hepatic AML12 cells were incubated with 30 μM of PLGA-based squalene NPs and PLGA NPs for 72 h. (**A**) normal mouse AML12 cells (wild-type (WT)), (**B**) TXNDC5-deficient AML12 cells (knockout (KO)). Statistical analyses were done according to Mann–Whitney's U-test; * $p < 0.05$.

3.4. Squalene Based PLGA NPs Could Effectively Protect against Oxidative Stress

Normal mouse hepatocyte AML12 cells (wild-type (WT)) and TXNDC5-deficient AML12 cells (knockout (KO)) were incubated with 30 μM of squalene loaded NPs for 72 h to assess the induction of intracellular ROS by PLGA-based squalene nanoparticles, and the amount of intracellular ROS was calculated according to the dichlorodihydrofluorescein (DCF) production. As shown in Figure 4(A1), WT cells treated with squalene NPs exhibited a significant decrease in ROS production compared with the PLGA group. However, squalene NPs increased the formation of ROS in KO samples (Figure 4(A2)). The comparison of the control group and the PLGA illustrates that PLGA nanoparticles did not induce ROS in both cell lines. To peruse whether 30 μM of squalene loaded NPs could effectually represent protection against oxidative stress, we initially developed an in vitro model of oxidative insult. When WT and KO cells were incubated with 25 mM H_2O_2 for 3 h, a significant reduction in intracellular reactive oxygen species was detected in AML12 WT cells treated with squalene NPs (Figure 4(B1)), whereas in the KO cells, the increment was observed (Figure 4(B2)). These results suggest that there was not any squalene protection in cells lacking TXNDC5 in exposure to the oxidative agent.

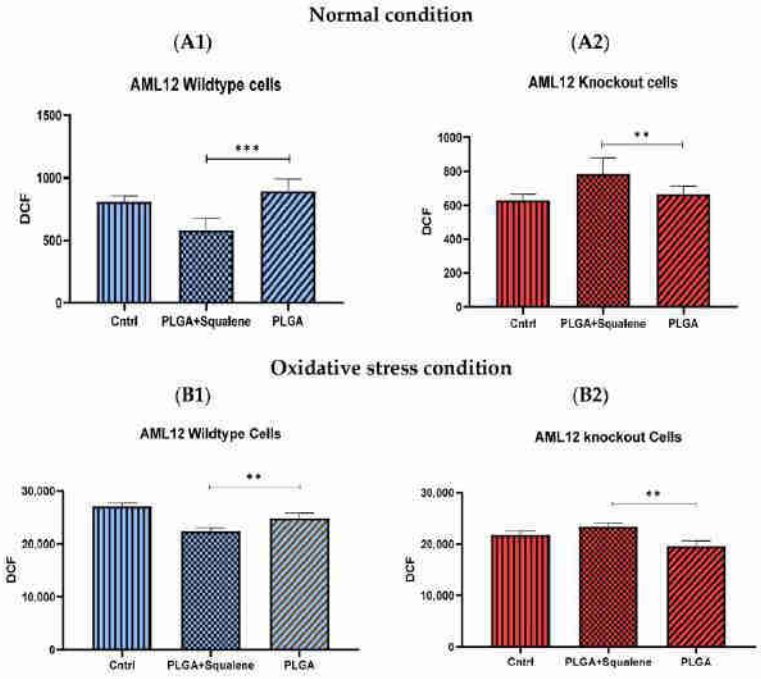

Figure 4. Assessment of ROS production in normal mouse AML12 cells cell line (AML12 wild-type (WT)) and TXNDC5-deficient AML12 cells (AML12 knockout (KO)). (**A**,**B**) After treatment of cells with 30 μM of squalene NPs for 72 h, (**A**) ROS was measured in normal conditions, (**B**) oxidative stress circumstance by 25 mM of H_2O_2 for 3 h. (**A1**) potent reduction of ROS in squalene group in WT cells, and (**A2**) significant enhancement in KO cells were observed. (**B1**) Considerable decrement of ROS in squalene group in WT cells and (**B2**) remarkable increase in KO cells are indicated. Statistical analyses were done according to Mann–Whitney's U-test; ** $p < 0.01$, *** $p < 0.001$.

The cell viability of WT and KO cells is shown in Figure 5. After 72 h exposure to 30 μM concentrations of both mixtures of PLGA and of the squalene loaded into the PLGA nanoparticles, the cells were treated with three different concentrations of H_2O_2 for 30 min.

The PLGA NPs did not produce notable alteration on the cell viability, according to the MTT assay, when compared to the control group. Squalene loaded PLGA NPs could significantly increase the viability of both cell lines (Figure 5A,B). Viability enhancement was calculated in the different H_2O_2 concentrations that were tested, and the results showed that the squalene delivered from PLGA nanoparticles incremented, on average, the viability in the wild-type mouse hepatocyte cells and knockout by 16 and 21%, respectively (Figure 5C).

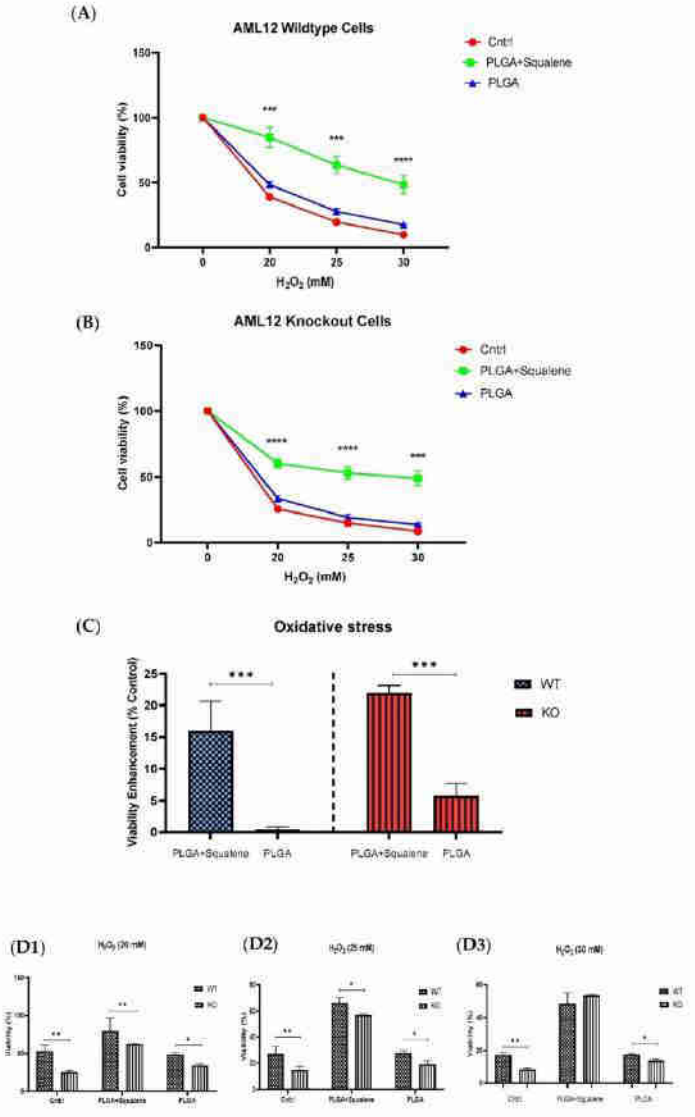

Figure 5. Squalene loaded PLGA NPs increased viability against oxidative stress. MTT was applied to evaluate the cell viability. (**A**) Normal mouse AML12 cells (AML12 wild-type (WT)) were exposed

to 30 μM PLGA based squalene NPs for 72 h had a significant increase in viability in presence of 20, 25 and 30 mM of H_2O_2, and (**B**) TXNDC5-deficient mouse hepatocyte cells (AML12 knockout (KO)) displayed a similar increment in viability. (**C**) Statistically, a significant difference of 16% and 21% was observed on average in viability enhancement of WT and KO cell lines, respectively, related to respective control in 20, 25 and 30 mM of H_2O_2. (**D**) TXNDC5 deletion can drastically lower the viability of the mouse hepatocyte in the absence of squalene at all concentrations tested; however, when the cells were treated with squalene, the viability of both cell lines increased. Although (**D3**) there were no significant differences between WT and KO cells at 30 mM H_2O_2, (**D1**,**D2**) a statistical difference was seen in samples treated with squalene loaded in PLGA nanoparticles in presence of 20 and 25 mM H_2O_2. Statistical analysis was carried out according to two-way ANOVA and Mann–Whitney's U-test for pairwise comparisons; * $p < 0.05$, ** $p < 0.01$, *** $p < 0.001$, **** $p < 0.0001$.

3.5. Effect of Squalene Protection on Oxidative Stress Response In Vitro by Gpx4 Induction

After treatment for 72 h with squalene-loaded PLGA based NPs (30 μM), we examined the levels of glutathione peroxidase 4 in both cell lines. Specifically, we discovered that *Gpx4*, which is involved in the antioxidant defense to neutralize oxidative stress, significantly increased its mRNA level in the squalene-treated samples (Figure 6A,B). Compared with the control group (Figure 6C,D), mRNA levels of *Gpx4* were significantly downregulated by the oxidative challenge (25 mM H_2O_2), irrespective of squalene supplementation. However, in squalene-treated samples, there was not any considerable reduction in mRNA levels of *Gpx4* in the presence of hydrogen peroxide.

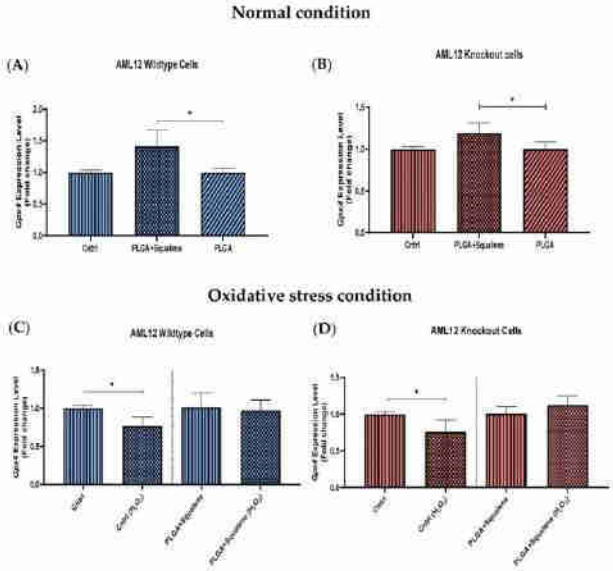

Figure 6. Effect of 30 μM PLGA based squalene nanoparticles on the *Gpx4* gene expression levels of oxidative-challenged (**A**,**C**) in wild-type mouse hepatic cells, and (**B**,**D**) knockout mouse hepatic cells. (**A**,**B**) Significant *Gpx4* induction after 72 h treatment with squalene encapsulated by PLGA in WT and KO cell line, respectively, (**C**,**D**) H_2O_2 can significantly downregulate *Gpx4* mRNA level after 30 min exposure to the 25 mM in the control group; whereas squalene encapsulated by PLGA prevented this reduction in both cell lines. The Mann–Whitney U-test was used in the statistical analysis; * $p < 0.05$.

3.6. Squalene Enhanced the Cell Viability of Mouse Hepatocytes in Harsh ER Stress

ER stress is an adaptive stress response program that is induced by thapsigargin. In AMI12 cells, MTT revealed an IC_{50} of 12.5 nM for thapsigargin. The cell viability under harsh ER stress conditions was evaluated after 72 h of treatment with 30 µM squalene loaded in PLGA and 24 h exposure to the 18 nM of thapsigargin. The PLGA nanoparticles without the squalene revealed no changes (Figure 7). After exposure to ER stress, both cell lines (i.e., AML12 wild-type and knockout) exhibited a fairly remarkable increase in the cell viability when using squalene-containing nanoparticles, i.e., at 18 nM cell viability reached values of 6.73% for WT (Figure 7A) and 6.55% for KO in average (Figure 7B), compared to the unexposed control.

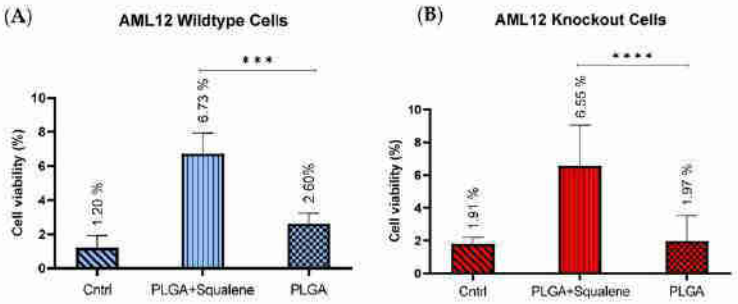

Figure 7. The cell viability evaluation of mouse hepatocytes upon ER stress. After 72 h, treated with 30 µM of squalene-loaded PLGA nanoparticles, ER stress was induced by 18 nM of thapsigargin for 24 h. (**A**,**B**) PLGA NPs did not produce a substantial difference in cell viability when compared to the untreated cells. PLGA based squalene nanoparticles at the 18 nM of thapsigargin (**A**) produced an enhancement of approximately 6% on the cell viability in WT cells (cell viability is 2.60% in control); likewise, (**B**) similar result was observed in KO cells. Statistical analyses were conducted according to two-way ANOVA; *** $p < 0.001$, **** $p < 0.0001$.

3.7. Squalene Protects Thapsigargin-Induced ER Stress by Ern1 and Eif2ak3 Pathways

To understand the effect of squalene on ER stress markers, we considered whether *Atf6*, *Ern1* and *Eif2ak3* expressions were caused by the squalene presence in mouse hepatocytes. The expression of ER stress-related genes in the presence of 30 µM of squalene loaded in PLGA NPs for 72 h did not show notable differences in AML12 WT cells (Figure 8A). However, in TXNDC5-deficient cells, mRNA abundance of *Atf6* and *Ern1* was significantly up-regulated by squalene treatment; furthermore, there was a significant difference in *Eif2ak3* expression (Figure 8B). When exposed to 12.5 nM of thapsigargin for 24 h to induce ER stress, for evaluating the function of squalene-PLGA NPs, wild-type cells exhibited a substantial attenuation in *Ern1* transcription rate; whereas, *Atf6* and *Eif2ak3* presented no significant decrement in mRNA levels (Figure 8C). The results in TXNDC5 knockout cells indicated that the *Eif2ak3* expression had a profound reduction in the presence of squalene in exposure to agents that cause ER stress, while no difference in *Atf6* and *Ern1* expression was observed between the squalene loaded in PLGA NPs and the PLGA nanoparticles (Figure 8D). These findings suggest that squalene plays an important role in maintaining the viability of mouse hepatocytes by repressing *Ern1* and *Eif2ak3* signaling in wild-type and knockout cells, respectively.

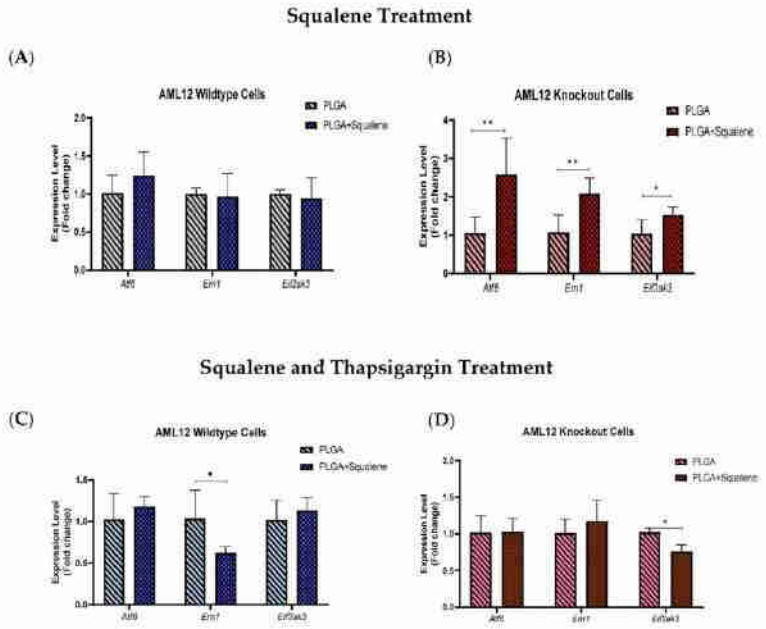

Figure 8. The mRNA expressions of *Atf6*, *Ern1* and *Eif2ak3* in presence of squalene-PLGA nanoparticles under the ER stress challenge. After 72 h of treatment with 30 µM PLGA based squalene NPs, (**A**) the results of three genes (*Atf6*, *Ern1* and *Eif2ak3*) represented a non-significant difference in WT cells. (**B**) Squalene with PLGA NPs induced a striking discrepancy in mRNA levels of *Atf6*, *Ern1* and *Eif2ak3* in TXNDC5 knockout cells. In order to evaluate the protective activity of squalene-PLGA NPs, when the cells were treated with 12.5 nM thapsigargin for 24 h to produce ER stress, (**C**) wild-type cells showed a significant reduction in *Ern1* mRNA rate, but no significant decline in *Atf6* or *Eif2ak3* mRNA levels. (**D**) TXNDC5 knockout cells revealed that the presence of squalene reduced *Eif2ak3* expression when exposed to a compound that generates ER stress, but there was no difference in *Atf6* and *Ern1* expression. The two-way ANOVA and Mann–Whitney's U-test were used in the data analysis; * $p < 0.05$, ** $p < 0.01$.

4. Discussion

The goals of this study were to vindicate the influence of squalene, the main ingredient of the unsaponifiable fraction in virgin olive oil, loaded into PLGA nanoparticles on oxidative and ER stress in a mouse hepatic cell line. Furthermore, the dependence or independence on TXNDC5 putative molecular pathways involved in hepatic stress has been investigated. In this context, PLGA, as a naturally derived and biodegradable polymer, is being explored for its ability to transport compounds of therapeutic relevance. Squalene is a naturally occurring cholesterol precursor that forms stable colloidal phases in water [54], and itself is a carrier of many substances and, considering the biological action of squalene, the effect could be a sum of actions [55]. As a result, our findings revealed that squalene was effectively encapsulated in PLGA NPs, resulting in stable NPs. Overall, the synthesis of squalene/PLGA NPs using the single-emulsion solvent evaporation method is a simple preparation procedure, which could facilitate their successful clinical translation.

Based on microscopic observations of PLGA NPs encapsulating fluorescent probes and/or the measurement of the probe's intracellular levels, many investigations have indicated quick and efficient cellular uptake of PLGA NPs [56–58]. The assessment of squalene content in our study revealed that PLGA nanoparticles have a great ability to

transfer squalene as a nanocarrier in mouse hepatocytes (Figure 3). As described in different studies, PLGA nanoparticles are effective nanocarriers for the encapsulation and delivery of various anti-cancer agents such as oleanolic (OA) and ursolic (UA) acids in three different cell lines, i.e., HepG2 (human hepatoma cell line), Caco-2 (human epithelial colorectal adenocarcinoma cell line) and Y-79 (human retinoblastoma cell line) [16]; also, for the encapsulation of several pharmaceuticals including haloperidol, estradiol, etc. [20]. For instance, the PLGA-based curcumin NPs have displayed entrapment efficiency in the range of 77 to 85% [59].

Intracellular ROS production is necessary for regular cellular activities and physiological processes, but when its production exceeds the intrinsic antioxidant capacity, oxidative stress occurs, causing severe damage to cellular macromolecules [60]. Squalene's antioxidant properties are intimately linked to the unique and stable triterpene structure that allows it to effectively scavenge harmful free radicals [61]. The protective effects of squalene versus oxidative destruction have been formerly documented in rodents [6,62–65]. Squalene can protect murine macrophages [32], Chinese hamster pulmonary fibroblasts (V79 cells) [66], human monocytes [32] and mammary epithelial cells (MCF10A) from hydrogen peroxide-induced damage in cell culture assays by directly scavenging ROS in a dose-dependent manner [34] and our finding in the present study reveal that squalene can reduce the ROS induction in mouse hepatic cells. Next, we investigated whether TXNDC5 deletion contributes to squalene protection against oxidative stress. ROS influences ER homeostasis and protein folding directly or indirectly, causing ER stress and possibly cell death in the case of extreme ER stress [67,68]. TXNDC5 appears to be involved in the formation of ROS and ER stress, according to growing data [69,70]. Inhibiting TXNDC5 expression via knockdown has previously been shown to induce ROS and ER stress in pancreatic cancer cells [69]; however, increasing TXNDC5 expression in lipid endothelial cells effectively reduces ROS production and protects cells [70]. The present study demonstrates that, in AML12 cells, as reflected in Figure 4A, an inverse and statistically significant difference was found between ROS content and TXNDC5 in exposure to squalene so that, in absence of TXNDC5, ROS was increased, while the ROS was decreased in WT samples. When cells were challenged to an oxidative stimulus (Figure 4B), a significant decrease of ROS in the squalene treated group in WT cells was observed, being the opposite in TXNDC5-KO cells. This finding reinforces previous research that found that oxidative stress-induced TXNDC5 was involved in proper protein folding via its disulfide isomerase activity [71]. Overall, these results evidence that squalene can alter ROS production in oxidative stress, in dependence of TXNDC5 (Figure 9). In the evaluation of the viability of cells in different concentrations of H_2O_2 based on the TXNDC5 elimination, in all concentrations that we tested, in the absence of squalene, TXNDC5 deletion significantly reduced the viability of mouse hepatocytes (Figure 5D). However, when the cells were treated with squalene, the viability of both cell lines was increased using 20 and 25 mM concentrations of H_2O_2 (Figure 5(D1,D2)). With these results in consideration, TXNDC5 can increase the squalene efficiency in AML12 cell viability and act as an oxidative stress-induced survival factor that regulates ROS/ER stress signaling, allowing AML12 cells to remain viable under oxidative stress, but it is not the only factor, and squalene could bypass it.

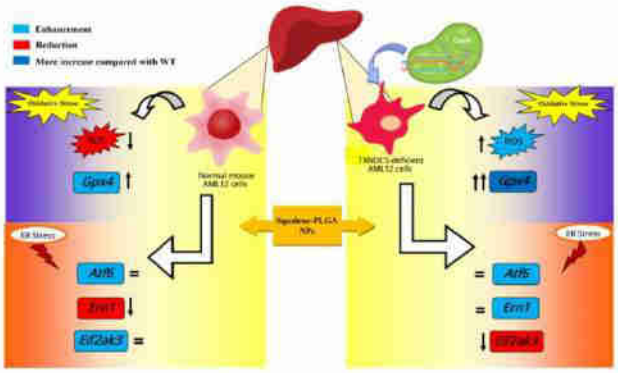

Figure 9. Scheme showing the effects of squalene on cells involved in oxidative and ER stress in the presence and absence of TXNDC5. In presence of squalene, wild-type and TXNDC5 deficient AML12 cell lines were exposed to oxidative and ER stress. The scheme reveals that in absence of TXNDC5, ROS abundance and *Gpx4* mRNA expression are enhanced, and *Eif2ak3* expression is decreased; whereas, in presence of TXNDC5, the ROS amount and *Ern1* mRNA level are reduced. This scheme was designed using Microsoft Publisher Document version 2010. ↑Increased,↓Decreased.

Since lipid peroxide accumulation is harmful to cell viability, most mammalian cells repair lipid damage with the phospholipid peroxidase glutathione peroxidase 4 (GPX4), whose blockage results in ferroptosis [72–74]. Previous studies have shown that oxidative stress decreased GPX activities and increased MDA accumulation (a substantial product of lipid peroxidation) in plasma and in the liver of piglets [44,75]; whereas our current study results, as shown in Figure 6C,D, confirmed that H_2O_2-induced oxidative stress reduced the mRNA level of *Gpx4* in WT and KO mouse hepatic cells. Squalene accumulation in cholesterol auxotrophic lymphomas inhibits oxidative cell death by *Gpx4* induction [76]. Oral administration of squalene improved rats' redox status after being exposed to cyclophosphamide-induced oxidative stress by boosting GPX activity in the heart, testis and urine bladder and normalize the alteration of *Gpx4* in the heart and hemolysate of red blood cells [62,63]. Our results also evidence the induction of *Gpx4* in the presence of squalene in WT and TXNDC5-deficient cells. When both kinds of cells were exposed to H_2O_2, squalene incubation rescued the decreased *Gpx4* expression with independence of TXNDC5 (Figure 6). This mechanism could partly explain that TXNDC5-deficient mouse hepatocyte cells could survive against H_2O_2-induced oxidative stress by the therapeutic action of squalene (Figure 9).

TXNDC5 is a thioredoxin with a protein disulfide isomerase-like domain that is expected to catalyze disulfide formation to facilitate protein folding or to control protein function in the face of endoplasmic reticulum stress [77]. When cells were exposed to thapsigargin that compels ER stress, WT and KO cell lines exhibited analogous cell viability (Figure 7A,B). Sullivan et al. found that TXNDC5 could protect endothelial cells from ER stress-induced apoptosis [37]. The major ER stress-induced pro-apoptotic mediators have so far been identified as DDIT3, JNK and cleaved caspase-12. As a downstream protein, DDIT3 is involved in ER stress-induced apoptosis and can be triggered by EIF2AK3, ERN1 and ATF6 [78]. ERN1 is a transmembrane protein that regulates its own expression and functions as a protein kinase and endoribonuclease [79,80]. ATF6, a type II transmembrane protein, is another ER stress sensor, up-regulating chaperones and ERAD pathway components [81], and EIF2AK3 is important for reducing workload by blocking mRNA translation, stopping additional synthesis and, consequently, protein folding under ER stress [82]. To identify the TXNDC5 mediators' role in endoplasmic reticulum stress, we performed gene expression analysis on *Atf6*, *Ern1* and *Eif2ak3* in the presence of squalene loaded in PLGA (Figure 8).

In the context of ER stress-induced effects, Chawsheen et al. found that the knockdown of TXNDC5 in human lung cancer cells accelerates the unfolded proteins and induces ER stress that increases the expression of *Eif2ak3*, *Ern1* and *Atf6* [83].

Accordingly, our results demonstrated that the downregulation of TXNDC5 increased the mRNA level of ER stress markers in mouse hepatic cells (Supplementary Figure S2). In the presence of induced ER stress, squalene decreased *Ern1* expression in WT cells in comparison to KO (Figure 8C). However, the opposite result was observed regarding *Eif2ak3* expression that decreased in TXNDC5 knockout cells, and no significant change was seen in *Atf6* (Figure 8C,D). Multiple experiments showed that knockout of ATF6 prevented the upregulation of *Txndc5* mRNA; TXNDC5 is located downstream of the ATF6 in cardiac, kidney fibroblasts and stelae cells [84–86]. Consistent with these results, we found that TXNDC5 may be posited downstream of the ATF6 and upstream of EIF2AK3 and ERN1 in hepatic cells. Based on this hypothesis, we suggest that TXNDC5 may regulate ER activity through distinct signaling pathways in stressful circumstances; moreover, squalene could reduce cell mortality by decreasing *Ern1* or *Eif2ak3* expression as ER stress markers in hepatic cells depending on TXNDC5.

5. Conclusions

The current study shows that squalene was successfully encapsulated in PLGA NPs, yielding stable nanoparticles with rapid and efficient cellular uptake. Squalene-based PLGA NPs effectively reduced ROS levels in normal mouse hepatocytes, whereas ROS was increased in TXNDC5-deficient AML12 cells. The cell viability of WT and KO cells under oxidative stress conditions was increased in the presence of squalene by *Gpx4* induction. Squalene also enhanced the cell viability of mouse hepatocytes in thapsigargin-induced ER stress by repressing *Ern1* or *Eif2ak3* expression in wild-type or knockout cells, respectively. Thus, TXNDC5 represented a crucial role in regulating ER activity through different signaling pathways in stressful circumstances. Likewise, squalene-loaded PLGA-NPs protect mouse hepatocytes from oxidative and endoplasmic reticulum stress by variable mechanisms depending on TXNDC5 presence. While this study was successful, there were some limitations in the PLGA encapsulation efficiency of squalene, which was variable in the amount of squalene in each batch of nanoparticle synthesized. Additionally, there was a limitation in PLGA-squalene NP cell treatment, so the cells underwent osmotic stress when exposed to high doses of PLGA-squalene NPs. Hence, high doses of squalene may not be useful in these experiments.

Supplementary Materials: The following supporting information can be downloaded at: https://www.mdpi.com/article/10.3390/antiox11030581/s1, Figure S1: Characterization of AML12 cell lines; Figure S2: The mRNA expressions of *Atf6*, *Ern1* and *Eif2ak3* in WT and KO cells; Table S1: Sequences of real-time PCR primers according to MIQE guidelines.

Author Contributions: Conceptualization, S.H.B., T.A., J.S.-M., R.M.-B., R.A., J.C.B., R.L., M.J.R.-Y., M.A. and J.O.; methodology, S.H.B., T.A., V.S., J.S.-M., R.M.-B., R.A., J.C.B. and R.L.; software, S.H.B., T.A., J.S.-M., J.C.B. and R.L.; validation, S.H.B., T.A., J.S.-M., J.C.B. and R.L.; formal analysis, S.H.B., T.A., V.S., J.S.-M., R.M.-B., R.A., J.C.B. and R.L.; investigation, S.H.B., T.A., J.S.-M., R.M.-B., R.A., J.C.B. and R.L.; resources, M.J.R.-Y., M.A. and J.O.; data curation, S.H.B., R.A. and J.O.; writing—original draft preparation, S.H.B.; writing—review and editing, S.H.B., T.A., V.S., J.S.-M., R.M.-B., R.A., J.C.B., R.L., M.J.R.-Y., M.A. and J.O.; visualization, S.H.B.; supervision, T.A., R.M.-B., M.J.R.-Y., M.A. and J.O.; project administration, M.J.R.-Y., M.A. and J.O.; funding acquisition, M.J.R.-Y., M.A. and J.O. All authors have read and agreed to the published version of the manuscript.

Funding: This research was supported by grants (CIBEROBN, CB06/03/1012, 1 January 2008) from CIBER Fisiopatología de la Obesidad y Nutrición as initiative of FEDER-ISCIII, Ministerio de Ciencia e Innovación-Fondo Europeo de Desarrollo Regional (PID2019-104915RB-I00, 1 June 2020) and Fondo Social Europeo-Gobierno de Aragón (B16_20R, 26 March 2020). S.H.B. was recipient of a joint fellowship from the Universities of Zaragoza and Pau and J.S.-M. was recipient of a Fundación Cuenca Villoro fellowship.

Institutional Review Board Statement: Not applicable.

Informed Consent Statement: Not applicable.

Data Availability Statement: Data is contained within the article and supplementary material.

Acknowledgments: We thank Cristina Barranquero and Tania Herrero-Continente for their help in maintaining the lab. We thank Isabel Ortiz de Solórzano for her help and assistance during the nanoparticle synthesis. V.S. acknowledges the use of the National Facility ELECMI ICTS, node "Laboratorio de Microscopias Avanzadas" at Universidad de Zaragoza.

Conflicts of Interest: The authors declare no conflict of interest.

Abbreviations

PLGA	Poly lactic-co-glycolic acid
NPs	Nanoparticles
ROS	Reactive oxygen species
AML12	Alpha mouse liver cell line
WT	Wild-type
KO	Knock-out
CRISPR	Clustered regularly interspaced short palindromic repeats
MDA-MB-231	M.D. Anderson-metastatic breast 231
ER	Endoplasmic reticulum
UPR	Unfolded protein response
HL-60	Human leukemic cell line 60
PDI	Protein disulfide isomerase
SEM	Scanning electron microscope
TEM	Transmission electron microscopy
DLS	Dynamic light scattering
HPLC	High performance liquid chromatography
MTT	3-(4 5-dimethylthiazol- 2-yl)-2 5-diphenyltetrazolium bromide
DCFH-DA	2,7-dichlorofluorescein diacetate
DCF	Dichlorofluorescein
Ppib	Peptidylprolyl isomerase B
Tbp	TATA box binding protein
Gpx4	Glutathione peroxidase 4
Eif2ak3	Eukaryotic translation initiation factor 2 alpha kinase 3
Atf6	Activating transcription factor 6
Ern1	Endoplasmic reticulum (ER) to nucleus signaling 1
Txndc5	Thioredoxin domain containing 5

References

1. Guasch-Ferré, M.; Willett, W. The Mediterranean diet and health: A comprehensive overview. *J. Intern. Med.* **2021**, *290*, 549–566. [CrossRef]
2. Shannon, O.M.; Ashor, A.W.; Scialo, F.; Saretzki, G.; Martin-Ruiz, C.; Lara, J.; Matu, J.; Griffiths, A.; Robinson, N.; Lillà, L. Mediterranean diet and the hallmarks of ageing. *Eur. J. Clin. Nutr.* **2021**, *75*, 1–17. [CrossRef]
3. Guasch-Ferré, M.; Li, Y.; Willett, W.C.; Sun, Q.; Sampson, L.; Salas-Salvadó, J.; Martínez-González, M.A.; Stampfer, M.J.; Hu, F.B. Consumption of olive oil and risk of total and cause-specific mortality among US adults. *J. Am. Coll. Cardiol.* **2022**, *79*, 101–112. [CrossRef]
4. Martínez-Beamonte, R.; Sánchez-Marco, J.; Felices, M.J.; Barranquero, C.; Gascón, S.; Arnal, C.; Burillo, J.C.; Lasheras, R.; Busto, R.; Lasunción, M.A. Dietary squalene modifies plasma lipoproteins and hepatic cholesterol metabolism in rabbits. *Food Funct.* **2021**, *12*, 8141–8153. [CrossRef]
5. Hu, F.B. The Mediterranean diet and mortality-olive oil and beyond. *N. Engl. J. Med.* **2003**, *348*, 2595–2596. [CrossRef]
6. Gabás-Rivera, C.; Barranquero, C.; Martínez-Beamonte, R.; Navarro, M.A.; Surra, J.C.; Osada, J. Dietary squalene increases high density lipoprotein-cholesterol and paraoxonase 1 and decreases oxidative stress in mice. *PLoS ONE* **2014**, *9*, e104224. [CrossRef] [PubMed]
7. Martakos, I.; Kostakis, M.; Dasenaki, M.; Pentogennis, M.; Thomaidis, N. Simultaneous determination of pigments, tocopherols, and squalene in Greek olive oils: A study of the influence of cultivation and oil-production parameters. *Foods* **2020**, *9*, 31. [CrossRef]

8. Lou-Bonafonte, J.M.; Martínez-Beamonte, R.; Sanclemente, T.; Surra, J.C.; Herrera-Marcos, L.V.; Sanchez-Marco, J.; Arnal, C.; Osada, J. Current insights into the biological action of squalene. *Mol. Nutr. Food Res.* **2018**, *62*, 1800136. [CrossRef] [PubMed]
9. Gaforio, J.J.; Sánchez-Quesada, C.; López-Biedma, A.; del Carmen Ramírez-Tortose, M.; Warleta, F. Molecular Aspects of Squalene and Implications for Olive Oil and the Mediterranean Diet. In *The Mediterranean Diet*; Elsevier: Amsterdam, The Netherlands, 2015; pp. 281–290.
10. Katdare, M.; Singhal, H.; Newmark, H.; Osborne, M.P.; Telang, N.T. Prevention of mammary preneoplastic transformation by naturally-occurring tumor inhibitors. *Cancer Lett.* **1997**, *111*, 141–147. [CrossRef]
11. Sánchez-Quesada, C.; Gutiérrez-Santiago, F.; Rodríguez-García, C.; Gaforio, J.J. Synergistic Effect of Squalene and Hydroxytyrosol on Highly Invasive MDA-MB-231 Breast Cancer Cells. *Nutrients* **2022**, *14*, 255. [CrossRef]
12. Murakoshi, M.; Nishino, H.; Tokuda, H.; Iwashima, A.; Okuzumi, J.; Kitano, H.; Iwasaki, R. Inhibition by squalene of the tumor-promoting activity of 12-O-Tetradecanoylphorbol-13-acetate in mouse-skin carcinogenesis. *Int. J. Cancer* **1992**, *52*, 950–952. [CrossRef] [PubMed]
13. Carbone, C.; Martins-Gomes, C.; Caddeo, C.; Silva, A.; Musumeci, T.; Pignatello, R.; Puglisi, G.; Souto, E. Mediterranean essential oils as precious matrix components and active ingredients of lipid nanoparticles. *Int. J. Pharm.* **2018**, *548*, 217–226. [CrossRef] [PubMed]
14. Santos, I.S.; Ponte, B.M.; Boonme, P.; Silva, A.M.; Souto, E.B. Nanoencapsulation of polyphenols for protective effect against colon–rectal cancer. *Biotechnol. Adv.* **2013**, *31*, 514–523. [CrossRef]
15. Alvarado, H.L.; Abrego, G.; Garduno-Ramirez, M.L.; Clares, B.; García, M.L.; Calpena, A.C. Development and validation of a high-performance liquid chromatography method for the quantification of ursolic/oleanic acids mixture isolated from *Plumeria obtusa*. *J. Chromatogr. B* **2015**, *983*, 111–116. [CrossRef]
16. Silva, A.M.; Alvarado, H.L.; Abrego, G.; Martins-Gomes, C.; Garduño-Ramirez, M.L.; García, M.L.; Calpena, A.C.; Souto, E.B. In vitro cytotoxicity of oleanolic/ursolic acids-loaded in PLGA nanoparticles in different cell lines. *Pharmaceutics* **2019**, *11*, 362. [CrossRef]
17. Jiang, H.; Sheng, Y.; Ngai, T. Pickering emulsions: Versatility of colloidal particles and recent applications. *Curr. Opin. Colloid Interface Sci.* **2020**, *49*, 1–15. [CrossRef]
18. Kumari, A.; Yadav, S.K.; Yadav, S.C. Biodegradable polymeric nanoparticles based drug delivery systems. *Colloids Surf. B Biointerfaces* **2010**, *75*, 1–18. [CrossRef]
19. Vasir, J.K.; Labhasetwar, V. Biodegradable nanoparticles for cytosolic delivery of therapeutics. *Adv. Drug Deliv. Rev.* **2007**, *59*, 718–728. [CrossRef]
20. Danhier, F.; Ansorena, E.; Silva, J.M.; Coco, R.; Le Breton, A.; Préat, V. PLGA-based nanoparticles: An overview of biomedical applications. *J. Control. Release* **2012**, *161*, 505–522. [CrossRef]
21. Hotamisligil, G.S. Endoplasmic reticulum stress and atherosclerosis. *Nat. Med.* **2010**, *16*, 396–399. [CrossRef]
22. Cnop, M.; Foufelle, F.; Velloso, L.A. Endoplasmic reticulum stress, obesity and diabetes. *Trends Mol. Med.* **2012**, *18*, 59–68. [CrossRef] [PubMed]
23. Fu, S.; Yang, L.; Li, P.; Hofmann, O.; Dicker, L.; Hide, W.; Lin, X.; Watkins, S.M.; Ivanov, A.R.; Hotamisligil, G.S. Aberrant lipid metabolism disrupts calcium homeostasis causing liver endoplasmic reticulum stress in obesity. *Nature* **2011**, *473*, 528–531. [CrossRef] [PubMed]
24. Fu, S.; Watkins, S.M.; Hotamisligil, G.S. The role of endoplasmic reticulum in hepatic lipid homeostasis and stress signaling. *Cell Metab.* **2012**, *15*, 623–634. [CrossRef]
25. Xu, C.; Bailly-Maitre, B.; Reed, J.C. Endoplasmic reticulum stress: Cell life and death decisions. *J. Clin. Investig.* **2005**, *115*, 2656–2664. [CrossRef]
26. Oliván, S.; Martínez-Beamonte, R.; Calvo, A.C.; Surra, J.C.; Manzano, R.; Arnal, C.; Osta, R.; Osada, J. Extra virgin olive oil intake delays the development of amyotrophic lateral sclerosis associated with reduced reticulum stress and autophagy in muscle of SOD1G93A mice. *J. Nutr. Biochem.* **2014**, *25*, 885–892. [CrossRef] [PubMed]
27. Ramírez-Torres, A.; Barceló-Batllori, S.; Martínez-Beamonte, R.; Navarro, M.A.; Surra, J.C.; Arnal, C.; Guillén, N.; Acín, S.; Osada, J. Proteomics and gene expression analyses of squalene-supplemented mice identify microsomal thioredoxin domain-containing protein 5 changes associated with hepatic steatosis. *J. Proteom.* **2012**, *77*, 27–39. [CrossRef] [PubMed]
28. Persson, T.; Popescu, B.O.; Cedazo-Minguez, A. Oxidative stress in Alzheimer's disease: Why did antioxidant therapy fail? *Oxidative Med. Cell. Longev.* **2014**, *2014*, 427318. [CrossRef]
29. Pisoschi, A.M.; Pop, A. The role of antioxidants in the chemistry of oxidative stress: A review. *Eur. J. Med. Chem.* **2015**, *97*, 55–74. [CrossRef]
30. Chen, Y.; Gu, Y.; Zhao, H.; Zhou, Y. Dietary squalene supplementation alleviates diquat-induced oxidative stress and liver damage of broiler chickens. *Poult. Sci.* **2021**, *100*, 100919. [CrossRef]
31. Albano, E.; Mottaran, E.; Occhino, G.; Reale, E.; Vidali, M. role of oxidative stress in the progression of non-alcoholic steatosis. *Aliment. Pharmacol. Ther.* **2005**, *22*, 71–73. [CrossRef]
32. Cárdeno, A.; Aparicio-Soto, M.; Montserrat-de la Paz, S.; Bermudez, B.; Muriana, F.J.G.; Alarcón-de-la-Lastra, C. Squalene targets pro-and anti-inflammatory mediators and pathways to modulate over-activation of neutrophils, monocytes and macrophages. *J. Func. Food* **2015**, *14*, 779–790. [CrossRef]

33. Yoshimura, T.; Harashima, M.; Kurogi, K.; Suiko, M.; Liu, M.-C.; Sakakibara, Y. A novel procedure for the assessment of the antioxidant capacity of food components. *Anal. Biochem.* **2016**, *507*, 7–12. [CrossRef] [PubMed]
34. Warleta, F.; Campos, M.; Allouche, Y.; Sánchez-Quesada, C.; Ruiz-Mora, J.; Beltrán, G.; Gaforio, J.J. Squalene protects against oxidative DNA damage in MCF10A human mammary epithelial cells but not in MCF7 and MDA-MB-231 human breast cancer cells. *Food Chem. Toxicol.* **2010**, *48*, 1092–1100. [CrossRef] [PubMed]
35. Starkov, A.A. The role of mitochondria in reactive oxygen species metabolism and signaling. *Ann. N. Y. Acad. Sci.* **2008**, *1147*, 37. [CrossRef] [PubMed]
36. Gabás-Rivera, C.; Jurado-Ruiz, E.; Sánchez-Ortiz, A.; Romanos, E.; Martínez-Beamonte, R.; Navarro, M.A.; Surra, J.C.; Arnal, C.; Rodríguez-Yoldi, M.J.; Andrés-Lacueva, C. Dietary Squalene Induces Cytochromes Cyp2b10 and Cyp2c55 Independently of Sex, Dose, and Diet in Several Mouse Models. *Mol. Nutr. Food Res.* **2020**, *64*, 2000354. [CrossRef]
37. Sullivan, D.C.; Huminiecki, L.; Moore, J.W.; Boyle, J.J.; Poulsom, R.; Creamer, D.; Barker, J.; Bicknell, R. EndoPDI, a novel protein-disulfide isomerase-like protein that is preferentially expressed in endothelial cells acts as a stress survival factor. *J. Biol. Chem.* **2003**, *278*, 47079–47088. [CrossRef]
38. Zhang, L.; Hou, Y.; Li, N.; Wu, K.; Zhai, J. The influence of $TXNDC_5$ gene on gastric cancer cell. *J. Cancer Res. Clin. Oncol.* **2010**, *136*, 1497–1505. [CrossRef]
39. Horna-Terrón, E.; Pradilla-Dieste, A.; Sánchez-de-Diego, C.; Osada, J. TXNDC5, a newly discovered disulfide isomerase with a key role in cell physiology and pathology. *Int. J. Mol. Sci.* **2014**, *15*, 23501–23518. [CrossRef]
40. Edman, J.C.; Ellis, L.; Blacher, R.W.; Roth, R.A.; Rutter, W.J. Sequence of protein disulphide isomerase and implications of its relationship to thioredoxin. *Nature* **1985**, *317*, 267–270. [CrossRef]
41. Freedman, R.B.; Hirst, T.R.; Tuite, M.F. Protein disulphide isomerase: Building bridges in protein folding. *Trends Biochem. Sci.* **1994**, *19*, 331–336. [CrossRef]
42. Lacoma, A.; Usón, L.; Mendoza, G.; Sebastián, V.; Garcia-Garcia, E.; Muriel-Moreno, B.; Domínguez, J.; Arruebo, M.; Prat, C. Novel intracellular antibiotic delivery system against *Staphylococcus aureus*: Cloxacillin-loaded poly (d,l-lactide-co-glycolide) acid nanoparticles. *Nanomedicine* **2020**, *15*, 1189–1203. [CrossRef] [PubMed]
43. Andreu, V.; Larrea, A.; Rodriguez-Fernandez, P.; Alfaro, S.; Gracia, B.; Lucía, A.; Usón, L.; Gomez, A.-C.; Mendoza, G.; Lacoma, A. Matryoshka-type gastro-resistant microparticles for the oral treatment of *Mycobacterium tuberculosis*. *Nanomedicine* **2019**, *14*, 707–726. [CrossRef] [PubMed]
44. Martínez-Beamonte, R.; Alda, O.; Sanclemente, T.; Felices, M.J.; Escusol, S.; Arnal, C.; Herrera-Marcos, L.V.; Gascón, S.; Surra, J.C.; Osada, J. Hepatic subcellular distribution of squalene changes according to the experimental setting. *J. Physiol. Biochem.* **2018**, *74*, 531–538. [CrossRef] [PubMed]
45. Huang, Z.; Wang, H.; Gao, C.; Shen, H.; Fa, X.e. Drug loaded gold nano-particulates for therapeutics of myocardial infarction in rat model. *J. Bionater. Tissue Eng.* **2018**, *8*, 197–205. [CrossRef]
46. Kumar, L.R.; Chatterjee, N.; Tejpal, C.; Vishnu, K.; Anas, K.; Asha, K.; Anandan, R.; Mathew, S. Evaluation of chitosan as a wall material for microencapsulation of squalene by spray drying: Characterization and oxidative stability studies. *Int. J. Biol. Macromol.* **2017**, *104*, 1986–1995. [CrossRef]
47. Jiao, L.; Liu, Z.; Zhang, Y.; Feng, Z.; Gu, P.; Huang, Y.; Liu, J.; Wu, Y.; Wang, D. Lentinan PLGA-stabilized pickering emulsion for the enhanced vaccination. *Int. J. Pharm.* **2022**, *611*, 121348. [CrossRef]
48. Hu, Y.; Hoerle, R.; Ehrich, M.; Zhang, C. Engineering the lipid layer of lipid–PLGA hybrid nanoparticles for enhanced in vitro cellular uptake and improved stability. *Acta Biomater.* **2015**, *28*, 149–159. [CrossRef]
49. Alejo, T.; Uson, L.; Landa, G.; Prieto, M.; Yus Argón, C.; Garcia-Salinas, S.; de Miguel, R.; Rodriguez-Largo, A.; Irusta, S.; Sebastian, V. Nanogels with High Loading of Anesthetic Nanocrystals for Extended Duration of Sciatic Nerve Block. *ACS Appl. Mater. Interfaces* **2021**, *13*, 17220–17235. [CrossRef]
50. Garms, B.C.; Poli, H.; Baggley, D.; Han, F.Y.; Whittaker, A.K.; Anitha, A.; Grøndahl, L. Evaluating the effect of synthesis, isolation, and characterisation variables on reported particle size and dispersity of drug loaded PLGA nanoparticles. *Mater. Adv.* **2021**, *2*, 5657–5671. [CrossRef]
51. Wu, D.; Xu, Z.; Li, Z.; Yuan, W.; Wang, H.-Q.; Xie, X. Reduction and temperature dually-triggered size-shrinkage and drug release of micelles for synergistic photothermal-chemotherapy of cancer. *Eur. Polym. J.* **2021**, *154*, 110535. [CrossRef]
52. Raval, N.; Maheshwari, R.; Kalyane, D.; Youngren-Ortiz, S.R.; Chougule, M.B.; Tekade, R.K. Importance of Physicochemical Characterization of Nanoparticles in Pharmaceutical Product Development. In *Basic Fundamentals of Drug Delivery*; Elsevier: Amsterdam, The Netherlands, 2019; pp. 369–400.
53. Alejo, T.; Andreu, V.; Mendoza, G.; Sebastian, V.; Arruebo, M. Controlled release of bupivacaine using hybrid thermoresponsive nanoparticles activated via photothermal heating. *J. Colloid Interface Sci.* **2018**, *523*, 234–244. [CrossRef] [PubMed]
54. Desmaële, D.; Gref, R.; Couvreur, P. Squalenoylation: A generic platform for nanoparticular drug delivery. *J. Control. Release* **2012**, *161*, 609–618. [CrossRef]
55. Arias, J.L.; Reddy, L.H.; Othman, M.; Gillet, B.; Desmaele, D.; Zouhiri, F.; Dosio, F.; Gref, R.; Couvreur, P. Squalene based nanocomposites: A new platform for the design of multifunctional pharmaceutical theragnostics. *ACS Nano* **2011**, *5*, 1513–1521. [CrossRef] [PubMed]
56. Panyam, J.; Sahoo, S.K.; Prabha, S.; Bargar, T.; Labhasetwar, V. Fluorescence and electron microscopy probes for cellular and tissue uptake of poly (D,L-lactide-co-glycolide) nanoparticles. *Int. J. Pharm.* **2003**, *262*, 1–11. [CrossRef]

57. Sahoo, S.K.; Panyam, J.; Prabha, S.; Labhasetwar, V. Residual polyvinyl alcohol associated with poly (D,L-lactide-co-glycolide) nanoparticles affects their physical properties and cellular uptake. *J. Control. Release* **2002**, *82*, 105–114. [CrossRef]
58. Panyam, J.; Zhou, W.Z.; Prabha, S.; Sahoo, S.K.; Labhasetwar, V. Rapid endo-lysosomal escape of poly (DL-lactide-coglycolide) nanoparticles: Implications for drug and gene delivery. *FASEB J.* **2002**, *16*, 1217–1226. [CrossRef]
59. Rakotoarisoa, M.; Angelov, B.; Garamus, V.M.; Angelova, A. Curcumin-and fish oil-loaded spongosome and cubosome nanoparticles with neuroprotective potential against H2O2-induced oxidative stress in differentiated human SH-SY5Y cells. *ACS Omega* **2019**, *4*, 3061–3073. [CrossRef]
60. Nita, M.; Grzybowski, A. The role of the reactive oxygen species and oxidative stress in the pathomechanism of the age-related ocular diseases and other pathologies of the anterior and posterior eye segments in adults. *Oxidative Med. Cell. Longev.* **2016**, *2016*, 3164734. [CrossRef]
61. Kohno, Y.; Egawa, Y.; Itoh, S.; Nagaoka, S.-i.; Takahashi, M.; Mukai, K. Kinetic study of quenching reaction of singlet oxygen and scavenging reaction of free radical by squalene in n-butanol. *Biochim. Et Biophys. Acta (BBA)-Lipids Lipid Metab.* **1995**, *1256*, 52–56. [CrossRef]
62. Motawi, T.M.; Sadik, N.A.; Refaat, A. Cytoprotective effects of DL-alpha-lipoic acid or squalene on cyclophosphamide-induced oxidative injury: An experimental study on rat myocardium, testicles and urinary bladder. *Food Chem. Toxicol.* **2010**, *48*, 2326–2336. [CrossRef]
63. Senthilkumar, S.; Yogeeta, S.K.; Subashini, R.; Devaki, T. Attenuation of cyclophosphamide induced toxicity by squalene in experimental rats. *Chem. Biol. Interact.* **2006**, *160*, 252–260. [CrossRef]
64. Farvin, K.S.; Anandan, R.; Kumar, S.H.S.; Shiny, K.; Sankar, T.; Thankappan, T. Effect of squalene on tissue defense system in isoproterenol-induced myocardial infarction in rats. *Pharmacol. Res.* **2004**, *50*, 231–236.
65. Farvin, K.S.; Kumar, S.H.S.; Anandan, R.; Mathew, S.; Sankar, T.; Nair, P.V. Supplementation of squalene attenuates experimentally induced myocardial infarction in rats. *Food Chem.* **2007**, *105*, 1390–1395. [CrossRef]
66. Skorkowska-Telichowska, K.; Hasiewicz-Derkacz, K.; Gębarowski, T.; Kulma, A.; Moreira, H.; Kostyn, K.; Gębczak, K.; Szyjka, A.; Wojtasik, W.; Gąsiorowski, K. Emulsions made of oils from seeds of GM flax protect V79 cells against oxidative stress. *Oxidative Med. Cell. Longev.* **2016**, *2016*, 7510759. [CrossRef]
67. Clarke, R.; Cook, K.L.; Hu, R.; Facey, C.O.; Tavassoly, I.; Schwartz, J.L.; Baumann, W.T.; Tyson, J.J.; Xuan, J.; Wang, Y. Endoplasmic reticulum stress, the unfolded protein response, autophagy, and the integrated regulation of breast cancer cell fate. *Cancer Res.* **2012**, *72*, 1321–1331. [CrossRef]
68. Wang, W.-A.; Groenendyk, J.; Michalak, M. Endoplasmic reticulum stress associated responses in cancer. *Biochim. Et Biophys. Acta Mol. Cell Res.* **2014**, *1843*, 2143–2149. [CrossRef]
69. Lee, S.-O.; Jin, U.-H.; Kang, J.H.; Kim, S.B.; Guthrie, A.S.; Sreevalsan, S.; Lee, J.-S.; Safe, S. The orphan nuclear receptor NR4A1 (Nur77) regulates oxidative and endoplasmic reticulum stress in pancreatic cancer cells. *Mol. Cancer Res.* **2014**, *12*, 527–538. [CrossRef]
70. Gu, M.-X.; Fu, Y.; Sun, X.-L.; Ding, Y.-Z.; Li, C.-H.; Pang, W.; Pan, S.; Zhu, Y. Proteomic analysis of endothelial lipid rafts reveals a novel role of statins in antioxidation. *J. Proteome Res.* **2012**, *11*, 2365–2373. [CrossRef]
71. Kojima, R.; Okumura, M.; Masui, S.; Kanemura, S.; Inoue, M.; Saiki, M.; Yamaguchi, H.; Hikima, T.; Suzuki, M.; Akiyama, S. Radically different thioredoxin domain arrangement of ERp46, an efficient disulfide bond introducer of the mammalian PDI family. *Structure* **2014**, *22*, 431–443. [CrossRef]
72. Dixon, S.J.; Lemberg, K.M.; Lamprecht, M.R.; Skouta, R.; Zaitsev, E.M.; Gleason, C.E.; Patel, D.N.; Bauer, A.J.; Cantley, A.M.; Yang, W.S. Ferroptosis: An iron-dependent form of nonapoptotic cell death. *Cell* **2012**, *149*, 1060–1072. [CrossRef]
73. Angeli, J.P.F.; Schneider, M.; Proneth, B.; Tyurina, Y.Y.; Tyurin, V.A.; Hammond, V.J.; Herbach, N.; Aichler, M.; Walch, A.; Eggenhofer, E. Inactivation of the ferroptosis regulator Gpx4 triggers acute renal failure in mice. *Nat. Cell Biol.* **2014**, *16*, 1180–1191. [CrossRef] [PubMed]
74. Yang, W.S.; SriRamaratnam, R.; Welsch, M.E.; Shimada, K.; Skouta, R.; Viswanathan, V.S.; Cheah, J.H.; Clemons, P.A.; Shamji, A.F.; Clish, C.B. Regulation of ferroptotic cancer cell death by GPX4. *Cell* **2014**, *156*, 317–331. [CrossRef] [PubMed]
75. Lv, M.; Yu, B.; Mao, X.; Zheng, P.; He, J.; Chen, D. Responses of growth performance and tryptophan metabolism to oxidative stress induced by diquat in weaned pigs. *Animal* **2012**, *6*, 928–934. [CrossRef] [PubMed]
76. Garcia-Bermudez, J.; Baudrier, L.; Bayraktar, E.C.; Shen, Y.; La, K.; Guarecuco, R.; Yucel, B.; Fiore, D.; Tavora, B.; Freinkman, E. Squalene accumulation in cholesterol auxotrophic lymphomas prevents oxidative cell death. *Nature* **2019**, *567*, 118–122. [CrossRef]
77. Jessop, C.E.; Watkins, R.H.; Simmons, J.J.; Tasab, M.; Bulleid, N.J. Protein disulphide isomerase family members show distinct substrate specificity: P5 is targeted to BiP client proteins. *J. Cell Sci.* **2009**, *122*, 4287–4295. [CrossRef]
78. Oyadomari, S.; Mori, M. Roles of CHOP/GADD153 in endoplasmic reticulum stress. *Cell Death Differ.* **2004**, *11*, 381–389. [CrossRef]
79. Shamu, C.E.; Walter, P. Oligomerization and phosphorylation of the Ire1p kinase during intracellular signaling from the endoplasmic reticulum to the nucleus. *EMBO J.* **1996**, *15*, 3028–3039. [CrossRef]
80. Hassler, J.; Cao, S.S.; Kaufman, R.J. IRE1, a double-edged sword in pre-miRNA slicing and cell death. *Dev. Cell* **2012**, *23*, 921–923. [CrossRef]
81. Schuck, S.; Prinz, W.A.; Thorn, K.S.; Voss, C.; Walter, P. Membrane expansion alleviates endoplasmic reticulum stress independently of the unfolded protein response. *J. Cell Biol.* **2009**, *187*, 525–536. [CrossRef]

82. Cullinan, S.B.; Diehl, J.A. PERK-dependent activation of Nrf2 contributes to redox homeostasis and cell survival following endoplasmic reticulum stress. *J. Biol. Chem.* **2004**, *279*, 20108–20117. [CrossRef]
83. Chawsheen, H.A.; Jiang, H.; Ying, Q.; Ding, N.; Thapa, P.; Wei, Q. The redox regulator sulfiredoxin forms a complex with thioredoxin domain–containing 5 protein in response to ER stress in lung cancer cells. *J. Biol. Chem.* **2019**, *294*, 8991–9006. [CrossRef]
84. Shih, Y.-C.; Chen, C.-L.; Zhang, Y.; Mellor, R.L.; Kanter, E.M.; Fang, Y.; Wang, H.-C.; Hung, C.-T.; Nong, J.-Y.; Chen, H.-J. Endoplasmic reticulum protein TXNDC5 augments myocardial fibrosis by facilitating extracellular matrix protein folding and redox-sensitive cardiac fibroblast activation. *Circ. Res.* **2018**, *122*, 1052–1068. [CrossRef]
85. Chen, Y.-T.; Jhao, P.-Y.; Hung, C.-T.; Wu, Y.-F.; Lin, S.-J.; Chiang, W.-C.; Lin, S.-L.; Yang, K.-C. Endoplasmic reticulum protein TXNDC5 promotes renal fibrosis by enforcing TGF-β signaling in kidney fibroblasts. *J. Clin. Investig.* **2021**, *131*, e143645. [CrossRef] [PubMed]
86. Hung, C.-T.; Su, T.-H.; Chen, Y.-T.; Wu, Y.-F.; Chen, Y.-T.; Lin, S.-J.; Lin, S.-L.; Yang, K.-C. Targeting ER protein TXNDC5 in hepatic stellate cell mitigates liver fibrosis by repressing non-canonical TGFβ signalling. *Gut* **2021**, *2021*, 325065. [CrossRef] [PubMed]

Supplementary Table S1. Sequences of real-time PCR primers according to MIQE guidelines
Abbreviations: *Ppib*, peptidylprolyl isomerase B; *Tbp*, TATA box binding protein; *Gpx4*, glutathione peroxidase 4;

Gene symbol	Accession	Primer sequence, sense/antisense ((5'->3')	Amplicon length	Exon	Concentration	Efficiency
Ppib	NM_011149.2	GGAGATGGCACAGGAGGAA TAGTGCTTCAGCTTGAAGTTCTCAT	71	3/4	0.2 µM	99%
Tbp	NM_013684.3	GTGAGTTGCTTGCTCTGTGC GCTGCGTTTTTGTGCAGAGT	359	8	0.2 µM	104%
Gpx4	NM_008162.4 NM_001037741.4 NM_001367995.1	ATGGATGAAAGTCCAGCCCAAG CGGCAGGTCCTTCTCTATCAC	148	4/7	0.2 µM	96%
Eif2ak3	NM_010121.3 XM_011241202.3 XM_006505501.2	TATGTTGGAAGGCTTGAGGTCC GTACATTCAGATGCAGCTGTGC	178	13/14	0.2 µM	95%
Atf6	NM_001081304.1 XM_030253420.2 XM_011238796.4	GGTTCTTCCTCATGGACCAGAT ATAGGTCTGACTCCCAAGGCAT	170	1/3	0.2 µM	102%
Ern1	NM_023913.2	AACAACCTGCCCAAACATCG TGGTCGGTGTGTTGTCTGAA	109	11/12	0.2 µM	93%
Txndc5	NM_001289599.1 NM_001289598.1 NM_145367.4	CAGGCTTGTCAGATGTCACCAT TAACCTCGTACCGAGTACTTGCTG	82	9/10	0.2 µM	92%

Eif2ak3, eukaryotic translation initiation factor 2 alpha kinase 3; *Atf6*, activating transcription factor 6; *Ern1*, endoplasmic reticulum (ER) to nucleus signaling 1; *Txndc5*, thioredoxin domain containing 5

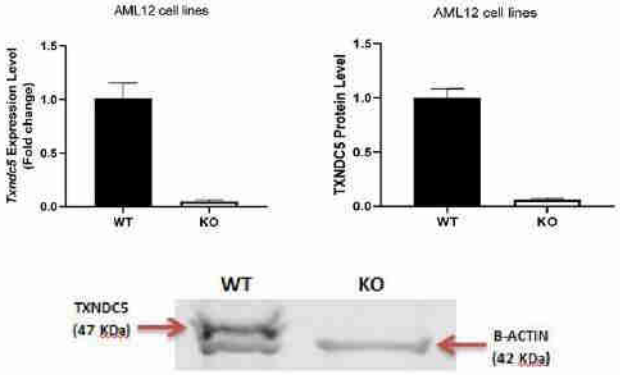

Supplementary Figure S1. Characterization of AML12 cell lines. *Txndc5* mRNA and protein levels in normal mouse hepatocyte AML12 cells (wildtype (WT)) and TXNDC5-deficient AML12 cells (knockout (KO))

ACS OMEGA

Open Access

http://pubs.acs.org/journal/acsodf

Article

Chitosan Nanoparticles, a Novel Drug Delivery System to Transfer Squalene for Hepatocyte Stress Protection

Seyed Hesamoddin Bidooki, Lea Spitzer, Arnaud Petitpas, Javier Sánchez-Marco, Roberto Martínez-Beamonte, Roberto Lasheras, Virginie Pellerin, María J. Rodríguez-Yoldi, María Angeles Navarro, Jesús Osada,* and Susana C. M. Fernandes*

Cite This: https://doi.org/10.1021/acsomega.4c08258

Read Online

ACCESS | Metrics & More | Article Recommendations | Supporting Information

ABSTRACT: The Mediterranean diet is a well-known dietary pattern that has gained considerable popularity worldwide for its ability to prevent the progression of nonalcoholic fatty liver disease. This is largely attributed to the use of virgin olive oil as the primary source of fat, which contains a substantial amount of squalene, a natural antioxidant. In order to enhance the delivery of squalene and amplify its effects due to its highly hydrophobic nature, herein, squalene has been incorporated into chitosan nanoparticles. The characterization of the resulting nanoparticles was conducted via scanning electron microscopy, dynamic light scattering, ζ potential, Fourier transform infrared spectroscopy, and gas chromatography−mass spectrometry. Reactive oxygen species (ROS) generation and cell viability assays were conducted in oxidative and endoplasmic reticulum (ER) stress in AML12 and a TXNDC5-deficient AML12 cell line, which was generated by CRISPR/Cas9 technology. The results demonstrated that squalene was successfully encapsulated in chitosan nanoparticles and exhibited rapid and efficient cellular uptake at a 150 μM squalene concentration within 48 h. In conclusion, the encapsulation of squalene in chitosan nanoparticles, compared to the poly(D,L-lactide-*co*-glycolic acid) and ethanol drug carriers, significantly enhanced its cellular uptake. This allows the administration of higher doses, which improve hepatocyte viability and reduce ROS levels, effectively compensating for the adverse effects of TXNDC5 deficiency under the context of hepatocyte stress protection.

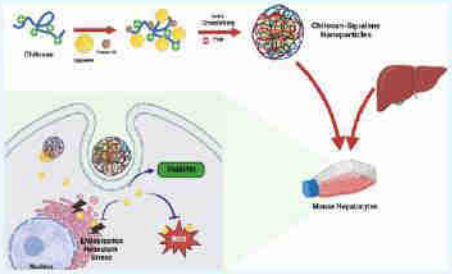

1. INTRODUCTION

Metabolic disease is a growing societal burden, leading to increased morbidity and mortality rates due to subsequent cardiovascular disease and cancer.[1] As a multifactorial metabolic disorder, nonalcoholic fatty liver disease (NAFLD) affects approximately 30% of the general population and is currently the most common liver disease in Western countries.[2] NAFLD develops naturally in the absence of alcohol abuse and initially presents as simple steatosis, which is the abnormal accumulation of lipids in the liver and eventually, it progresses to cirrhosis.[2,3] The Mediterranean diet is a well-known dietary pattern worldwide and has become popular for preventing the progression of NAFLD.[4,5] This dietary pattern includes a variety of plant-based foods, such as fruits, vegetables, nuts, and in particular olive oil.[5] The consumption of virgin olive oil has been associated with a reduced risk of general and cause-specific mortality in cardiovascular disease.[6] Virgin olive oil is high in monounsaturated fatty acids, particularly oleic acid, and other minor bioactive components including squalene which is a major unsaponifiable component, contributing to its anti-inflammatory and antioxidant properties.[5−8]

Squalene (SQ) is a terpenoid hydrocarbon that is widely present in nature (Figure 1). It can be found in substantial amounts in virgin olive oil, although the richest source of squalene is shark liver oil, which has been traditionally used as a source of this lipid.[9] Squalene is an intermediate in the biosynthesis of phytosterols in plants or cholesterol in animals.[10] It is synthesized in all types of cells because it is a key intermediate in the formation of eukaryotic sterols and bacterial hopanoids.[10] Squalene has several beneficial properties. It is a natural antioxidant and serves to hydrate the skin. Additionally, it is extensively used as an excipient in pharmaceutical formulations for disease management and therapy due to its biocompatibility, inertness, and other advantageous properties. Furthermore, it has been found to have a preventive effect on breast cancer and possesses tumor-

Received: September 8, 2024
Revised: October 29, 2024
Accepted: November 6, 2024

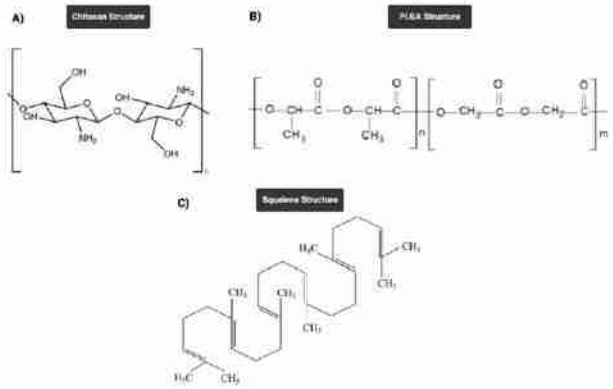

Figure 1. Chemical structures of (A) chitosan, (B) PLGA, and (C) squalene.

protective and cardio-protective properties.[10] It also decreases serum cholesterol levels.[10,11] Although squalene is a weak inhibitor of tumor cell proliferation, it has a potentiation effect that contributes to the treatment of cancer, either directly or indirectly.[11] Additionally, squalene is being investigated for vaccine delivery applications due to its ability to enhance the immune response to various associated antigens. These qualities make squalene a potentially interesting excipient for therapeutic applications.[11] Due to its high degree of unsaturation, squalene is susceptible to oxidation by a number of factors, including oxygen, temperature, moisture content, metals, and light. If squalene can be effectively encapsulated, it can be preserved without affecting the chemical and sensory attributes of the final product.[12] The administration of squalene has been demonstrated to reduce hepatic fat content and to induce the expression of proteins involved in lipid metabolism, which may result in reduced endoplasmic reticulum (ER) stress and intracellular reactive oxygen species (ROS) levels.[5] Thioredoxin domain-containing 5 (TXNDC5), a protein located in the ER, protects hepatocytes from stress-induced apoptosis by participating in protein modification and folding, and performs vital roles in antioxidative harm, antianoxia-induced apoptosis and cellular proliferation.[13]

Nanoparticles (NPs) have been demonstrated to offer superior performance to alternative drug delivery technologies, including enhanced circulation time, increased solubility for hydrophobic drugs, and targeted drug delivery.[14,15] The use of nanoparticles to encapsulate anticancer therapy and other disorder-specific compounds has been extensively studied with the objective of protecting sensitive chemicals from degradation, thus enhancing their bioavailability. Consequently, a plethora of naturally derived and biodegradable particles, including chitosan (CS), poly(D,L-lactide-*co*-glycolic acid) (PLGA) (Figure 1), and protein-based particles, have been developed.

PLGA is a particularly efficacious biodegradable polymer, as its hydrolysis results in the generation of endogenous monomer metabolites, namely lactic acid and glycolic acid. These monomers can be effectively degraded within the body via the Krebs cycle. Therefore, the low risk of systemic toxicity in PLGA applications such as drug delivery and tissue engineering can be attributed to the aforementioned factors.[5] Conversely, CS is employed as an encapsulation agent for a multitude of sensitive substances, including hydrophobic and lipophilic drugs, vitamins, astaxanthin, fish oil, and curcumin, among others.[12,16,17] CS is a modified natural polysaccharide obtained by the partial N-deacetylation of chitin, a natural biopolymer derived from the exoskeleton of crustaceans, including crabs, shrimps, and lobsters.[18−21] CS is soluble in aqueous acidic media and can be produced in a variety of molecular weights and with different degrees of deacetylation.[18,22] CS possesses a wide range of bioactivities, including antioxidant, antimicrobial, antifungal, antitumor, antiallergic, immune system activating, antihypertensive, and cholesterol-lowering properties.[12,15,23−27] Chitosan nanoparticles (CSNPs), with diameters ranging from 1 to 1,000 nm, have been widely used therapeutically as drug carriers, wherein the active ingredient is dissolved, entrapped, encapsulated, adsorbed, or chemically bound due to their biodegradability, biocompatibility and nontoxicity.[18,28−30] CSNPs possess the advantage of a slow and controlled drug release, which improves drug solubility and stability, enhances efficacy, and reduces toxicity. Due to their small size, they are capable of passing through biological barriers in vivo (such as the blood-brain barrier) and delivering drugs to the lesion site, thereby enhancing efficacy.[14]

In this context, the present study focuses on the preparation and characterization of CSNPs as a drug delivery system to enhance the therapeutic effect of squalene followed by its administration to hepatocytes. The cellular uptake of CSNP-squalene and the effects of initial squalene content, encapsulation efficiency, and mean particle size were also investigated. In comparison to alternative methodologies such as PLGA-squalene nanoparticles, the antioxidant properties of squalene have been examined using this innovative drug delivery system, particularly in the context of ER and oxidative stress. Furthermore, this investigation was conducted in the absence of TXNDC5 protein, which serves as a target gene.

2. MATERIALS AND METHODS

2.1. Materials. Low molecular weight chitosan (LMw CS) and high molecular weight chitosan (HMw CS) were obtained from Sigma-Aldrich/Merck Millipore (Darmstadt, Germany) and Mahtani Chitosan Pvt. Ltd. (India), respectively. The following materials were purchased from Sigma-Aldrich/Merck

https://doi.org/10.1021/acsomega.4c08258
ACS Omega XXXX, XXX, XXX−XXX

Millipore (Darmstadt, Germany): acetic acid, Tween 80, sodium tripolyphosphate (TPP), squalene (2.05 M, ≥98%, liquid), Resomer RG 503H poly(D,L-lactide-*co*-glycolic acid) (PLGA-COOH), ethanol, and ethyl acetate 99.6% ACS. Pluronic F68 was procured from Panreac Química S. L. U. (Barcelona, Spain). Cyclohexane was supplied by VWR (Radnor, Pennsylvania, USA).

The mouse hepatocyte cell line (AML12) was procured from the ATCC collection (Manassas, VA, USA). Dulbecco's modified Eagle's minimum essential medium (DMEM), fetal bovine serum, nonessential amino acids, amphotericin B, penicillin, streptomycin, trypsin, EDTA, and the Lipofectamine 2000 kit were obtained from Thermo Fisher Scientific (Waltham, MA, USA). The following materials were obtained from Sigma-Aldrich/Merck Millipore (Darmstadt, Germany): dexamethasone, 5α-cholestane, 3-(4,5-dimethylthiazol-2-yl)-2,5-diphenyltetrazolium bromide assay (MTT), hydrogen peroxide (H_2O_2), thapsigargin, dimethyl sulfoxide (DMSO), palmitic acid, and 2,7-dichlorofluorescein diacetate (DCFH-DA). F-12 Ham's medium was purchased from GE Healthcare Life Science (South Logan, UT, USA), and insulin-transferrin-selenium was obtained from Corning (Bedford, MA, USA). TXNDC5 CRISPR/Cas9 KO plasmids were provided by Santa Cruz Biotechnology (Dallas, TX, USA).

2.2. Preparation and Characterization of the Nanoparticles. *2.2.1. Synthesis of Squalene-Loaded Chitosan Nanoparticles.* Chitosan nanoparticles (CSNPs) were synthesized by the ionic gelation and ultrasonication approaches, as previously published.[12,16,31,32] Two different chitosan samples were used: (i) LMw CS with a Mw range of 50−190 kDa and a degree of deacetylation (DDA) range of 75−85% from Sigma-Aldrich, Merck Millipore (Darmstadt, Germany); and (ii) HMw CS presenting an average Mw of 500 kDa (determined by viscosimetry) and a DDA of 98% (determined by ^{1}H NMR spectroscopy in D_2O containing a 1% of CD_3COOD) and processed to medical grade from Mahtani Chitosan Pvt. Ltd. (India).

Briefly, 1 mg/mL solution was first prepared by dissolving chitosan (LMw CS or HMw CS) in aqueous acetic acid (1% v/v) at room temperature under vigorous stirring for 48 h. After, Tween 80 (0.5% v/v) (Sigma-Aldrich, Merck Millipore, Darmstadt, Germany) were added to the chitosan solution and the solution was filtered through a 0.45 μm filter and the pH adjusted to 4.5 with NaOH 1M. To this solution, 0.5 mg/mL of sodium tripolyphosphate (TPP, Sigma-Aldrich; Merck Millipore, Darmstadt, Germany) solution, prepared with double-distilled water (pH adjusted to 4.5 with HCl 1M) and filtered through a 0.45 μm filter, was added dropwise under stirring (CS:TPP ratio = 2.5:1). The solution was then sonicated using a Branson Digital Sonifier 450 (Danbury, CT, USA) in an ice bath for 25 s at 80% amplitude using a 2 mm diameter probe. The mixture was then stirred for cross-linking under a fume hood at 600 rpm for 3 h. Finally, the nanoparticles were collected by centrifugation (Thermo Fisher Scientific, Waltham, MA, USA) at 15,000 g for 15 min at 10 °C and dispersed in 2 mL of double-distilled water for subsequent cellular experiments. The preparation of chitosan-squalene nanoparticles (CS-SQ NPs) involved the dispersion of squalene (2.05 M, ≥98%, liquid; Sigma-Aldrich, Merck Millipore, Darmstadt, Germany) into CS-TPP solution. The solution was prepared with the different volumes of squalene (50, 100, and 200 μL) under stirring. The mixtures were then sonicated for 25 s and 80% amplitude in an ice bath, and stirred for 3 h. The unreacted chemicals and byproducts were removed by centrifugation (15,000g for 15 min at 10 °C). The final samples were stored at 4 °C in the dark prior to analysis.

2.2.2. Physicochemical and Morphological Characterization of the Chitosan Nanoparticles. The size, polydispersity index (PDI) and zeta potential of the nanoparticles were studied using the Malvern Zetasizer Nano ZS coupled to an MPT-2 auto titrator system (Malvern Instruments, Worcester, UK). The size reported is the z-average diameter (intensity based) of five measurements by Dynamic Light Scattering (DLS) at 25 °C and 90° scattering angle.

The chemical composition of the starting and final materials, such as pure squalene and squalene encapsulated with LMw or HMw chitosan, were confirmed using Attenuated Total Reflectance Fourier Transform Infrared (ATR-FTIR) spectroscopy on a Nicolet iS50 (ThermoFisher Scientific, Waltham, Massachusetts, USA) from wavenumber 400−4000 cm^{-1} with a resolution of 4 cm^{-1} and an accumulation of 64 scans.

The morphological features of CSNPs and CS-SQ NPs were analyzed using an Apreo 2 Scanning Electron Microscope (SEM, ThermoFisher Scientific, Waltham, MA, USA) operating at an acceleration voltage of 30 kV with a Scanning Transmission Electron Microscopy (STEM) detector. Prior to SEM analysis, the samples were coated with a thin layer of gold (Au) using a sputter coater (Cressington 108 Auto Sputter Coater, Watford, UK) to enhance conductivity and image resolution. For STEM analysis, NPs were dispersed in ultrapure water to obtain a suspension with a very low concentration. The mixture was then subjected to a sonication bath for 3 min. A 2 μL droplet of the sonicated suspension was placed on a 200 mesh Cu TEM grid type B (Ted Pella Inc., Redding, California, USA), and excess water was evaporated from the grid overnight under a fume hood at room temperature before being placed in the STEM chamber for morphological studies.

2.2.3. Chitosan Encapsulation Efficiency Experiment. CSNPs with different initial squalene volumes (200, 100, 50 μL of 2.05 M squalene) were synthesized and then washed twice with water using an ultrafiltration device (Amicon, molecular weight cutoff, 100 000 Da). Squalene was extracted from the NPs using cyclohexane and was then quantified by gas chromatography−mass spectrometry (GC/MS), as described in the Squalene Extraction subsection. The drug loading content (DLC) and encapsulation efficiency (EE) of the LMw CSNP and HMw CSNP were calculated according to the following equations:[32]

$$\mathrm{DLC} = \frac{\text{Weight of squalene in nanoparticles}}{\text{Chitosan nanoparticles weight}}$$

$$\mathrm{EE}\ (\%) = \frac{\text{Total squalene added} - \text{Nonentrapped squalene}}{\text{Total squalene added}} \times 100$$

2.2.4. Synthesis and Characterization of Squalene-Loaded PLGA Nanoparticles. PLGA-Squalene polymeric nanoparticles (PLGA-SQ NPs) were synthesized for comparison with CS-SQ NPs by the single emulsion solvent evaporation technique using Resomer RG 503H poly(D,L-lactide-*co*-glycolic acid) (PLGA-COOH, Mw 24−38 kDa) (Sigma-Aldrich; Merck Millipore, Darmstadt, Germany), Pluronic F68 (Panreac Quimica S. L.U; Barcelona, Spain)

https://doi.org/10.1021/acsomega.4c08258
ACS Omega XXXX, XXX, XXX−XXX

and ethyl acetate 99.6% ACS (Sigma-Aldrich, Merck Millipore, Darmstadt, Germany) as described previously.[5] A scanning electron microscope (SEM, FEG INSPECT-F50, Eindhoven, Netherlands), transmission electron microscopy (TEM) (Tecnai T20, FEI Company, Hillsboro, OR, USA) and DLS (Malvern Instruments, Worcester, UK) were used to determine the physicochemical characterization of these nanoparticles.

2.2.5. Preparation of Ethanol−Squalene System. An ethanol-squalene system (Eth-SQ) was prepared for comparison with CS-SQ NPs by the solvent displacement technique.[33,34] Squalene (2.05 M, ≥98%, liquid; Sigma-Aldrich, Merck Millipore, Darmstadt, Germany) was initially dissolved in 100% ethanol (Sigma-Aldrich; Merck Millipore, Darmstadt, Germany) to attain the requisite concentration. Subsequently, the squalene-ethanol solution was introduced to the cell culture medium, thereby enabling the dispersion of the squalene within the medium following the evaporation of the ethanol. The resulting squalene dispersion was then directly applied to the cells for the purpose of conducting biological experiments.

2.2.6. Viscosity Measurement. The viscosity of the drug delivery systems was quantified using the MCR302 DG23.04 Pressure Cell C-PDT200 (Anton Paar, Graz, Austria) with a bucket and cylinder (bucket diameter = 20.33 mm, cylinder diameter = 21.04 mm). All measurements were conducted at a temperature of 25 °C. For the purpose of measuring viscosity, approximately 3 mL of each sample was collected and subsequently loaded onto the rheometer. The viscosity of the nanoparticles was determined in accordance with the manufacturer's instructions.

2.3. Biological Assays. *2.3.1. AML12 Cell Culture.* The mouse hepatocyte cell line (AML12) (ATCC collection, Manassas, VA, USA) was cultured in 25 cm^2 plastic flasks at a density of 5×10^5 cells/cm^2 (in duplicate) at 37 °C in a humidified atmosphere of 5% CO_2 in Dulbecco's modified Eagle's minimum essential medium (DMEM; Thermo Fisher Scientific, Waltham, MA, USA): F-12 Ham's medium (GE Healthcare Life Science, South Logan, UT, USA) at a 1:1 ratio supplemented with 10% fetal bovine serum (Thermo Fisher Scientific, Waltham, MA, USA), 1:500 insulin-transferrin-selenium (Corning, Bedford, MA, USA), 40 ng/mL dexamethasone (Sigma-Aldrich; Merck Millipore, Darmstadt, Germany), 1% nonessential amino acids (Thermo Fisher Scientific, Waltham, MA, USA), 1% amphotericin B (1000 mg/mL; Thermo Fisher Scientific, Waltham, MA, USA), 1% penicillin (1000 U/mL; Thermo Fisher Scientific, Waltham, MA, USA), and 1% streptomycin (1000 mg/mL; Thermo Fisher Scientific, Waltham, MA, USA). The culture medium was changed every 2 days. After the AML12 cells reached 90−100% confluence, the medium was removed and the cells were washed with PBS and trypsinized with 0.25% trypsin (DMEM; Thermo Fisher Scientific, Waltham, MA, USA) and 1 mM EDTA (DMEM; Thermo Fisher Scientific, Waltham, MA, USA).

2.3.2. Generating a Stable TXNDC5 Knockout AML12 Cell Line. The stable TXNDC5-deficient clones were expanded as described previously.[5] Briefly, AML12 cells were transfected with TXNDC5/ERp46 HDR and TXNDC5 CRISPR/Cas9 KO plasmids (Santa Cruz Biotechnology, Dallas, TX, USA) using Lipofectamine 2000 (Thermo Fisher Scientific, Waltham, MA, USA). The gRNA sequence 5′-TTATCAAG-TTCTTCGCTCCG-3′ in the TXNDC5 CRISPR/Cas9 KO plasmid caused a double-strand break in the fifth exon of Txndc5. AML12 KO cells that were resistant to puromycin were selected after repeated puromycin incubations. Finally, the absence of TXNDC5 was confirmed by Western blot.

2.3.3. Cellular Uptake Assay. AML12 cells were seeded in 25 cm^2 plastic flasks at a density of 5×10^5 cells/cm^2 (in triplicate) in complete growth medium. After the cells reached 90% confluence, they were treated with CS-SQ NPs, PLGA-SQ NPs or Eth-SQ at two different concentrations (30 and 150 μM) and two different incubation time (48 and 72 h) in medium without fetal bovine serum and amphotericin B. The cells were then trypsinized and washed three times with PBS, pH 7.4 and centrifuged at 3900 rpm for 5 min and collected for squalene extraction.

2.3.4. Squalene Extraction. Squalene was extracted from CS-SQ NPs, PLGA-SQ NPs and cells treated with different drug delivery systems, and analyzed by GC/MS as previously described.[35] Briefly, according to the weight of the samples and the volumes used in each step, the samples were transferred to a centrifuge glass tube and homogenized in 1 mL of PBS, 10 μL of 1 mM 5α-cholestane (Sigma-Aldrich; Merck Millipore, Darmstadt, Germany) in cyclohexane (VWR, Radnor, Pennsylvania, USA) as an internal standard to determine the efficiency of the extraction and 1 mL of cyclohexane and vortexed for 10 s. After centrifugation, the organic phase was transferred to a clean tube. The eluted samples were dried with a nitrogen gas in a thermostatic bath at 55 °C. They were then dissolved in 200 μL of 50 μM squalane solution (Sigma-Aldrich; Merck Millipore, Darmstadt, Germany) in cyclohexane for chromatographic analysis. CG analyses were performed in an Agilent 6890 CG with a 7683B injector and a 5975B MS acquisition parameter unit (Agilent Technologies, Santa Clara, CA, USA), using a J&W122-5532 column (Agilent) with a nominal length of 30 m and a diameter of 0.25 mm and a helium flow of 1 mL/min. The oven temperature was set to run from 280 to 290 °C in 15 min with a ramp from 5 to 13 min.

2.3.5. Cell Viability Assay. Cellular viability was determined using the 3-(4 5-dimethylthiazol-2-yl)-2 5-diphenyltetrazolium bromide assay (MTT; Sigma-Aldrich, Merck Millipore, Darmstadt, Germany).[36] Cells were seeded on a 96-well plate at 5000 cells/well and exposed for 24, 48, and 72 h to the range of 15 to 600 μM CS-SQ NPs diluted in medium without fetal bovine serum and amphotericin B. In another assay, cells after treatment with 150 μM CS-SQ NPs were exposed for 24 h to 8 mM H_2O_2 (Sigma-Aldrich, Merck Millipore, Darmstadt, Germany) for oxidative stress, 12.5 nM thapsigargin (Sigma-Aldrich, Merck Millipore, Darmstadt, Germany) dissolved in DMSO and 600 μM palmitic acid (Sigma-Aldrich, Merck Millipore, Darmstadt, Germany) dissolved in ethanol for ER stress. Then, 1 mg/mL MTT was added to the culture medium. After 3 h of incubation, the cell growth medium was replaced with DMSO and the absorbance was measured with a SPECTROstar Nano Microplate Reader (Omega, BMG Labtech, Ortenberg, Germany) at 570 nm.

2.3.6. Reactive Oxygen Species Assay. AML12 cells (5000 cells per well) were seeded in a 96-well plate and cultured at 37 °C for 72 h. Cells were treated with CS-SQ NPs or CSNPs diluted in medium without fetal bovine serum and amphotericin B at a concentration of 150 μM for 48 h, followed by treatment with 8 mM H_2O_2 (Sigma-Aldrich, Merck Millipore, Darmstadt, Germany), 12.5 nM thapsigargin (Sigma-Aldrich, Merck Millipore, Darmstadt, Germany)

https://doi.org/10.1021/acsomega.4c08258
ACS Omega XXXX, XXX, XXX−XXX

dissolved in DMSO or 600 μM palmitic acid (Sigma-Aldrich, Merck Millipore, Darmstadt, Germany) dissolved in ethanol. 10 μL of 2.0 mg/mL 2,7-dichlorofluorescein diacetate (DCFH-DA; Sigma-Aldrich, Merck Millipore, Darmstadt, Germany) dissolved in fresh PBS was added to the cells. After 3 h, the medium was removed and the presence of ROS was assessed by measuring the conversion of DCFH-DA to fluorescent dichlorofluorescein (DCF) at excitation and emission wavelengths of 485 and 520 nm, respectively, in a microplate reader (FLUOstar, Omega, BMG Labtech, Ortenberg, Germany).

2.3.7. Characterization of Cell Morphology in the Presence of Chitosan, PLGA, and Ethanol Drug Delivery Systems. Both WT and KO AML12 cells (2000 cells per well) were cultured in a 12-well plate (in duplicate). Cells were incubated for 48 h in the presence of 150 μM CS-SQ NPs and uncharged CSNPs as control, 150 μM PLGA-SQ NPs and uncharged PLGA NPs as control, and 150 μM Eth-SQ and ethanol as control. After three washes with PBS, a Floid Cell Imaging System (Thermo Fisher Scientific, Waltham, MA, USA) was used to detect the influence of different drug delivery systems on the AML12 cell line.

2.3.8. Statistical Analysis. Statistical analyses were performed using GraphPad Prism 8 for Windows (GraphPad, San Diego, CA, USA). The Shapiro–Wilk test was used to determine the normal distribution of the data, and Bartlett's or Levene's test was used to determine the homology of variance between groups. Factors meeting both criteria were examined using one-way ANOVA with Dunnett's multiple comparison test and two-tailed Student's t test. If any of the hypotheses failed, statistical analysis was performed using the Mann–Whitney U test. A p-value of less than 0.05 was used to indicate statistical significance. Means and standard deviations of the results are presented.

3. RESULTS AND DISCUSSION

3.1. Encapsulation of Squalene in the Chitosan Nanoparticles. Chitosan-based systems have found a multitude of applications in the food and biochemical industries due to their ability to encapsulate a wide range of ingredients.[37] The initial method described in the literature for the preparation of CSNPs involved emulsification and cross-linking. Herein, the CSNPs were prepared by the addition of a negatively charged TPP solution to a positively charged chitosan solution under magnetic stirring at room temperature followed by ultrasound approach.[38,39] Initial experiments were conducted using two chitosan samples with low and high molecular weights (LMw and HMw). As the biophysical characterization of PLGA-squalene was previously documented in our previous publication,[5] the particle size, surface charge, and EE% of all CSNPs were also evaluated and are presented in Table 1 and Table 2. The average diameter of LMw CSNPs was 262.5 ± 80.1 nm, with a polydispersity index (PDI) of 0.35. However, HMw CSNPs exhibited an average diameter of 473.4 ± 62.3 nm and a PDI of 0.53. The increase in chitosan Mw resulted in an increase in the average particle size from 262 to 473 nm and PDI change from 0.35 to 0.53. These findings were consistent with previous observations that higher Mw chitosan produces larger nanoparticles.[19,40,41] The PDI was found to be low for all NPs evaluated, indicating that a homogeneous dispersion was obtained and it was observed that a higher variety of particle sizes were obtained when a solution of larger polymer chains was used. The positive charge of chitosan enables it to form a robust interaction with negatively charged molecules such as TPP, while maintaining its intrinsic activity.[42] Upon mixing chitosan and TPP, they spontaneously formed compact complexes with an overall positive surface charge of 20 ± 4 mV in LMw CSNPs and 35.5 ± 3 mV in HMw CSNPs, as confirmed by zeta potential measurements. In accordance with the literature, an analysis of the differences between the two CSNPs revealed a similar trend as observed for the particle size: a higher surface charge was obtained for particles formed by polymers with a longer chain.[43]

Table 1. Diameter, Polydispersity Index (PDI), and Zeta Potential of Chitosan Nanoparticles without and with Squalene

Sample	Diameter (d.nm)	PDI	Zeta potential (mV)
LMw CSNPs	262.5 ± 80.1	0.35 ± 0.03	20 ± 4.0
HMw CSNPs	473.4 ± 62.3	0.53 ± 0.06	35.5 ± 3.0
LMw CS-SQ NPs	330.7 ± 77.4	0.27 ± 0.02	25 ± 6.0
HMw CS-SQ NPs	673.2 ± 38.8	0.45 ± 0.09	40.9 ± 1.7

The size and PDI of a nanoparticle formulation have a significant impact on the loading and release of a drug.[44] Table 1 illustrates that the particle size and PDI of the developed CS-SQ NPs exhibited a range of 330.7 ± 77.4 nm with a 0.27 PDI in LMw CS-SQ NPs and 673.2 ± 38.8 nm with a 0.45 PDI in HMw CS-SQ NPs, which is conducive to passive targeting of tumors.[45] The results indicated that the CS-SQ NPs were comparatively larger than CSNPs, which is consistent with the findings of Keawchaoon and Yoksan using carvacrol.[46] The surface charge of CS-SQ NPs remained positive at 25 ± 6 mV and 40.9 ± 1.7 mV in LMw and HMw CS-SQ NPs, respectively. The positive surface charge of CS-SQ NPs is mainly due to the cationic nature of chitosan, which has protonated amine groups in aqueous solutions at neutral to slightly acidic pH. Squalene, which is hydrophobic, is encapsulated within the nanoparticle by hydrophobic interactions. Therefore, the positive surface charge is maintained due to the protonation of chitosan.[29]

FTIR analysis was conducted to confirm the encapsulation of squalene within the NPs (Figure 2). The various synthesized samples were studied in comparison with squalene and chitosan.[29] The ATR-FTIR spectra of the chitosan-squalene NPs revealed the presence of characteristic peaks at 2800–3000 cm^{-1}, which correspond to the C–H stretching of squalene,[47] and peaks at 1000–1100 cm^{-1}, which are indicative of the C–O–C vibration of chitosan. The selection of these peaks was based on their capacity to provide a qualitative measure of the encapsulation process. The C–H stretching bands of squalene were selected due to their pronounced intensity under the specified experimental conditions, providing a straightforward method for evaluating the relative quantity of squalene present in the nanoparticle system. While the C=C stretching (approximately 1640 cm^{-1}) was also a characteristic feature of squalene, the C–H stretching bands provided more discernible signals for monitoring the encapsulation process. Despite the fact that both chitosan and squalene display C–H stretching vibrations, the presence of squalene was substantiated by identifying specific C–H peaks that were exclusive to this compound in terms of wavenumber and intensity. These peaks were then validated by comparing them with individual and combined

https://doi.org/10.1021/acsomega.4c08258
ACS Omega XXXX, XXX, XXX−XXX

Table 2. Squalene Content and Encapsulation Efficiency Based on the Squalene Initial Volume in LMw and HMw Chitosan Nanoparticles

Chitosan sample	Squalene initial volume	Squalene concentration (μM)	Squalene encapsulation (%)	Squalene/Chitosan (W/W)
LMw	200 μL	8015 ± 1065	61.5 ± 12.0	0.184
	100 μL	1838 ± 795	27.4 ± 3.0	0.042
	50 μL	1296 ± 676	38.9 ± 5.4	0.029
HMw	200 μL	1989 ± 247	14.7 ± 8.0	0.045
	100 μL	738 ± 335	11.3 ± 4.1	0.016
	50 μL	396 ± 290	13.2 ± 2.7	0.009

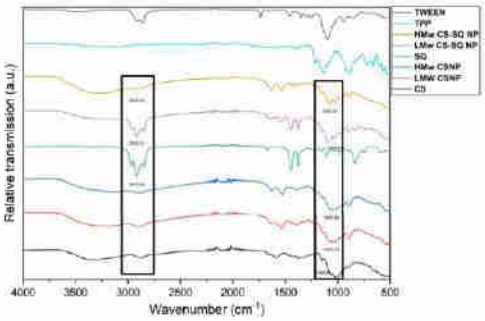

Figure 2. ATR-FTIR spectra of the different raw materials and chitosan-squalene nanoparticles. The black squares in Figure 2 indicate the typical peaks associated with the C−H stretching in the molecules of SQ and the C−O−C vibration bonds of CS, respectively. CS: chitosan. LMw CSNP: low molecular weight chitosan nanoparticle. HMw CSNP: high molecular weight chitosan nanoparticle. SQ: squalene. LMw CS-SQ NP: low molecular weight chitosan-squalene nanoparticle. HMw CS-SQ NP: high molecular weight chitosan-squalene nanoparticles. TPP: sodium tripolyphosphate. TWEEN: Tween 80. FTIR spectrum labels: broad O−H stretching (3200−3600 cm^{-1}), N−H stretching (3300−3500 cm^{-1}), C−H stretching (2800−3000 cm^{-1}), C═C stretching (1600−1680 cm^{-1}), C−O stretching (1000−1300 cm^{-1}), C−N stretching (1000−1350 cm^{-1}), C═O stretching (1650−1750 cm^{-1}), C−O−C stretching (900−1200 cm^{-1}).

spectra. This approach permitted the differentiation of the C−H stretching vibrations of squalene from those of chitosan within the CS-SQ NPs.[29,47] For chitosan, the C−O−C vibration (1000−1100 cm^{-1}) was selected as it is indicative of the glycosidic bond structure of the polysaccharide, thereby confirming its presence in the nanoparticles. Although other signals, such as the amide II band (around 1550 cm^{-1}) and the CO−H band (around 1410 cm^{-1}), are also characteristic of chitosan, the C−O−C peak enabled the reliable identification of chitosan within the system, without interference from other bands.[48]

By calculating the intensity ratios of squalene:chitosan bands (at 2800−3000 vs 1000−1100 cm^{-1}), we observed that the LMw CS-SQ NPs (0.8) exhibited a higher ratio than the HMw CS-SQ NPs (0.3), supporting our claim of higher encapsulation efficiency in LMw chitosan. These findings were consistent with the results of GC-MS, which indicated higher amounts of squalene in LMw CS-SQ NPs than the HMw CS-SQ NPs (Table 2), by using the equations provided in the experimental section. The maximum squalene loading in CSNPs was found to occur when using 200 μL of initial squalene volume, which reached 8015 ± 1065 μM of squalene loading (Table 2). This corresponded to an encapsulation efficiency of 61.5 ± 12%. Among the tested formulations in our study, this represented the highest encapsulation efficiency achieved for squalene within chitosan nanoparticles. The encapsulation efficiency of squalene-loaded NPs has been reported in the literature to vary considerably, depending on the type of NP and the synthetic method employed, with values ranging from 26 to 82%.[12,49]

The results of this study confirmed that the LMw CSNPs with a positive charge have favorable properties for encapsulating squalene and could significantly influence their encapsulation efficiency of squalene. Consequently, these nanoparticles were selected for further investigation.

3.2. Morphology of the LMw Chitosan Nanoparticles. SEM and scanning transmission electron microscopy in scanning electron microscopy (STEM in SEM) were employed to examine the morphology of the LMw NPs. Selected SEM and STEM in SEM micrographs of the CSNPs and CS-SQ NPs are presented in Figure 3A,B. As displayed in Figure 3A, the SEM image of the morphological construction of CSNPs revealed slightly spherical-like particles. Moreover, upon evaluating the SEM images, we acknowledge that while the nanoparticles are indeed isolated, discrete, and nonaggregated, they exhibit some variability in size. For CS-SQ NPs, the NPs exhibited an increase in size and different shapes due to the presence of squalene and also some aggregation. Another effective approach for elucidating the morphology of CSNPs is STEM in SEM (Figure 3B). The introduction of STEM in SEM images has led to a more expansive conceptualization than that of the SEM, particularly with regard to the nonaggregation and lower agglomeration status of CSNPs in comparison to the CS-SQ NPs. The loading of squalene on CSNPs has been demonstrated to exert an influence on the shape of the NPs, as previously observed by other research groups.[12,29] It can be concluded that squalene affects both the shape and size of chitosan nanoparticles during the synthesis process. This observation was consistent with previous findings indicating that the presence of diverse components, including curcumin, oregano essential oil, and lipids, can enhance the size of CSNPs while maintaining their spherical shape.[15,29,30,32] Also, the sizes obtained by SEM and STEM in SEM were smaller than those observed with DLS. For example, the mean size of the CSNPs and CS-SQ NPs exhibited a wide range, between 40 and 150 nm. This result was anticipated, as the particles were dried prior to observation. Conversely, DLS provided insight into the hydrodynamic diameter of the particles, and it was known that chitosan particles exhibited significant swelling in aqueous solution.[50]

3.3. Cytotoxicity Evaluation of the Chitosan−Squalene Nanoparticles as Drug Carrier. Currently, chitosan is widely regarded as a safe and benign polymer for the delivery of pharmaceuticals. The United States Food and Drug

https://doi.org/10.1021/acsomega.4c08258
ACS Omega XXXX, XXX, XXX−XXX

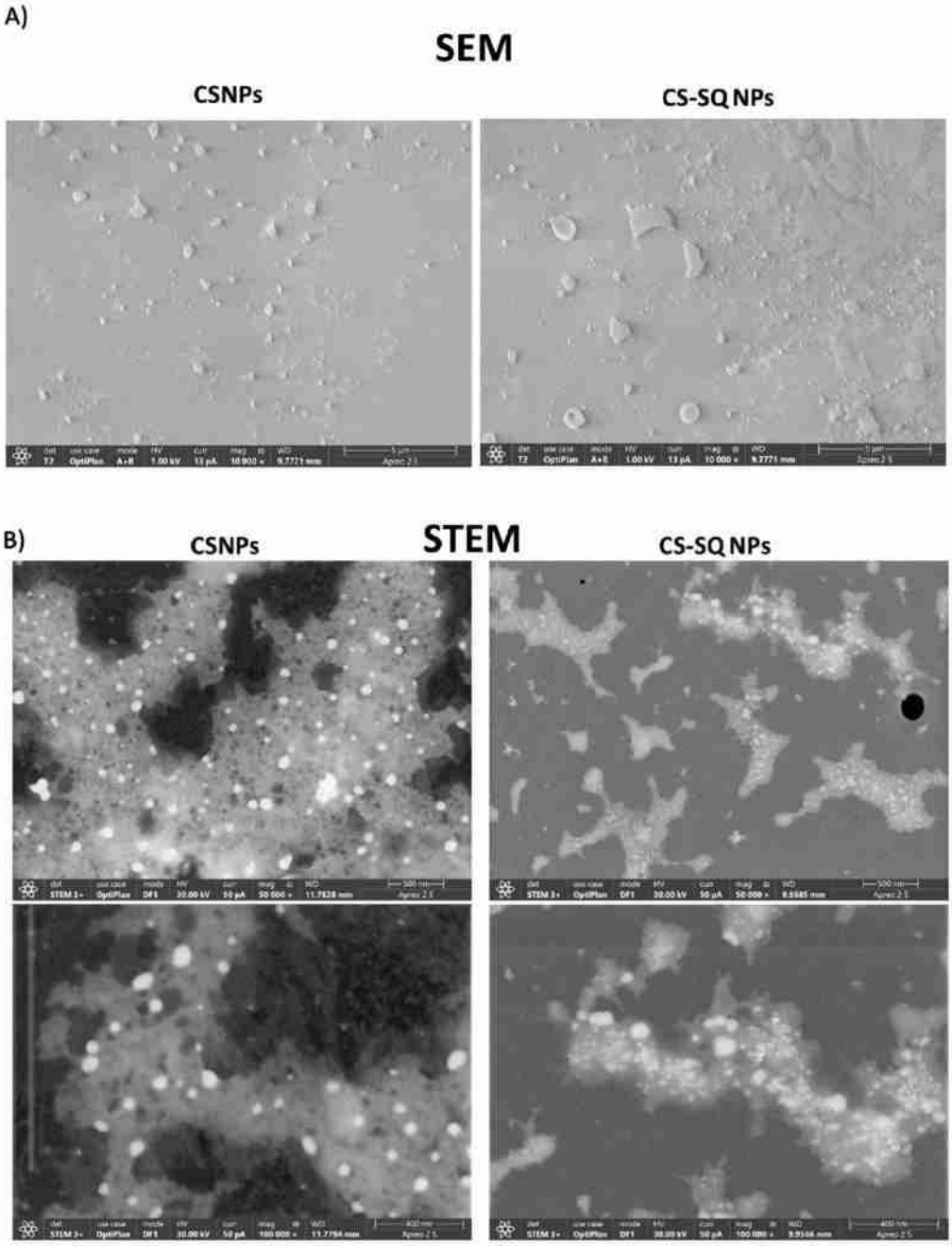

Figure 3. (A) SEM and (B) STEM in SEM pictures of chitosan nanoparticles (CSNPs) and chitosan-squalene nanoparticles (CS-SQ NPs) (×50,000 and ×100,000).

https://doi.org/10.1021/acsomega.4c08258
ACS Omega XXXX, XXX, XXX−XXX

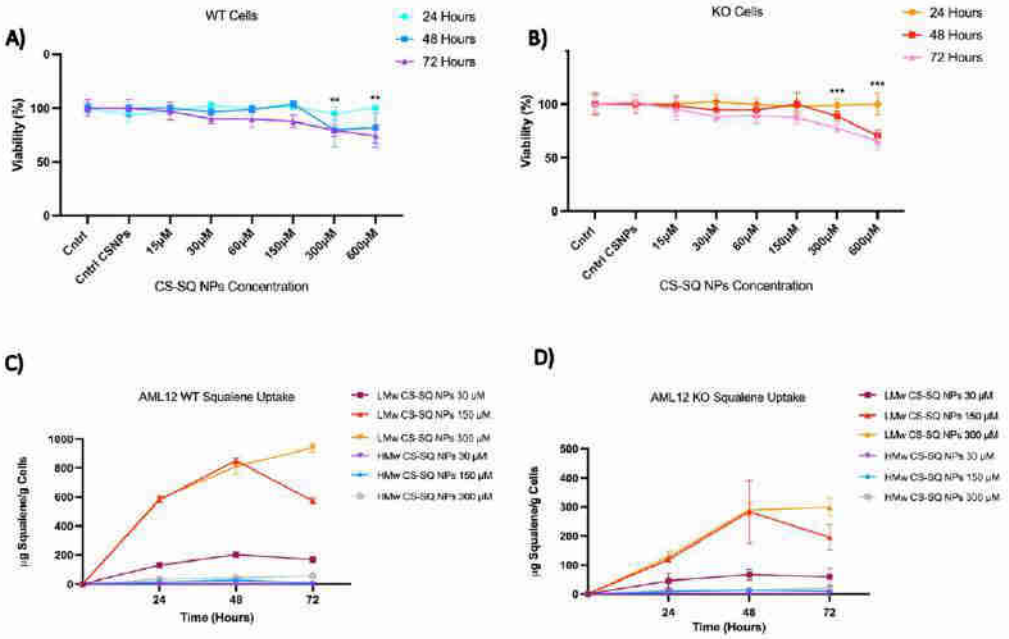

Figure 4. The viability of (A) AML12 WT cells and (B) AML12 KO cells was assessed following 24, 48, and 72 h of treatment with varying concentrations of CS-SQ NPs. A significant difference was observed between the 300 and 600 μM CS-SQ NPs and control groups. (C, D) Cellular uptake of squalene by the AML12 WT and KO cell lines, respectively. A notable enhancement in squalene uptake was observed in both WT and KO AML12 cells at 150 μM following a 48 h incubation period, as evidenced by the results of the squalene extraction. Statistical analyses were done according to Mann–Whitney's *U*-test: $^{**}p < 0.01$, $^{***}p < 0.001$.

Administration has approved its use as a wound dressing.[51] Different results demonstrated that, due to the prolonged circulation time *in vivo* and enhanced permeability and efficacy of the drug, chitosan nanoparticles loaded with drugs were successfully concentrated in tumor tissues of mice, with a superior antitumor effect and reduced toxicity.[52] The cytotoxicities of the CS-SQ NPs and CSNPs were evaluated using MTT colorimetric assays on two distinct cell lines: AML12 WT, mouse hepatocyte cells, and AML12 KO, mouse hepatocyte cells lacking the expression of TXNDC5 protein. Both cell lines served as effective models for the investigation of hepatotoxicity associated with novel materials. In regard to the MTT assays, three-time frames and six distinct nanoparticle concentrations were selected for testing. Both cell lines demonstrated heightened sensitivity within 72 h of treatment. In fact, at 600 μM, the highest concentration tested, the cell viability was approximately 75% on the AML12 WT cell line (Figure 4A) and 65% on the AML12 KO cell line (Figure 4B). The MTT assays indicated that 24 and 48 h were safe for a maximum concentration of 150 μM on both cells, with cell viability exceeding 85%. There was no difference in cell viability between the control and CSNPs. The results of this assay indicated that neither CS-SQ NPs nor CSNPs exhibited cytotoxicity in either cell line at concentrations up to 150 μM at 24 and 48 h of treatment (Figure 4A,B). The results of this study confirmed the lack of cytotoxicity observed in previous studies involving chitosan-curcumin nanoparticles and doxorubicin–chitosan polymeric micelles for targeting the liver and spleen, with a significant reduction in drug toxicity to the heart and kidney.[30,53] In contrast to toxic compounds such as sulfide, which exhibited toxicity against MCF7 and COS7 cells, chitosan has been demonstrated to be nontoxic. However, it is important to note that the concentration of chitosan may affect cell viability at high doses or for long periods of time. For example, intravenous injection of excessive amounts of chitosan has been associated with blood clotting, which could lead to adverse outcomes such as death. However, this phenomenon typically occurred at very high concentrations.[54] Consequently, in the development of CSNPs, it is important to consider the NPs concentration to minimize potential toxicity.[55]

3.4. Cellular Uptake of Squalene in AML12 Cells. A cell uptake study is an essential tool for evaluating the delivery potential of the nanoparticle system. Cellular uptake was studied with squalene extracted from hepatocytes by GC/MS. Three different LMw and HMw CS-SQ NP ratios (30, 150, and 300 μM) were tested over 24, 48, and 72 h to identify optimal conditions. As the CS-SQ NPs ratio increased, the uptake efficiency increased. Interestingly, for all CS-SQ NPs except 300 μM, the maximum cellular uptake efficiency was observed for the 150 μM ratio at 48 h, after which a decrease in uptake was observed (Figure 4C,D). This could be due to the saturation of the endocytosis pathway by the nanosystems.[56] It is our contention that saturation was reflected in the time and

https://doi.org/10.1021/acsomega.4c08258
ACS Omega XXXX, XXX, XXX−XXX

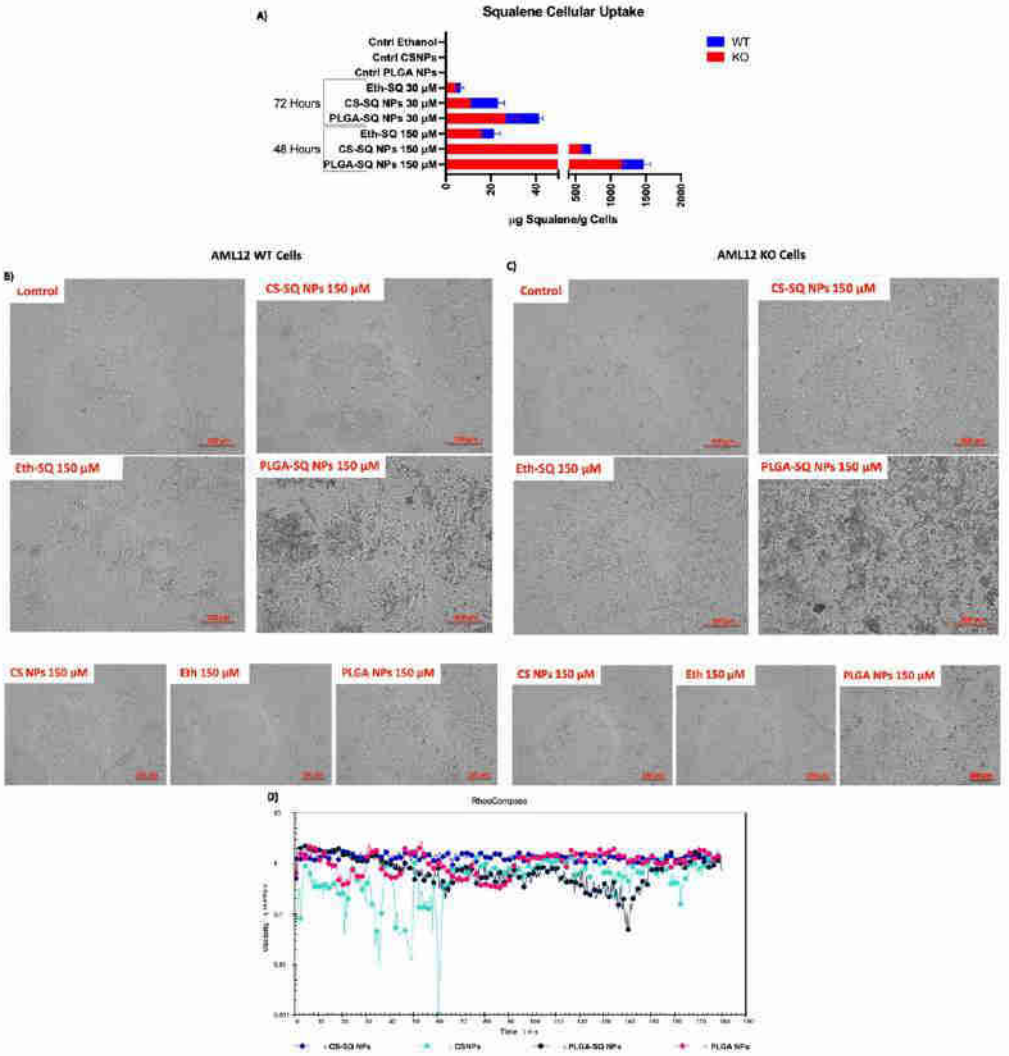

Figure 5. (A) *In vitro* cellular uptake of squalene using different carriers. WT and KO hepatic AML12 cells were incubated with 30 and 150 μM PLGA, CS-SQ NPs, and Eth-SQ for 48 and 72 h. (B, C) The effect of 48 h of exposure to different carriers at a concentration of 150 μM squalene on the morphology of AML12 WT and KO cell lines. The control group refers to untreated cells with none of the carriers. (D) Viscosity measurements of chitosan and PLGA nanoparticle solutions containing squalene compared to control nanoparticle solution.

concentration of squalene. In LMw CS-SQ NPs 150 and 300 μM, in the concentration of 150, the absorption finished after 48 h, as indicated by the decrease in cellular squalene amount at 72 h. Conversely, the cellular amount of squalene increased continuously because there were more squalene molecules to absorb. These data might be used to determine the optimal concentration for subsequent doses of charged NPs and the appropriate time interval between doses. Among the LMw and HMw CS-SQ NPs, squalene carried by LMw CS into the cells was the most efficient in terms of the amount of squalene per gram of cells. The results indicated that the nature and molar ratios of chitosan play a significant role in their internalization process.[57] Another hypothesis regarding the In HMw CS-SQ NPs was that they are unable to be absorbed due to their larger size, which prevents them from being absorbed by cells. This indicated a loss of function of the NPs. Previous studies have shown that for a comparable number of polymer units, the use of smaller Mw chitosan on lipid nanoparticle surfaces was more

https://doi.org/10.1021/acsomega.4c08258
ACS Omega XXXX, XXX, XXX−XXX

favorable for efficient cellular uptake.[58−60] Chitosan has been demonstrated to enhance the bioavailability of drugs by facilitating their absorption, which prolongs the contact time between the substrate and cell membrane.[18] Furthermore, their nanoscale dimensions facilitate the uptake of drugs through the cell membrane. This feature has been observed in A2780 ovarian cancer cells, indicating that CSNPs could deliver drugs to the perinuclear space.[61] Other studies have indicated that paclitaxel, glycol, cyclosporin A, and ovalbumin−chitosan nanoparticles had a higher cell uptake rate than the free drugs in MDA-MB-231, HeLa, RCE, and RAW264.7.[62−65] In conclusion, the results of squalene extraction indicated that there was a considerable increase in the uptake of squalene as compared to the control in 150 μM at 48 h in both WT and KO AML12 cells. The internalization and uptake of squalene-particles might be favored due to the presence of positively charged chitosan.[62] In general, the surface charge of particles is considered a crucial factor in determining their uptake by cells. For example, positively charged gold nanoparticles were preferentially captured by cells in comparison to their negatively charged counterparts.[66] CS-SQ NPs had a high positive charge, and studies have shown that cationic nanoparticles could significantly increase the endocytosis of particles.[67]

3.5. Chitosan Nanoparticles vs PLGA or Ethanol as Carriers. The transfer of squalene into cells can be achieved through the use of various carriers, including PLGA and ethanol.[5,68] However, the optimal carrier for this purpose remains to be determined. In our experimental design, we included ethanol-squalene as a non-nanoparticle carrier to serve as a control for comparison with PLGA and CS drug delivery systems. The ethanol-squalene formulation provided a relevant baseline for the investigation of the cellular uptake and delivery efficiency of squalene when not encapsulated in NPs. Also, prior studies have evaluated the use of free CS for drug delivery, demonstrating its limited ability to encapsulate and effectively deliver hydrophobic compounds like squalene, clove essential oil, and doxorubicin without nanoparticle formulation. These studies demonstrated that CS in non-nanoparticle form provided significantly lower encapsulation efficiency and stability for hydrophobic compounds compared to nanoparticle formulations, which utilize chitosan's capacity to form stable carriers.[69−72] Previous investigations have indicated that PLGA NPs, due to their smaller size, are rapidly and efficiently taken up by cells.[73,74] In order to identify the optimal carrier for the transfer of squalene into hepatocytes, two doses of squalene (30 μM and 150 μM) were selected for comparison. These doses were carried by LMw chitosan, PLGA and ethanol,[5,68] and were administered over a 48- or 72-h exposure period. The results of squalene cellular uptake by AML12 WT and KO cells indicated that the chitosan and PLGA have higher efficiency compared to ethanol (Figure 5A). However, the PLGA-SQ NPs in both doses exhibited the highest efficiency at 48 and 72 h. These results confirmed previous findings that PLGA has superior cellular uptake compared to other polymers used for drug and gene delivery.[75] As evidenced by numerous studies, PLGA nanoparticles are highly efficient nanocarriers for the encapsulation and delivery of a diverse array of anticancer agents, including oleanolic and ursolic acids, in three distinct cell lines: HepG2, Caco-2, and Y-79.[76] For instance, PLGA-based curcumin nanoparticles have exhibited an entrapment efficiency of 77 to 85%.[77] However, the previous study conducted by our group revealed certain limitations associated with PLGA nanoparticles. In this regard, the influence of 150, 60, 30, and 15 μM doses of squalene loaded into PLGA nanoparticles was qualitatively examined by microscopy after 72 h of incubation with AML12 cells. The 150 μM PLGA NPs caused the cell to undergo complete shrinkage due to osmotic stress. However, this shrinkage was mitigated by lowering the nanoparticle dosage. Due to the observed morphological impact of the highest doses, the 30 μM of squalene loaded in the PLGA nanoparticles was selected to carry out the subsequent studies on AML12 cells. Hence, high doses of squalene were not applicable in the PLGA carrier.[5] To ascertain the impact of CS-SQ NPs on hepatocyte morphology in the presence of high concentrations of squalene, the influence of 150 μM CS-SQ NPs, PLGA-SQ NPs, and Eth-SQ was qualitatively examined by microscopy after 48 h of incubation with WT and KO AML12 cells. Consequently, the 150 μM PLGA-SQ NPs induced a change in cell morphology (Figure 5B,C), whereas no such change was observed in CS-SQ NPs and Eth-SQ due to the presence of osmotic stress. Therefore, based on the observed morphological impact of the highest doses of squalene, chitosan was selected as the most efficient and productive carrier for high doses of squalene to conduct subsequent studies on hepatocytes.

The viscosity of polymer solution is a parameter of great interest from a technological standpoint, as highly viscous solutions present significant challenges in their management.[22] The molecular weight and viscosity of chitosan in aqueous solution also play a significant role in its biochemical and pharmacological applications.[78] The viscosity of chitosan is dependent upon the molecular weight of the polymer and the degree of deacetylation, with a reduction in viscosity observed as the molecular weight of chitosan is diminished. In fact, viscosity can be employed to ascertain the stability of the polymer in solution, as a reduction was observed during polymer storage due to polymer degradation.[79] It was evident that a certain quantity of larger nanoparticles was tolerated by the human body. In contrast to small nanoparticles, capillary blockage will occur if the particle size exceeds the diameter of the blood vessel. The gelation of the low-viscosity CS-SQ NPs and PLGA-SQ NPs dispersion in the syringe needle may occur, resulting in the immediate formation of a viscous suspension with unacceptable particle sizes. These were significant challenges for the development of squalene nanoparticle dispersions suitable for intravenous injection in clinical practice. In this context, the viscosity of the CS-SQ NPs and PLGA-SQ NPs was quantified using Pressure Cell C-PDT200. The results demonstrated that the squalene did not show any significant alterations in the viscosity of both drug delivery carriers. In addition, the viscosity of CS-SQ NPs and PLGA-SQ NPs demonstrated their ease of administration due to the formulations with lower viscosity (Figure 5D).

3.6. Squalene Protects Hepatocytes against Oxidative and Endoplasmic Reticulum Stress. The administration of squalene has been demonstrated to induce significant alterations in hepatic proteins involved in lipid metabolism, oxidative stress, and lipoprotein secretion, as well as a reduction in hepatic triglycerides in mice.[80] Squalene's antioxidant properties are closely associated with its distinctive and stable structure, which enables it to effectively neutralize harmful free radicals.[81] Hepatic TXNDC5 is a member of the protein disulfide isomerase family, which has been associated with antisteatotic properties of squalene and regulation of ER

https://doi.org/10.1021/acsomega.4c08258
ACS Omega XXXX, XXX, XXX−XXX

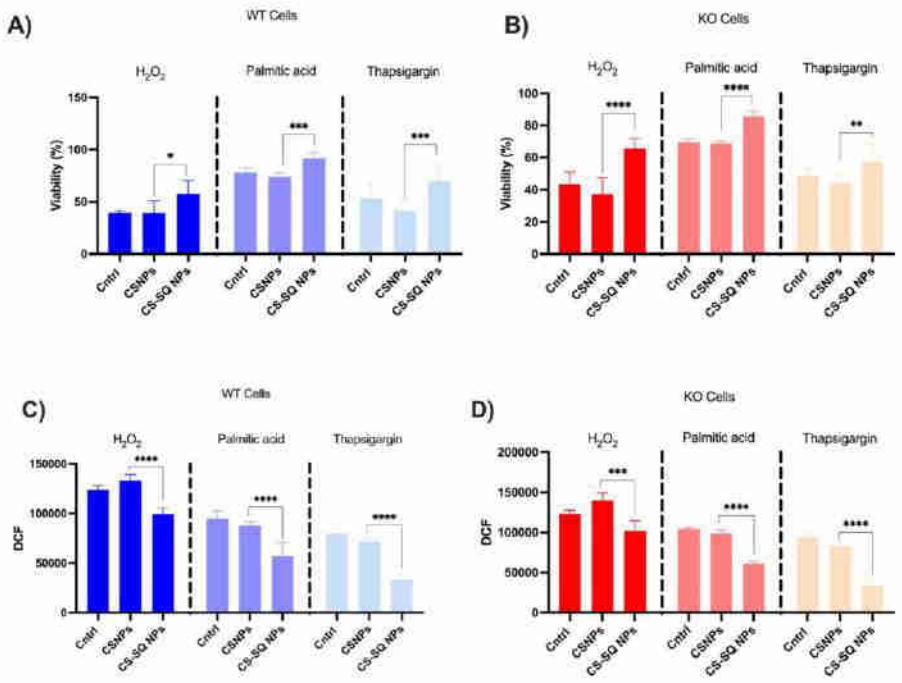

Figure 6. (A, B) The evaluation of cell viability in WT and KO AML12 hepatocytes subjected to oxidative and ER stress. Following a 48 h treatment with 150 μM of CS-SQ NPs, ER stress was induced by 12.5 nM of thapsigargin, 600 μM of palmitic acid, and oxidative stress was induced by 8 mM of H_2O_2 for 24 h. (C, D) Assessment of ROS production in AML12 WT and KO cells, respectively. Following the treatment of cells with 150 μM of CS-SQ NPs for 48 h, ROS was measured in oxidative and ER stress circumstances induced by 8 mM of H_2O_2, 600 μM of palmitic acid, and 12.5 nM of thapsigargin for 24 h. Statistical analyses were conducted according to two-way ANOVA: $^{**}p < 0.01$, $^{***}p < 0.001$, $^{***}p < 0.001$, $^{****}p < 0.0001$.

stress.[82,83] Furthermore, TXNDC5 has demonstrated potential for the diagnosis and treatment of various diseases by reducing oxidative stress and levels of inflammatory cytokines. Consequently, TXNDC5 acts as a protective agent, safeguarding cells against oxidative and ER stress.[13] AML12 cells were incubated with 150 μM of CS-SQ NPs for 48 h to assess the induction of intracellular ROS and viability by squalene. Following exposure to squalene, the cells were treated with H_2O_2 as an oxidative stress inducer, palmitic acid and thapsigargin as moderate and harsh ER stressors for 24 h. The CSNPs did not produce a notable alteration in cell viability when compared to the control group, as determined by the MTT assay. CS-SQ NPs demonstrated the capacity to significantly enhance the viability of both cell lines (Figure 6A,B). Viability enhancement was calculated in the different stressors that were tested, and the results demonstrated that the squalene delivered from chitosan nanoparticles increased the viability of the WT hepatocyte cells and KO cells by 18 and 25% in oxidative stress, respectively, and 21 and 15% in ER stress, respectively. To ascertain whether 150 μM of squalene-loaded NPs could effectively provide protection against oxidative and ER stress, we initially developed an in vitro model of them. The comparison of the control group and the CSNPs demonstrates that chitosan nanoparticles did not induce a significant ROS in both cell lines. As illustrated in Figure 6C, WT cells treated with CS-SQ NPs exhibited a significant reduction in ROS production compared with the CS group in all stress conditions. This data was also observed in KO samples (Figure 6D), although previous data from our group indicated that squalene protection was absent in cells lacking TXNDC5 when exposed to 30 μM of squalene in an oxidative stress context.[5] The protective effects of squalene against oxidative destruction have been formally documented in rodents and multiple cell lines, including murine macrophages, human monocytes, and mammary epithelial cells.[84] Previous studies have demonstrated that inhibiting TXNDC5 expression via knockdown induced ROS and ER stress in pancreatic cancer cells. Conversely, increasing TXNDC5 expression in lipid endothelial cells effectively reduced ROS production and protects cells.[85,86] Additionally, the overexpression of TXNDC5 resulted in reduced sensitivity to ER stress when exposed to tunicamycin and thapsigargin. However, TXNDC5 knockout human prostate adenocarcinoma cells exhibited a loss of the ability to upregulate protein disulfide isomerase following tunicamycin-induced ER stress.[87] Overall, the results demonstrated that TXNDC5 could modulate ROS production in oxidative stress, contingent on the optimal dose of squalene, and enhanced the efficacy of squalene in AML12 cell viability and functioned as an oxidative stress-induced survival factor that regulated ROS/ER stress

https://doi.org/10.1021/acsomega.4c08258
ACS Omega XXXX, XXX, XXX−XXX

signaling, thereby enabling AML12 cells to persist under oxidative stress.

4. CONCLUSIONS

The present study demonstrates that low molecular weight chitosan nanoparticles, which form a spherical shape, are an effective encapsulation agent for squalene based on GC-MS measurement and semiquantitative FTIR analysis. The results demonstrated that squalene-loaded chitosan nanoparticles did not exhibit any cytotoxicity to hepatocytes up to 150 μM and exhibited efficient cellular uptake within 48 h. In comparison to PLGA and ethanol, the chitosan nanoparticles were identified as the most efficient and productive carriers for high doses of squalene and PLGA for lower doses of squalene, thus justifying further investigation in hepatocytes. The cell viability of WT and KO AML12 cells was increased in the presence of squalene under oxidative and endoplasmic reticulum stress conditions induced by palmitic acid and thapsigargin. Furthermore, squalene-based chitosan nanoparticles effectively reduced ROS levels in mouse hepatocytes. Chitosan nanoparticles demonstrated the potential to overcome the limitations of PLGA drug carriers, suggesting that the proper dose of squalene can modulate ROS production in oxidative stress, independent of TXNDC5.

■ ASSOCIATED CONTENT

Data Availability Statement

Data are contained within the article and Supporting Information.

Supporting Information

The Supporting Information is available free of charge at https://pubs.acs.org/doi/10.1021/acsomega.4c08258.

Figure S1 showing characterization of AML12 cell lines (PDF)

■ AUTHOR INFORMATION

Corresponding Authors

Jesús Osada − *Departamento de Bioquímica y Biología Molecular y Celular, Facultad de Veterinaria, Instituto de Investigación Sanitaria de Aragón, Universidad de Zaragoza, E-50013 Zaragoza, Spain; Instituto Agroalimentario de Aragón, CITA-Universidad de Zaragoza, E-50013 Zaragoza, Spain; Centro de Investigación Biomédica en Red de Fisiopatología de la Obesidad y Nutrición (CIBEROBN), Instituto de Salud Carlos III, E-28029 Madrid, Spain; Departamento de Farmacología, Fisiología, Medicina Legal y Forense, Facultad de Veterinaria, Instituto de Investigación Sanitaria de Aragón-Universidad de Zaragoza, E-50013 Zaragoza, Spain;* Phone: +34-976-761-644; Email: josada@unizar.es; Fax: +34-976-761-612

Susana C. M. Fernandes − *Institute of Analytical Sciences and Physico-Chemistry for Environment and Materials (IPREM), E2S UPPA, CNRS, Université de Pau et des Pays de l'Adour, 64 012 Pau, France; MANTA—Marine Materials Research Group, Universite de Pau et des Pays de l'Adour, 64 053 Pau, France;* orcid.org/0000-0002-1295-5010; Phone: +33 (0) 5 40 17 50 15; Email: susana.fernandes@univ-pau.fr

Authors

Seyed Hesamoddin Bidooki − *Departamento de Bioquímica y Biología Molecular y Celular, Facultad de Veterinaria, Instituto de Investigación Sanitaria de Aragón, Universidad de Zaragoza, E-50013 Zaragoza, Spain; Institute of Analytical Sciences and Physico-Chemistry for Environment and Materials (IPREM), E2S UPPA, CNRS, Université de Pau et des Pays de l'Adour, 64 012 Pau, France; MANTA—Marine Materials Research Group, Universite de Pau et des Pays de l'Adour, 64 053 Pau, France;* orcid.org/0000-0002-5612-5000

Lea Spitzer − *Institute of Analytical Sciences and Physico-Chemistry for Environment and Materials (IPREM), E2S UPPA, CNRS, Université de Pau et des Pays de l'Adour, 64 012 Pau, France; MANTA—Marine Materials Research Group, Universite de Pau et des Pays de l'Adour, 64 053 Pau, France*

Arnaud Petitpas − *Institute of Analytical Sciences and Physico-Chemistry for Environment and Materials (IPREM), E2S UPPA, CNRS, Université de Pau et des Pays de l'Adour, 64 012 Pau, France; MANTA—Marine Materials Research Group, Universite de Pau et des Pays de l'Adour, 64 053 Pau, France*

Javier Sánchez-Marco − *Departamento de Bioquímica y Biología Molecular y Celular, Facultad de Veterinaria, Instituto de Investigación Sanitaria de Aragón, Universidad de Zaragoza, E-50013 Zaragoza, Spain*

Roberto Martínez-Beamonte − *Departamento de Bioquímica y Biología Molecular y Celular, Facultad de Veterinaria, Instituto de Investigación Sanitaria de Aragón, Universidad de Zaragoza, E-50013 Zaragoza, Spain; Instituto Agroalimentario de Aragón, CITA-Universidad de Zaragoza, E-50013 Zaragoza, Spain; Centro de Investigación Biomédica en Red de Fisiopatología de la Obesidad y Nutrición (CIBEROBN), Instituto de Salud Carlos III, E-28029 Madrid, Spain*

Roberto Lasheras − *Laboratorio Agroambiental, Servicio de Seguridad Agroalimentaria de la Dirección General de Alimentación y Fomento Agroalimentario, Gobierno de Aragón, E-50192 Zaragoza, Spain*

Virginie Pellerin − *Institute of Analytical Sciences and Physico-Chemistry for Environment and Materials (IPREM), E2S UPPA, CNRS, Université de Pau et des Pays de l'Adour, 64 012 Pau, France*

María J. Rodríguez-Yoldi − *Instituto Agroalimentario de Aragón, CITA-Universidad de Zaragoza, E-50013 Zaragoza, Spain; Centro de Investigación Biomédica en Red de Fisiopatología de la Obesidad y Nutrición (CIBEROBN), Instituto de Salud Carlos III, E-28029 Madrid, Spain; Departamento de Farmacología, Fisiología, Medicina Legal y Forense, Facultad de Veterinaria, Instituto de Investigación Sanitaria de Aragón-Universidad de Zaragoza, E-50013 Zaragoza, Spain*

María Ángeles Navarro − *Departamento de Bioquímica y Biología Molecular y Celular, Facultad de Veterinaria, Instituto de Investigación Sanitaria de Aragón, Universidad de Zaragoza, E-50013 Zaragoza, Spain; Instituto Agroalimentario de Aragón, CITA-Universidad de Zaragoza, E-50013 Zaragoza, Spain; Centro de Investigación Biomédica en Red de Fisiopatología de la Obesidad y Nutrición (CIBEROBN), Instituto de Salud Carlos III, E-28029 Madrid, Spain*

Complete contact information is available at: https://pubs.acs.org/10.1021/acsomega.4c08258

https://doi.org/10.1021/acsomega.4c08258
ACS Omega XXXX, XXX, XXX−XXX

Author Contributions

Conceptualization: S.H.B., L.S., A.P., V.P., J.S.-M., R.M.-B., R.L., M.A.N., M.J.R.-Y., J.O., and S.C.M.F. Methodology: S.H.B., L.S., A.P., V.P., J.S.-M., R.M.-B., and R.L. Software: S.H.B., A.P., and V.P. Validation: S.H.B. Formal analysis: S.H.B., L.S., A.P., V.P., J.S.-M., R.M.-B., and R.L. Investigation: S.H.B., J.O., and S.C.M.F. Resources: M.J.R.-Y., J.O., and S.C.M.F. Data curation: M.A.N., M.J.R.-Y., J.O. and S.C.M.F. Writing—original draft preparation: S.H.B. Writing—review and editing: S.H.B., L.S., A.P., V.P., J.S.-M., R.M.-B., R.L., M.A.N., M.J.R.-Y., J.O., and S.C.M.F. Visualization: S.H.B., A.P., V.P. Supervision: M.A.N., J.O., and S.C.M.F. Project administration: M.J.R.-Y., J.O., and S.C.M.F. Funding acquisition: M.J.R.-Y., J.O., and S.C.M.F. All authors have read and agreed to the published version of the manuscript.

Funding

This research was supported by grants (CIBEROBN, CB06/03/1012) from CIBER Fisiopatología de la Obesidad y Nutrición as an initiative of FEDER-ISCIII, Ministerio de Ciencia e Innovación-Fondo Europeo de Desarrollo Regional (Grant PID2022-136414OB-I00) and Fondo Social Europeo-Gobierno de Aragón (Grant B16_23R). S.H.B. was recipient of a joint fellowship from the Universities of Zaragoza and Pau and short-term fellowship from Universidad de Zaragoza, Fundación Bancaria Ibercaja, and Fundación CAI (Grant CM 4/24, June 4, 2024). It was also carried under the framework of E2S UPPA Partnership Chair MANTA (Marine Materials) funded by the "Investissements d'Avenir' French program managed by ANR, Grant ANR-16-IDEX-0002.

Notes

The authors declare no competing financial interest.

■ ACKNOWLEDGMENTS

We thank Cristina Barranquero for her help in maintaining the lab.

■ REFERENCES

(1) Hatchwell, L.; Harney, D. J.; Cielesh, M.; Young, K.; Koay, Y. C.; O'Sullivan, J. F.; Larance, M. Multi-omics analysis of the intermittent fasting response in mice identifies an unexpected role for HNF4α. *Cell Reports* **2020**, *30* (10), 3566−3582.

(2) Herrera-Marcos, L. V.; Martínez-Beamonte, R.; Macías-Herranz, M.; Arnal, C.; Barranquero, C.; Puente-Lanzarote, J. J.; Gascón, S.; Herrero-Continente, T.; Gonzalo-Romeo, G.; Alastrué-Vera, V.; et al. Hepatic galectin-3 is associated with lipid droplet area in non-alcoholic steatohepatitis in a new swine model. *Sci. Rep.* **2022**, *12* (1), 1024.

(3) Tu, L. N.; Showalter, M. R.; Cajka, T.; Fan, S.; Pillai, V. V.; Fiehn, O.; Selvaraj, V. Metabolomic characteristics of cholesterol-induced non-obese nonalcoholic fatty liver disease in mice. *Sci. Rep.* **2017**, *7* (1), 6120.

(4) Guasch-Ferré, M.; Willett, W. The Mediterranean diet and health: A comprehensive overview. *Journal of internal medicine* **2021**, *290* (3), 549−566.

(5) Bidooki, S. H.; Alejo, T.; Sánchez-Marco, J.; Martínez-Beamonte, R.; Abuobeid, R.; Burillo, J. C.; Lasheras, R.; Sebastian, V.; Rodríguez-Yoldi, M. J.; Arruebo, M.; Osada, J. Squalene loaded nanoparticles effectively protect hepatic AML12 cell lines against oxidative and endoplasmic reticulum stress in a TXNDC5-dependent way. *Antioxidants* **2022**, *11* (3), 581.

(6) Guasch-Ferré, M.; Li, Y.; Willett, W. C.; Sun, Q.; Sampson, L.; Salas-Salvadó, J.; Martínez-González, M. A.; Stampfer, M. J.; Hu, F. B. Consumption of olive oil and risk of total and cause-specific mortality among US adults. *Journal of the American College of Cardiology* **2022**, *79* (2), 101−112.

(7) Martínez-Beamonte, R.; Sánchez-Marco, J.; Felices, M. J.; Barranquero, C.; Gascón, S.; Arnal, C.; Burillo, J. C.; Lasheras, R.; Busto, R.; Lasunción, M. A.; et al. Dietary squalene modifies plasma lipoproteins and hepatic cholesterol metabolism in rabbits. *Food Funct.* **2021**, *12* (17), 8141−8153.

(8) Gabás-Rivera, C.; Barranquero, C.; Martínez-Beamonte, R.; Navarro, M. A.; Surra, J. C.; Osada, J. Dietary squalene increases high density lipoprotein-cholesterol and paraoxonase 1 and decreases oxidative stress in mice. *PloS one* **2014**, *9* (8), No. e104224.

(9) Spanova, M.; Daum, G. Squalene-biochemistry, molecular biology, process biotechnology, and applications. *European journal of lipid science and technology* **2011**, *113* (11), 1299−1320.

(10) Lou-Bonafonte, J. M.; Martínez-Beamonte, R.; Sanclemente, T.; Surra, J. C.; Herrera-Marcos, L. V.; Sanchez-Marco, J.; Arnal, C.; Osada, J. Current insights into the biological action of squalene. *Mol. Nutr. Food Res.* **2018**, *62* (15), 1800136.

(11) Reddy, L. H.; Couvreur, P. Squalene: A natural triterpene for use in disease management and therapy. *Advanced drug delivery reviews* **2009**, *61* (15), 1412−1426.

(12) Kumar, L. R.; Chatterjee, N.; Tejpal, C.; Vishnu, K.; Anas, K.; Asha, K.; Anandan, R.; Mathew, S. Evaluation of chitosan as a wall material for microencapsulation of squalene by spray drying: Characterization and oxidative stability studies. *Int. J. Biol. Macromol.* **2017**, *104*, 1986−1995.

(13) Bidooki, S. H.; Navarro, M. A.; Fernandes, S. C. M.; Osada, J. Thioredoxin Domain Containing 5 (TXNDC5): Friend or Foe? *Current Issues in Molecular Biology* **2024**, *46* (4), 3134−3163.

(14) Wang, J. J.; Zeng, Z. W.; Xiao, R. Z.; Xie, T.; Zhou, G. L.; Zhan, X. R.; Wang, S. L. Recent advances of chitosan nanoparticles as drug carriers. *Int. J. Nanomed.* **2011**, 765−774.

(15) Khan, M. M.; Madni, A.; Torchilin, V.; Filipczak, N.; Pan, J.; Tahir, N.; Shah, H. Lipid-chitosan hybrid nanoparticles for controlled delivery of cisplatin. *Drug delivery* **2019**, *26* (1), 765−772.

(16) Lekshmi, R. K.; Rahima, M.; Chatterjee, N.; Tejpal, C.; Anas, K.; Vishnu, K.; Sarika, K.; Asha, K.; Anandan, R.; Suseela, M. Chitosan-Whey protein as efficient delivery system for squalene: Characterization and functional food application. *Int. J. Biol. Macromol.* **2019**, *135*, 855−863.

(17) Fernández-Marín, R.; Fernandes, S. C. M.; Sánchez, M. Á. A.; Labidi, J. Halochromic and antioxidant capacity of smart films of chitosan/chitin nanocrystals with curcuma oil and anthocyanins. *Food Hydrocolloids* **2022**, *123*, 107119.

(18) Tiyaboonchai, W. Chitosan nanoparticles: a promising system for drug delivery. *Naresuan University Journal: Science and Technology (NUJST)* **2003**, *11* (3), 51−66.

(19) Rampino, A.; Borgogna, M.; Blasi, P.; Bellich, B.; Cesaro, A. Chitosan nanoparticles: Preparation, size evolution and stability. *International journal of pharmaceutics* **2013**, *455* (1−2), 219−228.

(20) Salaberria, A. M.; Diaz, R. H.; Labidi, J.; Fernandes, S. C. M. Preparing valuable renewable nanocomposite films based exclusively on oceanic biomass-Chitin nanofillers and chitosan. *React. Funct. Polym.* **2015**, *89*, 31−39.

(21) Claverie, M.; McReynolds, C.; Petitpas, A.; Thomas, M.; Fernandes, S. C. M. Marine-derived polymeric materials and biomimetics: An overview. *Polymers* **2020**, *12* (5), 1002.

(22) Aranaz, I.; Alcántara, A. R.; Civera, M. C.; Arias, C.; Elorza, B.; Heras Caballero, A.; Acosta, N. Chitosan: An overview of its properties and applications. *Polymers* **2021**, *13* (19), 3256.

(23) Bekmukhametova, A.; Uddin, M. M. N.; Houang, J.; Malladi, C.; George, L.; Wuhrer, R.; Barman, S. K.; Wu, M. J.; Mawad, D.; Lauto, A. Fabrication and characterization of chitosan nanoparticles using the coffee-ring effect for photodynamic therapy. *Lasers in Surgery and Medicine* **2022**, *54* (5), 758−766.

(24) Gan, Q.; Wang, T. Chitosan nanoparticle as protein delivery carrier—systematic examination of fabrication conditions for efficient loading and release. *Colloids Surf., B* **2007**, *59* (1), 24−34.

(25) Cardoso, M. J.; Costa, R. R.; Mano, J. F. Marine origin polysaccharides in drug delivery systems. *Marine drugs* **2016**, *14* (2), 34.

https://doi.org/10.1021/acsomega.4c08258
ACS Omega XXXX, XXX, XXX−XXX

(26) Pinto, R. J.; Fernandes, S. C. M.; Freire, C. S.; Sadocco, P.; Causio, J.; Neto, C. P.; Trindade, T. Antibacterial activity of optically transparent nanocomposite films based on chitosan or its derivatives and silver nanoparticles. *Carbohydr. Res.* **2012**, *348*, 77−83.
(27) Zubillaga, V. n.; Salaberria, A. M.; Palomares, T.; Alonso-Varona, A.; Kootala, S.; Labidi, J.; Fernandes, S. C. M. Chitin nanoforms provide mechanical and topological cues to support growth of human adipose stem cells in chitosan matrices. *Biomacromolecules* **2018**, *19* (7), 3000−3012.
(28) Divya, K.; Jisha, M. Chitosan nanoparticles preparation and applications. *Environmental chemistry letters* **2018**, *16*, 101−112.
(29) Lepeltier, E.; Loretz, B.; Desmaële, D.; Zapp, J.; Herrmann, J.; Couvreur, P.; Lehr, C.-M. Squalenoylation of chitosan: a platform for drug delivery? *Biomacromolecules* **2015**, *16* (9), 2930−2939.
(30) Ma, S.; Moser, D.; Han, F.; Leonhard, M.; Schneider-Stickler, B.; Tan, Y. Preparation and antibiofilm studies of curcumin loaded chitosan nanoparticles against polymicrobial biofilms of Candida albicans and Staphylococcus aureus. *Carbohydr. Polym.* **2020**, *241*, 116254.
(31) Tezgel, Ö.; Szarpak-Jankowska, A.; Arnould, A.; Auzély-Velty, R.; Texier, I. Chitosan-lipid nanoparticles (CS-LNPs): Application to siRNA delivery. *J. Colloid Interface Sci.* **2018**, *510*, 45−56.
(32) Hosseini, S. F.; Zandi, M.; Rezaei, M.; Farahmandghavi, F. Two-step method for encapsulation of oregano essential oil in chitosan nanoparticles: Preparation, characterization and in vitro release study. *Carbohydr. Polym.* **2013**, *95* (1), 50−56.
(33) Kumar, L.; Verma, S.; Singh, K.; Prasad, D. N.; Jain, A. K. Ethanol based vesicular carriers in transdermal drug delivery: nanoethosomes and transethosomes in focus. *NanoWorld J.* **2016**, *2*, 41.
(34) Chu, B.-S.; Ichikawa, S.; Kanafusa, S.; Nakajima, M. Preparation and characterization of β-carotene nanodispersions prepared by solvent displacement technique. *Journal of agricultural and food chemistry* **2007**, *55* (16), 6754−6760.
(35) Martínez-Beamonte, R.; Alda, O.; Sanclemente, T.; Felices, M. J.; Escusol, S.; Arnal, C.; Herrera-Marcos, L. V.; Gascón, S.; Surra, J. C.; Osada, J.; Rodríguez-Yoldi, M. J. Hepatic subcellular distribution of squalene changes according to the experimental setting. *J. Physiol. Biochem.* **2018**, *74*, 531−538.
(36) Bidooki, S. H.; Barranquero, C.; Sánchez-Marco, J.; Martínez-Beamonte, R.; Rodríguez-Yoldi, M. J.; Navarro, M. A.; Fernandes, S. C. M.; Osada, J. TXNDC5 Plays a Crucial Role in Regulating Endoplasmic Reticulum Activity through Different ER Stress Signaling Pathways in Hepatic Cells. *International Journal of Molecular Sciences* **2024**, *25* (13), 7128.
(37) Zhao, L.-M.; Shi, L.-E.; Zhang, Z.-L.; Chen, J.-M.; Shi, D.-D.; Yang, J.; Tang, Z.-X. Preparation and application of chitosan nanoparticles and nanofibers. *Brazilian Journal of Chemical Engineering* **2011**, *28*, 353−362.
(38) Qi, L.; Xu, Z.; Jiang, X.; Hu, C.; Zou, X. Preparation and antibacterial activity of chitosan nanoparticles. *Carbohydrate research* **2004**, *339* (16), 2693−2700.
(39) De Campos, A. M.; Sánchez, A.; Alonso, M. a. J. Chitosan nanoparticles: a new vehicle for the improvement of the delivery of drugs to the ocular surface. Application to cyclosporin A. *International journal of pharmaceutics* **2001**, *224* (1−2), 159−168.
(40) Csaba, N.; Köping-Höggård, M.; Alonso, M. J. Ionically crosslinked chitosan/tripolyphosphate nanoparticles for oligonucleotide and plasmid DNA delivery. *International journal of pharmaceutics* **2009**, *382* (1−2), 205−214.
(41) Luangtana-anan, M.; Opanasopit, P.; Ngawhirunpat, T.; Nunthanid, J.; Sriamornsak, P.; Limmatvapirat, S.; Lim, L. Y. Effect of chitosan salts and molecular weight on a nanoparticulate carrier for therapeutic protein. *Pharm. Dev. Technol.* **2005**, *10* (2), 189−196.
(42) Mohammadpour Dounighi, N.; Eskandari, R.; Avadi, M. R.; Zolfagharian, H.; Mir Mohammad Sadeghi, A.; Rezayat, M. Preparation and in vitro characterization of chitosan nanoparticles containing Mesobuthus eupeus scorpion venom as an antigen delivery system. *Journal of Venomous Animals and Toxins Including Tropical Diseases* **2012**, *18*, 44−52.
(43) Gan, Q.; Wang, T.; Cochrane, C.; McCarron, P. Modulation of surface charge, particle size and morphological properties of chitosan-TPP nanoparticles intended for gene delivery. *Colloids Surf., B* **2005**, *44* (2−3), 65−73.
(44) Souza, M. P.; Vaz, A. F.; Correia, M. T.; Cerqueira, M. A.; Vicente, A. A.; Carneiro-da-Cunha, M. G. Quercetin-loaded lecithin/chitosan nanoparticles for functional food applications. *Food and bioprocess technology* **2014**, *7*, 1149−1159.
(45) Cho, K.; Wang, X.; Nie, S.; Chen, Z.; Shin, D. M. Therapeutic nanoparticles for drug delivery in cancer. *Clinical cancer research* **2008**, *14* (5), 1310−1316.
(46) Keawchaoon, L.; Yoksan, R. Preparation, characterization and in vitro release study of carvacrol-loaded chitosan nanoparticles. *Colloids Surf., B* **2011**, *84* (1), 163−171.
(47) Ceruti, M.; Viola, F.; Balliano, G.; Milla, P.; Roma, G.; Grossi, G.; Rocco, F. Synthesis of (E)-and (Z)-29-methylidyne-2, 3-oxidosqualene derivatives as inhibitors of liver and yeast oxidosqualene cyclase. *Journal of the Chemical Society, Perkin Transactions 1* **2002**, No. 12, 1477−1486.
(48) Liu, G.; Gan, J.; Chen, A.; Liu, Q.; Zhao, X. Synthesis and characterization of an amphiphilic chitosan bearing octyl and methoxy polyethylene. *Nat. Sci.* **2010**, *2* (07), 707.
(49) Huang, Z.; Wang, H.; Gao, C.; Shen, H.; Fa, X. e. Drug loaded gold nano-particulates for therapeutics of myocardial infarction in rat model. *Journal of Biomaterials and Tissue Engineering* **2018**, *8* (2), 197−205.
(50) de Moura, M. R.; Aouada, F. A.; Mattoso, L. H. Preparation of chitosan nanoparticles using methacrylic acid. *J. Colloid Interface Sci.* **2008**, *321* (2), 477−483.
(51) Wedmore, I.; McManus, J. G.; Pusateri, A. E.; Holcomb, J. B. A special report on the chitosan-based hemostatic dressing: experience in current combat operations. *Journal of Trauma and Acute Care Surgery* **2006**, *60* (3), 655−658.
(52) Kim, J.-H.; Kim, Y.-S.; Park, K.; Lee, S.; Nam, H. Y.; Min, K. H.; Jo, H. G.; Park, J. H.; Choi, K.; Jeong, S. Y.; et al. Antitumor efficacy of cisplatin-loaded glycol chitosan nanoparticles in tumor-bearing mice. *J. Controlled Release* **2008**, *127* (1), 41−49.
(53) Xu, X.; Zhou, J.; Li, L.; Zhang, Y.; Huo, M.; Wang, X.; Lü, L. Preparation of doxorubicin-loaded chitosan polymeric micelle and study on its tissue biodistribution in mice. *Yao Xue Xue Bao* **2008**, *43* (7), 743−748.
(54) Kean, T.; Thanou, M. Biodegradation, biodistribution and toxicity of chitosan. *Advanced drug delivery reviews* **2010**, *62* (1), 3−11.
(55) Ghormade, V.; Deshpande, M. V.; Paknikar, K. M. Perspectives for nano-biotechnology enabled protection and nutrition of plants. *Biotechnology advances* **2011**, *29* (6), 792−803.
(56) Sato, T.; Ishii, T.; Okahata, Y. In vitro gene delivery mediated by chitosan. Effect of pH, serum, and molecular mass of chitosan on the transfection efficiency. *Biomaterials* **2001**, *22* (15), 2075−2080.
(57) Nguyen, J.; Szoka, F. C. Nucleic acid delivery: the missing pieces of the puzzle? *Accounts of chemical research* **2012**, *45* (7), 1153−1162.
(58) Ragelle, H.; Vandermeulen, G.; Préat, V. Chitosan-based siRNA delivery systems. *J. Controlled Release* **2013**, *172* (1), 207−218.
(59) Dash, M.; Chiellini, F.; Ottenbrite, R. M.; Chiellini, E. Chitosan—A versatile semi-synthetic polymer in biomedical applications. *Prog. Polym. Sci.* **2011**, *36* (8), 981−1014.
(60) Ying, X.-Y.; Cui, D.; Yu, L.; Du, Y.-Z. Solid lipid nanoparticles modified with chitosan oligosaccharides for the controlled release of doxorubicin. *Carbohydr. Polym.* **2011**, *84* (4), 1357−1364.
(61) Yue, Z.-G.; Wei, W.; Lv, P.-P.; Yue, H.; Wang, L.-Y.; Su, Z.-G.; Ma, G.-H. Surface charge affects cellular uptake and intracellular trafficking of chitosan-based nanoparticles. *Biomacromolecules* **2011**, *12* (7), 2440−2446.
(62) Gokce, E. H.; Sandri, G.; Bonferoni, M. C.; Rossi, S.; Ferrari, F.; Güneri, T.; Caramella, C. Cyclosporine A loaded SLNs: evaluation

https://doi.org/10.1021/acsomega.4c08258
ACS Omega XXXX, XXX, XXX−XXX

of cellular uptake and corneal cytotoxicity. *International journal of pharmaceutics* **2008**, *364* (1), 76−86.
(63) Nam, H. Y.; Kwon, S. M.; Chung, H.; Lee, S.-Y.; Kwon, S.-H.; Jeon, H.; Kim, Y.; Park, J. H.; Kim, J.; Her, S.; et al. Cellular uptake mechanism and intracellular fate of hydrophobically modified glycol chitosan nanoparticles. *J. Controlled Release* **2009**, *135* (3), 259−267.
(64) Trickler, W.; Nagvekar, A.; Dash, A. K. A novel nanoparticle formulation for sustained paclitaxel delivery. *AAPS PharmSciTech* **2008**, *9*, 486−493.
(65) Gao, X.; Gong, J.; Cai, Y.; Wang, J.; Wen, J.; Peng, L.; Ji, H.; Jiang, S.; Guo, D. Chitosan modified squalene nanostructured lipid carriers as a promising adjuvant for freeze-dried ovalbumin vaccine. *Int. J. Biol. Macromol.* **2021**, *188*, 855−862.
(66) Boisselier, E.; Astruc, D. Gold nanoparticles in nanomedicine: preparations, imaging, diagnostics, therapies and toxicity. *Chem. Soc. Rev.* **2009**, *38* (6), 1759−1782.
(67) Yue, H.; Wei, W.; Yue, Z.; Lv, P.; Wang, L.; Ma, G.; Su, Z. Particle size affects the cellular response in macrophages. *European journal of pharmaceutical sciences* **2010**, *41* (5), 650−657.
(68) Abuobeid, R.; Sánchez-Marco, J.; Felices, M. J.; Arnal, C.; Burillo, J. C.; Lasheras, R.; Busto, R.; Lasunción, M. A.; Rodríguez-Yoldi, M. J.; Martínez-Beamonte, R.; Osada, J. Squalene through Its Post-Squalene Metabolites Is a Modulator of Hepatic Transcriptome in Rabbits. *Int. J. Mol. Sci.* **2022**, *23* (8), 4172.
(69) Agnihotri, S. A.; Mallikarjuna, N. N.; Aminabhavi, T. M. Recent advances on chitosan-based micro-and nanoparticles in drug delivery. *Journal of controlled release* **2004**, *100* (1), 5−28.
(70) Janes, K. A.; Fresneau, M. P.; Marazuela, A.; Fabra, A.; Alonso, M. a. J. Chitosan nanoparticles as delivery systems for doxorubicin. *Journal of controlled Release* **2001**, *73* (2−3), 255−267.
(71) Singh, A.; Mittal, A.; Benjakul, S. Chitosan nanoparticles: Preparation, food applications and health benefits. *Sci. Asia* **2021**, *47* (2021), 1−10.
(72) Vllasaliu, D.; Exposito-Harris, R.; Heras, A.; Casettari, L.; Garnett, M.; Illum, L.; Stolnik, S. Tight junction modulation by chitosan nanoparticles: comparison with chitosan solution. *International journal of pharmaceutics* **2010**, *400* (1−2), 183−193.
(73) Panyam, J.; Sahoo, S. K.; Prabha, S.; Bargar, T.; Labhasetwar, V. Fluorescence and electron microscopy probes for cellular and tissue uptake of poly (D, L-lactide-co-glycolide) nanoparticles. *International journal of pharmaceutics* **2003**, *262* (1−2), 1−11.
(74) Sahoo, S. K.; Panyam, J.; Prabha, S.; Labhasetwar, V. Residual polyvinyl alcohol associated with poly (D, L-lactide-co-glycolide) nanoparticles affects their physical properties and cellular uptake. *Journal of controlled release* **2002**, *82* (1), 105−114.
(75) Panyam, J.; Zhou, W. Z.; Prabha, S.; Sahoo, S. K.; Labhasetwar, V. Rapid endo-lysosomal escape of poly (DL-lactide-coglycolide) nanoparticles: implications for drug and gene delivery. *FASEB J.* **2002**, *16* (10), 1217−1226.
(76) Silva, A. M.; Alvarado, H. L.; Abrego, G.; Martins-Gomes, C.; Garduño-Ramirez, M. L.; García, M. L.; Calpena, A. C.; Souto, E. B. In vitro cytotoxicity of oleanolic/ursolic acids-loaded in PLGA nanoparticles in different cell lines. *Pharmaceutics* **2019**, *11* (8), 362.
(77) Rakotoarisoa, M.; Angelov, B.; Garamus, V. M.; Angelova, A. Curcumin-and fish oil-loaded spongosome and cubosome nanoparticles with neuroprotective potential against H2O2-induced oxidative stress in differentiated human SH-SY5Y cells. *ACS omega* **2019**, *4* (2), 3061−3073.
(78) Rinaudo, M. Chitin and chitosan: Properties and applications. *Prog. Polym. Sci.* **2006**, *31* (7), 603−632.
(79) Chattopadhyay, D.; Inamdar, M. S. Aqueous behaviour of chitosan. *Int. J. Polym. Sci.* **2010**, *2010*, 1.
(80) Abuobeid, R.; Herrera-Marcos, L. V.; Arnal, C.; Bidooki, S. H.; Sánchez-Marco, J.; Lasheras, R.; Surra, J. C.; Rodríguez-Yoldi, M. J.; Martínez-Beamonte, R.; Osada, J. Differentially Expressed Genes in Response to a Squalene-Supplemented Diet Are Accurate Discriminants of Porcine Non-Alcoholic Steatohepatitis. *International Journal of Molecular Sciences* **2023**, *24* (16), 12552.
(81) Kohno, Y.; Egawa, Y.; Itoh, S.; Nagaoka, S.-i.; Takahashi, M.; Mukai, K. Kinetic study of quenching reaction of singlet oxygen and scavenging reaction of free radical by squalene in n-butanol. *Biochimica et Biophysica Acta (BBA)-Lipids and Lipid Metabolism* **1995**, *1256* (1), 52−56.
(82) Sánchez-Marco, J.; Bidooki, S. H.; Abuobeid, R.; Barranquero, C.; Herrero-Continente, T.; Arnal, C.; Martínez-Beamonte, R.; Lasheras, R.; Surra, J. C.; Navarro, M. A.; et al. Thioredoxin domain containing 5 is involved in the hepatic storage of squalene into lipid droplets in a sex-specific way. *J. Nutr. Biochem.* **2024**, *124*, 109503.
(83) Bidooki, S. H.; Sánchez-Marco, J.; Martínez-Beamonte, R.; Herrero-Continente, T.; Navarro, M. A.; Rodríguez-Yoldi, M. J.; Osada, J. Endoplasmic Reticulum Protein TXNDC5 Interacts with PRDX6 and HSPA9 to Regulate Glutathione Metabolism and Lipid Peroxidation in the Hepatic AML12 Cell Line. *International Journal of Molecular Sciences* **2023**, *24* (24), 17131.
(84) Cárdeno, A.; Aparicio-Soto, M.; Montserrat-de la Paz, S.; Bermúdez, B.; Muriana, F. J.; Alarcón-de-la-Lastra, C. Squalene targets pro-and anti-inflammatory mediators and pathways to modulate over-activation of neutrophils, monocytes and macrophages. *Journal of Functional Foods* **2015**, *14*, 779−790.
(85) Lee, S.-O.; Jin, U.-H.; Kang, J. H.; Kim, S. B.; Guthrie, A. S.; Sreevalsan, S.; Lee, J.-S.; Safe, S. The orphan nuclear receptor NR4A1 (Nur77) regulates oxidative and endoplasmic reticulum stress in pancreatic cancer cells. *Molecular Cancer Research* **2014**, *12* (4), 527−538.
(86) Gu, M.-X.; Fu, Y.; Sun, X.-L.; Ding, Y.-Z.; Li, C.-H.; Pang, W.; Pan, S.; Zhu, Y. Proteomic analysis of endothelial lipid rafts reveals a novel role of statins in antioxidation. *J. Proteome Res.* **2012**, *11* (4), 2365−2373.
(87) Duivenvoorden, W.; Hopmans, S. N.; Austin, R. C.; Pinthus, J. H. Endoplasmic reticulum protein ERp46 in prostate adenocarcinoma. *Oncology Letters* **2017**, *13* (5), 3624−3630.

https://doi.org/10.1021/acsomega.4c08258
ACS Omega XXXX, XXX, XXX−XXX

V. DISCUSSION

DISCUSSION

The present thesis employs a variety of methodologies to expand the understanding of the biological characteristics of minor components of EVOO, such as squalene, on hepatocytes. These findings led our research group to identify TXNDC5 as a novel protein–protein interaction partner of PRDX6 and HSPA9. The lack of interaction between TXNDC5 and PRDX6/HSPA9 in mouse hepatocytes may contribute to the impairment of the glutathione mechanism and lipid peroxidation, which in turn may contribute to the development of liver disease and its possible repercussions. However, the molecular mechanisms of TXNDC5 have not been extensively investigated, including its role in liver metabolism and ER stress. In this context, the study aimed at understanding how TXNDC5 protein interacts specifically through the three main ER-stress-activated signaling pathways: ATF6, EIF2AK3, and ERN1. Such an experimental setup afforded the necessary comprehensive understanding of TXNDC5 functional relevance to the maintenance of cellular homeostasis upon the development of ER stress. Among the extensive beneficial effects of the MD, as elucidated by the minor component of EVOO, squalene has been shown to enhance the metabolic characteristics of hepatocytes and to safeguard against oxidative and ER stress, malignancy, and inflammatory responses. Therefore, this thesis describes the protective function of PLGA and chitosan-based squalene nanoparticles in regard to oxidative and ER stress in mouse hepatocytes. To address these issues and gain a deeper insight into the mechanisms of cellular uptake underlying the potential role of squalene, the function of TXNDC5 and the primary ER molecular mechanisms in stressful conditions were investigated.

The first objective was to identify novel protein interactions involving TXNDC5 in the liver and to assess the impact of TXNDC5 deficiency on these interactions. This was addressed in the first manuscript of this thesis, entitled:

1. Endoplasmic Reticulum Protein TXNDC5 Interacts with PRDX6 and HSPA9 to Regulate Glutathione Metabolism and Lipid Peroxidation in the Hepatic AML12 Cell Line

The objective of this study was twofold: first, to uncover novel protein interactions involving TXNDC5 in the liver and second, to assess the effects of TXNDC5 deficiency on these interactions. Furthermore, we investigated the impact of these interactions on the activity of $iPLA_2$, glutathione (GSH), and lipid peroxidation, as well as the mRNA levels of key genes associated with HSPA9, PRDX6, and TXNDC5. TXNDC5 interacts with a wide array of proteins, playing essential roles in processes such as histone modification, DNA transcription, mRNA splicing, cell cycle regulation, signaling, mobility, metabolism, and protein degradation [161]. These interactions may contribute to the progression of diseases such as diabetes, neurological disorders, vitiligo, arthritis, and liver cancer [122,271]. For example, TXNDC5's

interactions with proteins such as NENF, PPP1R2, ALDOC, LDH, and PGD may elucidate its role in diabetes. Additionally, its dysregulation may affect the cell cycle via interactions with CDK5, histones, or transcription factors like ATF2 and ZNHIT2, which are linked to carcinogenesis [272,273]. Moreover, hepatic fat appears to regulate TXNDC5, particularly in the context of ER stress and its role in apolipoprotein B (APOB) regulation, which contributes to the development of steatosis [46].

The results of the co-immunoprecipitation (co-IP) and mass spectrometry experiments identified HSPA9 and PRDX6 as novel TXNDC5-interacting proteins in the AML12 cell line (Figure 1, Manuscript 1). HSPA9, a member of the heat shock protein 70 family and a ubiquitous molecular chaperone in mammalian cells, has been linked to a variety of biological processes, including protein folding, the assembly of multi-protein complexes, protein trafficking, stress responses, mitochondrial biogenesis, and differentiation [274–276]. A number of malignancies, including leukemia, brain cancer, colorectal adenocarcinoma, and hepatocellular carcinoma, have been associated with elevated levels of *Hspa9* expression [277–280]. Increased HSPA9 expression has been linked to metastasis and early tumor recurrence in liver cancer. Furthermore, evidence indicates that overexpression of *Hspa9* is sufficient to render breast cancer cells more aggressive. These findings suggest that HSPA9 may represent a promising target for cancer therapy. Additionally, numerous studies have established a correlation between elevated TXNDC5 expression and cancer [280,281]. There is a possibility that this may be linked to HSPA9. As illustrated in Figures 2A–C, Manuscript 1, TXNDC5 inactivation has been demonstrated to reduce the expression of HSPA9 mRNA and protein levels, thereby inducing cell growth arrest and enhancing cell apoptosis. These findings are analogous to those of the RNA interference-based selective knockdown of *Hspa9* expression [282].

The reduction of a variety of cellular peroxides is catalyzed by the peroxiredoxin family of proteins, which represent an evolutionarily conserved group of antioxidants that protect cells from oxidative damage [283,284]. The peroxiredoxin family of proteins has been linked to a number of biological activities, including the oxidative stress response, cell proliferation, and differentiation [285]. PRDX6 is capable of reducing H_2O_2 and a number of phospholipid peroxides in the cytosol. It is highly expressed in several organs, including the liver, lung, and keratinocytes [283–286]. The current study demonstrates that TXNDC5 deficiency does not influence the mRNA level of *Prdx6* in the AML12 cell line, although it induces a notable reduction in the protein level (Figure 3C–E, Manuscript 1). In pathological situations, there is evidence that *Prdx6* differential expression may be impacted. Recent studies have indicated that *Prdx6* mRNA levels decrease upon serum deprivation, and that keratinocyte growth factor is a strong inducer of *Prdx6* expression in both liver cells and keratinocytes. The results demonstrated that H_2O_2 enhanced the expression of *Prdx6* in mouse liver cells. The ubiquitin/proteasome system (UPS) plays a pivotal role in regulating fundamental biological processes such as cell growth, proliferation, the cell cycle, and apoptosis [287]. Dysregulation of these processes can lead to malignant transformation. Given that numerous cancer cells, including those of the colon and breast, exhibit a defective UPS and elevated proteasome activity, the inhibition of proteasomes in tumor cells has been demonstrated to facilitate the

accumulation of inhibitors of cyclin-dependent kinases, pro-apoptotic proteins, and tumor suppressor proteins, ultimately leading to cell cycle arrest and apoptosis [288–290]. To ascertain whether TXNDC5 could interact with the proteasome and thereby inhibit PRDX6 protein expression, we used a proteasome inhibitor, MG-132, in the WT and KO AML12 cell lines. However, the results did not reveal any significant effect on PRDX6 protein expression in the cells, indicating that the proteasome is not the cellular target of these complexes (Figure 2F, Manuscript 1).

Recent research has demonstrated that increased *Prdx6* expression can protect lung cells from oxidative stress-induced membrane lipid peroxidation and apoptosis in transfected cells and adenovirus-mediated transfer in mice [291,292]. Conversely, *Prdx6* antisense suppression has been shown to increase oxidative stress susceptibility and cell death. However, our findings demonstrate a notable reduction in lipid peroxidation in the AML12 cell line following the absence of TXNDC5 and a decline in PRDX6 protein levels (Figure 3A, Manuscript 1). In addition to its role in lipid peroxidation, PRDX6 has been demonstrated to possess glutathione peroxidase and phospholipase A_2 activities, which are increased concomitantly with *Prdx6* expression. Accordingly, this protein plays a significant role in membrane phospholipid metabolism [293,294]. As illustrated in Figure 3B–D, Manuscript 1, the present study confirmed that the GSH and $iPLA_2$ activities were reduced in the AML12 knockout cells. This finding is consistent with the results of PRDX6 knockdown in A549, NCI-H460, and H1299 cell lines via siRNA, in which a reduction in the $iPLA_2$ and glutathione peroxidase activities was observed [294,295].

To evaluate the influence of *Txndc5 in vivo*, RNA sequencing was previously conducted. However, to ascertain its impact *in vitro*, a next-generation transcriptomic assay was performed [184]. Following the analysis of RNAseq data from both normal and TXNDC5-deficient AML12 cell lines, the data were summarized based on the liver transcripts using the aforementioned databases (Figure 4D, Manuscript 1). The impact of TXNDC5 on hepatic transcripts associated with HSPA9 was examined in the AML12 cell line. From the data presented in Table 1, Manuscript 1, the transcripts *Dnaja3*, *Hsp90aa1*, *Mfn2*, and *Rps14* were selected for further analysis. The results demonstrate that there is an elevated *in vitro* expression of *Dnaja3*. The J-protein *Dnaja3* is responsible for attracting substrates to *Hspa9* and is linked to the non-mitochondrial import functions of *Hspa9 [296]*. In two IL-7 responsive B-cell lines (human 697 pre-B and mouse mIL-7R expressing Ba/F3 cells), overexpression of *Dnaja3* has been demonstrated to inhibit Stat5 phosphorylation and cell proliferation. A reduction in the abundance of *Hspa9* may result in an increase in the amount of *Dnaja3* in hematopoietic and mouse β-cell lines. However, it should be noted that *Hspa9* and *Dnaja3* have also been established as regulators of p53 via a similar mechanism [297,298]. However, in liver cells, the absence of TXNDC5 has been shown to result in a reduction in both *Hspa9* and *Dnaja3*. It has been demonstrated that the level of *Hsp90* expression in cancerous tissues, with particular relevance to hepatocellular carcinoma, is associated with a poorer prognosis and less favorable therapeutic outcomes [299,300]. Hsp90's anti-proliferative effects on cancer cells are largely mediated by the degradation of client proteins, including AKT and P53, which ultimately induce cancer cell apoptosis. The combined inhibition of *Hsp90* and *Hspa9* was

found to markedly diminish tumor growth in a liver cancer xenograft model. Additionally, the *Hsp90* inhibitor was observed to enhance the expression of *Hspa9 [300,301]*. The present study indicates that *Hsp90aa1* is downregulated in the absence of TXNDC5, and that *Hspa9* is also downregulated. These findings are consistent with previous studies conducted in the liver. It is hypothesized that contact points between the ER and mitochondria (referred to as MAMs) in the liver may serve as important nodes for the control of lipid metabolism. However, ER stress was directly associated with altered triglyceride metabolism after *Hspa9* or *Mfn2* overexpression in Huh7 cells, underscoring the significance of the two key partners in maintaining MAM integrity and activity [128,302]. Nevertheless, *Mfn2* overexpression has been observed *in vitro* when *Hspa9* expression is reduced and TXNDC5 is deleted. The deletion of HSPA9 has been demonstrated to result in an increase in reactive oxygen species formation in other biological systems. Consequently, cellular stress is induced by the deletion of RPS14, a gene that is frequently lost alongside HSPA9 on 5q-deletion as a result of ribosomal insufficiency and P53 activation [297]. It is postulated that haploinsufficiency of deleted genes, such as RPS14 and HSPA9, may play a role in bone marrow failure and inadequate hematopoiesis in hematopoietic cells by activating wild-type TP53 and inducing apoptosis [303]. Nevertheless, deletion of TXNDC5 has been observed to induce mRNA activation failure of *Hspa9* and *Rps14* in hepatic cells (Figure 4E, Manuscript 1).

As illustrated in Figure 4F, Manuscript 1, the downregulation of TXNDC5 resulted in a reduction in the protein level of PRDX6 in the AML12 cell line. This may potentially influence the expression of numerous hepatic genes that are associated with PRDX6 (Table 2, Manuscript 1). In the AML12 KO cells, the expression of several genes involved in glutathione metabolism, including *Oplah*, *Gstm6*, *Gstt1*, and *Gstp3*, was found to be decreased [304]. It is established that glutathione synthase deficiency results in oxidative damage to the red blood cell membrane. Furthermore, another known metabolic defect of the gamma-glutamyl cycle affects an ATP-hydrolyzing enzyme (5-oxo-L-prolinase) encoded by the *OPLAH* gene [305]. Furthermore, under conditions of oxidative stress, the expression of *Gstm6*, *Gstt1*, and *Gstp3* is decreased in glial cells of the retina, liver, and hepatocytes of rats, respectively [306–308]. The results demonstrated that *Prdx5* was upregulated in AML12 cells in the absence of TXNDC5, whereas *Prdx5* was downregulated in PRDX6 knockout HepG2 cells [309]. It has recently been demonstrated that *Npm1*, a DNA/RNA chaperone, stimulates *Prdx6* expression and that *Npm1* gene knockdown suppresses *Prdx6* expression. Conversely, an increase in the *Npm1* level has been shown to result in an increase in the *Prdx6* level. Moreover, they are implicated in the ROS-P53 pathway, and their downregulation has been demonstrated to enhance the expression level of phosphorylated p53 and ROS content in HepG2 cells [293,310]. Therefore, our findings corroborate the observed reduction in *Npm1* levels in AML12 cells concomitant with a decline in PRDX6 protein expression. Finally, the mRNA patterns of the predominantly liver-produced *Serpina1a*, *Serpina1b*, and *Serpina3m* demonstrated a significant reduction in expression *in vitro* when TXNDC5 was absent. Proteins associated with inflammation, such as the SERPINA1 family and TXNDC5, exhibit differential positive alterations in cutaneous squamous cell carcinoma and hepatocytes [186,311]. While the *Serpina3m* transcript levels exhibited a marked decline in liver cells, adenomas, and carcinomas, they demonstrated a tendency to decrease in non-neoplastic liver

cells. Serpin peptidase inhibitor, clade A (alpha-1 antiproteinase, antitrypsin) is the *Serpina3m* gene product that inhibits neutrophil elastase. Given its capacity to damage tissue, it has been proposed that elevated neutrophil elastase activity may contribute to the development of carcinogenic responses [312,313]. These findings suggest that the TXNDC5 and PRDX6 complex, as observed in the current study, may be associated with the reduced neutrophil elastase activity resulting from *Serpina3m* deficiency. In line with these results, it is possible that TXNDC5 and its role in protein folding and the SERPINA family may interact with PRDX6 in the liver through an as yet unknown mechanism. A comprehensive summary of the findings is presented in Figure 22.

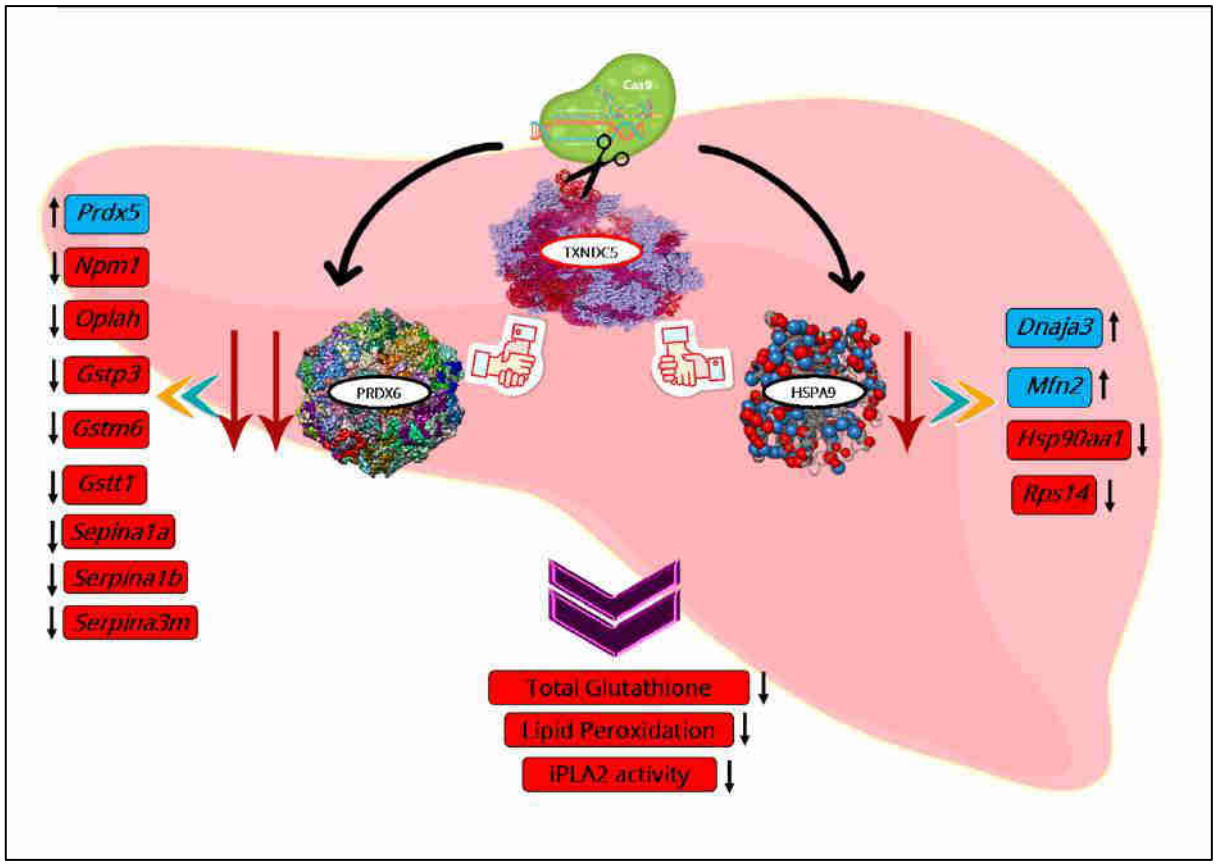

Figure 22. A synopsis of the findings that were obtained in this objective.

The second objective, which was to determine the influence of TXNDC5 on the gene and protein expressions associated with the ER stress pathways, was addressed in the second manuscript of this thesis, entitled:

2. TXNDC5 Plays a Crucial Role in Regulating Endoplasmic Reticulum Activity through Different ER Stress Signaling Pathways in Hepatic Cells

This work aimed to elucidate the impact of TXNDC5 on gene and protein expressions pertaining to ER stress pathways. The results demonstrated that TXNDC5 deficiency resulted in a reduction in *Ern1*, *Xbp1*, *Eif2ak3*, and *Sec61a1* expression and an increase in *Hspa5*, *Atf4*, and *Ddit3* expression. No change was observed in *Atf6* and *Ssr2* expression. At the protein level, the absence of TXNDC5 was associated with a reduction in ERN1 and EIF2AK3 expression, while the HSPA5 protein was upregulated. However, no change was observed in the ATF6 protein. The absence of TXNDC5 did not affect the pattern of mortality induced by the three known ER stressors, tunicamycin, palmitic acid, and thapsigargin, in the AML12 cell line. This was despite the observed enhancement of cellular ROS levels in TXNDC5-deficient cells. It is evident that TXNDC5 is the sole factor responsible for maintaining mitochondrial ROS levels during tunicamycin-induced ER stress. The application of these three agents resulted in increased *Atf6, Hspa5, Atf4, Ddit3, Ern1*, and *Sec61a1* expressions in WT AML12 cells, with the exception of a lack of induction of *Eif2ak3*, *Xbp1*, and *Ssr2* in the presence of palmitic acid, thapsigargin, and tunicamycin, respectively. A more complex outcome was observed in cells lacking TXNDC5. In this context, while ATF6, HSPA5, and EIF2AK3 exhibited no evidence of expression induction in the presence of palmitic acid and tunicamycin, ERN1 demonstrated such induction. The expression patterns of *Xbp1* and *Ssr2* were found to be analogous to those observed in WT cells. However, in the presence of thapsigargin, the absence of TXNDC5 facilitated the splicing of *Xbp1*. However, the expression of *Sec61a1* was disrupted by the absence of TXNDC5 in the presence of tunicamycin. In conclusion, TXNDC5 appears to regulate the activity of the ER, particularly affecting the induction of ATF6 and HSPA5 genes in response to palmitic acid, while also influencing the signaling cascade of EIF2AK3.

Prior research has established a connection between TXNDC5 and a multitude of cellular processes as an ER molecular chaperone [161]. As demonstrated in Table 1, Manuscript 2, TXNDC5 deficiency has been linked to a decrease in the expression of ERN1, EIF2AK3, *Xbp1*, and *Sec61a1*, while there has been an increase in the expression of HSPA5, *Atf4*, and *Ddit3*. Other studies have also demonstrated a correlation between TXNDC5 and these proteins. In this context, the fragmentation of the ER and the altered expression of numerous ER proteins, including ATF6, HSPA5, ATF4, and CCAAT/enhancer-binding protein homologous protein, are caused by the downregulation of TXNDC5 in pancreatic β-cells. Furthermore, reduced TXNDC5 levels have been linked to elevated expression of HSPA5, *Ddit3*, and *eIF2a*, which collectively contribute to ER stress and an increase in misfolded proteins in pancreatic β-cells [314,315]. In conclusion, TXNDC5 can activate ER stress cascades via HSPA5, either directly or indirectly.

In this report, three stressors have been utilized. Tunicamycin, which acts as an inhibitor of GlcNAc phosphotransferase, has been demonstrated to induce a significant accumulation of unfolded proteins, activate the UPR, increase *Txndc5* expression levels, and ultimately result in apoptosis of human head and neck carcinoma cells [149]. Palmitic acid is a saturated fatty acid that has been demonstrated to induce ER stress and elevate UPR levels in well-differentiated hepatocyte cell lines [316]. Thapsigargin, an inhibitor of Ca^{2+} ATPase, has been demonstrated to alter the concentration of Ca^{2+} within the ER lumen of mouse hepatocytes [317]. In the present study, all of the agents demonstrated a dose-dependent mortality in AML12 cells (Figure 1, Manuscript 2) and promoted TXNDC5 expression (Figure 4, Manuscript 2). The overexpression of *Txndc5* has been observed in various studies to occur in laryngeal squamous carcinoma cells, colorectal cancer cells, and liver and kidney cells under circumstances of ER stress. In consideration of the aforementioned observations, it can be postulated that TXNDC5 plays a role in the ER stress response induced by these agents, potentially acting as a protective factor. However, the absence of TXNDC5 did not result in any alterations to the survival patterns, in stark contrast with other agents such as H_2O_2 [187,318–320]. Therefore, the absence of TXNDC5 is insufficient to alter cell survival in response to these ER stressors.

Our findings indicate that the deficiency of TXNDC5 can markedly induce cellular ROS in hepatocytes, as illustrated in Figure 2, Manuscript 2. These findings corroborate those of previous studies which demonstrated an enhancement of ROS in the absence of TXNDC5 in endometrial, ovarian, and colorectal tissues. The silencing of NR4A1 in endometrial cancer cells has been shown to result in a significant increase in ROS levels, which can be attributed to a reduction in TXNDC5 and IDH1 expression levels. This is corroborated by a notable elevation in ROS and oxidative/ER stress following TXNDC5 silencing [122]. The ER maintains dynamic contact with mitochondria, which are collectively referred to as mitochondria–ER contacts. This contact plays an essential role in regulating mitochondrial function. For instance, calcium transfer at these sites may lead to mitochondrial calcium overload, which can subsequently induce apoptosis. Mitochondrial malfunction and disruption of protein translocation, translation, and folding within this organelle can result in the phenomenon of "mitochondrial stress." ER stress and mitochondrial stress initiate a shared downstream signaling pathway involving the phosphorylation of eIF2α, which represses global translation [321]. The results demonstrated that the absence of TXNDC5 was unable to induce mitochondrial ROS in hepatocytes, thus indicating that this process is TXNDC5-dependent. Nevertheless, these findings are not consistent with regard to the role of ER stress. All ER stressors resulted in a reduction of the mitochondrial membrane potential in TXNDC5-KO cells. In cells lacking TXNDC5, tunicamycin caused a reduction in mitochondrial membrane potential (Figure 3, Manuscript 2). In contrast, the presence of the chemical did not have this effect on WT cells. In this context, our previous findings indicate that TXNDC5 directly interacts with HSPA9 as a mitochondrial chaperone protein involved in protein folding and transport. The downregulation of HSPA9 in hepatocytes following the knockdown of TXNDC5 suggests that this protein may play a significant role in protecting mitochondria against tunicamycin [45].

The lack of TXNDC5 had no impact on the expression of ATF6 in the presence of tunicamycin and thapsigargin (Figure 5A, Manuscript 2). Conversely, it effectively attenuated the induction observed in response to palmitic acid. Prior research has identified a distinctive positive feedback loop comprising the TGF1–ATF6–TXNDC5–TGFBR1 signaling axis in kidney, heart, and lung fibroblasts. The loop begins with TGF1, which causes the induction of TXNDC5 through ER stress and ATF6-mediated transcriptional control. Our findings indicate that TXNDC5 may play a role in certain circumstances [125,175,176,322]. Two ER stressors, tunicamycin and thapsigargin, do not appear to influence ATF6 levels, whereas palmitic acid appears to require TXNDC5 to induce this ATF6 effect (Figure 9, Manuscript 2).

The detachment of the chaperone HSPA5 from the luminal region of the ER integral membrane proteins EIF2AK3, ERN1, and ATF6 represents a pivotal step in the induction of ER stress in human leukemia and bladder carcinoma cell lines [323]. Lee et al. demonstrated that the orphan nuclear receptor 4A1 (NR4A1) is closely associated with *Txndc5*-induced transcriptional activity. Furthermore, they showed that ER fragmentation and altered expression of *Hspa5* are outcomes of *Txndc5* downregulation in pancreatic malignant cells. The data acquired from the hepatic AML12 cell line demonstrate that the expression of HSPA5 is modified by the absence of TXNDC5 (see Table 1, Manuscript 2). Furthermore, our results demonstrate that, in the absence of TXNDC5, ER stressors modify the protein level of HSPA5, with the exception of palmitic acid as a saturated fatty acid (Figure 5B, Manuscript 2). This observation provides compelling evidence that HSPA5 may be a key regulator of lipid metabolism, in addition to TXNDC5 [188]. Indeed, our findings revealed elevated protein and mRNA levels of HSPA5, something observed in the group of rats fed a high-fat diet, which lends further support to this notion [271]. Moreover, obese mice demonstrated elevated hepatic levels of *Hspa5* mRNA in response to ATF6 and EIF2AK3 activation. In contrast, the overexpression of *Hspa5* in hepatocytes has been observed to reduce indicators of ER stress, inhibit the cleavage of SREBP1c, and suppress the transcription of SREBP1c and SREBP2 target genes. This has been shown to result in a significant reduction in hepatic cholesterol levels [324]. Moreover, the activation of JNK, which serves as a central mediator of palmitic acid-induced hepatic lipoapoptosis, has been observed to result in the suppression of *Hspa5* in this cell line. This saturated fatty acid has been demonstrated to induce lipotoxicity and insulin resistance in both mouse and human hepatocytes [147,325]. Additionally, our previous findings indicate that TXNDC5 plays a direct role in regulating PRDX6. The absence of TXNDC5 has been shown to result in the downregulation of PRDX6. Thus, the findings of the present study provide further evidence supporting the hypothesis that TXNDC5 is linked to the HSPA5 response to palmitic acid, and it is possible that PRDX6 plays a part in this pathway through a protein depalmitoylation process [45,326].

The influence of TXNDC5 depletion on the EIF2AK3 cascade, previously designated as PERK, was also investigated. In the wild-type cell line, the mRNA expression levels of ER stress-related markers, including *Eif2ak3*, *Atf4*, and *Ddit3*, were observed to increase in response to various ER stressors. The protein expression of EIF2AK3 displayed a divergent pattern in tunicamycin and palmitic acid exposure, suggesting that these stressors are involved in post-transcriptional regulation. Nevertheless, TXNDC5-deficient AML12 hepatocytes

demonstrated a disruption in EIF2AK3 expression when subjected to tunicamycin and palmitic acid (Figure 6A, Manuscript 2). Negative feedback loops intrinsic to the UPR lead to a rapid downregulation of EIF2AK3-EIF2α signaling in CHO cells, largely due to the upregulation of *Ddit3* and its downstream targets [129]. Moreover, the diminution of EIF2AK3-EIF2α signaling has been evidenced to precipitate the emergence of diabetes phenotypes in murine models of EIF2AK3 deficiency [327]. Conversely, the disruption of the EIF2AK3 pathway has been observed to result in the enhanced production of ROS during ER stress in mouse fibroblasts [328]. The expression levels of *Eif2ak3* and *Txndc5* in NIH-3T3 fibroblasts demonstrated a gradual increase over time under stressful conditions, indicating the presence of a coordinated regulatory mechanism [125]. Conversely, thapsigargin was observed to facilitate the phosphorylation of EIF2AK3, which was significantly diminished by the overexpression of *Hspa5* in the context of hepatic steatosis in mice [317]. In contrast to the aforementioned observations, thapsigargin proved to be an exception in our experimental setting. Notably, the presence of this compound led to a notable stimulation of EIF2AK3 expression, even in the absence of TXNDC5. These findings suggest that TXNDC5 may serve as a critical factor in the induction of EIF2AK3 in hepatocytes under specific stressful conditions (as illustrated in Figure 10, Manuscript 2).

The absence of TXNDC5 had no discernible impact on the expression of *Atf4* and *Ddit3* in AML12 cells subjected to ER stress, as evidenced by the data presented in Figures 6B and 6C, Manuscript 2. The results of recently conducted studies indicate that the expression patterns of *Atf4*, *Ddit3*, and apoptosis, induced by silencing of NR4A1; a modulator of TXNDC5, regulate ER stress in a number of cellular lines, including MCF-7, RKO, MDA-MB-231, and Jurkat. Deletion of DDIT3 has been observed to partially protect both cells and animals from ER stress-induced cell death; this is in contrast to the effects observed with overexpression of *Ddit3*, which in the absence of other stimuli has been demonstrated to trigger cell death [329]. DDIT3 has been linked to the overexpression of death receptor 5 (DR5) and the downregulation of the anti-apoptotic protein BCL2 [330,331]. Conversely, DNA damage-inducible 34 protein (GADD34) has recently been identified in mouse fibroblasts as a target of DDIT3. Therefore, the deletion of either DDIT3 or GADD34 protects cells against acute ER stress-induced cell death [332]. Furthermore, the absence of TXNDC5 does not appear to suppress *Atf4* and *Ddit3* expression in AML12 cells under ER stress, indicating that these cells may undergo apoptosis. Additionally, our findings suggest that TXNDC5 is not directly involved in the upregulation of *Atf4* and *Ddit3* expression in hepatocytes under ER stress conditions.

A reduction in one of the three ER stress markers commonly leads to the activation of other ER stress markers in secretory goblet cells [333]. The EIF2AK3 and ERN1 pathways have been demonstrated to regulate ER chaperones, ER-associated degradation, and other protective activities in a range of cell types, including mouse embryonic cells, NIH-3T3 fibroblasts, human embryonic kidney 293 cells, and Phoenix-Eco cells [131,334,335]. Additionally, Tsuchiya et al. observed an increase in Eif2ak3 expression in MIN6 cells lacking ERN1 protein [123]. It can therefore be surmised from the evidence that disruptions to EIF2AK3 in TXNDC5-deficient AML12 cells may result in increased ER stress and the consequent activation of other ER stress sensors (Figure 10, Manuscript 2), such as ERN1.

Indeed, hepatocyte expression patterns demonstrated that the expression of ERN1 may be enhanced in the presence of ER stress when the expression of EIF2AK3 is disrupted in the absence of TXNDC5, as compared to the WT cells (Figures 6A and 7A, Manuscript 2). It may be proposed that TXNDC5 exerts a dynamic role in the protection of the ER from stress in the EIF2AK3 and ERN1 pathways in mouse hepatocytes, which is independent of the pro-apoptotic Bax (BCL2-associated X protein) and Bak (BCL2 antagonist of cell death) proteins [336]. These have the potential to enhance ERN1 signaling. This could provide an explanation for why, in spite of the observed increase in ERN1 expression and EIF2AK3 disturbance, no changes in cell mortality were observed in TXNDC5-deficient hepatocytes.

The endoribonuclease ERN1 acts on *Xbp1* mRNA as a substrate, cleaving a 26-base intron [134]. Evidence has emerged indicating that mice lacking ERN1 and XBP1 display embryonic abnormalities in liver development and B lymphocyte differentiation [337,338]. The evidence suggests a link between the ERN1–XBP-1 signaling pathway and TXNDC5, as demonstrated by observations indicating that pharmacological inhibition of ERN1 and knockdown of XBP1 result in reduced TXNDC5 expression in pulmonary fibroblasts [125]. However, the present study in mouse hepatocytes indicates that the absence of TXNDC5 is associated with a reduction in *Xbp1* expression compared to the WT cells (Figure 7B, Manuscript 2). Furthermore, it was observed that the absence or presence of TXNDC5 did not result in the induction of *Xbp1* by palmitic acid and thapsigargin.

Chen et al. put forth the hypothesis that ERN1 may regulate TXNDC5 through *Xbp1* mRNA splicing in lung fibroblasts [125,339], and that it plays a role in MASLD, in which DDIT3, caspase-12, and JNK participate in ER stress by enhancing its activities [339]. In contrast, autophosphorylation of ERN1 may activate downstream genes without causing *Xbp1* mRNA splicing, indicating that ERN1 can exist in a state other than "on" or "off" in mouse embryonic fibroblasts and human pancreatic beta cells [340,341]. It has been postulated that XBP1 may interact with TXNDC5 indirectly, by binding to the regulatory regions of downstream target genes. This has been observed in C2C12 myoblasts and MIN6 cells, where XBP1 has been seen to interact with HSPA5. This interaction may serve to modulate *Txndc5* expression [342]. The present study demonstrates that thapsigargin is an effective agent for converting *Xbp1* from its unspliced form to the spliced variant. Moreover, TXNDC5 deficiency has been observed to result in an increased prevalence of the latter form in AML12 cells (Figure 7C, D, Manuscript 2). To conclude, the lack of TXNDC5 in hepatocytes modulates *Xbp1* splicing following thapsigargin exposure in the ERN1 cascade, suggesting a potential role for TXNDC5 and its mRNA expression in this specific splicing pathway. It is plausible that ERN1 influences *Xbp1* splicing not solely at the transcriptional level.

ERN1 and XBP1 have been observed to target the translocon and translocon auxiliary components in mouse embryonic fibroblasts and HEK293T cells [131,133]. Studies conducted on HeLa and Cos-7 cells have demonstrated that XBP1 splicing is optimized when ERN1 interacts with the translocons and SRP facilitates the recruitment of unspliced XBP1 (XBP1u) to the ER [343]. This indicates that ERN1 may function in a physical association with the translocons, in contrast to the observed behavior of ATF6 or EIF2AK3. SEC61A1, which

encodes an ER protein–translocation channel, and SSR2, a translocon auxiliary protein, are involved in the targeting of proteins to the ER via the SRP pathway. Moreover, the repression of the SEC61A1 translocon subunits appeared to exclusively and specifically activate the ERN1 branch, while also upregulating the SSR2 in human embryonic kidney cells and mouse embryonic fibroblasts [126,344]. As illustrated in Figure 8A, Manuscript 2, the present report indicates that *Ssr2* expression was not significantly induced by ER stress in TXNDC5 knockout cells. This is in contrast to the findings observed in WT cells, where *Ssr2* was induced by palmitic acid alone. Conversely, the expression of *Sec61a1* was augmented in WT cells via all ER stressors, however no alterations in tunicamycin exposure were exhibited by TXNDC5-KO cells (Figure 8B, Manuscript 2). This observation is consistent with previous findings that *Sec61a1* expression is uniquely regulated by the ERN1 cascade. Furthermore, it is possible that translocons may be regulated by other mediators, such as DDIT3 and HSPA5. The downregulation of SEC61A1 and SEC61B has been observed to stimulate *Ddit3* expression in myelogenous leukemia cells [130,344,345]. However, DDIT3 was found to be upregulated in SEC61A1-induced HeLa cells, which is consistent with the findings presented here. Furthermore, *Txndc5*, *Sec61a1*, and *Ssr2* are observed to be upregulated in XBP-1-transduced NIH-3T3 fibroblasts and murine macrophage cells. However, an alternative study demonstrated that in the presence of sertraline, an anti-stress drug, the mRNA level of *Txndc5* was reduced, while *Ssr2* and *Ern1* were increased in HepG2 cells [133,346]. It seems reasonable to conclude that the regulation of translocons by DDIT3 and HSPA5 is dependent on the specific tissue under consideration. These findings suggest a feedback mechanism whereby TXNDC5 can regulate translocon expression by modulating the expression of the ERN1 cascade via the XBP1 mediator in conditions of ER stress [126,133,347]. Moreover, ERN1 may be employed to assess the status of the translocon in mouse hepatocytes. Additionally, the expression of *Ssr2* and *Sec61α1* ER protein–translocon channels is subject to selective influence by the absence of TXNDC5, with the extent of influence contingent upon the source of ER stress. A summary of the findings is provided in Figure 23.

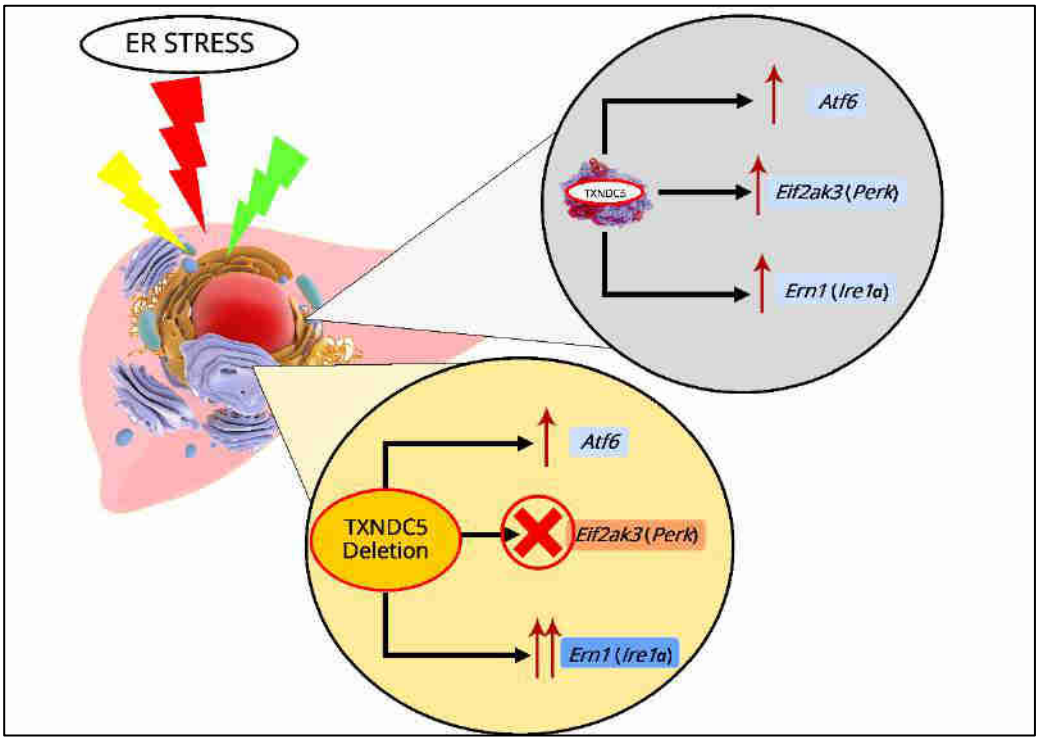

Figure 23. A synopsis of the findings that were obtained in this objective.

The third objective, which sought to elucidate the influence of squalene loaded into PLGA nanoparticles on oxidative and ER stress in a mouse hepatic cell line, was addressed in the third manuscript of this thesis, entitled:

3. Squalene Loaded Nanoparticles Effectively Protect Hepatic AML12 Cell Lines against Oxidative and Endoplasmic Reticulum Stress in a TXNDC5-Dependent Way

The objective of this study was to substantiate the impact of squalene, the primary component of the unsaponifiable fraction in virgin olive oil, encapsulated in PLGA nanoparticles (PLGA NPs), on oxidative and ER stress in a mouse hepatic cell line. Moreover, an investigation has been conducted to ascertain whether TXNDC5 putative molecular pathways are dependent or independent of those involved in hepatic stress. In this context, PLGA, a naturally derived and biodegradable polymer, is being investigated for its potential to facilitate the transport of compounds with therapeutic relevance. Squalene is a naturally occurring cholesterol precursor that forms stable colloidal phases in water [348]. It is also a carrier of many substances, and considering the biological action of squalene, the effect could be a sum of actions [349]. Our findings demonstrated that squalene was successfully encapsulated in PLGA NPs, resulting in stable NPs. The synthesis of squalene/PLGA NPs using the single-emulsion solvent evaporation method is a straightforward preparation procedure that could facilitate their successful clinical translation.

A substantial body of evidence, derived from microscopic observations of PLGA NPs encapsulating fluorescent probes and/or the measurement of the probe's intracellular levels, indicates that PLGA NPs are rapidly and efficiently taken up by cells [350,351]. The assessment of squalene content in our study demonstrated that PLGA nanoparticles possess a remarkable capacity to transfer squalene as a nanocarrier in mouse hepatocytes (Figure 3, Manuscript 3). As has been demonstrated in a number of studies, PLGA nanoparticles are highly effective nanocarriers for the encapsulation and delivery of a range of anti-cancer agents, including oleanolic and ursolic acids, in three different cell lines: the human hepatoma cell line (HepG2), the human epithelial colorectal adenocarcinoma cell line (Caco-2), and the human retinoblastoma cell line (Y-79) [261,352]. Additionally, PLGA nanoparticles have been utilized for the encapsulation of several pharmaceuticals, such as haloperidol and estradiol. For instance, PLGA-based curcumin nanoparticles have demonstrated an entrapment efficiency range of 77 to 85% [353].

Intracellular ROS production is essential for the normal functioning of cells and the maintenance of physiological processes. However, when the production of ROS exceeds the intrinsic antioxidant capacity of cells, oxidative stress occurs, leading to significant damage to cellular macromolecules [354]. The antioxidant properties of squalene are closely associated with its distinctive triterpene structure, which enables it to effectively scavenge detrimental free radicals [355]. The protective effects of squalene against oxidative destruction have been previously documented in rodent models. In cell culture assays, squalene can protect a number of different cell types, including murine macrophages, Chinese hamster pulmonary fibroblasts (V79 cells), human monocytes, and mammary epithelial cells (MCF10A), from damage caused

by hydrogen peroxide [356–359]. This occurs in a dose-dependent manner, with the antioxidant effect of squalene increasing with higher doses. Furthermore, our findings indicate that squalene can also reduce the level of ROS produced in mouse hepatic cells. The objective of the subsequent investigation was to ascertain whether TXNDC5 deletion contributes to squalene protection against oxidative stress. ROS influence ER homeostasis and protein folding directly or indirectly, causing ER stress and potentially leading to cell death in cases of extreme ER stress [360,361]. TXNDC5 appears to be involved in the formation of ROS and ER stress, as evidenced by an accumulating body of data. It has previously been demonstrated that inhibiting TXNDC5 expression via knockdown induces ROS and ER stress in pancreatic cancer cells. Conversely, increasing TXNDC5 expression in lipid endothelial cells effectively reduces ROS production and protects cells [362,363]. The results of the present study demonstrate that in AML12 cells, as illustrated in Figure 4A, Manuscript 3, there was an inverse and statistically significant difference between ROS content and TXNDC5 in response to squalene exposure. Specifically, in the absence of TXNDC5, ROS levels were elevated, while in WT samples, ROS levels were decreased. Upon exposure to an oxidative stimulus (Figure 4B, Manuscript 3), a notable decline in ROS levels was observed in the squalene-treated WT cells, whereas an opposite trend was evident in TXNDC5-KO cells. This finding corroborates previous research indicating that oxidative stress-induced TXNDC5 plays a role in proper protein folding through its disulfide isomerase activity [364]. In conclusion, these results demonstrate that squalene can alter ROS production in oxidative stress, depending on TXNDC5 (Figure 9, Manuscript 3). The viability of cells was evaluated in different concentrations of H_2O_2 based on TXNDC5 elimination. In all concentrations tested, the absence of squalene resulted in a significant reduction in the viability of mouse hepatocytes in the absence of TXNDC5 (Figure 5D, Manuscript 3). However, the viability of both cell lines was enhanced when the cells were treated with squalene and exposed to 20- and 25-mM concentrations of H_2O_2 (Figure 5D1 and D2, Manuscript 3). In light of these findings, TXNDC5 may enhance the efficacy of squalene in promoting AML12 cell viability. Additionally, it may function as an oxidative stress-induced survival factor that regulates ROS/ER stress signaling, enabling AML12 cells to withstand oxidative stress. However, it is not the sole factor, and squalene may circumvent its influence.

Given that the accumulation of lipid peroxides is detrimental to cell viability, the majority of mammalian cells utilize the phospholipid peroxidase glutathione peroxidase 4 (GPx4) to repair damaged lipids. The inhibition of this process can lead to ferroptosis. Prior research has demonstrated that oxidative stress diminishes GPx activity and elevates MDA accumulation (a primary product of lipid peroxidation) in the plasma and liver of piglets [365,366]. Our present study findings, as illustrated in Figure 6C and D, Manuscript 3, substantiate that H_2O_2 -induced oxidative stress reduces the mRNA level of *Gpx4* in WT and KO mouse hepatic cells. The accumulation of squalene in cholesterol auxotrophic lymphomas has been demonstrated to inhibit oxidative cell death through the induction of GPx4 [367]. The oral administration of squalene was observed to improve the redox status of rats following exposure to cyclophosphamide-induced oxidative stress, as evidenced by an increase in GPx activity within the heart, testis, and urine bladder, and the normalization of the alterations observed in *Gpx4* within the heart and hemolysate of red blood cells [368,369]. Furthermore,

our findings indicate that *Gpx4* is induced in the presence of squalene in WT and TXNDC5-deficient cells. When both cell types were exposed to H_2O_2, incubation with squalene rescued the decreased *Gpx4* expression regardless of TXNDC5 (Figure 6, Manuscript 3). This mechanism may contribute to the survival of TXNDC5-deficient mouse hepatocyte cells against H_2O_2-induced oxidative stress through the therapeutic action of squalene (Figure 9, Manuscript 3).

TXNDC5 is a thioredoxin comprising a protein disulfide isomerase-like domain, which is postulated to catalyze disulfide formation for the purposes of facilitating protein folding or controlling protein function when faced with ER stress [370]. Following exposure to thapsigargin, which induces ER stress, the viability of WT and KO cell lines was observed to be analogous (Figure 7A, B, Manuscript 3). Sullivan et al. demonstrated that TXNDC5 could protect endothelial cells from ER stress-induced apoptosis [371]. To date, the principal mediators of ER stress-induced apoptosis have been identified as DDIT3, JNK, and cleaved caspase-12. As a downstream protein, DDIT3 plays a role in ER stress-induced apoptosis and can be triggered by EIF2AK3, ERN1, and ATF6 [329]. The ER stress sensor protein, ERN1, functions as both a protein kinase and an endoribonuclease, and is a transmembrane protein that can regulate its own expression [124,372]. Another ER stress sensor, ATF6, is a type II transmembrane protein that up-regulates chaperones and ERAD pathway components [373]. EIF2AK3 is important for reducing workload by blocking mRNA translation and, in consequence, stopping further protein synthesis [127]. To ascertain the role of TXNDC5 mediators in ER stress, gene expression analysis was conducted on *Atf6*, *Ern1*, and *Eif2ak3* in the presence of squalene loaded in PLGA (Figure 8, Manuscript 3). In the context of ER stress-induced effects, Chawsheen et al. observed that the knockdown of TXNDC5 in human lung cancer cells accelerates the unfolded proteins and induces ER stress, which in turn increases the expression of *Eif2ak3*, *Ern1*, and *Atf6* [151].

In accordance with the aforementioned findings, the downregulation of TXNDC5 was observed to elevate the mRNA levels of ER stress markers in mouse hepatic cells (see Supplementary Figure S2, Manuscript 3). In the presence of induced ER stress, squalene was observed to decrease *Ern1* expression in WT cells in comparison to KO (Figure 8C, Manuscript 3). However, an inverse outcome was noted with respect to *Eif2ak3* expression, which exhibited a decline in TXNDC5-deficient cells, while no notable alteration was discerned in *Atf6* (Figure 8C, D, Manuscript 3). A series of experiments demonstrated that the knockout of ATF6 impeded the elevation of *Txndc5* mRNA. TXNDC5 occupies a downstream position with respect to ATF6 in cardiac, kidney fibroblasts, and stellate cells [173,176,177]. In accordance with the aforementioned outcomes, it was postulated that TXNDC5 may be located downstream of ATF6 and upstream of EIF2AK3 and ERN1 in hepatic cells. Based on this hypothesis, it can be proposed that TXNDC5 may regulate ER activity through disparate signaling pathways during periods of stress; additionally, squalene may reduce cellular mortality by diminishing *Ern1* or *Eif2ak3* expression as ER stress markers in hepatic cells, contingent on TXNDC5. A synopsis of the results is presented in Figure 24.

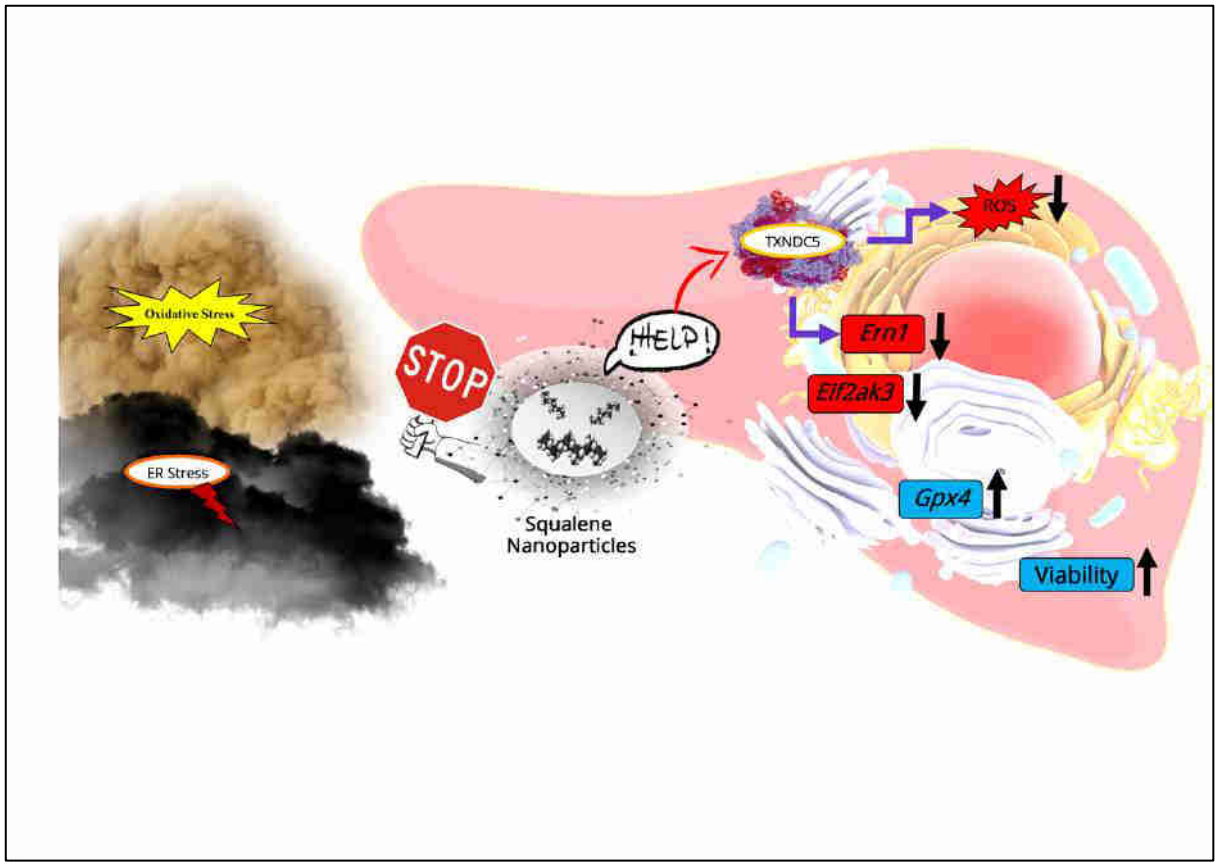

Figure 24. A synopsis of the findings that were obtained in this objective.

The fourth objective, which concerns the enhancement of the therapeutic effect of squalene through the development of a novel drug delivery system for hepatocytes based on chitosan, is addressed in the fourth manuscript of this thesis, entitled:

4. Chitosan Nanoparticles, a Novel Drug Delivery System to Transfer Squalene for Hepatocyte Stress Protection

Chitosan-based systems have been employed in a plethora of applications within the food and biochemical industries, largely due to their capacity to encapsulate a diverse array of ingredients [374]. The initial method described in the literature for the preparation of CSNPs involved emulsification and cross-linking. In this study, CSNPs were prepared by the addition of a negatively charged sodium tripolyphosphate solution to a positively charged chitosan solution under magnetic stirring at room temperature, followed by an ultrasound approach [375,376]. Initial experiments were conducted using two chitosan samples with distinct molecular weights, namely low (LMw) and high (HMw) molecular weight. As the biophysical characterization of PLGA-squalene was previously documented in our previous publication [187], the particle size, surface charge, and EE% of all CSNPs were also evaluated and are presented in Tables 1 and 2, Manuscript 4. An increase in chitosan Mw was observed to result in an increase in the average particle size from 262 to 473 nm, accompanied by a change in PDI from 0.35 to 0.53. These findings align with previous observations that higher Mw chitosan yields larger nanoparticles [377–379]. The PDI was found to be low for all NPs evaluated, indicating that a homogeneous dispersion was obtained. Additionally, it was observed that a higher variety of particle sizes were obtained when a solution of larger polymer chains was used. The positive charge of chitosan enables it to form a robust interaction with negatively charged molecules, such as sodium tripolyphosphate, while maintaining its intrinsic activity. In accordance with the existing literature, an analysis of the differences between the two CSNPs revealed a similar trend as observed for the particle size, namely that a higher surface charge was obtained for particles formed by polymers with a longer chain [380,381]. The size and PDI of a nanoparticle formulation exert a considerable influence on the loading and release of a drug [382]. The results indicated that the CS-SQ NPs were comparatively larger than CSNPs, which is consistent with the findings of Keawchaoon and Yoksan using carvacrol [383,384]. The positive surface charge of CS-SQ NPs is primarily attributable to the cationic nature of chitosan, which exhibits protonated amine groups in aqueous solutions at neutral to slightly acidic pH. The hydrophobic substance squalene is encapsulated within the nanoparticle by means of hydrophobic interactions. Consequently, the positive surface charge is sustained as a result of the protonation of chitosan [385].

To confirm the encapsulation of squalene within the NPs, a Fourier transform infrared (FTIR) analysis was conducted (Figure 2, Manuscript 4). The various synthesized samples were studied in comparison with squalene and chitosan [385,386]. The ATR-FTIR spectra of the chitosan-squalene NPs exhibited the presence of characteristic peaks in the range of 2 800–3 000 cm^{-1}, which corresponded to the C–H stretching of squalene, and in the range of 1 000–1 100 cm^{-1}, which were indicative of the C–O–C vibration of chitosan. The selection of these peaks was based on their capacity to provide a qualitative measure of the encapsulation process.

The C–H stretching bands of squalene were selected due to their pronounced intensity under the specified experimental conditions, thereby providing a straightforward method for evaluating the relative quantity of squalene present in the nanoparticle system. While the C=C stretching (approximately 1 640 cm^{-1}) is also a distinctive feature of squalene, the C-H stretching bands yielded more conspicuous signals for monitoring the encapsulation process with greater accuracy. This approach enabled the differentiation of the C-H stretching vibrations of squalene from those of chitosan within the CS-SQ NPs. For chitosan, the C–O–C vibration (1 000–1 100 cm^{-1}) was selected as it is indicative of the glycosidic bond structure of the polysaccharide, thereby confirming its presence in the nanoparticles. While other signals, such as the amide II band (approximately 1 550 cm^{-1}) and the CO–H band (approximately 1 410 cm^{-1}), are also characteristic of chitosan, the C–O–C peak enabled the reliable identification of chitosan within the system, without interference from other bands [387–389]. By calculating the intensity ratios of the squalene:chitosan bands (at 2 800-3 000 vs. 1 000-1 100 cm^{-1}), it was observed that the LMw CS-SQ NPs (0.8) exhibited a higher ratio than the HMw CS-SQ NPs (0.3), thereby supporting the aforementioned claim of a higher encapsulation efficiency in LMw chitosan. These findings were corroborated by the results of GC-MS, which indicated higher amounts of squalene in LMw CS-SQ NPs than in HMw CS-SQ NPs (Table 2, Manuscript 4), using the equations provided in the experimental section. The encapsulation efficiency of squalene-loaded NPs has been documented in the literature to exhibit considerable variability, contingent on the NP type and the synthetic methodology employed, with reported values spanning a range of 26 to 82% [385,387,389].

Scanning electron microscopy (SEM) and scanning transmission electron microscopy in scanning electron microscopy (STEM in SEM) were employed to examine the morphology of the LMw NPs. As illustrated in Figure 3A Manuscript 4, the SEM image of the morphological construction of CSNPs exhibited particles with a slightly spherical morphology. The CS-SQ NPs exhibited an increase in size and a range of shapes due to the presence of squalene and the occurrence of aggregation. Another effective approach for elucidating the morphology of CSNPs is STEM in SEM (Figure 3B, Manuscript 4). The loading of squalene on CSNPs has been demonstrated to exert an influence on the shape of the NPs, as previously observed by other research groups [385,389]. It can be concluded that the addition of squalene during the synthesis process affects both the shape and size of chitosan nanoparticles. This observation was consistent with previous findings indicating that the presence of diverse components, including curcumin, oregano essential oil, and lipids, can enhance the size of CSNPs while maintaining their spherical shape [390–392]. Furthermore, the sizes obtained by SEM were smaller than those observed with DLS. This outcome was anticipated, given that the particles were subjected to desiccation prior to observation. In contrast, the DLS method provided insight into the hydrodynamic diameter of the particles. It was established that chitosan particles exhibited significant swelling in aqueous solution [393].

At present, chitosan is widely regarded as a safe polymer for the delivery of pharmaceuticals. The United States Food and Drug Administration has granted approval for its use as a wound dressing [394]. The results demonstrated that, due to the prolonged circulation time *in vivo* and enhanced permeability and efficacy of the drug, chitosan nanoparticles loaded

with drugs were successfully concentrated in tumor tissues of mice, with a superior antitumor effect and reduced toxicity [395]. The cytotoxicities of the CS-SQ NPs and CSNPs were evaluated using MTT colorimetric assays on two distinct cell lines: The cell lines used in this study were AML12 WT, which are mouse hepatocyte cells, and AML12 KO, which are mouse hepatocyte cells lacking the expression of TXNDC5 protein. Both cell lines exhibited heightened sensitivity within 72 hours of treatment. The MTT assays indicated that 24 and 48 hours were safe for a maximum concentration of 150 μM on both cells, with cell viability exceeding 85% (Figure 4, Manuscript 4). The results of this study corroborate those of previous studies involving chitosan-curcumin nanoparticles and doxorubicin–chitosan polymeric micelles for targeting the liver and spleen, confirming the absence of cytotoxicity and demonstrating a notable reduction in drug toxicity to the heart and kidney [390,396]. In contrast to toxic compounds such as sulfide, which have been demonstrated to exhibit toxicity against MCF7 and COS7 cells, chitosan has been shown to be non-toxic. It is important to note, however, that the concentration of chitosan may affect cell viability at high doses or for extended periods of time. For instance, the intravenous administration of an excessive quantity of chitosan has been linked to the formation of blood clots, which could potentially result in adverse effects, including mortality. However, this phenomenon typically occurred at concentrations that were exceedingly high. Therefore, it is crucial to take the concentration of CSNPs into account during their development in order to reduce the potential for toxicity [397,398].

The results of squalene extraction indicated a notable increase in the uptake of squalene relative to the control in 150 μM at 48 hours in both WT and KO AML12 cells (Figure 4C, D, Manuscript 4). Among the LMw and HMw CS-SQ NPs, the LMw CS-mediated delivery of squalene into cells exhibited the highest efficiency in terms of the amount of squalene per gram of cells. The results demonstrated that the nature and molar ratios of chitosan exert a considerable influence on the internalization process [399]. An additional hypothesis regarding the HMw CS-SQ NPs is that they are unable to be absorbed due to their larger size, which prevents them from being absorbed by cells. This indicated a loss of function of the NPs [400]. Prior research has demonstrated that, for an equivalent number of polymer units, the utilization of smaller Mw chitosan on lipid nanoparticle surfaces is more conducive to efficient cellular uptake. Chitosan has been demonstrated to enhance the bioavailability of drugs by facilitating their absorption, which prolongs the contact time between the substrate and cell membrane. Moreover, their nanoscale dimensions facilitate the uptake of drugs through the cell membrane [401–403]. This phenomenon has been observed in A2780 ovarian cancer cells, indicating that CSNPs may be a viable delivery system for drugs to the perinuclear space [404]. Other studies have indicated that paclitaxel, glycol, cyclosporin A, and ovalbumin–chitosan nanoparticles exhibited a higher cell uptake rate than the free drugs in MDA-MB-231, HeLa, RCE, and RAW264.7 cells [405–408]. The internalization and uptake of squalene particles may be facilitated by the presence of positively charged chitosan. In general, the surface charge of particles is considered a crucial factor in determining their cellular uptake. For instance, positively charged gold nanoparticles were selectively internalized by cells to a greater extent than their negatively charged counterparts. CS-SQ NPs exhibited a high positive charge, and

previous studies have demonstrated that cationic nanoparticles can markedly enhance the endocytosis of particles [409,410].

The transfer of squalene into cells can be achieved through the use of various carriers, including PLGA and ethanol [187,411]. Nevertheless, the most suitable carrier for this objective remains to be established. In our experimental design, we included ethanol-squalene as a non-nanoparticle carrier to serve as a control for comparison with PLGA and CS drug delivery systems [412]. Prior research has demonstrated that PLGA NPs, due to their smaller size, are rapidly and efficiently internalized by cells [187]. The results of this study demonstrated that the chitosan and PLGA carriers exhibited higher efficiency in the uptake of squalene by AML12 WT and KO cells, as compared to ethanol (Figure 5A, Manuscript 4). Nevertheless, the PLGA-SQ NPs demonstrated the highest efficiency at both 48 and 72 hours. These results corroborate previous findings that PLGA has superior cellular uptake compared to other polymers utilized for drug and gene delivery. As evidenced by numerous studies, PLGA nanoparticles are highly efficient nanocarriers for the encapsulation and delivery of a diverse array of anti-cancer agents, including oleanolic and ursolic acids, in three distinct cell lines: The aforementioned studies were conducted using HepG2, Caco-2, and Y-79 cell lines [350–353,413–415]. For example, PLGA-based curcumin nanoparticles have demonstrated an encapsulation efficiency of 77 to 85% [353]. However, a previous study conducted by our research group identified certain limitations associated with PLGA nanoparticles [187]. The application of 150 µM PLGA NPs resulted in the complete shrinkage of the cell, a consequence of osmotic stress. Nevertheless, this shrinkage was alleviated by reducing the dosage of nanoparticles. Given the observed morphological impact of the highest doses, the 30 µM of squalene loaded in the PLGA nanoparticles was selected for subsequent studies on AML12 cells. Therefore, high doses of squalene were not suitable for use in the PLGA carrier. As a result, the 150 µM PLGA-SQ NPs prompted a transformation in cellular morphology (Figure 5B, C, Manuscript 4), while no such alteration was discerned in CS-SQ NPs and Eth-SQ due to the presence of osmotic stress. Consequently, based on the observed morphological impact of the highest doses of squalene, chitosan was selected as the most efficacious and productive carrier for high doses of squalene to conduct subsequent studies on hepatocytes.

The viscosity of a polymer solution represents a key parameter of interest from a technological standpoint. The management of highly viscous solutions presents significant challenges due to the inherent complexities associated with such materials. Furthermore, the molecular weight and viscosity of chitosan in aqueous solution are of considerable importance with regard to its biochemical and pharmacological applications [416]. Viscosity is dependent upon the molecular weight and degree of deacetylation of the polymer. As the molecular weight of chitosan is diminished, a reduction in viscosity has been observed. Indeed, viscosity can be utilized to ascertain the stability of the polymer in solution, as a reduction was observed during polymer storage due to polymer degradation. It was evident that a certain quantity of larger nanoparticles was tolerated by the human body. In contrast to small nanoparticles, the occurrence of capillary blockage is inevitable when the particle size exceeds the diameter of the blood vessel [416–418]. The gelation of the low-viscosity CS-SQ NPs and PLGA-SQ NPs dispersion in the syringe needle may occur, resulting in the immediate formation of a viscous

suspension with unacceptable particle sizes. These were significant challenges for the development of squalene nanoparticle dispersions suitable for intravenous injection in clinical practice. In this context, the viscosity of the CS-SQ NPs and PLGA-SQ NPs demonstrated that the viscosity of the squalene did not undergo any significant alterations in either drug delivery carrier. Furthermore, the viscosity of the CS-SQ NPs and PLGA-SQ NPs demonstrated that these formulations facilitate ease of administration due to their lower viscosity (Figure 5D, Manuscript 4).

The administration of squalene has been demonstrated to induce significant alterations in hepatic proteins involved in lipid metabolism, oxidative stress, and lipoprotein secretion [216]. Additionally, a reduction in hepatic triglycerides has been observed in mice following the administration of squalene. Squalene's antioxidant properties are closely associated with its distinctive and stable structure, which enables it to effectively neutralize harmful free radicals [355]. Hepatic TXNDC5 is a member of the protein disulfide isomerase family, which has been linked to the anti-steatotic properties of squalene and the regulation of ER stress [45,188]. Consequently, TXNDC5 functions as a protective agent, safeguarding cells against oxidative and ER stress [122]. Following exposure to squalene, the cells were treated with H_2O_2 as an oxidative stress inducer, palmitic acid and thapsigargin as moderate and harsh ER stressors for 24 hours. The viability enhancement was calculated for the various stressors that were tested, and the results demonstrated that the squalene delivered from chitosan nanoparticles increased the viability of the WT hepatocyte cells and KO cells by 18 and 25%, respectively, in oxidative stress, and by 21 and 15%, respectively, in ER stress (Figure 6, Manuscript 4). Prior findings from our research group indicated that squalene protection was absent in cells devoid of TXNDC5 when subjected to 30 μM of squalene in an oxidative stress context [187]. The protective effects of squalene against oxidative destruction have been formally documented in rodents and multiple cell lines, including murine macrophages, human monocytes, and mammary epithelial cells [359]. Prior research has shown that the knockdown of TXNDC5 expression has been observed to induce ROS and ER stress in pancreatic cancer cells. Conversely, the elevation of TXNDC5 expression in lipid endothelial cells has been demonstrated to effectively diminish ROS production and safeguard cells [362,363]. Furthermore, the overexpression of TXNDC5 resulted in reduced sensitivity to ER stress when exposed to tunicamycin and thapsigargin. However, TXNDC5 knockout human prostate adenocarcinoma cells demonstrated a loss of the capacity to upregulate protein disulfide isomerase in response to tunicamycin-induced ER stress [419]. In sum, the findings revealed that TXNDC5 can modulate ROS production in oxidative stress, contingent on the optimal dosage of squalene, thereby enhancing the efficacy of squalene in AML12 cell viability and functioning as an oxidative stress-induced survival factor that regulates ROS/ER stress signaling, thereby enabling AML12 cells to persist under oxidative stress. A brief overview of the findings is presented in Figure 25.

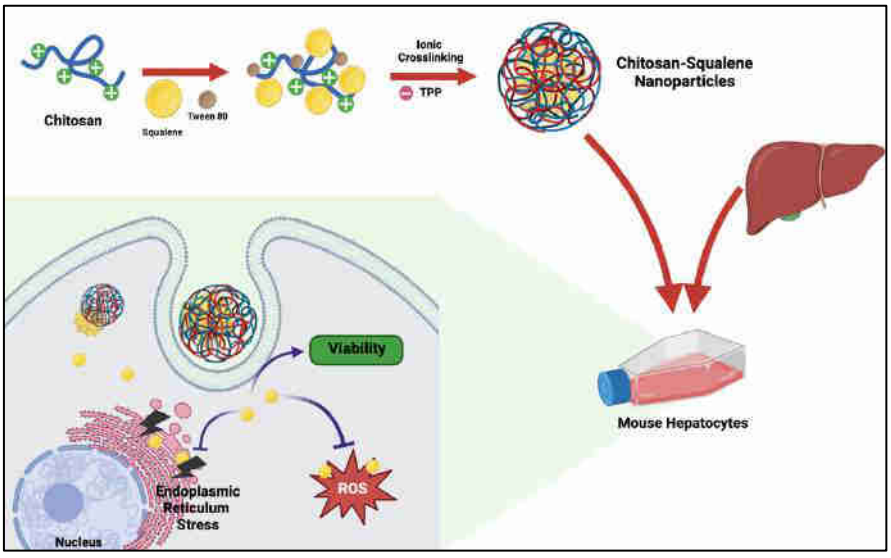

Figure 25. A brief overview of the findings that were obtained in this objective.

FUTURE DIRECTIONS AND RESEARCH OPPORTUNITIES

This study has laid the foundation for understanding the role of TXNDC5 and squalene in cellular stress responses and MASLD mechanisms. However, several key areas remain unexplored, providing exciting research opportunities for future investigations. One critical direction is the investigation of TXNDC5 promoter activity. By analyzing different promoter sequences, it will be identified the functional unit responsible for squalene responsiveness and its associated transcription factors. Additionally, squalene's effect on liver metabolism may involve CYP2B10, a key enzyme in xenobiotic metabolism. Using different promoter sequences, it will be explored the transcription factors mediating CYP2B10 expression in response to squalene, contributing to a better understanding of its metabolic regulation. To assess the role of endogenous squalene, it will be inhibited squalene epoxidase using terbinafine and NB598 to evaluate how intracellular squalene levels affect stress responses and cellular homeostasis. Additionally, to strengthen the findings from in vitro studies, in vivo experiments will be conducted using wild-type (WT) and TXNDC5 knockout (KO) mice, which will confirm and validate squalene's protective role, particularly in oxidative and ER stress conditions. Another critical aspect is PRDX6 and Serpina downregulation in TXNDC5 KO cells, which raises important mechanistic questions. Future research will identify the molecular pathways linking TXNDC5 to PRDX6 and Serpina regulation, potentially revealing novel insights into redox homeostasis and stress response. Additionally, given the interplay between ER stress and mitochondrial dysfunction, it would be interesting to explore whether squalene can mitigate mitochondrial damage under ER stress conditions, thereby establishing it as a mitochondrial-protective compound. As squalene has been proposed to exhibit anticancer properties, its effects on Caco-2 cells, a human colorectal cancer model, to assess whether squalene influences cancer cell proliferation, apoptosis, and stress responses require testing. Moreover, the differential effects of squalene on differentiated vs. undifferentiated Caco-2 cells will be investigated to determine whether cellular differentiation status influences its mode of action and identify biomarker responses to squalene treatment. A broader

perspective involves cross-species meta-analysis of squalene response biomarkers by integrating RNAseq datasets from mice, rabbits, pigs, and AML12 cells treated with squalene. This will allow the identification of conserved squalene response biomarkers across species, highlighting evolutionary conserved mechanisms and validating key molecular targets. Lastly, nanoparticle-based drug delivery plays a critical role in squalene administration. By conducting RNAseq analysis on AML12 cells, treated with squalene-loaded chitosan and PLGA nanoparticles, will allow to compare gene expression differences and determine the most efficient squalene delivery system. These future studies will provide a comprehensive understanding of squalene's role in cellular regulation, stress response, and chronic disease mechanisms, with implications for drug development, metabolic regulation, cancer therapy, and nanomedicine.

VI. CONCLUSIONS

CONCLUSIONS (ENGLISH)

1. The HSPA9 and PRDX6 proteins have been observed to interact with TXNDC5 in AML12 cells. TXNDC5 deficiency resulted in a reduction in PRDX6 protein levels, without changes in its mRNA. In contrast, the expression of the HSPA9 protein and mRNA was found to be decreased. The levels of lipid peroxidation, reduced GSH, and $iPLA_2$ activity were significantly diminished in TXNDC5-deficient cells, whereas the total PLA_2 exhibited an increase. The inactivation of the proteasome using MG-132 in the WT and KO AML12 cell lines revealed no considerable effect on PRDX6 protein expression changes. This suggests that the proteasome is not the biological target of the TXNDC5–PRDX6 complex. The impact of TXNDC5 on hepatic transcripts linked to PRDX6 and HSPA9 indicated that in the AML12 KO cells, *Dnaja3*, *Mfn2*, and *Prdx5* were increased while *Hsp90aa1*, *Rsp14*, *Oplah*, *Gstp3*, *Gstm6*, *Gstt1*, *Serpina1a*, *Serpina1b*, and *Serpina3m* were downregulated.

2. The depletion of TXNDC5 decreased the mRNA expression of *Ern1*, *Xbp1*, *Eif2ak3*, and *Sec61a1*, while increased that of *Atf4*, *Hspa5*, and *Ddit3* in mouse hepatocytes. The expression of *Atf6* and *Ssr2* was not modified in the absence of TXNDC5. The protein expression results for the most prominent ER stress markers indicated a downregulation of ERN1 and EIF2AK3 proteins and an upregulation of HSPA5 protein. Furthermore, no changes were observed in the ATF6 protein in the absence of TXNDC5 at the protein level. It has been demonstrated that the knockout of TXNDC5 increases cellular ROS production in AML12 cells. Moreover, TXNDC5 activity is necessary for the maintenance of normal mitochondrial function during tunicamycin-induced ER stress. The elevation of TXNDC5 expression in AML12 cells is contingent upon the development of ER stress through the administration of thapsigargin, palmitic acid, or tunicamycin. Tunicamycin has been demonstrated to disrupt the protein levels of HSPA5, ERN1, and EIF2AK3 in TXNDC5-deficient cells. Furthermore, tunicamycin has been demonstrated to influence the mRNA levels of *Eif2ak3* and *Sec61a1* in TXNDC5-deficient cells. It should be noted, however, that palmitic acid can disrupt the protein and gene expression levels of ATF6, HSPA5, and EIF2AK3 in TXNDC5 knockout cells. The absence of TXNDC5 did not influence any ER stress cascades in thapsigargin-induced ER stress in hepatocytes, despite the activation of the ERN1–XBP1 pathway under these conditions. Moreover, the absence of TXNDC5 has been demonstrated to induce the *Xbp1* spliced form. Alternatively, the ERN1 upregulation may impact splicing rather than expression of *Xbp1* mRNA. Finally, TXNDC5 specifically activated different cascades of ER stress depending on the cause of ER stress via HSPA5. In turn, TXNDC5 deficiency disrupted EIF2AK3 cascade.

3. Squalene was effectively encapsulated in PLGA NPs, resulting in the formation of stable nanoparticles with rapid and efficient cellular uptake. The administration of squalene-based PLGA NPs significantly reduced ROS levels in normal mouse hepatocytes, whereas ROS levels were markedly elevated in TXNDC5-deficient AML12 cells. Squalene-induced *Gpx4* expression increased the viability of WT and KO cells under oxidative stress. Furthermore, squalene increased the viability of thapsigargin-treated mouse hepatocytes through the repression of *Ern1* in WT or of *Eif2ak3* in KO cells. Therefore, TXNDC5 was

identified as a critical regulator of ER activity through diverse signaling pathways in response to stress. Similarly, the administration of squalene-loaded PLGA NPs was shown to protect mouse hepatocytes from oxidative and ER stress through a range of mechanisms, which appear to be contingent upon the presence of TXNDC5.

4. Nanoparticles of low molecular weight chitosan, which adopt a spherical configuration, represent an effective encapsulation agent for squalene, based on the results of a analyses of GC-MS and semi-quantitative FTIR. The results demonstrated that hepatocytes were not adversely affected by squalene-loaded chitosan nanoparticles at concentrations up to 150 μM, and the nanoparticles exhibited efficient cellular uptake within 48 hours. In comparison to PLGA and ethanol, the chitosan nanoparticles exhibited the greatest efficiency and productivity as carriers for high doses of squalene and PLGA for lower doses of squalene, thus justifying further investigation in hepatocytes. The viability of WT and KO AML12 cells was enhanced in the presence of squalene, particularly under conditions of oxidative and ER stress induced by palmitic acid and thapsigargin. Moreover, the administration of squalene-based chitosan nanoparticles was observed to effectively reduce the levels of ROS in mouse hepatocytes. The results suggest that chitosan nanoparticles may offer a means of overcoming the limitations of PLGA drug carriers. It is further proposed that the appropriate dose of squalene may modulate ROS production in oxidative stress, independently of TXNDC5.

CONCLUSIONES (ESPAÑOL)

1. Se ha observado que las proteínas HSPA9 y PRDX6 interactúan con TXNDC5 en células AML12. La deficiencia de TXNDC5 resultó en una reducción en los niveles de proteína PRDX6, sin cambios en su RNA. En contraste, se encontró que la expresión de la proteína HSPA9 y el ARNm disminuían. Los niveles de peroxidación lipídica, glutatión reducido y actividad de $iPLA_2$ disminuyeron significativamente en las células deficientes en TXNDC5, mientras que la PLA_2 total mostró un aumento. La inactivación del proteasoma con MG-132 en las líneas celulares WT y KO AML12 no modificó la expresión de la proteína PRDX6. Esto sugiere que el proteasoma no es el objetivo biológico del complejo TXNDC5-PRDX6. El impacto de TXNDC5 en los transcritos hepáticos vinculadas a PRDX6 y HSPA9 indicó que en las células AML12 KO, *Dnaja3*, *Mfn2* y *Prdx5* estaban incrementados mientras que *Hsp90aa1*, *Rsp14*, *Oplah*, *Gstp3*, *Gstm6*, *Gstt1*, *Serpina1a*, *Serpina1b* y *Serpina3m* estaban regulados negativamente.

2. La depleción de TXNDC5 se ha relacionado con una disminución en la expresión de ARNm para *Ern1*, *Xbp1*, *Eif2ak3* y *Sec61a1*, mientras que se ha observado un aumento en la expresión de ARNm de *Atf4*, *Hspa5* y *Ddit3* en hepatocitos de ratón. La expresión de *Atf6* y *Ssr2* no se alteró significativamente en ausencia de TXNDC5. Los resultados de la expresión de proteínas para los marcadores de estrés de RE más destacados indicaron una regulación negativa de las proteínas ERN1 y EIF2AK3 y una regulación positiva de la proteína HSPA5. Además, no se observaron alteraciones notables en la proteína ATF6 en ausencia de TXNDC5 a nivel proteico. Se ha demostrado que la inactivación de TXNDC5 aumenta la producción celular de ROS en células AML12. Además, la actividad de TXNDC5 es necesaria para el mantenimiento de la función mitocondrial normal durante el estrés de RE inducido por tunicamicina. La elevación de la expresión de TXNDC5 en células AML12 depende del agente de inducción del estrés del RE: tapsigargina, ácido palmítico o tunicamicina. Así, la tunicamicina altera los niveles de proteína de HSPA5, ERN1 y EIF2AK3 en células deficientes en TXNDC5. Además, este agente influye en los niveles de ARNm de *Eif2ak3* y *Sec61a1* en células deficientes en TXNDC5. Sin embargo, el ácido palmítico puede alterar los niveles de expresión de la proteína y RNA de ATF6, HSPA5 y EIF2AK3 en células carentes de TXNDC5. La ausencia de TXNDC5 no influyó en ninguna cascada de estrés del RE inducido por tapsigargina en estas células, a pesar de la activación de la vía ERN1–XBP1 en estas condiciones. Además, se ha demostrado que la ausencia de TXNDC5 induce un corte y empalme específico de *Xbp1*. Alternativamente, la sobreexpresión de ERN1 puede afectar el corte y empalme en lugar de la expresión del ARNm de *Xbp1*. Finalmente, TXNDC5 activó específicamente diferentes cascadas de estrés del RE dependiendo de la causa del estrés del RE a través de HSPA5. A su vez, la deficiencia de TXNDC5 interrumpió la cascada de EIF2AK3.

3. El escualeno se encapsuló de manera efectiva en nanopartículas de PLGA, lo que resultó en la formación de nanopartículas estables con una captación celular rápida y eficiente. La administración de nanopartículas de PLGA basadas en escualeno redujo significativamente los niveles de ROS en hepatocitos de ratón normales, mientras que dichos niveles se elevaron notablemente en células AML12 deficientes en TXNDC5. La viabilidad de las células WT y

KO en condiciones de estrés oxidativo mejoró en presencia de escualeno, que indujo la expresión de *Gpx4*. Además, se observó que el escualeno mejoraba la viabilidad de los hepatocitos de ratón sometidos a estrés de RE inducido por tapsigargina al reprimir la expresión de *Ern1* o *Eif2ak3* en células WT o KO, respectivamente. Por lo tanto, se identificó a TXNDC5 como un regulador crítico de la actividad de RE a través de diversas vías de señalización en respuesta al estrés. De manera similar, se ha demostrado que la administración de nanopartículas de PLGA cargadas con escualeno protege a los hepatocitos de ratón del estrés oxidativo y del RE a través de una variedad de mecanismos, que parecen depender de la presencia de TXNDC5.

4. Las nanopartículas de quitosano de bajo peso molecular, que adoptan una configuración esférica, representan un agente de encapsulación eficaz para el escualeno, según los análisis de GC-MS y FTIR semicuantitativo. Los resultados demostraron que los hepatocitos no se vieron afectados negativamente por las nanopartículas de quitosano cargadas con escualeno en concentraciones de hasta 150 μM, y las nanopartículas exhibieron una captación celular eficiente en 48 horas. En comparación con PLGA y etanol, las nanopartículas de quitosano exhibieron la mayor eficiencia y productividad como portadores para dosis altas de escualeno y PLGA para dosis más bajas de escualeno, lo que justifica una mayor investigación en hepatocitos. La viabilidad de las células AML12 WT y KO se mejoró en presencia de escualeno, particularmente en condiciones de estrés oxidativo y de ER inducido por ácido palmítico y tapsigargina. Además, se observó que la administración de nanopartículas de quitosano con escualeno reducía eficazmente los niveles de ROS en los hepatocitos de ratón. Los hallazgos sugieren que las nanopartículas de quitosano pueden ofrecer un medio para superar las limitaciones del PLGA como portador de fármacos. Se propone además que la dosis adecuada de escualeno puede modular la producción de ROS en el estrés oxidativo, independientemente de TXNDC5.

VII. REFERENCES

[1] Häussinger D, Lammert E, Zeeb M. Anatomy and Physiology of the Liver. Metabolism of Human Diseases: Organ Physiology and Pathophysiology 2014:173.

[2] Sibulesky L. Normal liver anatomy. Clin Liver Dis (Hoboken) 2013;2:S1–3.

[3] Juza RM, Pauli EM. Clinical and surgical anatomy of the liver: a review for clinicians. Clinical Anatomy 2014;27:764–9.

[4] Sumadewi KT. Embryology, anatomy and physiology of the liver. Indian J Clin Anat Physiol 2023;10:138–44.

[5] Messina A, Luce E, Dubart-Kupperschmitt A. Directed Differentiation of Human-induced Pluripotent Stem Cells into Hepatic Cells: A Transposable Example of Disease Modeling and Regenerative Medicine Applications. Stem Cell Biology and Regenerative Medicine, River Publishers; 2022, p. 181–205.

[6] McCuskey R. Anatomy of the liver. Zakim and Boyer's Hepatology: A Textbook of Liver Disease 2012;6:3–19.

[7] Ross MH, Pawlina W. Histología: texto y atlas color con biología celular y molecular. Ed. Médica Panamericana; 2007.

[8] Singh P, Kesharwani RK, Keservani RK. Protein, carbohydrates, and fats: Energy metabolism. Sustained Energy for Enhanced Human Functions and Activity, Elsevier; 2017, p. 103–15.

[9] Vargas M, Toniasso S de CC, Riedel PG, Baldin CP, Dos Reis FL, Pereira RM, et al. Metabolic disease and the liver: A review. World J Hepatol 2024;16:33.

[10] Berg JM, Tymoczko JL, Stryer L, Gatto GJ. Bioquímica con aplicaciones clínicas. Reverté; 2013.

[11] Hall JE. Guyton y Hall. Tratado de fisiología médica. Elsevier Health Sciences; 2021.

[12] Han H-S, Kang G, Kim JS, Choi BH, Koo S-H. Regulation of glucose metabolism from a liver-centric perspective. Exp Mol Med 2016;48:e218–e218.

[13] Scoditti E, Sabatini S, Carli F, Gastaldelli A. Hepatic glucose metabolism in the steatotic liver. Nat Rev Gastroenterol Hepatol 2024;21:319–34.

[14] Stanley LA. Drug metabolism. Pharmacognosy, Elsevier; 2024, p. 597–624.

[15] Ozougwu JC. Physiology of the liver. International Journal of Research in Pharmacy and Biosciences 2017;4:13–24.

[16] Esteller A. Physiology of bile secretion. World Journal of Gastroenterology: WJG 2008;14:5641.

[17] Kubes P, Jenne C. Immune responses in the liver. Annu Rev Immunol 2018;36:247–77.

[18] Blaner WS, Li Y, Brun P-J, Yuen JJ, Lee S-A, Clugston RD. Vitamin A absorption, storage and mobilization. The Biochemistry of Retinoid Signaling II: The Physiology of Vitamin A-Uptake, Transport, Metabolism and Signaling, Springer; 2016, p. 95–125.

[19] Taniguchi H, Toyoshima T, Fukao K, Nakauchi H. Presence of hematopoietic stem cells in the adult liver. Nat Med 1996;2:198–203.

[20] Abo T, Watanabe H, Iiai T, Kimura M, Ohtsuka K, Sato K, et al. Extrathymic pathways of T-cell differentiation in the liver and other organs. Int Rev Immunol 1994;11:61–102.

[21] Mitra V, Metcalf J. Metabolic functions of the liver. Anaesthesia & Intensive Care Medicine 2009;10:334–5.

[22] Zhang Y-Y, Meng Z-J. Definition and classification of acute-on-chronic liver diseases. World J Clin Cases 2022;10:4717.

[23] Bahramirad S, Mustapha A, Eshraghi M. Classification of liver disease diagnosis: A comparative study. 2013 Second International Conference on Informatics & Applications (ICIA), IEEE; 2013, p. 42–6.
[24] Suva MA. A brief review on liver cirrhosis: epidemiology, etiology, pathophysiology, symptoms, diagnosis and its management. Inventi Rapid: Molecular Pharmacology 2014;2:1–5.
[25] Seitz HK, Bataller R, Cortez-Pinto H, Gao B, Gual A, Lackner C, et al. Alcoholic liver disease. Nat Rev Dis Primers 2018;4:16.
[26] Guidotti LG, Chisari F V. Immunobiology and pathogenesis of viral hepatitis. Annu Rev Pathol Mech Dis 2006;1:23–61.
[27] Scorza M, Elce A, Zarrilli F, Liguori R, Amato F, Castaldo G. Genetic diseases that predispose to early liver cirrhosis. Int J Hepatol 2014;2014:713754.
[28] Barton JC, McDonnell SM, Adams PC, Brissot P, Powell LW, Edwards CQ, et al. Management of hemochromatosis. Ann Intern Med 1998;129:932–9.
[29] Ala A, Walker AP, Ashkan K, Dooley JS, Schilsky ML. Wilson's disease. The Lancet 2007;369:397–408.
[30] Köhnlein T, Welte T. Alpha-1 antitrypsin deficiency: pathogenesis, clinical presentation, diagnosis, and treatment. Am J Med 2008;121:3–9.
[31] Carbone M, Neuberger JM. Autoimmune liver disease, autoimmunity and liver transplantation. J Hepatol 2014;60:210–23.
[32] Carey EJ, Ali AH, Lindor KD. Primary biliary cirrhosis. The Lancet 2015;386:1565–75.
[33] Lleo A, Wang G-Q, Gershwin ME, Hirschfield GM. Primary biliary cholangitis. The Lancet 2020;396:1915–26.
[34] Rinella ME, Lazarus J V, Ratziu V, Francque SM, Sanyal AJ, Kanwal F, et al. A multisociety Delphi consensus statement on new fatty liver disease nomenclature. Hepatology 2023;78:1966–86.
[35] Buzzetti E, Pinzani M, Tsochatzis EA. The multiple-hit pathogenesis of non-alcoholic fatty liver disease (NAFLD). Metabolism 2016;65:1038–48.
[36] Yki-Järvinen H. Diagnosis of non-alcoholic fatty liver disease (NAFLD). Diabetologia 2016;59:1104–11.
[37] Glen J, Floros L, Day C, Pryke R. Non-alcoholic fatty liver disease (NAFLD): summary of NICE guidance. Bmj 2016;354:i4428.
[38] Jiang X, Zheng J, Zhang S, Wang B, Wu C, Guo X. Advances in the Involvement of Gut Microbiota in Pathophysiology of NAFLD. Front Med (Lausanne) 2020;7:361.
[39] Kořínková L, Pražienková V, Černá L, Karnošová A, Železná B, Kuneš J, et al. Pathophysiology of NAFLD and NASH in experimental models: the role of food intake regulating peptides. Front Endocrinol (Lausanne) 2020;11:597583.
[40] Rowe IA. Lessons from epidemiology: the burden of liver disease. Digestive Diseases 2017;35:304–9.
[41] Younossi ZM, Koenig AB, Abdelatif D, Fazel Y, Henry L, Wymer M. Global epidemiology of nonalcoholic fatty liver disease—meta-analytic assessment of prevalence, incidence, and outcomes. Hepatology 2016;64:73–84.
[42] Caballería L, Pera G, Auladell MA, Torán P, Muñoz L, Miranda D, et al. Prevalence and factors associated with the presence of nonalcoholic fatty liver disease in an adult population in Spain. Eur J Gastroenterol Hepatol 2010;22:24–32.
[43] Burt AD, Lackner C, Tiniakos DG. Diagnosis and assessment of NAFLD: definitions and histopathological classification. Semin Liver Dis 2015;35:207–20.

[44] Piazzolla VA, Mangia A. Noninvasive Diagnosis of NAFLD and NASH. Cells 2020;9:1005.
[45] Bidooki SH, Sánchez-Marco J, Martínez-Beamonte R, Herrero-Continente T, Navarro MA, Rodríguez-Yoldi MJ, et al. Endoplasmic Reticulum Protein TXNDC5 Interacts with PRDX6 and HSPA9 to Regulate Glutathione Metabolism and Lipid Peroxidation in the Hepatic AML12 Cell Line. Int J Mol Sci 2023;24:17131.
[46] Ramírez-Torres A, Barceló-Batllori S, Martínez-Beamonte R, Navarro MA, Surra JC, Arnal C, et al. Proteomics and gene expression analyses of squalene-supplemented mice identify microsomal thioredoxin domain-containing protein 5 changes associated with hepatic steatosis. J Proteomics 2012;77:27–39.
[47] Manne V, Handa P, Kowdley K V. Pathophysiology of nonalcoholic fatty liver disease/nonalcoholic steatohepatitis. Clin Liver Dis 2018;22:23–37.
[48] Duseja A, Chalasani N. Epidemiology and risk factors of nonalcoholic fatty liver disease (NAFLD). Hepatol Int 2013;7:755–64.
[49] Young EN, Dogan M, Watkins C, Bajwa A, Eason JD, Kuscu C, et al. A review of defatting strategies for non-alcoholic fatty liver disease. Int J Mol Sci 2022;23:11805.
[50] Reddy JK, Sambasiva Rao M. Lipid metabolism and liver inflammation. II. Fatty liver disease and fatty acid oxidation. American Journal of Physiology-Gastrointestinal and Liver Physiology 2006;290:G852–8.
[51] Ipsen DH, Lykkesfeldt J, Tveden-Nyborg P. Molecular mechanisms of hepatic lipid accumulation in non-alcoholic fatty liver disease. Cellular and Molecular Life Sciences 2018;75:3313–27.
[52] Bechmann LP, Gieseler RK, Sowa J, Kahraman A, Erhard J, Wedemeyer I, et al. Apoptosis is associated with CD36/fatty acid translocase upregulation in non-alcoholic steatohepatitis. Liver International 2010;30:850–9.
[53] Bechmann LP, Hannivoort RA, Gerken G, Hotamisligil GS, Trauner M, Canbay A. The interaction of hepatic lipid and glucose metabolism in liver diseases. J Hepatol 2012;56:952–64.
[54] Mashek DG. Hepatic fatty acid trafficking: multiple forks in the road. Advances in Nutrition 2013;4:697–710.
[55] Koonen DPY, Jacobs RL, Febbraio M, Young ME, Soltys C-LM, Ong H, et al. Increased hepatic CD36 expression contributes to dyslipidemia associated with diet-induced obesity. Diabetes 2007;56:2863–71.
[56] Endo M, Masaki T, Seike M, Yoshimatsu H. TNF-α induces hepatic steatosis in mice by enhancing gene expression of sterol regulatory element binding protein-1c (SREBP-1c). Exp Biol Med 2007;232:614–21.
[57] Wang G, Bonkovsky HL, de Lemos A, Burczynski FJ. Recent insights into the biological functions of liver fatty acid binding protein 1. J Lipid Res 2015;56:2238–47.
[58] Dentin R, Girard J, Postic C. Carbohydrate responsive element binding protein (ChREBP) and sterol regulatory element binding protein-1c (SREBP-1c): two key regulators of glucose metabolism and lipid synthesis in liver. Biochimie 2005;87:81–6.
[59] Ricchi M, Odoardi MR, Carulli L, Anzivino C, Ballestri S, Pinetti A, et al. Differential effect of oleic and palmitic acid on lipid accumulation and apoptosis in cultured hepatocytes. J Gastroenterol Hepatol 2009;24:830–40.
[60] Sanders FWB, Griffin JL. De novo lipogenesis in the liver in health and disease: more than just a shunting yard for glucose. Biological Reviews 2016;91:452–68.
[61] Ferre P, Foufelle F. Hepatic steatosis: a role for de novo lipogenesis and the transcription factor SREBP-1c. Diabetes Obes Metab 2010;12:83–92.

[62] Sun L-P, Seemann J, Goldstein JL, Brown MS. Sterol-regulated transport of SREBPs from endoplasmic reticulum to Golgi: Insig renders sorting signal in Scap inaccessible to COPII proteins. Proceedings of the National Academy of Sciences 2007;104:6519–26.
[63] Ricoult SJH, Manning BD. The multifaceted role of mTORC1 in the control of lipid metabolism. EMBO Rep 2013;14:242–51.
[64] Ma L, Tsatsos NG, Towle HC. Direct role of ChREBP· Mlx in regulating hepatic glucose-responsive genes. Journal of Biological Chemistry 2005;280:12019–27.
[65] Dentin R, Tomas-Cobos L, Foufelle F, Leopold J, Girard J, Postic C, et al. Glucose 6-phosphate, rather than xylulose 5-phosphate, is required for the activation of ChREBP in response to glucose in the liver. J Hepatol 2012;56:199–209.
[66] Zhang D, Yin L. Transcriptional Regulation of De Novo Lipogenesis in Liver. In: Ntambi JM, editor. Hepatic De Novo Lipogenesis and Regulation of Metabolism, Cham: Springer International Publishing; 2016, p. 1–31.
[67] Zelber-Sagi S. Dietary treatment for NAFLD: new clinical and epidemiological evidence and updated recommendations. Semin Liver Dis 2021;41:248–62.
[68] Dirkx R, Vanhorebeek I, Martens K, Schad A, Grabenbauer M, Fahimi D, et al. Absence of peroxisomes in mouse hepatocytes causes mitochondrial and ER abnormalities. Hepatology 2005;41:868–78.
[69] Rao MS, Reddy JK. Peroxisomal β-oxidation and steatohepatitis. Semin Liver Dis 2001;21:43–55.
[70] Akkaoui M, Cohen I, Esnous C, Lenoir V, Sournac M, Girard J, et al. Modulation of the hepatic malonyl-CoA–carnitine palmitoyltransferase 1A partnership creates a metabolic switch allowing oxidation of de novo fatty acids. Biochemical Journal 2009;420:429–38.
[71] Reddy JK, Hashimoto T. Peroxisomal β-oxidation and peroxisome proliferator–activated receptor α: an adaptive metabolic system. Annu Rev Nutr 2001;21:193–230.
[72] Kersten S, Stienstra R. The role and regulation of the peroxisome proliferator activated receptor alpha in human liver. Biochimie 2017;136:75–84.
[73] Heeren J, Scheja L. Metabolic-associated fatty liver disease and lipoprotein metabolism. Mol Metab 2021;50:101238.
[74] Friedman SL, Neuschwander-Tetri BA, Rinella M, Sanyal AJ. Mechanisms of NAFLD development and therapeutic strategies. Nat Med 2018;24:908–22.
[75] Claudel T, Inoue Y, Barbier O, Duran-Sandoval D, Kosykh V, Fruchart J, et al. Farnesoid X receptor agonists suppress hepatic apolipoprotein CIII expression. Gastroenterology 2003;125:544–55.
[76] Lefebvre P, Cariou B, Lien F, Kuipers F, Staels B. Role of bile acids and bile acid receptors in metabolic regulation. Physiol Rev 2009;89:147–91.
[77] Caron S, Samanez CH, Dehondt H, Ploton M, Briand O, Lien F, et al. Farnesoid X receptor inhibits the transcriptional activity of carbohydrate response element binding protein in human hepatocytes. Mol Cell Biol 2013;33:2202–11.
[78] Rinella ME, Sanyal AJ. Management of NAFLD: a stage-based approach. Nat Rev Gastroenterol Hepatol 2016;13:196–205.
[79] Bellanti F, Mitarotonda D, Tamborra R, Blonda M, Iannelli G, Petrella A, et al. Oxysterols induce mitochondrial impairment and hepatocellular toxicity in non-alcoholic fatty liver disease. Free Radic Biol Med 2014;75:S16–7.

[80] Arguello G, Balboa E, Arrese M, Zanlungo S. Recent insights on the role of cholesterol in non-alcoholic fatty liver disease. Biochimica et Biophysica Acta (BBA)-Molecular Basis of Disease 2015;1852:1765–78.
[81] Mota M, Banini BA, Cazanave SC, Sanyal AJ. Molecular mechanisms of lipotoxicity and glucotoxicity in nonalcoholic fatty liver disease. Metabolism 2016;65:1049–61.
[82] Singh R, Kaushik S, Wang Y, Xiang Y, Novak I, Komatsu M, et al. Autophagy regulates lipid metabolism. Nature 2009;458:1131–5.
[83] Porstmann T, Santos CR, Griffiths B, Cully M, Wu M, Leevers S, et al. SREBP activity is regulated by mTORC1 and contributes to Akt-dependent cell growth. Cell Metab 2008;8:224–36.
[84] Jung CH, Ro S-H, Cao J, Otto NM, Kim D-H. mTOR regulation of autophagy. FEBS Lett 2010;584:1287–95.
[85] Nordlie RC, Foster JD, Lange AJ. Regulation of glucose production by the liver. Annu Rev Nutr 1999;19:379–406.
[86] Krawczyk M, Rau M, Schattenberg JM, Bantel H, Pathil A, Demir M, et al. Combined effects of the PNPLA3 rs738409, TM6SF2 rs58542926, and MBOAT7 rs641738 variants on NAFLD severity: A multicenter biopsy-based study1. J Lipid Res 2017;58:247–55.
[87] Ducheix S, Montagner A, Theodorou V, Ferrier L, Guillou H. The liver X receptor: a master regulator of the gut–liver axis and a target for non alcoholic fatty liver disease. Biochem Pharmacol 2013;86:96–105.
[88] Evans RM, Mangelsdorf DJ. Nuclear receptors, RXR, and the big bang. Cell 2014;157:255–66.
[89] McClain CJ, Barve S, Deaciuc I. Good fat/bad fat. Hepatology 2007;45:1343–6.
[90] Gautheron J, Vucur M, Reisinger F, Cardenas DV, Roderburg C, Koppe C, et al. A positive feedback loop between RIP 3 and JNK controls non-alcoholic steatohepatitis. EMBO Mol Med 2014;6:1062–74.
[91] Li Y, Yang P, Ye J, Xu Q, Wu J, Wang Y. Updated mechanisms of MASLD pathogenesis. Lipids Health Dis 2024;23:117.
[92] Zheng J, Conrad M. Ferroptosis: when metabolism meets cell death. Physiol Rev 2025;105:651–706.
[93] Petrasek J, Bala S, Csak T, Lippai D, Kodys K, Menashy V, et al. IL-1 receptor antagonist ameliorates inflammasome-dependent alcoholic steatohepatitis in mice. J Clin Invest 2012;122:3476–89.
[94] Wree A, Eguchi A, McGeough MD, Pena CA, Johnson CD, Canbay A, et al. NLRP3 inflammasome activation results in hepatocyte pyroptosis, liver inflammation, and fibrosis in mice. Hepatology 2014;59:898–910.
[95] Gregersen N, Bross P. Protein misfolding and cellular stress: an overview. Protein Misfolding and Cellular Stress in Disease and Aging: Concepts and Protocols, Springer; 2010, p. 3–23.
[96] Fulda S, Gorman AM, Hori O, Samali A. Cellular stress responses: cell survival and cell death. Int J Cell Biol 2010;2010:214074.
[97] Tilokani L, Nagashima S, Paupe V, Prudent J. Mitochondrial dynamics: overview of molecular mechanisms. Essays Biochem 2018;62:341–60.
[98] Tutar L, Tutar Y. Heat shock proteins; an overview. Curr Pharm Biotechnol 2010;11:216–22.
[99] Schoffl F, Prandl R, Reindl A. Regulation of the heat-shock response. Plant Physiol 1998;117:1135–41.

[100] Luo H, Chiang H-H, Louw M, Susanto A, Chen D. Nutrient sensing and the oxidative stress response. Trends in Endocrinology & Metabolism 2017;28:449–60.
[101] Mackinnon E, Stone SL. The ubiquitin proteasome system and nutrient stress response. Front Plant Sci 2022;13:867419.
[102] Lee P, Chandel NS, Simon MC. Cellular adaptation to hypoxia through hypoxia inducible factors and beyond. Nat Rev Mol Cell Biol 2020;21:268–83.
[103] Barzilai A, Yamamoto K-I. DNA damage responses to oxidative stress. DNA Repair (Amst) 2004;3:1109–15.
[104] Davies KJA. An overview of oxidative stress. IUBMB Life 2000;50:241–4.
[105] Sosa V, Moliné T, Somoza R, Paciucci R, Kondoh H, LLeonart ME. Oxidative stress and cancer: an overview. Ageing Res Rev 2013;12:376–90.
[106] Vona R, Gambardella L, Cittadini C, Straface E, Pietraforte D. Biomarkers of oxidative stress in metabolic syndrome and associated diseases. Oxid Med Cell Longev 2019;2019:8267234.
[107] Schröder M, Kaufman RJ. ER stress and the unfolded protein response. Mutation Research/Fundamental and Molecular Mechanisms of Mutagenesis 2005;569:29–63.
[108] Chen Z, Tian R, She Z, Cai J, Li H. Role of oxidative stress in the pathogenesis of nonalcoholic fatty liver disease. Free Radic Biol Med 2020;152:116–41.
[109] Delli Bovi AP, Marciano F, Mandato C, Siano MA, Savoia M, Vajro P. Oxidative stress in non-alcoholic fatty liver disease. An updated mini review. Front Med (Lausanne) 2021;8:595371.
[110] Dandekar A, Mendez R, Zhang K. Cross talk between ER stress, oxidative stress, and inflammation in health and disease. Stress responses: methods and protocols, Springer; 2015, p. 205–14.
[111] Alberts B, Johnson A, Lewis J, Raff M, Roberts K, Walter P. From DNA to RNA. Molecular Biology of the Cell. 4th edition, Garland Science; 2002.
[112] Görlich D, Prehn S, Hartmann E, Kalies K-U, Rapoport TA. A mammalian homolog of SEC61p and SECYp is associated with ribosomes and nascent polypeptides during translocation. Cell 1992;71:489–503.
[113] Seiser RM, Nicchitta C V. The fate of membrane-bound ribosomes following the termination of protein synthesis. Journal of Biological Chemistry 2000;275:33820–7.
[114] Schwarz DS, Blower MD. The endoplasmic reticulum: structure, function and response to cellular signaling. Cellular and Molecular Life Sciences 2016;73:79–94.
[115] Maxfield FR, Wüstner D. Intracellular cholesterol transport. J Clin Invest 2002;110:891–8.
[116] Stornaiuolo M, Lotti L V, Borgese N, Torrisi M-R, Mottola G, Martire G, et al. KDEL and KKXX retrieval signals appended to the same reporter protein determine different trafficking between endoplasmic reticulum, intermediate compartment, and Golgi complex. Mol Biol Cell 2003;14:889–902.
[117] de Seny D, Bianchi E, Baiwir D, Cobraiville G, Collin C, Deliège M, et al. Proteins involved in the endoplasmic reticulum stress are modulated in synovitis of osteoarthritis, chronic pyrophosphate arthropathy and rheumatoid arthritis, and correlate with the histological inflammatory score. Sci Rep 2020;10:14159.
[118] Yang L, Li P, Fu S, Calay ES, Hotamisligil GS. Defective hepatic autophagy in obesity promotes ER stress and causes insulin resistance. Cell Metab 2010;11:467–78.
[119] Zhang J, Zhang K, Li Z, Guo B. ER stress-induced inflammasome activation contributes to hepatic inflammation and steatosis. J Clin Cell Immunol 2016;7:457.

[120] Dufey E, Sepúlveda D, Rojas-Rivera D, Hetz C. Cellular mechanisms of endoplasmic reticulum stress signaling in health and disease. 1. An overview. American Journal of Physiology-Cell Physiology 2014;307:C582–94.
[121] Maiers JL, Malhi H. Endoplasmic reticulum stress in metabolic liver diseases and hepatic fibrosis. Semin Liver Dis 2019;39:235–48.
[122] Bidooki SH, Navarro MA, Fernandes SCM, Osada J. Thioredoxin Domain Containing 5 (TXNDC5): Friend or Foe? Curr Issues Mol Biol 2024;46:3134–63.
[123] Tsuchiya Y, Saito M, Kadokura H, Miyazaki J, Tashiro F, Imagawa Y, et al. IRE1–XBP1 pathway regulates oxidative proinsulin folding in pancreatic β cells. Journal of Cell Biology 2018;217:1287–301.
[124] Hassler J, Cao SS, Kaufman RJ. IRE1, a double-edged sword in pre-miRNA slicing and cell death. Dev Cell 2012;23:921–3.
[125] Chen X, Li C, Liu J, He Y, Wei Y, Chen J. Inhibition of ER stress by targeting the IRE1α–TXNDC5 pathway alleviates crystalline silica-induced pulmonary fibrosis. Int Immunopharmacol 2021;95:107519.
[126] Lin JH, Han L, Yasumura D, Cohen HR, Zhang C, Panning B, et al. IRE1 signaling affects cell fate during the unfolded protein response. Sciences 2007;318:944–9.
[127] Cullinan SB, Diehl JA. PERK-dependent activation of Nrf2 contributes to redox homeostasis and cell survival following endoplasmic reticulum stress. Journal of Biological Chemistry 2004;279:20108–17.
[128] Muñoz JP, Ivanova S, Sánchez-Wandelmer J, Martínez-Cristóbal P, Noguera E, Sancho A, et al. Mfn2 modulates the UPR and mitochondrial function via repression of PERK. EMBO J 2013;32:2348–61.
[129] Novoa I, Zeng H, Harding HP, Ron D. Feedback inhibition of the unfolded protein response by GADD34-mediated dephosphorylation of eIF2α. J Cell Biol 2001;153:1011–22.
[130] Wang Y, Shen J, Arenzana N, Tirasophon W, Kaufman RJ, Prywes R. Activation of ATF6 and an ATF6 DNA binding site by the endoplasmic reticulum stress response. Journal of Biological Chemistry 2000;275:27013–20.
[131] Yamamoto K, Sato T, Matsui T, Sato M, Okada T, Yoshida H, et al. Transcriptional induction of mammalian ER quality control proteins is mediated by single or combined action of ATF6α and XBP1. Dev Cell 2007;13:365–76.
[132] Paxman R, Plate L, Blackwood EA, Glembotski C, Powers ET, Wiseman RL, et al. Pharmacologic ATF6 activating compounds are metabolically activated to selectively modify endoplasmic reticulum proteins. Elife 2018;7:e37168.
[133] Shoulders MD, Ryno LM, Genereux JC, Moresco JJ, Tu PG, Wu C, et al. Stress-independent activation of XBP1s and/or ATF6 reveals three functionally diverse ER proteostasis environments. Cell Rep 2013;3:1279–92.
[134] Yoshida H, Matsui T, Yamamoto A, Okada T, Mori K. XBP1 mRNA is induced by ATF6 and spliced by IRE1 in response to ER stress to produce a highly active transcription factor. Cell 2001;107:881–91.
[135] Fagone P, Jackowski S. Membrane phospholipid synthesis and endoplasmic reticulum function. J Lipid Res 2009;50:S311–6.
[136] Wang S, Chen Z, Lam V, Han J, Hassler J, Finck BN, et al. IRE1α-XBP1s induces PDI expression to increase MTP activity for hepatic VLDL assembly and lipid homeostasis. Cell Metab 2012;16:473–86.

[137] Ji C, Kaplowitz N, Lau MY, Kao E, Petrovic LM, Lee AS. Liver-specific loss of glucose-regulated protein 78 perturbs the unfolded protein response and exacerbates a spectrum of liver diseases in mice. Hepatology 2011;54:229–39.
[138] Rutkowski DT, Wu J, Back S-H, Callaghan MU, Ferris SP, Iqbal J, et al. UPR pathways combine to prevent hepatic steatosis caused by ER stress-mediated suppression of transcriptional master regulators. Dev Cell 2008;15:829–40.
[139] Lloyd DJ, Wheeler MC, Gekakis N. A point mutation in Sec61α1 leads to diabetes and hepatosteatosis in mice. Diabetes 2010;59:460–70.
[140] So J-S, Hur KY, Tarrio M, Ruda V, Frank-Kamenetsky M, Fitzgerald K, et al. Silencing of lipid metabolism genes through IRE1α-mediated mRNA decay lowers plasma lipids in mice. Cell Metab 2012;16:487–99.
[141] Lee A-H, Scapa EF, Cohen DE, Glimcher LH. Regulation of hepatic lipogenesis by the transcription factor XBP1. Sciences 2008;320:1492–6.
[142] Herrema H, Zhou Y, Zhang D, Lee J, Hernandez MAS, Shulman GI, et al. XBP1s is an anti-lipogenic protein. Journal of Biological Chemistry 2016;291:17394–404.
[143] Zhang K, Wang S, Malhotra J, Hassler JR, Back SH, Wang G, et al. The unfolded protein response transducer IRE1α prevents ER stress-induced hepatic steatosis. EMBO J 2011;30:1357–75.
[144] Zeng L, Lu M, Mori K, Luo S, Lee AS, Zhu Y, et al. ATF6 modulates SREBP2-mediated lipogenesis. EMBO J 2008;27:2941.
[145] Basseri S, Austin RC. Endoplasmic reticulum stress and lipid metabolism: mechanisms and therapeutic potential. Biochem Res Int 2012;2012:841362.
[146] Yoshida H. ER stress and diseases. FEBS J 2007;274:630–58.
[147] Pardo V, González-Rodríguez Á, Muntané J, Kozma SC, Valverde ÁM. Role of hepatocyte S6K1 in palmitic acid-induced endoplasmic reticulum stress, lipotoxicity, insulin resistance and in oleic acid-induced protection. Food and Chemical Toxicology 2015;80:298–309.
[148] Zeng X, Zhu M, Liu X, Chen X, Yuan Y, Li L, et al. Oleic acid ameliorates palmitic acid induced hepatocellular lipotoxicity by inhibition of ER stress and pyroptosis. Nutr Metab (Lond) 2020;17:1–14.
[149] Noda I, Fujieda S, Seki M, Tanaka N, Sunaga H, Ohtsubo T, et al. Inhibition of N-linked glycosylation by tunicamycin enhances sensitivity to cisplatin in human head-and-neck carcinoma cells. Int J Cancer 1999;80:279–84.
[150] Bidooki SH, Barranquero C, Sánchez-Marco J, Martínez-Beamonte R, Rodríguez-Yoldi MJ, Navarro MA, et al. TXNDC5 Plays a Crucial Role in Regulating Endoplasmic Reticulum Activity through Different ER Stress Signaling Pathways in Hepatic Cells. Int J Mol Sci 2024;25:7128.
[151] Chawsheen HA, Jiang H, Ying Q, Ding N, Thapa P, Wei Q. The redox regulator sulfiredoxin forms a complex with thioredoxin domain–containing 5 protein in response to ER stress in lung cancer cells. Journal of Biological Chemistry 2019;294:8991–9006.
[152] Wang X, Li H, Chang X. The role and mechanism of TXNDC5 in diseases. Eur J Med Res 2022;27:145.
[153] Hung C-T, Tsai Y-W, Wu Y-S, Yeh C-F, Yang K-C. The novel role of ER protein TXNDC5 in the pathogenesis of organ fibrosis: mechanistic insights and therapeutic implications. J Biomed Sci 2022;29:63.

[154] Okumura M, Kadokura H, Inaba K. Structures and functions of protein disulfide isomerase family members involved in proteostasis in the endoplasmic reticulum. Free Radic Biol Med 2015;83:314–22.
[155] Kuribara T, Totani K. Structural insights into N-linked glycan-mediated protein folding from chemical and biological perspectives. Curr Opin Struct Biol 2021;68:41–7.
[156] Janssen-Heininger Y, Reynaert NL, van der Vliet A, Anathy V. Endoplasmic reticulum stress and glutathione therapeutics in chronic lung diseases. Redox Biol 2020;33:101516.
[157] Hirayama C, Machida K, Noi K, Murakawa T, Okumura M, Ogura T, et al. Distinct roles and actions of protein disulfide isomerase family enzymes in catalysis of nascent-chain disulfide bond formation. IScience 2021;24:102296.
[158] Smirnova OA, Bartosch B, Zakirova NF, Kochetkov SN, Ivanov A V. Polyamine metabolism and oxidative protein folding in the ER as ROS-producing systems neglected in virology. Int J Mol Sci 2018;19:1219.
[159] Victor P, Sarada D, Ramkumar KM. Crosstalk between endoplasmic reticulum stress and oxidative stress: Focus on protein disulfide isomerase and endoplasmic reticulum oxidase 1. Eur J Pharmacol 2021;892:173749.
[160] Sandamalika WMG, Samaraweera AV, Yang H, Lee J. A newly discovered teleost disulfide isomerase, thioredoxin domain containing 5 (TXNDC5), from big-belly seahorse (Hippocampus abdominalis): Insights into its molecular and functional properties and immune regulatory functions. Dev Comp Immunol 2021;114:103827.
[161] Horna-Terrón E, Pradilla-Dieste A, Sánchez-de-Diego C, Osada J. TXNDC5, a newly discovered disulfide isomerase with a key role in cell physiology and pathology. Int J Mol Sci 2014;15:23501–18.
[162] Tassano E, Uccella S, Severino M, Giacomini T, Nardi F, Gimelli G, et al. Expanding the phenotype associated with interstitial 6p25. 1p24. 3 microdeletion: a new case and review of the literature. J Genet 2021;100:1–6.
[163] Li P, Li Y, Ma L. Potential role of chimeric genes in pathway-related gene co-expression modules. World J Surg Oncol 2021;19:149.
[164] Mallén-Ponce MJ, Huertas MJ, Florencio FJ. Exploring the diversity of the thioredoxin systems in cyanobacteria. Antioxidants 2022;11:654.
[165] Marcuello C, Frempong GA, Balsera M, Medina M, Lostao A. Atomic force microscopy to elicit conformational transitions of ferredoxin-dependent flavin thioredoxin reductases. Antioxidants 2021;10:1437.
[166] Cheng F, Ji Q, Wang L, Wang C, Liu G, Wang L. Reducing oxidative protein folding alleviates senescence by minimizing ER-to-nucleus H2O2 release. EMBO Rep 2023;24:e56439.
[167] Arai K, Ueno H, Asano Y, Chakrabarty G, Shimodaira S, Mugesh G, et al. Protein Folding in the Presence of Water-Soluble Cyclic Diselenides with Novel Oxidoreductase and Isomerase Activities. ChemBioChem 2018;19:207–11.
[168] Matsusaki M, Okada R, Tanikawa Y, Kanemura S, Ito D, Lin Y, et al. Functional interplay between p5 and pdi/erp72 to drive protein folding. Biology (Basel) 2021;10:1112.
[169] Varadi M, Bertoni D, Magana P, Paramval U, Pidruchna I, Radhakrishnan M, et al. AlphaFold Protein Structure Database in 2024: providing structure coverage for over 214 million protein sequences. Nucleic Acids Res 2024;52:D368–75.
[170] Jumper J, Evans R, Pritzel A, Green T, Figurnov M, Ronneberger O, et al. Highly accurate protein structure prediction with AlphaFold. Nature 2021;596:583–9.

[171] Rauluseviciute I, Riudavets-Puig R, Blanc-Mathieu R, Castro-Mondragon JA, Ferenc K, Kumar V, et al. JASPAR 2024: 20th anniversary of the open-access database of transcription factor binding profiles. Nucleic Acids Res 2024;52:D174–82.
[172] Yeh C-F, Cheng S-H, Lin Y-S, Shentu T-P, Huang R-T, Zhu J, et al. Targeting mechanosensitive endothelial TXNDC5 to stabilize eNOS and reduce atherosclerosis in vivo. Sci Adv 2022;8:eabl8096.
[173] Shih Y-C, Chen C-L, Zhang Y, Mellor RL, Kanter EM, Fang Y, et al. Endoplasmic reticulum protein TXNDC5 augments myocardial fibrosis by facilitating extracellular matrix protein folding and redox-sensitive cardiac fibroblast activation. Circ Res 2018;122:1052–68.
[174] Wynn T. Cellular and molecular mechanisms of fibrosis. The Journal of Pathology: A Journal of the Pathological Society of Great Britain and Ireland 2008;214:199–210.
[175] Lee T-H, Yeh C-F, Lee Y-T, Shih Y-C, Chen Y-T, Hung C-T, et al. Fibroblast-enriched endoplasmic reticulum protein TXNDC5 promotes pulmonary fibrosis by augmenting TGFβ signaling through TGFBR1 stabilization. Nat Commun 2020;11:4254.
[176] Chen Y-T, Jhao P-Y, Hung C-T, Wu Y-F, Lin S-J, Chiang W-C, et al. Endoplasmic reticulum protein TXNDC5 promotes renal fibrosis by enforcing TGF-β signaling in kidney fibroblasts. J Clin Invest 2021;131:e143645.
[177] Hung C-T, Su T-H, Chen Y-T, Wu Y-F, Chen Y-T, Lin S-J, et al. Targeting ER protein TXNDC5 in hepatic stellate cell mitigates liver fibrosis by repressing non-canonical TGFβ signalling. Gut 2022;71:1876–91.
[178] Lampropoulou E, Lymperopoulou A, Charonis A. Reduced expression of ERp46 under diabetic conditions in β-cells and the effect of liraglutide. Metabolism 2016;65:7–15.
[179] Li J, Chen Y, Liu Q, Tian Z, Zhang Y. Mechanistic and therapeutic links between rheumatoid arthritis and diabetes mellitus. Clin Exp Med 2023;23:287–99.
[180] Turkyilmaz A, Lee Y, Lee MK. Fermented extract of mealworm (Tenebrio molitor larvae) as a dietary protein source modulates hepatic proteomic profiles in C57BLKS/J-db/db mice. J Insects Food Feed 2023;9:1199–210.
[181] Cheng SH, Yeh CF, Fang Y, Yang KC. P593 Endoplasmic reticulum protein thioredoxin domain containing 5 (TXNDC5) is a novel mediator of endothelial dysfunction and atherosclerosis. Eur Heart J 2018;39:ehy564-P593.
[182] Zhou J, Wu Y, Rauova L, Koma G, Wang L, Poncz M, et al. A novel role for endoplasmic reticulum protein 46 (ERp46) in platelet function and arterial thrombosis in mice. Blood, The Journal of the American Society of Hematology 2022;139:2050–65.
[183] Nassar A, El-Rauf A, Mohammed S, Mostafa A. Evaluation of Serum Level of Thioredoxin and its Gene Polymorphism in Diagnosis of Hepatocellular Carcinoma of HCV-Infected Patients. Benha Medical Journal 2020;37:111–30.
[184] Sánchez-Marco J, Martínez-Beamonte R, Diego A De, Herrero-Continente T, Barranquero C, Arnal C, et al. Thioredoxin domain containing 5 suppression elicits serum amyloid A-containing high-density lipoproteins. Biomedicines 2022;10:709.
[185] Kern P, Balzer NR, Blank N, Cygon C, Wunderling K, Bender F, et al. Creld2 function during unfolded protein response is essential for liver metabolism homeostasis. FASEB J 2021;35:e21939.
[186] Karatas E, Raymond A-A, Leon C, Dupuy J-W, Di-Tommaso S, Senant N, et al. Hepatocyte proteomes reveal the role of protein disulfide isomerase 4 in alpha 1-antitrypsin deficiency. JHEP Reports 2021;3:100297.

[187] Bidooki SH, Alejo T, Sánchez-Marco J, Martínez-Beamonte R, Abuobeid R, Burillo JC, et al. Squalene loaded nanoparticles effectively protect hepatic AML12 cell lines against oxidative and endoplasmic reticulum stress in a TXNDC5-dependent way. Antioxidants 2022;11:581.
[188] Sánchez-Marco J, Bidooki SH, Abuobeid R, Barranquero C, Herrero-Continente T, Arnal C, et al. Thioredoxin domain containing 5 is involved in the hepatic storage of squalene into lipid droplets in a sex-specific way. J Nutr Biochem 2024;124:109503.
[189] Davis C, Bryan J, Hodgson J, Murphy K. Definition of the Mediterranean diet: a literature review. Nutrients 2015;7:9139–53.
[190] Hidalgo-Mora JJ, García-Vigara A, Sánchez-Sánchez ML, García-Pérez M-Á, Tarín J, Cano A. The Mediterranean diet: A historical perspective on food for health. Maturitas 2020;132:65–9.
[191] Guasch-Ferré M, Willett WC. The Mediterranean diet and health: A comprehensive overview. J Intern Med 2021;290:549–66.
[192] Nestle M. Mediterranean diets: historical and research overview. Am J Clin Nutr 1995;61:1313S-1320S.
[193] Anania C, Perla FM, Olivero F, Pacifico L, Chiesa C. Mediterranean diet and nonalcoholic fatty liver disease. World J Gastroenterol 2018;24:2083.
[194] Wahrburg U, Kratz M, Cullen P. Mediterranean diet, olive oil and health. European Journal of Lipid Science and Technology 2002;104:698–705.
[195] Lou-Bonafonte JM, Arnal C, Navarro MA, Osada J. Efficacy of bioactive compounds from extra virgin olive oil to modulate atherosclerosis development. Mol Nutr Food Res 2012;56:1043–57.
[196] Sofi F, Macchi C, Abbate R, Gensini GF, Casini A. Mediterranean diet and health. Biofactors 2013;39:335–42.
[197] Battino M, Ferreiro MS. Ageing and the Mediterranean diet: a review of the role of dietary fats. Public Health Nutr 2004;7:953–8.
[198] Scoditti E, Capurso C, Capurso A, Massaro M. Vascular effects of the Mediterranean diet—Part II: Role of omega-3 fatty acids and olive oil polyphenols. Vascul Pharmacol 2014;63:127–34.
[199] Ortega RM. Importance of functional foods in the Mediterranean diet. Public Health Nutr 2006;9:1136–40.
[200] Jimenez-Lopez C, Carpena M, Lourenço-Lopes C, Gallardo-Gomez M, Lorenzo JM, Barba FJ, et al. Bioactive compounds and quality of extra virgin olive oil. Foods 2020;9:1014.
[201] Marquez-Martin A, De La Puerta R, Fernandez-Arche A, Ruiz-Gutierrez V, Yaqoob P. Modulation of cytokine secretion by pentacyclic triterpenes from olive pomace oil in human mononuclear cells. Cytokine 2006;36:211–7.
[202] Oliveras-López M-J, Molina JJM, Mir MV, Rey EF, Martín F, de la Serrana HL-G. Extra virgin olive oil (EVOO) consumption and antioxidant status in healthy institutionalized elderly humans. Arch Gerontol Geriatr 2013;57:234–42.
[203] Nocella C, Cammisotto V, Fianchini L, D'Amico A, Novo M, Castellani V, et al. Extra virgin olive oil and cardiovascular diseases: Benefits for human health. Endocrine, Metabolic & Immune Disorders-Drug Targets (Formerly Current Drug Targets-Immune, Endocrine & Metabolic Disorders) 2018;18:4–13.
[204] Yubero-Serrano EM, Lopez-Moreno J, Gomez-Delgado F, Lopez-Miranda J. Extra virgin olive oil: More than a healthy fat. Eur J Clin Nutr 2019;72:8–17.

[205] Presti G, Guarrasi V, Gulotta E, Provenzano F, Provenzano A, Giuliano S, et al. Bioactive compounds from extra virgin olive oils: Correlation between phenolic content and oxidative stress cell protection. Biophys Chem 2017;230:109–16.
[206] Morgan NR, Magalingam KB, Radhakrishnan AK, Arumugam M, Jamil A, Bhuvanendran S. Explicating the multifunctional roles of tocotrienol and squalene in promoting skin health. Skin Health and Disease 2024;4:e448.
[207] Alongi M, Lucci P, Clodoveo ML, Schena FP, Calligaris S. Oleogelation of extra virgin olive oil by different oleogelators affects the physical properties and the stability of bioactive compounds. Food Chem 2022;368:130779.
[208] Lee O-H, Kim Y-C, Kim K-J, Kim Y-C, Lee B-Y. The effects of bioactive compounds and fatty acid compositions on the oxidative stability of extra virgin olive oil varieties. Food Sci Biotechnol 2007;16:415–20.
[209] Ambra R, Natella F, Lucchetti S, Forte V, Pastore G. α-Tocopherol, β-carotene, lutein, squalene and secoiridoids in seven monocultivar Italian extra-virgin olive oils. Int J Food Sci Nutr 2017;68:538–45.
[210] Popa O, Băbeanu NE, Popa I, Niță S, Dinu-Pârvu CE. Methods for obtaining and determination of squalene from natural sources. Biomed Res Int 2015;2015:367202.
[211] Simon SA, Lis LJ, MacDonald RC, Kauffman JW. The noneffect of a large linear hydrocarbon, squalene, on the phosphatidylcholine packing structure. Biophys J 1977;19:83–90.
[212] Lou-Bonafonte JM, Martínez-Beamonte R, Sanclemente T, Surra JC, Herrera-Marcos L V, Sanchez-Marco J, et al. Current insights into the biological action of squalene. Mol Nutr Food Res 2018;62:1800136.
[213] Spanova M, Daum G. Squalene–biochemistry, molecular biology, process biotechnology, and applications. European Journal of Lipid Science and Technology 2011;113:1299–320.
[214] Shahidi F, Varatharajan V, Peng H, Senadheera R. Utilization of marine by-products for the recovery of value-added products. Journal of Food Bioactives 2019;6:10–61.
[215] Rajaratnam RA, Gylling H, Miettinen TA. Serum squalene in postmenopausal women without and with coronary artery disease. Atherosclerosis 1999;146:61–4.
[216] Abuobeid R, Herrera-Marcos L V, Arnal C, Bidooki SH, Sánchez-Marco J, Lasheras R, et al. Differentially Expressed Genes in Response to a Squalene-Supplemented Diet Are Accurate Discriminants of Porcine Non-Alcoholic Steatohepatitis. Int J Mol Sci 2023;24:12552.
[217] Reddy LH, Couvreur P. Squalene: A natural triterpene for use in disease management and therapy. Adv Drug Deliv Rev 2009;61:1412–26.
[218] Kelly GS. Squalene and its potential clinical uses. Altern Med Rev 1999;4:29–36.
[219] Strandberg TE, Tilvis RS, Miettinen TA. Metabolic variables of cholesterol during squalene feeding in humans: comparison with cholestyramine treatment. J Lipid Res 1990;31:1637–43.
[220] Pham D, Boussouira B, Moyal D, Nguyen QL. Oxidization of squalene, a human skin lipid: a new and reliable marker of environmental pollution studies. Int J Cosmet Sci 2015;37:357–65.
[221] Ronco AL, De Stéfani E. Squalene: a multi-task link in the crossroads of cancer and aging. Functional Foods in Health and Disease 2013;3:462–76.

[222] Sheares BT, White SS, Molowa DT, Chan K, Ding VDH, Kroon PA, et al. Cloning, analysis, and bacterial expression of human farnesyl pyrophosphate synthetase and its regulation in Hep G2 cells. Biochemistry 1989;28:8129–35.
[223] Herrera-Marcos L V, Martínez-Beamonte R, Arnal C, Barranquero C, Puente-Lanzarote JJ, Herrero-Continente T, et al. Dietary squalene supplementation decreases triglyceride species and modifies phospholipid lipidomic profile in the liver of a porcine model of non-alcoholic steatohepatitis. J Nutr Biochem 2023;112:109207.
[224] Martínez-Beamonte R, Alda O, Sanclemente T, Felices MJ, Escusol S, Arnal C, et al. Hepatic subcellular distribution of squalene changes according to the experimental setting. J Physiol Biochem 2018;74:531–8.
[225] Kouvedaki I, Pappas AC, Surai PF, Zoidis E. Nutrigenomics of natural antioxidants in broilers. Antioxidants 2024;13:270.
[226] Luke SS, Raj MN, Ramesh S, Bhatt NP. Network pharmacology prediction and molecular docking-based strategy to explore the potential mechanism of squalene against inflammation. In Silico Pharmacol 2024;12:44.
[227] Widyawati T, Syahputra RA, Syarifah S, Sumantri IB. Analysis of Antidiabetic Activity of Squalene via In Silico and In Vivo Assay. Molecules 2023;28:3783.
[228] Cheng Y, Ferdousi F, Foronda BA, Linh TN, Ganbold M, Yada A, et al. A comparative transcriptomics analysis reveals ethylene glycol derivatives of squalene ameliorate excessive lipogenesis and inflammatory response in 3T3-L1 preadipocytes. Heliyon 2024;10:e26867.
[229] Nathan JA. Squalene and cholesterol in the balance at the ER membrane. Proceedings of the National Academy of Sciences 2020;117:8228–30.
[230] Porter FD, Herman GE. Malformation syndromes caused by disorders of cholesterol synthesis. J Lipid Res 2011;52:6–34.
[231] Kandutsch AA, Russell AE. Preputial Gland Tumor Sterols: II. THE IDENTIFICATION OF 4α-METHYL-Δ8-CHOLESTEN-3β-OL. Journal of Biological Chemistry 1960;235:2253–5.
[232] Lee J, Roh J-L. Cholesterol-ferroptosis nexus: Unveiling novel cancer therapeutic avenues. Cancer Lett 2024;597:217046.
[233] Cerqueira NM, Oliveira EF, Gesto DS, Santos-Martins D, Moreira C, Moorthy HN, et al. Cholesterol biosynthesis: a mechanistic overview. Biochemistry 2016;55:5483–506.
[234] Woodward RB, Bloch K. The cyclization of squalene in cholesterol synthesis. J Am Chem Soc 1953;75:2023–4.
[235] Kumar P, Robins A, Vardoulakis S, Britter R. A review of the characteristics of nanoparticles in the urban atmosphere and the prospects for developing regulatory controls. Atmos Environ 2010;44:5035–52.
[236] Khan S, Hossain MK. Classification and properties of nanoparticles. Nanoparticle-based polymer composites, Elsevier; 2022, p. 15–54.
[237] Altammar KA. A review on nanoparticles: characteristics, synthesis, applications, and challenges. Front Microbiol 2023;14:1155622.
[238] Mody V V, Siwale R, Singh A, Mody HR. Introduction to metallic nanoparticles. J Pharm Bioallied Sci 2010;2:282–9.
[239] Kumar H, Venkatesh N, Bhowmik H, Kuila A. Metallic nanoparticle: a review. Biomed J Sci Tech Res 2018;4:3765–75.
[240] Thakkar KN, Mhatre SS, Parikh RY. Biological synthesis of metallic nanoparticles. Nanomedicine 2010;6:257–62.

[241] C Thomas S, Kumar Mishra P, Talegaonkar S. Ceramic nanoparticles: fabrication methods and applications in drug delivery. Curr Pharm Des 2015;21:6165–88.
[242] Singh D, Singh S, Sahu J, Srivastava S, Singh MR. Ceramic nanoparticles: Recompense, cellular uptake and toxicity concerns. Artif Cells Nanomed Biotechnol 2016;44:401–9.
[243] D'Amato R, Falconieri M, Gagliardi S, Popovici E, Serra E, Terranova G, et al. Synthesis of ceramic nanoparticles by laser pyrolysis: from research to applications. J Anal Appl Pyrolysis 2013;104:461–9.
[244] Vollath D, Szabo DV, Hauβelt J. Synthesis and properties of ceramic nanoparticles and nanocomposites. J Eur Ceram Soc 1997;17:1317–24.
[245] Dizaj SM, Mennati A, Jafari S, Khezri K, Adibkia K. Antimicrobial activity of carbon-based nanoparticles. Adv Pharm Bull 2015;5:19.
[246] Markovic ZM, Harhaji-Trajkovic LM, Todorovic-Markovic BM, Kepić DP, Arsikin KM, Jovanović SP, et al. In vitro comparison of the photothermal anticancer activity of graphene nanoparticles and carbon nanotubes. Biomaterials 2011;32:1121–9.
[247] Nasr MS, Esmaeilnezhad E, Choi HJ. Effect of carbon-based and metal-based nanoparticles on enhanced oil recovery: A review. J Mol Liq 2021;338:116903.
[248] Morimoto Y, Horie M, Kobayashi N, Shinohara N, Shimada M. Inhalation toxicity assessment of carbon-based nanoparticles. Acc Chem Res 2013;46:770–81.
[249] Zhang G, Niu A, Peng S, Jiang M, Tu Y, Li M, et al. Formation of novel polymeric nanoparticles. Acc Chem Res 2001;34:249–56.
[250] Elsabahy M, Wooley KL. Design of polymeric nanoparticles for biomedical delivery applications. Chem Soc Rev 2012;41:2545–61.
[251] Lai P, Daear W, Löbenberg R, Prenner EJ. Overview of the preparation of organic polymeric nanoparticles for drug delivery based on gelatine, chitosan, poly(d,l-lactide-co-glycolic acid) and polyalkylcyanoacrylate. Colloids Surf B Biointerfaces 2014;118:154–63.
[252] Astete CE, Sabliov CM. Synthesis and characterization of PLGA nanoparticles. J Biomater Sci Polym Ed 2006;17:247–89.
[253] Divya K, Jisha MS. Chitosan nanoparticles preparation and applications. Environ Chem Lett 2018;16:101–12.
[254] Govender T, Riley T, Ehtezazi T, Garnett MC, Stolnik S, Illum L, et al. Defining the drug incorporation properties of PLA–PEG nanoparticles. Int J Pharm 2000;199:95–110.
[255] Nagavarma BVN, Yadav HKS, Ayaz A, Vasudha LS, Shivakumar HG. Different techniques for preparation of polymeric nanoparticles-a review. Asian J Pharm Clin Res 2012;5:16–23.
[256] Crucho CIC, Barros MT. Polymeric nanoparticles: A study on the preparation variables and characterization methods. Materials Science and Engineering: C 2017;80:771–84.
[257] Sarkar C, Kommineni N, Butreddy A, Kumar R, Bunekar N, Gugulothu K. PLGA nanoparticles in drug delivery. Nanoengineering of Biomaterials, Wiley Online Library; 2022, p. 217–60.
[258] Khan I, Gothwal A, Sharma AK, Kesharwani P, Gupta L, Iyer AK, et al. PLGA nanoparticles and their versatile role in anticancer drug delivery. Crit Rev Ther Drug Carrier Syst 2016;33:159–93.
[259] Bala I, Hariharan S, Kumar MNVR. PLGA nanoparticles in drug delivery: the state of the art. Crit Rev Ther Drug Carrier Syst 2004;21:387–422.
[260] Zhang L, Gu FX, Chan JM, Wang AZ, Langer RS, Farokhzad OC. Nanoparticles in medicine: therapeutic applications and developments. Clin Pharmacol Ther 2008;83:761–9.

[261] Danhier F, Ansorena E, Silva JM, Coco R, Le Breton A, Préat V. PLGA-based nanoparticles: an overview of biomedical applications. Journal of Controlled Release 2012;161:505–22.
[262] Garg U, Chauhan S, Nagaich U, Jain N. Current advances in chitosan nanoparticles based drug delivery and targeting. Adv Pharm Bull 2019;9:195.
[263] Tajmir-Riahi HA, Nafisi S, Sanyakamdhorn S, Agudelo D, Chanphai P. Applications of chitosan nanoparticles in drug delivery. Drug Delivery System 2014;1141:165–84.
[264] Mohammed MA, Syeda JTM, Wasan KM, Wasan EK. An overview of chitosan nanoparticles and its application in non-parenteral drug delivery. Pharmaceutics 2017;9:53.
[265] Nagpal K, Singh SK, Mishra DN. Chitosan nanoparticles: a promising system in novel drug delivery. Chem Pharm Bull (Tokyo) 2010;58:1423–30.
[266] Bashir SM, Ahmed Rather G, Patrício A, Haq Z, Sheikh AA, Shah MZ ul H, et al. Chitosan nanoparticles: a versatile platform for biomedical applications. Materials 2022;15:6521.
[267] Boominathan T, Sivaramakrishna A. Recent advances in the synthesis, properties, and applications of modified chitosan derivatives: challenges and opportunities. Top Curr Chem 2021;379:1–57.
[268] Wu JC, Merlino G, Fausto N. Establishment and characterization of differentiated, nontransformed hepatocyte cell lines derived from mice transgenic for transforming growth factor alpha. Proceedings of the National Academy of Sciences 1994;91:674–8.
[269] Dumenco L, Oguey D, Wu J, Messier N, Fausto N. Introduction of a murine p53 mutation corresponding to human codon 249 into a murine hepatocyte cell line results in growth advantage, but not in transformation. Hepatology 1995;22:1279–88.
[270] Castell J V, Jover R, Martnez-Jimnez CP, Gmez-Lechn MJ. Hepatocyte cell lines: their use, scope and limitations in drug metabolism studies. Expert Opin Drug Metab Toxicol 2006;2:183–212.
[271] Ao N, Yang J, Wang X, Du J. Glucagon-like peptide-1 preserves non-alcoholic fatty liver disease through inhibition of the endoplasmic reticulum stress-associated pathway. Hepatology Research 2016;46:343–53.
[272] Heiker JT, Kosel D, Beck-Sickinger AG. Molecular mechanisms of signal transduction via adiponectin and adiponectin receptors. Biol Chem 2010;391:1005–18.
[273] Charlton HK, Webster J, Kruger S, Simpson F, Richards AA, Whitehead JP. ERp46 binds to AdipoR1, but not AdipoR2, and modulates adiponectin signalling. Biochem Biophys Res Commun 2010;392:234–9.
[274] Dores-Silva PR, Cauvi DM, Kiraly VTR, Borges JC, De Maio A. Human HSPA9 (mtHsp70, mortalin) interacts with lipid bilayers containing cardiolipin, a major component of the inner mitochondrial membrane. Biochimica et Biophysica Acta (BBA)-Biomembranes 2020;1862:183436.
[275] Ornatsky OI, Connor MK, Hood DA. Expression of stress proteins and mitochondrial chaperonins in chronically stimulated skeletal muscle. Biochemical Journal 1995;311:119–23.
[276] Xu J, Xiao HH, Sartorelli AC. Attenuation of the induced differentiation of HL-60 leukemia cells by mitochondrial chaperone HSP70. Oncol Res 1999;11:429–35.
[277] Pizzatti L, Sá LA, de Souza JM, Bisch PM, Abdelhay E. Altered protein profile in chronic myeloid leukemia chronic phase identified by a comparative proteomic study. Biochimica et Biophysica Acta (BBA)-Proteins and Proteomics 2006;1764:929–42.

[278] Takano S, Wadhwa R, Yoshii Y, Nose T, Kaul SC, Mitsui Y. Elevated levels of mortalin expression in human brain tumors. Exp Cell Res 1997;237:38–45.
[279] Rozenberg P, Kocsis J, Saar M, Prohászka Z, Füst G, Fishelson Z. Elevated levels of mitochondrial mortalin and cytosolic HSP70 in blood as risk factors in patients with colorectal cancer. Int J Cancer 2013;133:514–8.
[280] Wadhwa R, Takano S, Kaur K, Deocaris CC, Pereira-Smith OM, Reddel RR, et al. Upregulation of mortalin/mthsp70/Grp75 contributes to human carcinogenesis. Int J Cancer 2006;118:2973–80.
[281] Yi X, Luk JM, Lee NP, Peng J, Leng X, Guan X-Y, et al. Association of mortalin (HSPA9) with liver cancer metastasis and prediction for early tumor recurrence. Molecular & Cellular Proteomics 2008;7:315–25.
[282] Wadhwa R, Takano S, Taira K, Kaul SC. Reduction in mortalin level by its antisense expression causes senescence-like growth arrest in human immortalized cells. The Journal of Gene Medicine: A Cross-disciplinary Journal for Research on the Science of Gene Transfer and Its Clinical Applications 2004;6:439–44.
[283] Hofmann B, Hecht H-J, Flohé L. Peroxiredoxins. Biol Chem 2002;383:347–64.
[284] Munz B, Frank S, Hubner G, Olsen E, Werner S. A novel type of glutathione peroxidase: expression and regulation during wound repair. Biochemical Journal 1997;326:579–85.
[285] Rhee SG, Chae HZ, Kim K. Peroxiredoxins: a historical overview and speculative preview of novel mechanisms and emerging concepts in cell signaling. Free Radic Biol Med 2005;38:1543–52.
[286] Sparling NE, Phelan SA. Identification of multiple transcripts for antioxidant protein 2 (Aop2): differential regulation by oxidative stress and growth factors. Redox Report 2003;8:87–94.
[287] Hershko A, Ciechanover A. The ubiquitin system. Annu Rev Biochem 1998;67:425–79.
[288] Chen L, Madura K. Increased proteasome activity, ubiquitin-conjugating enzymes, and eEF1A translation factor detected in breast cancer tissue. Cancer Res 2005;65:5599–606.
[289] Arlt A, Bauer I, Schafmayer C, Tepel J, Müerköster SS, Brosch M, et al. Increased proteasome subunit protein expression and proteasome activity in colon cancer relate to an enhanced activation of nuclear factor E2-related factor 2 (Nrf2). Oncogene 2009;28:3983–96.
[290] Quero J, Cabello S, Fuertes T, Mármol I, Laplaza R, Polo V, et al. Proteasome versus thioredoxin reductase competition as possible biological targets in antitumor mixed thiolate-dithiocarbamate gold (III) complexes. Inorg Chem 2018;57:10832–45.
[291] Pak JH, Manevich Y, Kim HS, Feinstein SI, Fisher AB. An antisense oligonucleotide to 1-cys peroxiredoxin causes lipid peroxidation and apoptosis in lung epithelial cells. Journal of Biological Chemistry 2002;277:49927–34.
[292] Manevich Y, Sweitzer T, Pak JH, Feinstein SI, Muzykantov V, Fisher AB. 1-Cys peroxiredoxin overexpression protects cells against phospholipid peroxidation-mediated membrane damage. Proceedings of the National Academy of Sciences 2002;99:11599–604.
[293] Sharapov MG, Novoselov VI, Gudkov S V. Radioprotective role of peroxiredoxin 6. Antioxidants 2019;8:15.
[294] Yun H-M, Park K-R, Lee HP, Lee DH, Jo M, Shin DH, et al. PRDX6 promotes lung tumor progression via its GPx and iPLA2 activities. Free Radic Biol Med 2014;69:367–76.

[295] Lu B, Chen X, Hong Y, Zhu H, He Q, Yang B, et al. Identification of PRDX6 as a regulator of ferroptosis. Acta Pharmacol Sin 2019;40:1334–42.
[296] Goswami AV, Chittoor B, D'Silva P. Understanding the functional interplay between mammalian mitochondrial Hsp70 chaperone machine components. Journal of Biological Chemistry 2010;285:19472–82.
[297] Krysiak K, Tibbitts JF, Shao J, Liu T, Ndonwi M, Walter MJ. Reduced levels of Hspa9 attenuate Stat5 activation in mouse B cells. Exp Hematol 2015;43:319–30.
[298] Dhennin-Duthille I, Nyga R, Yahiaoui S, Gouilleux-Gruart V, Regnier A, Lassoued K, et al. The tumor suppressor hTid1 inhibits STAT5b activity via functional interaction. Journal of Biological Chemistry 2011;286:5034–42.
[299] Gooljarsingh LT, Fernandes C, Yan K, Zhang H, Grooms M, Johanson K, et al. A biochemical rationale for the anticancer effects of Hsp90 inhibitors: slow, tight binding inhibition by geldanamycin and its analogues. Proceedings of the National Academy of Sciences 2006;103:7625–30.
[300] Pascale RM, Simile MM, Calvisi DF, Frau M, Muroni MR, Seddaiu MA, et al. Role of HSP90, CDC37, and CRM1 as modulators of P16INK4A activity in rat liver carcinogenesis and human liver cancer. Hepatology 2005;42:1310–9.
[301] Guo W, Yan L, Yang L, Liu X, E Q, Gao P, et al. Targeting GRP75 improves HSP90 inhibitor efficacy by enhancing p53-mediated apoptosis in hepatocellular carcinoma. PLoS One 2014;9:e85766.
[302] Bassot A, Prip-Buus C, Alves A, Berdeaux O, Perrier J, Lenoir V, et al. Loss and gain of function of Grp75 or mitofusin 2 distinctly alter cholesterol metabolism, but all promote triglyceride accumulation in hepatocytes. Biochimica et Biophysica Acta (BBA)-Molecular and Cell Biology of Lipids 2021;1866:159030.
[303] Liu T, Krysiak K, Shirai CL, Kim S, Shao J, Ndonwi M, et al. Knockdown of HSPA9 induces TP53-dependent apoptosis in human hematopoietic progenitor cells. PLoS One 2017;12:e0170470.
[304] Kanehisa M. Toward understanding the origin and evolution of cellular organisms. Protein Science 2019;28:1947–51.
[305] Almaghlouth IA, Mohamed JY, Al-Amoudi M, Al-Ahaidib L, Al-Odaib A, Alkuraya FS. 5-Oxoprolinase deficiency: report of the first human OPLAH mutation. Clin Genet 2012;82:193–6.
[306] Wiegand H, Boesch-Saadatmandi C, Regos I, Treutter D, Wolffram S, Rimbach G. Effects of quercetin and catechin on hepatic glutathione-S transferase (GST), NAD (P) H quinone oxidoreductase 1 (NQO1), and antioxidant enzyme activity levels in rats. Nutr Cancer 2009;61:717–22.
[307] Wang J, Shanmugam A, Markand S, Zorrilla E, Ganapathy V, Smith SB. Sigma 1 receptor regulates the oxidative stress response in primary retinal Müller glial cells via NRF2 signaling and system xc−, the Na+-independent glutamate–cystine exchanger. Free Radic Biol Med 2015;86:25–36.
[308] Parl FF. Glutathione S-transferase genotypes and cancer risk. Cancer Lett 2005;221:123–9.
[309] López-Grueso MJ, Lagal DJ, García-Jiménez ÁF, Tarradas RM, Carmona-Hidalgo B, Peinado J, et al. Knockout of PRDX6 induces mitochondrial dysfunction and cell cycle arrest at G2/M in HepG2 hepatocarcinoma cells. Redox Biol 2020;37:101737.

[310] Chen J, Cao X, Qin X, Liu H, Chen S, Zhong S, et al. Proteomic analysis of the molecular mechanism of curcumin/β-cyclodextrin polymer inclusion complex inhibiting HepG2 cells growth. J Food Biochem 2020;44:e13119.
[311] Azimi A, Kaufman KL, Ali M, Arthur J, Kossard S, Fernandez-Penas P. Differential proteomic analysis of actinic keratosis, Bowen's disease and cutaneous squamous cell carcinoma by label-free LC–MS/MS. J Dermatol Sci 2018;91:69–78.
[312] Yafune A, Kawai M, Itahashi M, Kimura M, Nakane F, Mitsumori K, et al. Global DNA methylation screening of liver in piperonyl butoxide-treated mice in a two-stage hepatocarcinogenesis model. Toxicol Lett 2013;222:295–302.
[313] Francavilla R, Castellaneta SP, Hadzic N, Chambers SM, Portmann B, Tung J, et al. Prognosis of alpha-1-antitrypsin deficiency-related liver disease in the era of paediatric liver transplantion. J Hepatol 2000;32:986–92.
[314] Alberti A, Karamessinis P, Peroulis M, Kypreou K, Kavvadas P, Pagakis S, et al. ERp46 is reduced by high glucose and regulates insulin content in pancreatic β-cells. American Journal of Physiology-Endocrinology and Metabolism 2009;297:E812–21.
[315] Chen D-L, Xiang J-N, Yang L-Y. Role of ERp46 in β-cell lipoapoptosis through endoplasmic reticulum stress pathway as well as the protective effect of exendin-4. Biochem Biophys Res Commun 2012;426:324–9.
[316] Zhou L, Zhang J, Fang Q, Liu M, Liu X, Jia W, et al. Autophagy-mediated insulin receptor down-regulation contributes to endoplasmic reticulum stress-induced insulin resistance. Mol Pharmacol 2009;76:596–603.
[317] Kammoun HL, Chabanon H, Hainault I, Luquet S, Magnan C, Koike T, et al. GRP78 expression inhibits insulin and ER stress–induced SREBP-1c activation and reduces hepatic steatosis in mice. J Clin Invest 2009;119:1201–15.
[318] Peng F, Zhang H, Du Y, Tan P. Cetuximab enhances cisplatin-induced endoplasmic reticulum stress-associated apoptosis in laryngeal squamous cell carcinoma cells by inhibiting expression of TXNDC5. Mol Med Rep 2018;17:4767–76.
[319] Tan F, Zhu H, He X, Yu N, Zhang X, Xu H, et al. Role of TXNDC5 in tumorigenesis of colorectal cancer cells: In vivo and in vitro evidence. Int J Mol Med 2018;42:935–45.
[320] DeZwaan-McCabe D, Sheldon RD, Gorecki MC, Guo D-F, Gansemer ER, Kaufman RJ, et al. ER stress inhibits liver fatty acid oxidation while unmitigated stress leads to anorexia-induced lipolysis and both liver and kidney steatosis. Cell Rep 2017;19:1794–806.
[321] Li T, Zhao H, Guo G, Xia S, Wang L. VMP1 affects endoplasmic reticulum stress sensitivity via differential modulation of the three unfolded protein response arms. Cell Rep 2023;42:112209.
[322] Bidoki SH, Bayatani A, Sarlak M, Rasouli M, Mostafaie P, Saghafi M, et al. Assessing expression of TGF-B2 and PCDH9 genes in breast cancer patients. Age (Omaha) 2018;7:20.
[323] Reddy RK, Mao C, Baumeister P, Austin RC, Kaufman RJ, Lee AS. Endoplasmic reticulum chaperone protein GRP78 protects cells from apoptosis induced by topoisomerase inhibitors: role of ATP binding site in suppression of caspase-7 activation. Journal of Biological Chemistry 2003;278:20915–24.
[324] Werstuck GH, Lentz SR, Dayal S, Hossain GS, Sood SK, Shi YY, et al. Homocysteine-induced endoplasmic reticulum stress causes dysregulation of the cholesterol and triglyceride biosynthetic pathways. J Clin Invest 2001;107:1263–73.

[325] Cazanave SC, Mott JL, Elmi NA, Bronk SF, Werneburg NW, Akazawa Y, et al. JNK1-dependent PUMA expression contributes to hepatocyte lipoapoptosis. Journal of Biological Chemistry 2009;284:26591–602.
[326] Howie J, Tulloch LB, Brown E, Reilly L, Ashford FB, Kennedy J, et al. Glutathione-dependent depalmitoylation of phospholemman by peroxiredoxin 6. Cell Rep 2024;43:113679.
[327] Harding HP, Zeng H, Zhang Y, Jungries R, Chung P, Plesken H, et al. Diabetes mellitus and exocrine pancreatic dysfunction in perk−/− mice reveals a role for translational control in secretory cell survival. Mol Cell 2001;7:1153–63.
[328] Harding HP, Zhang Y, Zeng H, Novoa I, Lu PD, Calfon M, et al. An integrated stress response regulates amino acid metabolism and resistance to oxidative stress. Mol Cell 2003;11:619–33.
[329] Oyadomari S, Mori M. Roles of CHOP/GADD153 in endoplasmic reticulum stress. Cell Death Differ 2004;11:381–9.
[330] McCullough KD, Martindale JL, Klotz L-O, Aw T-Y, Holbrook NJ. Gadd153 sensitizes cells to endoplasmic reticulum stress by down-regulating Bcl2 and perturbing the cellular redox state. Mol Cell Biol 2001;21:1249–59.
[331] Yamaguchi H, Wang H-G. CHOP is involved in endoplasmic reticulum stress-induced apoptosis by enhancing DR5 expression in human carcinoma cells. Journal of Biological Chemistry 2004;279:45495–502.
[332] Marciniak SJ, Yun CY, Oyadomari S, Novoa I, Zhang Y, Jungreis R, et al. CHOP induces death by promoting protein synthesis and oxidation in the stressed endoplasmic reticulum. Genes Dev 2004;18:3066–77.
[333] Tsuru A, Fujimoto N, Takahashi S, Saito M, Nakamura D, Iwano M, et al. Negative feedback by IRE1β optimizes mucin production in goblet cells. Proceedings of the National Academy of Sciences 2013;110:2864–9.
[334] Sriburi R, Jackowski S, Mori K, Brewer JW. XBP1: a link between the unfolded protein response, lipid biosynthesis, and biogenesis of the endoplasmic reticulum. J Cell Biol 2004;167:35–41.
[335] Novoa I, Zhang Y, Zeng H, Jungreis R, Harding HP, Ron D. Stress-induced gene expression requires programmed recovery from translational repression. EMBO J 2003;22:1180–7.
[336] Lisbona F, Rojas-Rivera D, Thielen P, Zamorano S, Todd D, Martinon F, et al. BAX inhibitor-1 is a negative regulator of the ER stress sensor IRE1α. Mol Cell 2009;33:679–91.
[337] Reimold AM, Etkin A, Clauss I, Perkins A, Friend DS, Zhang J, et al. An essential role in liver development for transcription factor XBP-1. Genes Dev 2000;14:152–7.
[338] Zhang K, Wong HN, Song B, Miller CN, Scheuner D, Kaufman RJ. The unfolded protein response sensor IRE1α is required at 2 distinct steps in B cell lymphopoiesis. J Clin Invest 2005;115:268–81.
[339] Loeuillard E, El Mourabit H, Lei L, Lemoinne S, Housset C, Cadoret A. Endoplasmic reticulum stress induces inverse regulations of major functions in portal myofibroblasts during liver fibrosis progression. Biochimica et Biophysica Acta (BBA)-Molecular Basis of Disease 2018;1864:3688–96.
[340] Zhou J, Liu CY, Back SH, Clark RL, Peisach D, Xu Z, et al. The crystal structure of human IRE1 luminal domain reveals a conserved dimerization interface required for activation

of the unfolded protein response. Proceedings of the National Academy of Sciences 2006;103:14343–8.
[341] Lipson KL, Fonseca SG, Ishigaki S, Nguyen LX, Foss E, Bortell R, et al. Regulation of insulin biosynthesis in pancreatic beta cells by an endoplasmic reticulum-resident protein kinase IRE1. Cell Metab 2006;4:245–54.
[342] Acosta-Alvear D, Zhou Y, Blais A, Tsikitis M, Lents NH, Arias C, et al. XBP1 controls diverse cell type-and condition-specific transcriptional regulatory networks. Mol Cell 2007;27:53–66.
[343] Kanda S, Yanagitani K, Yokota Y, Esaki Y, Kohno K. Autonomous translational pausing is required for XBP1u mRNA recruitment to the ER via the SRP pathway. Proceedings of the National Academy of Sciences 2016;113:E5886–95.
[344] Adamson B, Norman TM, Jost M, Cho MY, Nuñez JK, Chen Y, et al. A multiplexed single-cell CRISPR screening platform enables systematic dissection of the unfolded protein response. Cell 2016;167:1867–82.
[345] Gilbert LA, Horlbeck MA, Adamson B, Villalta JE, Chen Y, Whitehead EH, et al. Genome-scale CRISPR-mediated control of gene repression and activation. Cell 2014;159:647–61.
[346] Sriburi R, Bommiasamy H, Buldak GL, Robbins GR, Frank M, Jackowski S, et al. Coordinate regulation of phospholipid biosynthesis and secretory pathway gene expression in XBP-1 (S)-induced endoplasmic reticulum biogenesis. Journal of Biological Chemistry 2007;282:7024–34.
[347] Chen S, Xuan J, Couch L, Iyer A, Wu Y, Li Q-Z, et al. Sertraline induces endoplasmic reticulum stress in hepatic cells. Toxicology 2014;322:78–88.
[348] Desmaële D, Gref R, Couvreur P. Squalenoylation: a generic platform for nanoparticular drug delivery. Journal of Controlled Release 2012;161:609–18.
[349] Arias JL, Reddy LH, Othman M, Gillet B, Desmaele D, Zouhiri F, et al. Squalene based nanocomposites: a new platform for the design of multifunctional pharmaceutical theragnostics. ACS Nano 2011;5:1513–21.
[350] Panyam J, Sahoo SK, Prabha S, Bargar T, Labhasetwar V. Fluorescence and electron microscopy probes for cellular and tissue uptake of poly (D, L-lactide-co-glycolide) nanoparticles. Int J Pharm 2003;262:1–11.
[351] Sahoo SK, Panyam J, Prabha S, Labhasetwar V. Residual polyvinyl alcohol associated with poly (D, L-lactide-co-glycolide) nanoparticles affects their physical properties and cellular uptake. Journal of Controlled Release 2002;82:105–14.
[352] Silva AM, Alvarado HL, Abrego G, Martins-Gomes C, Garduño-Ramirez ML, García ML, et al. In vitro cytotoxicity of oleanolic/ursolic acids-loaded in PLGA nanoparticles in different cell lines. Pharmaceutics 2019;11:362.
[353] Rakotoarisoa M, Angelov B, Garamus VM, Angelova A. Curcumin-and fish oil-loaded spongosome and cubosome nanoparticles with neuroprotective potential against H2O2-induced oxidative stress in differentiated human SH-SY5Y cells. ACS Omega 2019;4:3061–73.
[354] Nita M, Grzybowski A. The role of the reactive oxygen species and oxidative stress in the pathomechanism of the age-related ocular diseases and other pathologies of the anterior and posterior eye segments in adults. Oxid Med Cell Longev 2016;2016:3164734.
[355] Kohno Y, Egawa Y, Itoh S, Nagaoka S, Takahashi M, Mukai K. Kinetic study of quenching reaction of singlet oxygen and scavenging reaction of free radical by squalene in n-

butanol. Biochimica et Biophysica Acta (BBA)-Lipids and Lipid Metabolism 1995;1256:52–6.
[356] Farvin KHS, Anandan R, Kumar SHS, Shiny KS, Sankar T V, Thankappan TK. Effect of squalene on tissue defense system in isoproterenol-induced myocardial infarction in rats. Pharmacol Res 2004;50:231–6.
[357] Farvin KHS, Kumar SHS, Anandan R, Mathew S, Sankar T V, Nair PGV. Supplementation of squalene attenuates experimentally induced myocardial infarction in rats. Food Chem 2007;105:1390–5.
[358] Skorkowska-Telichowska K, Hasiewicz-Derkacz K, Gębarowski T, Kulma A, Moreira H, Kostyn K, et al. Emulsions made of oils from seeds of GM flax protect V79 cells against oxidative stress. Oxid Med Cell Longev 2016;2016:7510759.
[359] Cárdeno A, Aparicio-Soto M, Montserrat-de la Paz S, Bermúdez B, Muriana FJG, Alarcón-de-la-Lastra C. Squalene targets pro-and anti-inflammatory mediators and pathways to modulate over-activation of neutrophils, monocytes and macrophages. J Funct Foods 2015;14:779–90.
[360] Clarke R, Cook KL, Hu R, Facey COB, Tavassoly I, Schwartz JL, et al. Endoplasmic reticulum stress, the unfolded protein response, autophagy, and the integrated regulation of breast cancer cell fate. Cancer Res 2012;72:1321–31.
[361] Wang W-A, Groenendyk J, Michalak M. Endoplasmic reticulum stress associated responses in cancer. Biochimica et Biophysica Acta (BBA)-Molecular Cell Research 2014;1843:2143–9.
[362] Lee S-O, Jin U-H, Kang JH, Kim SB, Guthrie AS, Sreevalsan S, et al. The orphan nuclear receptor NR4A1 (Nur77) regulates oxidative and endoplasmic reticulum stress in pancreatic cancer cells. Molecular Cancer Research 2014;12:527–38.
[363] Gu M-X, Fu Y, Sun X-L, Ding Y-Z, Li C-H, Pang W, et al. Proteomic analysis of endothelial lipid rafts reveals a novel role of statins in antioxidation. J Proteome Res 2012;11:2365–73.
[364] Kojima R, Okumura M, Masui S, Kanemura S, Inoue M, Saiki M, et al. Radically different thioredoxin domain arrangement of ERp46, an efficient disulfide bond introducer of the mammalian PDI family. Structure 2014;22:431–43.
[365] Dixon SJ, Lemberg KM, Lamprecht MR, Skouta R, Zaitsev EM, Gleason CE, et al. Ferroptosis: an iron-dependent form of nonapoptotic cell death. Cell 2012;149:1060–72.
[366] Yang WS, SriRamaratnam R, Welsch ME, Shimada K, Skouta R, Viswanathan VS, et al. Regulation of ferroptotic cancer cell death by GPX4. Cell 2014;156:317–31.
[367] Garcia-Bermudez J, Baudrier L, Bayraktar EC, Shen Y, La K, Guarecuco R, et al. Squalene accumulation in cholesterol auxotrophic lymphomas prevents oxidative cell death. Nature 2019;567:118–22.
[368] Senthilkumar S, Yogeeta SK, Subashini R, Devaki T. Attenuation of cyclophosphamide induced toxicity by squalene in experimental rats. Chem Biol Interact 2006;160:252–60.
[369] Motawi TMK, Sadik NAH, Refaat A. Cytoprotective effects of DL-alpha-lipoic acid or squalene on cyclophosphamide-induced oxidative injury: an experimental study on rat myocardium, testicles and urinary bladder. Food and Chemical Toxicology 2010;48:2326–36.

[370] Jessop CE, Watkins RH, Simmons JJ, Tasab M, Bulleid NJ. Protein disulphide isomerase family members show distinct substrate specificity: P5 is targeted to BiP client proteins. J Cell Sci 2009;122:4287–95.
[371] Sullivan DC, Huminiecki L, Moore JW, Boyle JJ, Poulsom R, Creamer D, et al. EndoPDI, a novel protein-disulfide isomerase-like protein that is preferentially expressed in endothelial cells acts as a stress survival factor. Journal of Biological Chemistry 2003;278:47079–88.
[372] Shamu CE, Walter P. Oligomerization and phosphorylation of the Ire1p kinase during intracellular signaling from the endoplasmic reticulum to the nucleus. EMBO J 1996;15:3028–39.
[373] Schuck S, Prinz WA, Thorn KS, Voss C, Walter P. Membrane expansion alleviates endoplasmic reticulum stress independently of the unfolded protein response. Journal of Cell Biology 2009;187:525–36.
[374] Zhao L-M, Shi L-E, Zhang Z-L, Chen J-M, Shi D-D, Yang J, et al. Preparation and application of chitosan nanoparticles and nanofibers. Brazilian Journal of Chemical Engineering 2011;28:353–62.
[375] Qi L, Xu Z, Jiang X, Hu C, Zou X. Preparation and antibacterial activity of chitosan nanoparticles. Carbohydr Res 2004;339:2693–700.
[376] De Campos AM, Sánchez A, Alonso MJ. Chitosan nanoparticles: a new vehicle for the improvement of the delivery of drugs to the ocular surface. Application to cyclosporin A. Int J Pharm 2001;224:159–68.
[377] Rampino A, Borgogna M, Blasi P, Bellich B, Cesàro A. Chitosan nanoparticles: Preparation, size evolution and stability. Int J Pharm 2013;455:219–28.
[378] Csaba N, Köping-Höggård M, Alonso MJ. Ionically crosslinked chitosan/tripolyphosphate nanoparticles for oligonucleotide and plasmid DNA delivery. Int J Pharm 2009;382:205–14.
[379] Luangtana-anan M, Opanasopit P, Ngawhirunpat T, Nunthanid J, Sriamornsak P, Limmatvapirat S, et al. Effect of chitosan salts and molecular weight on a nanoparticulate carrier for therapeutic protein. Pharm Dev Technol 2005;10:189–96.
[380] Mohammadpour Dounighi N, Eskandari R, Avadi MR, Zolfagharian H, Mir Mohammad Sadeghi A, Rezayat M. Preparation and in vitro characterization of chitosan nanoparticles containing Mesobuthus eupeus scorpion venom as an antigen delivery system. Journal of Venomous Animals and Toxins Including Tropical Diseases 2012;18:44–52.
[381] Gan Q, Wang T, Cochrane C, McCarron P. Modulation of surface charge, particle size and morphological properties of chitosan–TPP nanoparticles intended for gene delivery. Colloids Surf B Biointerfaces 2005;44:65–73.
[382] Cho K, Wang XU, Nie S, Chen Z, Shin DM. Therapeutic nanoparticles for drug delivery in cancer. Clinical Cancer Research 2008;14:1310–6.
[383] Souza MP, Vaz AFM, Correia MTS, Cerqueira MA, Vicente AA, Carneiro-da-Cunha MG. Quercetin-loaded lecithin/chitosan nanoparticles for functional food applications. Food Bioproc Tech 2014;7:1149–59.
[384] Keawchaoon L, Yoksan R. Preparation, characterization and in vitro release study of carvacrol-loaded chitosan nanoparticles. Colloids Surf B Biointerfaces 2011;84:163–71.
[385] Lepeltier E, Loretz B, Desmaële D, Zapp J, Herrmann J, Couvreur P, et al. Squalenoylation of chitosan: a platform for drug delivery? Biomacromolecules 2015;16:2930–9.

[386] Ceruti M, Viola F, Balliano G, Milla P, Roma G, Grossi G, et al. Synthesis of (E)-and (Z)-29-methylidyne-2, 3-oxidosqualene derivatives as inhibitors of liver and yeast oxidosqualene cyclase. J Chem Soc Perkin 1 2002:1477–86.
[387] Liu G, Gan J, Chen A, Liu Q, Zhao X. Synthesis and characterization of an amphiphilic chitosan bearing octyl and methoxy polyethylene. Nat Sci (Irvine) 2010;2:707.
[388] Huang Z, Wang H, Gao C, Shen H, Fa X. Drug loaded gold nano-particulates for therapeutics of myocardial infarction in rat model. J Biomater Tissue Eng 2018;8:197–205.
[389] Kumar LRG, Chatterjee NS, Tejpal CS, Vishnu K V, Anas KK, Asha KK, et al. Evaluation of chitosan as a wall material for microencapsulation of squalene by spray drying: Characterization and oxidative stability studies. Int J Biol Macromol 2017;104:1986–95.
[390] Ma S, Moser D, Han F, Leonhard M, Schneider-Stickler B, Tan Y. Preparation and antibiofilm studies of curcumin loaded chitosan nanoparticles against polymicrobial biofilms of Candida albicans and Staphylococcus aureus. Carbohydr Polym 2020;241:116254.
[391] Khan MM, Madni A, Torchilin V, Filipczak N, Pan J, Tahir N, et al. Lipid-chitosan hybrid nanoparticles for controlled delivery of cisplatin. Drug Deliv 2019;26:765–72.
[392] Hosseini SF, Zandi M, Rezaei M, Farahmandghavi F. Two-step method for encapsulation of oregano essential oil in chitosan nanoparticles: preparation, characterization and in vitro release study. Carbohydr Polym 2013;95:50–6.
[393] de Moura MR, Aouada FA, Mattoso LHC. Preparation of chitosan nanoparticles using methacrylic acid. J Colloid Interface Sci 2008;321:477–83.
[394] Huo MR, Zhou JP, Wei Y, Lü L. Preparation of paclitaxel-loaded chitosan polymeric micelles and influence of surface charges on their tissue biodistribution in mice. Yao Xue Xue Bao 2006;41:867–72.
[395] Wedmore I, McManus JG, Pusateri AE, Holcomb JB. A special report on the chitosan-based hemostatic dressing: experience in current combat operations. Journal of Trauma and Acute Care Surgery 2006;60:655–8.
[396] Kim J-H, Kim Y-S, Park K, Lee S, Nam HY, Min KH, et al. Antitumor efficacy of cisplatin-loaded glycol chitosan nanoparticles in tumor-bearing mice. Journal of Controlled Release 2008;127:41–9.
[397] Ghormade V, Deshpande M V, Paknikar KM. Perspectives for nano-biotechnology enabled protection and nutrition of plants. Biotechnol Adv 2011;29:792–803.
[398] Kean T, Thanou M. Biodegradation, biodistribution and toxicity of chitosan. Adv Drug Deliv Rev 2010;62:3–11.
[399] Sato T, Ishii T, Okahata Y. In vitro gene delivery mediated by chitosan. Effect of pH, serum, and molecular mass of chitosan on the transfection efficiency. Biomaterials 2001;22:2075–80.
[400] Nguyen J, Szoka FC. Nucleic acid delivery: the missing pieces of the puzzle? Acc Chem Res 2012;45:1153–62.
[401] Ragelle H, Vandermeulen G, Préat V. Chitosan-based siRNA delivery systems. Journal of Controlled Release 2013;172:207–18.
[402] Dash M, Chiellini F, Ottenbrite RM, Chiellini E. Chitosan—A versatile semi-synthetic polymer in biomedical applications. Prog Polym Sci 2011;36:981–1014.
[403] Ying X-Y, Cui D, Yu L, Du Y-Z. Solid lipid nanoparticles modified with chitosan oligosaccharides for the controlled release of doxorubicin. Carbohydr Polym 2011;84:1357–64.

[404] Yue Z-G, Wei W, Lv P-P, Yue H, Wang L-Y, Su Z-G, et al. Surface charge affects cellular uptake and intracellular trafficking of chitosan-based nanoparticles. Biomacromolecules 2011;12:2440–6.
[405] Gokce EH, Sandri G, Bonferoni MC, Rossi S, Ferrari F, Güneri T, et al. Cyclosporine A loaded SLNs: evaluation of cellular uptake and corneal cytotoxicity. Int J Pharm 2008;364:76–86.
[406] Nam HY, Kwon SM, Chung H, Lee S-Y, Kwon S-H, Jeon H, et al. Cellular uptake mechanism and intracellular fate of hydrophobically modified glycol chitosan nanoparticles. Journal of Controlled Release 2009;135:259–67.
[407] Trickler WJ, Nagvekar AA, Dash AK. A novel nanoparticle formulation for sustained paclitaxel delivery. AAPS PharmSciTech 2008;9:486–93.
[408] Gao X, Gong J, Cai Y, Wang J, Wen J, Peng L, et al. Chitosan modified squalene nanostructured lipid carriers as a promising adjuvant for freeze-dried ovalbumin vaccine. Int J Biol Macromol 2021;188:855–62.
[409] Boisselier E, Astruc D. Gold nanoparticles in nanomedicine: preparations, imaging, diagnostics, therapies and toxicity. Chem Soc Rev 2009;38:1759–82.
[410] Yue H, Wei W, Yue Z, Lv P, Wang L, Ma G, et al. Particle size affects the cellular response in macrophages. European Journal of Pharmaceutical Sciences 2010;41:650–7.
[411] Abuobeid R, Sánchez-Marco J, Felices MJ, Arnal C, Burillo JC, Lasheras R, et al. Squalene through Its Post-Squalene Metabolites Is a Modulator of Hepatic Transcriptome in Rabbits. Int J Mol Sci 2022;23:4172.
[412] Agnihotri SA, Mallikarjuna NN, Aminabhavi TM. Recent advances on chitosan-based micro-and nanoparticles in drug delivery. Journal of Controlled Release 2004;100:5–28.
[413] Singh A, Mittal A, Benjakul S. Chitosan nanoparticles: Preparation, food applications and health benefits. Sci Asia 2021;47:1–10.
[414] Vllasaliu D, Exposito-Harris R, Heras A, Casettari L, Garnett M, Illum L, et al. Tight junction modulation by chitosan nanoparticles: comparison with chitosan solution. Int J Pharm 2010;400:183–93.
[415] Panyam J, Zhou W, Prabha S, Sahoo SK, Labhasetwar V. Rapid endo-lysosomal escape of poly (DL-lactide-coglycolide) nanoparticles: implications for drug and gene delivery. The FASEB Journal 2002;16:1217–26.
[416] Rinaudo M. Chitin and chitosan: Properties and applications. Prog Polym Sci 2006;31:603–32.
[417] Chattopadhyay DP, Inamdar MS. Aqueous behaviour of chitosan. Int J Polym Sci 2010;2010:939536.
[418] Janes KA, Fresneau MP, Marazuela A, Fabra A, Alonso MJ. Chitosan nanoparticles as delivery systems for doxorubicin. Journal of Controlled Release 2001;73:255–67.
[419] Duivenvoorden W, Hopmans SN, Austin RC, Pinthus JH. Endoplasmic reticulum protein ERp46 in prostate adenocarcinoma. Oncol Lett 2017;13:3624–30.